

Fiscal Year 2017: Third Quarter

Progress Report
**Advanced Battery Materials
Research (BMR) Program**

Released September 2017
for the period of April – June 2017

Approved by

Tien Q. Duong, Advanced Battery Materials Research Program Manager
Vehicle Technologies Office, Energy Efficiency and Renewable Energy

TABLE OF CONTENTS

A Message from the Advanced Battery Materials Research Program Manager	xv
Task 1 – Advanced Electrode Architectures	1
Task 1.1 – Higher Energy Density via Inactive Components and Processing Conditions (Vincent Battaglia, Lawrence Berkeley National Laboratory)	2
Task 1.2 – Prelithiation of Silicon Anode for High-Energy Lithium-Ion Batteries (Yi Cui, Stanford University).....	4
Task 1.3 – Electrode Architecture-Assembly of Battery Materials and Electrodes (Karim Zaghib, Hydro-Quebec)	7
Task 2 – Silicon Anode Research	9
Task 2.1 – High-Capacity and Long Cycle Life Silicon-Carbon Composite Materials and Electrodes (Gao Liu, Lawrence Berkeley National Laboratory)	10
Task 2.2 – Stable Operation of Silicon-Based Anode for Lithium-Ion Batteries (Ji-Guang Zhang and Jun Liu, Pacific Northwest National Laboratory; Prashant Kumta, University of Pittsburgh).....	13
Task 3 – High-Energy-Density Cathodes for Advanced Lithium-Ion Batteries	16
Task 3.1 – Studies on High-Capacity Cathodes for Advanced Lithium-Ion Systems (Jagjit Nanda, Oak Ridge National Laboratory).....	17
Task 3.2 – High-Energy-Density Lithium Battery (Stanley Whittingham, SUNY Binghamton)	20
Task 3.3 – Development of High-Energy Cathode Materials (Ji-Guang Zhang and Jianming Zheng, Pacific Northwest National Laboratory).....	23
Task 3.4 – <i>In Situ</i> Solvothermal Synthesis of Novel High-Capacity Cathodes (Feng Wang and Jianming Bai, Brookhaven National Laboratory)	26
Task 3.5 – Novel Cathode Materials and Processing Methods (Michael M. Thackeray and Jason R. Croy, Argonne National Laboratory)	29
Task 3.6 – Advanced Cathode Materials for High-Energy Lithium-Ion Batteries (Marca Doeff, Lawrence Berkeley National Laboratory).....	32
Task 3.7 – Discovery of High-Energy Lithium-Ion Battery Materials (Wei Tong, Lawrence Berkeley National Laboratory)	35
Task 3.8 – Exploiting Cobalt and Nickel Spinel in Structurally Integrated Composite Electrodes (Michael M. Thackeray and Jason R. Croy, Argonne National Laboratory)	38

Task 4 – Electrolytes	41
Task 4.1 – Understanding and Mitigating Interfacial Reactivity between Electrode and Electrolyte (Khalil Amine, Larry A. Curtiss, and Nenad Markovic, Argonne National Laboratory)	43
Task 4.2 – Advanced Lithium-Ion Battery Technology: High-Voltage Electrolyte (Joe Sunstrom and Ron Hendershot, Daikin)	45
Task 4.3 – Multi-Functional, Self-Healing Polyelectrolyte Gels for Long-Cycle-Life, High-Capacity Sulfur Cathodes in Lithium-Sulfur Batteries (Alex Jen and Jihui Yang, University of Washington).....	48
Task 4.4 – Development of Ion-Conducting Inorganic Nanofibers and Polymers (Nianqiang (Nick) Wu, West Virginia University; Xiangwu Zhang, North Carolina State University).....	51
Task 4.5 – High Conductivity and Flexible Hybrid Solid-State Electrolyte (Eric Wachsman, Liangbing Hu, and Yifei Mo, University of Maryland)	54
Task 4.6 – Self-Forming Thin Interphases and Electrodes Enabling 3D Structured High-Energy-Density Batteries (Glenn Amatucci, Rutgers University).....	57
Task 4.7 – Dual Function Solid-State Battery with Self-Forming, Self-Healing Electrolyte and Separator (Esther Takeuchi, Stony Brook University).....	59
Task 5 – Diagnostics	62
Task 5.1 – Model System Diagnostics for High-Energy Cathode Development (Guoying Chen, Lawrence Berkeley National Laboratory).....	63
Task 5.2 – Interfacial Processes – Diagnostics (Robert Kostecki, Lawrence Berkeley National Laboratory)	66
Task 5.3 – Advanced <i>In Situ</i> Diagnostic Techniques for Battery Materials (Xiao-Qing Yang and Seongmin Bak, Brookhaven National Laboratory)	69
Task 5.4 – Nuclear Magnetic Resonance and Magnetic Resonance Imaging Studies of Solid Electrolyte Interphase, Dendrites, and Electrode Structures (Clare Grey, University of Cambridge).....	72
Task 5.5 – Advanced Microscopy and Spectroscopy for Probing and Optimizing Electrode- Electrolyte Interphases in High-Energy Lithium Batteries (Shirley Meng, University of California – San Diego)	75
Task 5.6 – <i>In Situ</i> Diagnostics of Coupled Electrochemical-Mechanical Properties of Solid Electrolyte Interphases on Lithium-Metal Rechargeable Batteries (Xingcheng Xiao, General Motors; Brian W. Sheldon, Brown University; Yue Qi, Michigan State University; and Y. T. Cheng, University of Kentucky).....	78
Task 5.7 – Microscopy Investigation on the Fading Mechanism of Electrode Materials (Chongmin Wang, Pacific Northwest National Laboratory).....	82
Task 5.8 – Characterization and Computational Modeling of Structurally Integrated Electrodes (Michael M. Thackeray and Jason R. Croy, Argonne National Laboratory)	85

Task 6 – Modeling Advanced Electrode Materials	88
Task 6.1 – Predicting and Understanding Novel Electrode Materials from First Principles (Kristin Persson, Lawrence Berkeley National Laboratory).....	89
Task 6.2 – Addressing Heterogeneity in Electrode Fabrication Processes (Dean Wheeler and Brian Mazzeo, Brigham Young University)	91
Task 6.3 – Understanding and Strategies for Controlled Interfacial Phenomena in Lithium-Ion Batteries and Beyond (Perla Balbuena, Jorge Seminario, and Partha Mukherjee, Texas A&M University).....	94
Task 6.4 – First Principles Modeling of SEI Formation on Bare and Surface/Additive Modified Silicon Anode (Perla Balbuena, Texas A&M University)	97
Task 6.5 – Electrode Materials Design and Failure Prediction (Venkat Srinivasan, Argonne National Laboratory).....	100
Task 6.6 – First Principles Calculations of Existing and Novel Electrode Materials (Gerbrand Ceder, Lawrence Berkeley National Laboratory)	103
Task 6.7 – Dendrite Growth Morphology Modeling in Liquid and Solid Electrolytes (Yue Qi, Michigan State University)	105
Task 6.8 – First Principles Modeling and Design of Solid-State Interfaces for the Protection and Use of Li-Metal Anodes (Gerbrand Ceder, UC Berkeley).....	108
Task 7 – Metallic Lithium and Solid Electrolytes	110
Task 7.1 – Mechanical Properties at the Protected Lithium Interface (Nancy Dudney, Oak Ridge National Laboratory; Erik Herbert, Michigan Technological University; Jeff Sakamoto, University of Michigan).....	112
Task 7.2 – Solid Electrolytes for Solid-State and Lithium-Sulfur Batteries (Jeff Sakamoto, University of Michigan).....	115
Task 7.3 – Composite Electrolytes to Stabilize Metallic Lithium Anodes (Nancy Dudney and Frank Delnick, Oak Ridge National Laboratory).....	118
Task 7.4 – Overcoming Interfacial Impedance in Solid-State Batteries (Eric Wachsman, Liangbing Hu, and Yifei Mo, University of Maryland, College Park).....	121
Task 7.5 – Nanoscale Interfacial Engineering for Stable Lithium-Metal Anodes (Yi Cui, Stanford University).....	124
Task 7.6 – Lithium Dendrite Prevention for Lithium-Ion Batteries (Wu Xu and Ji-Guang Zhang, Pacific Northwest National Laboratory).....	127
Task 7.7 – Lithium Batteries with Higher Capacity and Voltage (John B. Goodenough, University of Texas – Austin)	130
Task 7.8 – Advancing Solid State Interfaces in Lithium-Ion Batteries (Nenad Markovic and Larry A. Curtiss, Argonne National Laboratory)	133
Task 7.9 – Engineering Approaches to Dendrite-Free Lithium Anodes (Prashant Kumta, University of Pittsburgh).....	135
Task 7.10 – Self-Assembling and Self-Healing Rechargeable Lithium Batteries (Yet-Ming Chiang, Massachusetts Institute of Technology; Venkat Viswanathan, Carnegie Mellon University)	138

Task 8 – Lithium–Sulfur Batteries	141
Task 8.1 – New Lamination and Doping Concepts for Enhanced Lithium–Sulfur Battery Performance (Prashant N. Kumta, University of Pittsburgh)	143
Task 8.2 – Simulations and X-Ray Spectroscopy of Lithium–Sulfur Chemistry (Nitash Balsara, Lawrence Berkeley National Laboratory)	146
Task 8.3 – Novel Chemistry: Lithium Selenium and Selenium Sulfur Couple (Khalil Amine, Argonne National Laboratory)	149
Task 8.4 – Multi-Functional Cathode Additives for Lithium-Sulfur Battery Technology (Hong Gan, Brookhaven National Laboratory, and Co-PI Esther Takeuchi, Brookhaven National Laboratory and Stony Brook University)	152
Task 8.5 – Development of High-Energy Lithium–Sulfur Batteries (Jun Liu and Dongping Lu, Pacific Northwest National Laboratory)	155
Task 8.6 – Nanostructured Design of Sulfur Cathodes for High-Energy Lithium-Sulfur Batteries (Yi Cui, Stanford University)	158
Task 8.7 – Addressing Internal “Shuttle” Effect: Electrolyte Design and Cathode Morphology Evolution in Lithium-Sulfur Batteries (Perla Balbuena, Texas A&M University)	160
Task 8.8 – Investigation of Sulfur Reaction Mechanisms (Deyang Qu, University of Wisconsin - Milwaukee; Xiao-Qing Yang, Brookhaven National Laboratory)	163
Task 8.9 – Statically and Dynamically Stable Lithium–Sulfur Batteries (Arumugam Manthiram, U Texas Austin)	166
Task 8.10 – Electrochemically Responsive, Self-Formed Lithium-Ion Conductors for High-Performance Lithium-Metal Anodes (Donghai Wang, Pennsylvania State University)	169
Task 9 – Lithium-Air Batteries	171
Task 9.1 – Rechargeable Lithium–Air Batteries (Ji-Guang Zhang and Wu Xu, Pacific Northwest National Laboratory)	172
Task 9.2 – Efficient Rechargeable Li/O ₂ Batteries Utilizing Stable Inorganic Molten Salt Electrolytes (Vincent Giordani, Liox)	175
Task 9.3 – Lithium–Air Batteries (Khalil Amine and Larry A. Curtiss, Argonne National Laboratory)	177
Task 10 – Sodium-Ion Batteries	180
Task 10.1 – Exploratory Studies of Novel Sodium-Ion Battery Systems (Xiao-Qing Yang and Seongmin Bak, Brookhaven National Laboratory)	181

TABLE OF FIGURES

Figure 1. Cross section of a dry electrode.....	3
Figure 2. 30-sec resistance of four cells: with surface film, half surface film removed, and no film at all.	3
Figure 3. Resistance for three loadings.	3
Figure 4. Characterization and stability of LiF-coated Li_xSi nanoparticles (NPs). (a) Transmission electron microscopy image and (b) X-ray diffraction pattern of LiF-coated Li_xSi NPs. (c) First-cycle delithiation capacities of LiF-coated Li_xSi NPs (solid line) and bare Li_xSi NPs (dashed line) using different solvents to form the slurry. (d) The extraction capacities of LiF-coated Li_xSi NPs exposed to ambient air ($\sim 40\%$ RH) with varying durations. The inset shows the trend of capacity decay of LiF-coated Li_xSi NPs (red) and Li_2O -coated Li_xSi NPs (black) with varying durations.....	5
Figure 5. (a) Scanning electron microscopy image of nano-Si/C composite made by electrospray process and (b) first discharge/charge voltage profile of this.	8
Figure 6. Cell thickness monitoring during cycling with C/24 rate between 1.5 V and 0.005 V at room temperature.	8
Figure 7. Schematic illustrating the synthesis process of the SiO-PPy composite material.	11
Figure 8. Transmission electron microscopy (TEM) images of the SiO-PPy composite sintering at 500°C . (a, b) Low magnification TEM images of the SiO-PPy-500 composites. (c, d) High-resolution TEM image displaying details of the SiO submicron particles coated with sintered PPy.....	11
Figure 9. Cycling stability of anode prepared using silicon nano powder and different binders.....	14
Figure 10. The cycling performance and Coulombic efficiency of the porous silicon obtained from aluminum reduction.....	14
Figure 11. Long-term cycling data of nano-Si obtained from high-energy mechano chemical reduction using silicide reductant, tested at 0.1A/g for initial 3 cycles followed by 0.5A/g in Li/Li ⁺ system.	14
Figure 12. (a) X-ray diffraction patterns of Li_2MoO_3 , NMC-111, and NMC-111 doped with 5% molybdenum. Galvanostatic charge/discharge curves collected at 10 mA/g for undoped NMC-111 cathodes cycled between 2.0 – 4.3 V (b) and 2.0 – 4.8 V (c).....	18
Figure 13. The cycling behavior of the (a) former full cell of the $\text{Sn}_y\text{Fe}/\text{Li}_x\text{VOPO}_4$ electrochemical couple, (b) optimized Li_xVOPO_4 half-cell, and (c) presently optimized full cell of $\text{Sn}_y\text{Fe}/\text{Li}_x\text{VOPO}_4$ electrochemical couple.	21
Figure 14. (a-c) Scanning electron microscopy images of (a) pristine, (b) LPO-as-coated, and (c) LPO-infused $\text{LiNi}_{0.76}\text{Mn}_{0.14}\text{Co}_{0.10}\text{O}_2$ cathode materials, and (d) the corresponding cycling performance at C/3 between 2.7~4.5 V.....	24
Figure 15. Cross-section scanning electron microscopy images of pristine (a, c) and LPO-infused (b, d) $\text{LiNi}_{0.76}\text{Mn}_{0.14}\text{Co}_{0.10}\text{O}_2$ before (a, b) and after (c, d) 200 cycles at C/3 between 2.7~4.5 V.	24

Figure 16. (a) Representative time-resolved X-ray diffraction patterns from $\text{LiNi}_{0.7}\text{Mn}_{0.15}\text{Co}_{0.15}\text{O}_2$ during heat treatment. (b) Evolution of the reflections characteristic of layered structure. (c) Illustration of the atomic configuration and reflection planes of (104) and (003) in the layered structure. (d) Evolution of the integrated intensity of the (003) and (104) peaks.	27
Figure 17. Evolution of Li-slab distance and cationic disordering (that is, nickel ions at 3b sites) with holding. (Lines: fittings to $y=A_1\exp(-kx)+y_0$).	27
Figure 18. (a) Differential capacity plots (dQ/dV) for a $0.33\text{Li}_2\text{MnO}_3 \bullet 0.67\text{LiMn}_{0.365}\text{Ni}_{0.365}\text{Co}_{0.244}\text{M}_{0.02}\text{O}_2$ material with and without substituent $M = \text{Fe, Zn, and Cu}$. (b) Magnified view of the low-voltage processes in the dQ/dV shown in (a) associated with voltage fade. (c) First-cycle charge (uppermost closed symbols) and discharge (lowermost open symbols) capacities (left y axis) along with first-cycle Coulombic efficiencies (circled in red, right y axis) as a function of overall lithium to transition metal ratio in the tested compositions (x axis). Cycling was conducted between 4.6-2.0V in lithium half-cells at 15 mA/g and 30°C.	30
Figure 19. Statistical data from 3D nickel X-ray absorption near edge spectroscopy mapping transmission X-ray microscopy experiments, showing nickel K-edge energy as a function of distance from the surface. Results from a 50% delithiated NMC-622 sample are shown on the left, and a 100% delithiated sample on the right. Blue symbols are for data obtained on samples at room temperature, and green are for samples after heating to 350°C.	33
Figure 20. The first-cycle voltage profiles of $\text{Li}_{2-x-y}\text{Ni}_x\text{TM}_y\text{O}_2$ (TM = Mn, Ru, Mo and Nb). Cells were cycled between 4.8 and 2.0 V at 5 mA/g at room temperature.	36
Figure 21. The first dq/dV plots of $\text{Li}_{2-x-y}\text{Ni}_x\text{TM}_y\text{O}_2$ (TM = Mn, Ru, Mo and Nb). Cells were cycled between 4.8 and 2.0 V at 5 mA/g at room temperature.	36
Figure 22. (a) Synchrotron X-ray diffraction of Li_2MnO_3 , $\text{LiNi}_{0.5}\text{Mn}_{1.5}\text{O}_4$, a 1:1 physical blend of the two, and a $\text{Li}_2\text{MnO}_3 \bullet \text{LiNi}_{0.5}\text{Mn}_{1.5}\text{O}_4$ composite. (b) and (c) Enlarged regions ranging from 2.5° to 2.8° 2-theta and from 3.0° to 3.3° 2-theta, respectively.	39
Figure 23. (a) Initial voltage profiles of spinel $\text{LiNi}_{0.5}\text{Mn}_{1.5}\text{O}_4$, (b) layered Li_2MnO_3 , (c) a $\text{Li}_2\text{MnO}_3 \bullet \text{LiNi}_{0.5}\text{Mn}_{1.5}\text{O}_4$ composite, and (d) a 1:1 physical blend of the two components. 4.8-2.0V at $\sim C/15$ and 30°C against lithium metal.	39
Figure 24. Potential dependence on the static parasitic current for aluminum foil with surface coating of (a) carbon, (b) graphene, and (c) AlPO_4	44
Figure 25. Schematic showing the proposed coupled electrochemical chemical reaction on the aluminum surface at a relatively high potential.	44
Figure 26. Gas chromatography (top) and mass spectrometry (bottom) of the native D7 fluoroether used in Daikin electrolytes.	46
Figure 27. Thermogravimetric analysis traces for all cathodes used in this project (LCO, NMC-111, NMC-532, NMC-622, and NCA).	46
Figure 28. A polyelectrolyte gel prepared using ionic liquid, cross-linkable poly(ethylene glycol) chains, and ionic-liquid-like monomer.	49

Figure 29. Structures of PENDI-C3 and PENDI-C6.	49
Figure 30. (a, b) A film made of PENDI-C6 and pyrene (Py) Linker (1:1 naphthalene diimide [NDI]/Py molar ratio) self-healed after 4 hours at 40°C. (c, d) A film made of PENDI-C3 and Py Linker (1:1 NDI/Py molar ratio) was not self-healed at 40°C, even after 16 hours.	49
Figure 31. Cycling data (C/10) of as-received and phenylthiol-modified mesoporous carbons with majority pore sizes of (a) 4 nm, (b) 10 nm, (c) 30 nm, and (d) 150 nm.	50
Figure 32. Second-cycle voltage profile (C/10) of as-received and thiophenol-modified mesoporous carbons with majority pore sizes of (a) 4 nm, (b) 10 nm, (c) 30 nm, and (d) 150 nm.	50
Figure 33. (a) X-ray diffraction patterns. (b) Electrochemical impedance spectroscopy (EIS) curves of the PEO/LiTFSI/LLTO solid composite electrolytes with different LLTO nanofiber contents. (c) Arrhenius plots of PEO/LiTFSI and PEO/LiTFSI/LLTO. (d-e) Photograph and top scanning electron microscopy of flexible and bendable PVDF-HFP/LiTFSI/LLTO 0.5% membrane. (f) EIS curves of the PVDF-HFP/LiTFSI/LLTO solid composite electrolytes with different aluminum doping percentage.	52
Figure 34. Computer modeling of Li ⁺ transport in garnet nanofibers.	55
Figure 35. Lithium diffusion of garnet under strain.	55
Figure 36. Conductivity of Lil with x% AgI additive including error bars.	60
Figure 37. Conductivity of Lil with x% AgI + 20% Al ₂ O ₃ additive including error bars.	60
Figure 38. X-ray diffraction of KAg ₄ I ₅	60
Figure 39. Conductivity as a function of temperature for Lil _x MgAg ₄ I ₅ (x = 10, 20, M = K, Rb).	60
Figure 40. Manganese K-edge hard X-ray absorption spectroscopy (hXAS) measurements of Li _x Nb _{0.3} Mn _{0.4} O ₂ crystals: (a) hXAS spectra, (b) expanded view of the pre-edge region, (c) expanded view of the X-ray absorption near-edge spectroscopy (XANES) region, and (d) relationship between manganese XANES edge position and lithium content in the samples.	64
Figure 41. (a) Powder X-ray diffraction patterns of Li _{1.4-x} Nb _{0.4-x} Mn _{0.2+2x} O ₂ (x = 0, 0.1 and 0.2) and Li _{1.3} MMnO ₂ (M = Nb _{0.5} Ta _{0.5} and Ta) crystal samples. (b) Selected area (electron) diffraction pattern, high-angle annular dark field scanning transmission electron microscopy image, and elemental distributions on Li _{1.3} Nb _{0.3} Mn _{0.4} O ₂ crystals.	64
Figure 42. (a) Raman spectra of NMC powder (blue), pulsed laser deposition (PLD)-NMC/Al electrode (black), and PLD-NMC/Al electrode after 4.7 V charged (red). (b) Cyclic voltammogram of PLD-NMC/Al electrode at the 3rd cycle. (c) The voltage-time profile of electrode during <i>in situ</i> atomic force microscopy (AFM) experiment. The arrows point at the time when AFM images were acquired. Insert: <i>in situ</i> AFM cell.	67
Figure 43. Atomic force microscopy images of pulsed laser deposition (PLD)-NMC/Al electrode in 1 x 1 μm scale after staying in each target voltage for 30 minutes.	67

Figure 44. (a) <i>Ex situ</i> manganese K-edge and ruthenium K-edge X-ray absorption spectroscopy data of pristine $\text{Li}_2\text{Ru}_{0.5}\text{Mn}_{0.5}\text{O}$ sample, sample normally cycled 20 times, and sample cycled 20 times but first prelithiated, with references of Mn_2O_3 and MnO_2 shown. (b) <i>Ex situ</i> X-ray diffraction patterns of two cases (with [003], [108] and [110] peaks indexed according to the space group R3m): pristine sample, cycled 8 times and cycled 20 times for the normally cycled case (the part below the dash line); and pristine sample, cycled 8 times and cycled 20 times for the prelithiated case (the part above the dash line). (c) The ratio between lattice parameter <i>c</i> and lattice parameter <i>a</i> as a function of cycle numbers. The dash line shows the <i>c/a</i> ratio in perfect spinel.	70
Figure 45. ^1H solution NMR of (a) LP30, (b) LP30 + FEC, and (c) LP30 + 10 vol% ^{13}C -FEC before cycling (pristine), and after the 1 st and 30 th cycles. ^{13}C satellites are marked with an asterisk.	73
Figure 46. Multiplet pattern of LP30 + ^{13}C -FEC in region γ of Figure 45c, (a) experimental pattern and (b) simulated pattern of a four-spin system AA'XX' (cis-H-CR=CR-H).	73
Figure 47. ^1H - ^{13}C CP nuclear magnetic resonance (NMR) spectra of silicon nanowires after 30 cycles in (a) LP30 + 25 vol% ^{13}C -EC and (b) LP30 + 10 vol% ^{13}C -FEC electrolytes. The room-temperature spectra were measured by conventional solid-state NMR, whereas the 100 K spectra were measured with dynamic nuclear polarization (DNP) NMR. The dicyanobenzene was used as the radical solvent for DNP.	73
Figure 48. (a) The evolution of the superstructure peak intensity in the pristine state, after 50 cycles, and after the heat treatment. (b) Charge-discharge voltage curves of Li-rich layered oxide cathode with Li-metal as anode for the voltage range of 2.0-4.6 V versus Li^+/Li	76
Figure 49. Schematic cell configuration: (a) potential curve, (b) schematic cryo transmission electron microscopy (TEM) imaging of the EDLi for TEM observation, and (c) TEM images of the EDLi as a function of the electron radiation dose at 100 K (d-f at 19 kX magnification).	77
Figure 50. Tunneling probability for SEI components.	79
Figure 51. Bandgap change with anion distance.	79
Figure 52. The load-displacement curves of lithium metal in dry and wet conditions.	79
Figure 53. Microstructure of porous lithium obtained under current density (a) 2.4 mA/cm^2 and (b) 0.4 mA/cm^2 . (c) Typical load-displacement curves of bulk and porous lithium under the wet condition.	80
Figure 54. Schematic of a solid-state battery and pop-up modes of an electrode with a liquid electrolyte or a solid electrolyte.	80

Figure 55. Atomic resolution scanning transmission electron microscopy – electron energy loss spectroscopy (STEM-EELS) mapping of NMC-333. (a) From the pristine NMC-333 without cycling. (b–d) From NMC-333 after 100 cycles with a high cutoff voltage of 4.8 V. (b) From the well-preserved layered region. (c) From the disordered region. (d) From the heavily disordered region. The dashed blue frame at bottom right highlights transition metal maps with disordered structure. The white arrows in row b indicate a correspondence between the STEM – high-angle annular dark-field (HAADF) image and EELS map for identifying the nickel that migrates to the lithium layer. The scale bars in HAADF images are 0.5 nm.....	83
Figure 56. (a) Cross-sectional scanning electron microscopy image of Al-treated, layered-layered-spinel (LLS) particle. (b) Transmission electron microscopy image and fast Fourier transform (FFT) of surface and bulk regions showing spinel integration at the surface of the particle. (c). STEM-EDX analysis of Al-treated LLS particle showing distribution of Al (top left), Mn (top right), Co (bottom left), and Ni (bottom right).	86
Figure 57. The defect formation energy of each stable surface facet as compared to the bulk, covering defect transition metal, post-transition metal, and metalloid elements.....	90
Figure 58. Cross-section images from models of (a) CPG-A12, (b) Toda 523 (B), and (c) Toda HE5050; carbon-binder domain is red, active material is yellow, and larger pores are blue.....	92
Figure 59. Evolution of damage during lithiation-delithiation of an amorphous silicon particle for one cycle.....	95
Figure 60. Morphology change of a model LiF coating during cracking of a silicon nanoparticle.	95
Figure 61. Interaction energy (E) of one lithium ion with its nearest neighbors within a sphere of 6 Å radius during charging with $E = 1.0 \text{ V/Å}$. This is a particular trajectory of a lithium ion from the cathode (1) through the electrolyte (2) to the anode (3). [Ponce et al. <i>JPC</i> 121 (2017): 12959.].....	98
Figure 62. Concentration and potential contour within the electrolyte around the dendritic protrusion at high and low rates of current. Potential in lithium metal remains extremely close to zero. (a) Potential contour for $i_{\text{app}} = 0.01i_{\text{lim}}$. (b) Concentration contour for $i_{\text{app}} = 0.01i_{\text{lim}}$. (c) Potential contour for $i_{\text{app}} = 0.9i_{\text{lim}}$. (b) Concentration contour for $i_{\text{app}} = 0.9i_{\text{lim}}$	101
Figure 63. (a) Distribution of reaction current from the peak to the valley at two different applied current densities. (b) Reaction current ratio between protrusion peak and valley for different applied current densities. Model predictions are consistent with experiments.	101
Figure 64. (a) The first-cycle voltage profiles of LNTMO compounds. (b) Capacity evolution over 20 cycles.	104
Figure 65. (a) Proposed first-charge mechanism of LNTMO20, with voltage profile and corresponding lattice constant from <i>in situ</i> X-ray diffraction. (b) Illustrations of a LNTMO20 particle before and after oxygen loss with densified surface.	104

Figure 66. (a) Energy profile for Li^+ ion at the $\text{Li} \text{Li}_2\text{CO}_3 \text{EC}$ -electrolyte interface and (b) de-solvation barriers and diffusion barrier under the applied potential. (c) Snapshots of $\text{Li}_2\text{CO}_3 \text{EC}$ -electrolyte interface when lithium is away or at the interface under the different applied potentials.	106
Figure 67. Modeling of lithium dendrite growth in LLZO microstructure.	106
Figure 68. Schematic for the reverse design strategy overlaid on a Li-ion all-solid-state cell. Arrows show the lithium chemical potentials, which favor lithium percolation from the lithium anode (gray) toward the cathode (blue). The interfacial products, originating from the contact of electrodes and the ionic conductor, are identified by the ternary phase diagrams (triangular shapes) at the bottom.	109
Figure 69. Electrochemical stability ranges of binary lithium decomposition products.	109
Figure 70. (a) Hardness versus depth. (b) Data and rationalizations. (c) Dislocation avalanche threshold criterion.	113
Figure 71. Area specific resistance as a function of the adhesion strength of the Li-LLZO interface. Optical microscope images show the fracture surface of the lithium and LLZO disks at low and high area specific ionic resistance. The red dashed line indicates the measured tensile strength of lithium metal.	113
Figure 72. The critical current density increases with increasing grain size. Color maps indicate LLZO crystallographic orientations determined using electron backscatter diffraction.	116
Figure 73. Results for symmetrical cell $\text{Li}/\text{composite polymer electrolyte (CPE)}/\text{Li}$. At left, DC polarization and electrochemical impedance spectroscopy (EIS) response as inset. At center, voltage measured for +/- DC current of 8, 16, 32 $\mu\text{A}/\text{cm}^2$ at 5 min steps. At right, EIS response after each DC cycling test, and appearance of CPE and lithium when cell was disassembled.	119
Figure 74. Arrhenius plot of composite polymer electrolyte with Ohara acid/base treated.	119
Figure 75. (a) Calculated interphase equilibria and reaction energy between LLZO and lithium polysulfides. (b) X-ray photoelectron spectroscopy spectra of garnet interface in Li-S battery. Calculated Li^+ transport pathway (c) and energy barriers (d) of Li_2SO_4 . Calculated Li^+ transport pathway (e) and energy barriers (f) of Li_6ZrO_7	122
Figure 76. (a) Schematic showing surface treatment of lithium metal with Freon R134a. (b) Proposed major chemical reactions at the early stage of surface treatment.	125
Figure 77. High-resolution scanning electron microscopy images showing (a) surface morphology and (b) cross-section of LiF -coated lithium foil.	125
Figure 78. Time-dependent electrochemical impedance measurement on 3D Li-metal symmetric cells with LiF coating.	125
Figure 79. (a) Average lithium Coulombic efficiency in electrolytes of 1 M LiPF_6/PC with different additives (VC, FEC, and X) and additive mixtures (VC+X and FEC+X) tested in $\text{Li} \text{Cu}$ cells. (b) Cycling stability of these electrolytes in $\text{Li} \text{NMC-333}$ cells at C/3 rate.	128

Figure 80. Performances of Li NMC cells with different NMC areal capacity loadings. (a, b) First-cycle voltage profiles related to areal capacity (a) and specific capacity (b). (c) First-cycle efficiency. (d) Long-term cycling stability at 1.0 mA cm ⁻² charge and 2.0 mA cm ⁻² discharge between 2.7 and 4.3 V.....	128
Figure 81. Structure of cross-linked poly (ethylene glycol) methyl ether acrylate (CPMEA).....	131
Figure 82. Charge/discharge voltage curves of all-solid-state Li/CPMEA-LiTFSI/Cu cell at 70°C.....	131
Figure 83. X-ray photoelectron spectroscopy results for Ti 2p and Nb 3d peak to establish Li-cation interactions.....	134
Figure 84. (a) Crystal structure of the two STO LiCoO ₂ thin films. (b) Atomic force microscopy images showing the topography of the thin films. (c) X-ray absorption spectroscopy measurements demonstrating that (003) films are unaffected by lithium deposition, whereas bulk reduction takes place on (104) films.....	134
Figure 85. Very high porosity (60-80%) porous foams (PF) with hierarchical porosity. Post-cycled scanning electron microscopy images of the PF showing dendrite growth within the pores of the foam.	136
Figure 86. (a) Formation of lithium on stainless-steel spacer in coin cell tests. (b) Diffusion pathways causing plating of lithium on polymeric-coated stainless-steel spacers.	136
Figure 87. Lithium structurally isomorphous alloy (Li-SIA) electrodes demonstrate long-term stability, though there is a rise in overpotential due to possible phase segregation.	136
Figure 88. Li-Li asymmetric cell design and tests.	139
Figure 89. Electrochemical cycling performance of polysulfide trapping agent (PTA)-coated directly doped sulfur architecture electrodes.....	144
Figure 90. (a) Comparison of experimental and simulated X-ray diffraction patterns of sulfonic complex framework material (CFM). (b) Electrochemical cycling performance of the sulfonic CFM compared with commercial sulfur.	144
Figure 91. Schematic (left) and spectra (right) for an Li ₂ S complex with increasing number of diglyme solvent molecules embedded in a continuous implicit solvent medium that represents the bulk properties of diglyme.	147
Figure 92. Cycle performance of S/HPC composite with 85 wt% sulfur loading.....	150
Figure 93. High-precision leakage current measurement on S/HPC cathode in DOL/DME and DOL/ANL-1 electrolytes.....	150
Figure 94. E/C ratio effect on Li-S cell power.	153
Figure 95. Effect of LiNO ₃ concentration.....	153
Figure 96. Temperature versus sulfur utilization.	153
Figure 97. Li-S cell cycling after activation.	153

Figure 98. Visual comparison of polysulfide diffusion in H-cell using Celgard 2400 separator with (a) and without (b) cross-linked polyacrylic acid (C-PAA) coating for 1 h rest, (c) scanning electron microscopy image of C-PAA/carbon nanofiber (CNF)-coated separator, and (d) cycling capacity and Coulombic efficiency of Li-S cells using separator with and without C-PAA coating.	156
Figure 99. Li ₂ S ₆ polysulfide adsorption test. (a) Photograph of setup. (b) UV-Vis data of varying concentrations of Li ₂ S ₆ in DOL/DME solution without candidate materials. (c-d) With candidate materials added in 3 mM Li ₂ S ₆	159
Figure 100. Synthesis scheme and electrochemical tests of C/S composite.....	161
Figure 101. (a) Photograph of the two highly oriented pyrolytic graphite (HOPG) cylinders adopted in this paper. (b) Schematic illustration of the corresponding structures of HOPG-1 and HOPG-2. (c) Photographs of the geometrical configurations of the resulting working electrodes.	164
Figure 102. (a) iR-free CVs of sulfur electrochemical reduction and oxidation on highly oriented pyrolytic graphite (HOPG)-1T (basal plane), HOPG-1L (edge plane), HOPG-2T (edge plane), and HOPG-2L (step plane) at a scan rate of 20 mV/s. (b) The relation between peak potential obtained from (a) and I _D /I _G obtained from Raman analysis.	164
Figure 103. Cycling performance of the cells fabricated with LBL CNF-coated separators.	167
Figure 104. Cycling performance of the cells fabricated with (a) core-shell cathodes (sulfur loading of 4.0 – 30.0 mg cm ⁻²) and (b) cotton-carbon cathodes (sulfur loading of 30 mg cm ⁻²). The numbers in the legends CS4, CS6, ... CS30 in (a) refer to the sulfur loadings in mg cm ⁻²	167
Figure 105. Cycling performance of Li-S pouch cell.	170
Figure 106. Scanning electron microscopy images of C-SEI layer (a), S-SEI layer (b), and SCP-90-SEI layer (c).....	170
Figure 107. Atomic force microscopy images (10 × 10 μm ² scan size) of the C-SEI layer (a), S-SEI layer (b), and SCP-90-SEI layer (c).....	170
Figure 108. (a) Li-metal plating/stripping from Li Li cells cycled at 0.2 mA cm ⁻² in 1 M LiTf-Tetraglyme electrolytes with and without 2% LiDFOB additive. (b, c) Voltage profiles of Li-O ₂ cells cycled at 0.1 mA cm ⁻² in 1 M LiTf-TEGDME electrolytes with (b) and without 2% LiDFOB additive (c).	173
Figure 109. Li-O ₂ cells with optimized RuO ₂ /carbon nanotubes (CNTs) air-electrode and Li-metal anode (after 190 cycles, cells based on above cycled air-electrode and new lithium metal), and pristine RuO ₂ /CNTs air-electrode and lithium metal, cycled at 0.1 mA cm ⁻² in 1 M LiTf-Tetraglyme electrolyte.....	173
Figure 110. (left) Li/O ₂ cell voltage profile at 175°C using Super P Carbon:PTFE (95:5 wt%) cathode at 0.05 mA/cm ² current density (m _{carbon} = 3 mg, m _{nitrate} = 6.5 mg). (right) Molten nitrate lithium cell voltage profile at 175°C using nanoporous nickel cathode (Ni:LiNO ₃ -KNO ₃ eutectic 50:50 wt%) at 0.05 mA/cm ² current density (m _{Ni} = m _{nitrate} = 10 mg).	176

Figure 111. Reaction mechanisms for the hydrolysis of MO_2 (Reaction 1). For $\text{M}=\text{Li}$ the reaction bypasses the formation of H_2O_2 and forms LiOH , the quantity of which is measured by pH titration. 178

Figure 112. V $\text{L}_{2,3}$ -edge sXAS spectra collected on electrodes that are cycled to different voltages. (a) Bulk-sensitive total fluorescence yield (TFY), and (b) surface-sensitive total electron yield (TEY)..... 182

TABLE OF TABLES

Table 1. Gen 1/2 polymer properties.	49
Table 2. Simulated and experimental effective ionic transport results, following drying and calendering steps.....	92
Table 3. Density functional theory calculation for solvation energy of polysulfides in DME and ANL-1.	150

A MESSAGE FROM THE ADVANCED BATTERY MATERIALS RESEARCH PROGRAM MANAGER

This document summarizes the BMR investigators' activities performed during the period from April 1, 2017, through July 31, 2017. The Team continued to make incremental improvements in developing new battery materials and novel diagnostic techniques. Selected highlights from the various tasks are summarized below:

- Yi Cui's (Stanford University) group: A Freon gas reaction was used to prepare thin and conformal LiF passivation layers on 3D Li-metal anodes.
- Nancy Dudney's (Oak Ridge National Laboratory), Erik Herbert's (Michigan Technological University) and Jeff Sakamoto's (University of Michigan) groups: Tensile tests revealed the adhesive strength of the lithium electrode with an LLZO ceramic electrolyte. The adhesive strength exceeded the tensile strength of the Li-metal foil, ~ 8 MPa, for samples with very low interfacial area specific resistance.
- Kumta's (University of Pittsburgh) group: A new sulfonic Complex Framework Material demonstrated high sulfur loading and maintained a capacity of 1051 mAh/g for over 100 cycles with 0.0011% fade at 0.2C rate.
- Ji-Guang Zhang's (Pacific Northwest National Laboratory) group: A new low-temperature (210°C) thermic reduction method was developed to prepare porous silicon. The material demonstrated a specific capacity of ~2100 mAh g⁻¹ and retention of ~ 80% after 200 cycles.
- Khalil Amine's and Larry Curtiss' (Argonne National Laboratory) groups: A newly discovered approach to determine composition of the discharge product in Li-O₂ batteries is critical for further development of Li-O₂ batteries.

Last year, the DOE's goal of reducing the cost of vehicle battery technologies resulted in the formation of a consortium of investigators led by Pacific Northwest National Laboratory. The aim of the researchers is to develop batteries that have over twice the specific energy of batteries used in today's electric vehicles. The consortium includes Brookhaven National Laboratory, Idaho National Laboratory, SLAC National Accelerator Laboratory, Binghamton University (State University of New York), Stanford University, University of California at San Diego, University of Texas at Austin, and University of Washington. The DOE also provided support to "seedling projects" that will allow other organizations to share their ideas on how to meet these challenging goals.

On July 12, 2017, the DOE announced awards to 15 seedling projects that will support the Vehicle Technologies Office Battery500 Consortium Program. A list of the projects is presented below. These projects will be down selected for further funding after 18 months.

University of Maryland, College Park, MD

Research innovative iron-based materials for high-energy cathodes for high-energy Li-ion battery technologies.

Lawrence Berkeley National Laboratory, Berkeley, CA

Explore thick cathodes using freeze casting methods for solid-state lithium batteries.

Pennsylvania State University, University Park, PA

Research multifunctional Li-ion conducting interfacial materials that enable high-performance Li-metal anodes.

Mercedes-Benz Research & Development North America, Inc., Redford, MI

Investigate a scalable synthesis to enable very thin coatings on solid-state electrolyte membranes to enable high-performance Li-S battery.

University of Maryland, College Park, MD

Research 3D-printed, low-tortuosity frameworks to improve the specific energy of a solid-state Li-S battery containing a garnet electrolyte.

General Motors LLC, Pontiac, MI

Design, engineer, develop, and integrate pouch-format cells for Li-S batteries to achieve high energy density and long cycle life.

University of Pittsburgh, Pittsburgh, PA

Research sulfur electrodes utilizing Li-ion conductor (LIC) coatings for high-energy-density advanced Li-S batteries.

Cornell University, Ithaca, NY

Research highly loaded sulfur cathodes and conductive carbon-coated separators that enable high-energy batteries.

University of Maryland, College Park, MD

Investigate advanced electrolytes to limit dendrite growth in Li-metal cells.

Texas A&M Engineering Experiment Station, College Station, TX

Utilize an analytical and experimental approach to examine the interface between solid-state electrolytes and Li-metal anodes and identify potential methods for mitigating dendrite growth.

Navitas Advanced Solutions Group, LLC, Ann Arbor, MI

Research a solvent-free process to fabricate all-solid lithium batteries.

Wayne State University, Detroit, MI

Investigate a unique battery couple based on lithium-free cathodes of Ni-pillared MnO_2 /lithiated anodes.

Oregon State University, Corvallis, OR

Push the boundaries of energy density batteries by employing a compact configuration of the $\text{Li}_2\text{S}@$ Graphene cathode, formed by simple lithiothermic reactions.

Research Foundation of the State University of New York for Stony Brook University, Stony Brook, NY

Explore the benefit of novel MS_2 ($\text{M} = \text{Mo}, \text{Ti}$) nanosheets to generate 2D MS_2/S composites for advanced high-energy batteries.

University of Houston, Houston, TX

Investigate a new class of high-energy electrode materials, organic insertion materials, while employing solid-state electrolytes.

Sincerely,

Tien Q. Duong

Tien Q. Duong
Manager, Advanced Battery Materials Research (BMR) Program
Electrification R&D
Battery R&D
Vehicle Technologies Office
Energy Efficiency and Renewable Energy
U.S. Department of Energy

TASK 1 – ADVANCED ELECTRODE ARCHITECTURES

Summary and Highlights

Energy density is a critical characterization parameter for batteries for electric vehicles (EVs), as there is only so much room for the battery and the vehicle needs to travel nearly 300 miles. The U.S. Department of Energy (DOE) targets are 500 Wh/L on a system basis and 750 Wh/L on a cell basis. Not only must the batteries have high energy density, they need to do so and still deliver 1000 Wh/L for 30 seconds at 80% of its accessible capacity. To meet these requirements not only entails finding new, high-energy-density electrochemical couples, but also highly efficient electrode structures that minimize inactive material content, allow for expansion and contraction for several thousand cycles, and allow full access to the active materials by the electrolyte during pulse discharges. In that vein, the DOE Vehicle Technologies Office (VTO) supports three projects in the Advanced Battery Materials Research (BMR) Program under Advanced Electrode Architectures: (1) Higher Energy Density via Modifications to the Inactive Components at Lawrence Berkeley National Laboratory (LBNL), (2) Electrode Architecture – Assembly of Battery Materials and Electrodes at Hydro-Quebec (HQ), and (3) Prelithiation of Silicon Anode for High-Energy Li-Ion Batteries at Stanford University.

The three tasks take three distinct approaches to improving energy density. The first task attempts to increase energy density by making thicker electrodes and reducing the amount of inactive components per cell. The second task attempts to improve the energy density of the anode through different processing conditions and binders of silicon composites. The third task attempts to increase the energy density of Li-ion cells with high capacity, prelithiated Si-based active materials.

The problem being addressed with the first approach is that as electrode thickness increases, the drying time can decrease, which allows additional time for segregation of electrode components. For a thicker electrode, winding leads to more hoop stress on the outer portion of the laminate. Both problems can result in delamination of the laminate from the current collector. The other problem with thicker electrodes is that they tend to not cycle as well as thinner electrodes and thus reach the end-of-life condition sooner, delivering fewer cycles.

The problem being addressed by the second approach is that silicon expands three times its original size when fully lithiated. To lessen the stress of this event, composites of silicon are often used. These researchers hope to discover the proper processing conditions and binders to allow a silicon material to be substituted into a Li-ion cell.

The problem being addressed by the third approach is that silicon does not immediately form a passivating coating during the first charge of lithium ions. This results in an imbalance of lithium in the two electrodes, reducing the cyclable capacity of the cell.

Highlight. Cui's Group at Stanford is developing a means of pre-passivating silicon anodes using lithiated silicon and the fluoropolymer CYTOP.

Task 1.1 – Higher Energy Density via Inactive Components and Processing Conditions (Vincent Battaglia, Lawrence Berkeley National Laboratory)

Project Objective. Thicker electrodes with small levels of inactive components that can still deliver most of their energy at C-rates of C/3 should result in batteries of higher energy density. In turn, higher energy density should translate to more miles per charge or smaller, less expensive batteries. Unfortunately, the limit to making thicker electrodes is not based on power capability but on mechanical capability, that is, the thicker electrodes delaminate from the current collector during calendaring or slicing. The objective of this research is to produce a high-energy-density electrode with typical Li-ion components that does not easily delaminate and still meets the EV power requirements through changes to the components and concomitant changes to processing conditions.

Project Impact. Today's batteries cost too much on a per kWh basis and have too low of an energy density to allow cars to be driven over 300 miles on a single charge. This research simultaneously addresses both problems. By developing thicker, higher-energy-density electrodes, the fraction of cost relegated to inactive components is reduced and the amount of energy that can be introduced to a small volume can be increased. Macroscopic modeling suggests that this could have as much as a 20% impact on both numbers.

Out-Year Goals. In outgoing years, the project will make changes to the binder molecular weight, conductive additive, and size distribution of the active material and also whatever changes are necessitated by electrode processing conditions to increase the energy density while maintaining power capability. Changes in processing conditions can include the time of mixing, rate of casting, temperature of slurry during casting, drying conditions, and hot calendaring. Chemical modifications may include multiple binder molecular weights and changes in the conductive additive size and shape.

Collaborations. The project collaborates with several groups: Zaghbi's Group (HQ) for materials and cell testing; Wheeler's Group at Brigham Young University (BYU) for modeling analysis; Liu's group on polymer properties; Arkema for binders; and a commercial cathode material supplier.

Milestones

1. Fabricate "thick" laminates of NCM and establish the effect of calendaring at different temperatures. (Q1 – Completed December 2017)
2. Determine to what extent electrode performance can be improved through use of an active material of two particle size distributions. (Q2 – Delayed)
3. Determine the degree to which several updates in materials and processing are affecting cyclability. (Q3 – Delayed)
4. *Go/No-Go:* Determine if a binder of a mixture of molecular weights is worth pursuing to achieve thicker electrodes based on ease of processing and level of performance. If no, pursue a path of a single molecular weight binder. (Q4)

Progress Report

The second quarter milestone is delayed due to complexities in re-establishing a nondisclosure agreement with the material supplier. Those issues have been worked through, and efforts in this area will soon continue. The third quarter milestone is delayed, as the work in understanding the effect of material changes on electrode performance continues.

This quarter, work focused on the impact a surface layer has on cell performance and the ability to assess cell performance using a pouch cell with a reference electrode. As described in one of the project's first reports on fabrication of thick electrodes, if one follows typical procedures for making low- and mid-loading electrodes in the making of high-loading electrodes, a film of carbon and binder forms on the surface of the electrode. This quarter, the project investigated the impact this film has on cell performance.

Figure 1 shows a scanning electron microscopy (SEM) of a cross-sectioned electrode made using typical electrode fabrication procedures. A film can clearly be seen on the electrode surface. Energy-dispersive X-ray spectroscopy (EDX) indicates that this film consists almost entirely of carbon black and PVDF binder. This laminate was tested in a coin cell in three ways: (1) as is, (2) with the film removed from half of the surface, and (3) with the entire film removed. A fourth electrode of similar loading was also produced using the same electrode formulation, but modifying the processing conditions to prevent film formation.



Figure 1. Cross section of a dry electrode.

Figure 2 shows the 30-second pulse discharge resistance for the four different cells versus depth of discharge. The electrode with the surface film shows twice as much resistance as the electrode where the film was removed. The electrode with half of the film removed shows a resistance that is halfway between the two. The electrode prepared to have no surface film to begin with has nearly as low a resistance as the cell with the film removed. It is possible that this film consists of excess binder and carbon black. Next quarter, the project will attempt to measure the fraction of carbon black and polymer in the surface film and to fabricate a laminate without this excess. It will be interesting to see if electrodes can be produced that perform as well without the excess, and whether this might prove to be a method for determining the minimum amount of binder and conductive carbon one requires for making a thick electrode.

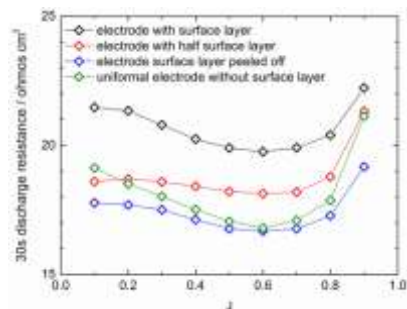


Figure 2. 30-sec resistance of four cells: with surface film, half surface film, surface film removed, and no film at all.

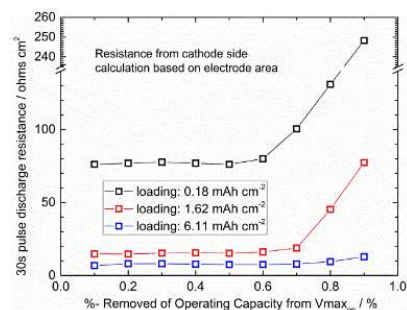


Figure 3. Resistance for three loadings.

Figure 3 is a plot of cell resistance of the cathode versus depth of discharge for three cells with reference electrodes. The data show that area specific resistance (ASR) drops with electrode thickness. If the resistance is normalized for cathode particle area, the order reverses, but the resistance is more closely bunched together. This suggests that the resistance of electrodes is dominated by the charge transfer resistance of the active material. This project intends to use similar cells to quantify cell failure modes of cycled thick electrodes.

Task 1.2 – Prelithiation of Silicon Anode for High-Energy Lithium Ion (Yi Cui, Stanford University)

Project Objective. Prelithiation of high-capacity electrode materials such as silicon is an important means to enable those materials in high-energy batteries. This study pursues two main directions: (1) developing facile and practical methods to increase first-cycle Coulombic efficiency (CE) of Li-ion batteries, and (2) synthesizing fully lithiated silicon and other lithium compounds for pre-storing lithium.

Project Impact. The first-cycle CE of Li-ion batteries will be increased dramatically via prelithiation. Prelithiation of high-capacity electrode materials will enable those materials in next generation, high-energy-density batteries. This project's success will make high-energy-density Li-ion batteries for EVs.

Out-Year Goals. Compounds containing a large quantity of lithium will be synthesized for pre-storing lithium ions inside batteries. First-cycle CE will be improved and optimized (over 95%) by prelithiation with the synthesized Li-rich compounds. The stability of prelithiation reagents in the air conditions and in solvents will be improved.

Collaborations. This project collaborates with BMR PIs, with Dr. Michael Toney at Stanford Linear Accelerator Center (SLAC) on *in situ* X-ray, and with Prof. Nix at Stanford University on mechanics.

Milestones

1. Synthesize Li_xGe nanoparticles and $\text{Li}_x\text{Ge-Li}_2\text{O}$ composites for anode prelithiation with improved air-stability. (January 15, 2017 – Complete)
2. Synthesize Li_xSn nanoparticles and $\text{Li}_x\text{Sn-Li}_2\text{O}$ composites for anode prelithiation with improved air stability. (April 15, 2017 – Complete)
3. Synthesize LiF-coated Li_xSi nanoparticles with improved stability in ambient air and polar solvents. (July 2017 – Complete)

Progress Report

In previous work, the team demonstrated that metallurgically synthesized Li_xSi nanoparticles (NPs) can serve as a high-capacity prelithiation reagent to effectively increase the first-cycle CE of anode materials. However, Li_xSi NPs are neither stable in air nor in standard slurry solvent N-methyl-2-pyrrolidinone (NMP). With low solubility in both water (0.134 g/100 mL at 25°C) and organic solvents, a LiF coating could be applicable to Li_xSi NPs to improve compatibility with industrial electrode fabrication processes. This project finds that the fluoropolymer CYTOP gradually decomposes and releases pure F_2 gas upon heating, which reacts with Li_xSi NPs to form a uniform and compact LiF coating.

The transmission electron microscopy (TEM) image in Figure 4a indicates a uniform and continuous coating with a thickness of 20 nm. Before an LiF coating, the synthesized Li_xSi NPs consist of crystalline $\text{Li}_{21}\text{Si}_5$ (PDF# 00-018-747) and intrinsic Li_2O (PDF# 04-001-8930). After coating, a new peak at 38.7° is indexed as LiF (PDF# 00-004-0857), confirming the crystalline nature of the coating (Figure 4b). The reaction between Li_xSi and NMP as well as the improved stability after LiF coating was studied by gas chromatography (GC). After soaking in NMP for 6 h, 20 mg Li_xSi NPs reacted with NMP vigorously to release 18145 ppm H_2 and 938 ppm CH_4 . With LiF coating, the reaction with NMP is considerably suppressed. The surface of the NPs is clean, and the core-shell structure remains almost unchanged. The GC signal of H_2 decreases to only 15% of that of uncoated Li_xSi , and no signal of CH_4 is detected.

To confirm stability of LiF-coated Li_xSi NPs in the slurry, LiF-coated Li_xSi NPs were mixed with Super P and PVDF (65:20:15 by weight) in 1,3-dioxolane (DOL) or NMP to form a slurry that was then drop cast on copper foil. Previously, the project found that bare Li_xSi NPs are stable in DOL, but react vigorously with NMP to leave almost no extraction capacity (dashed lines, Figure 4c). Consistently, LiF-coated Li_xSi NPs show a high capacity of 2879 mAh/g using DOL as the slurry

solvent, based on the mass of silicon in the cell. Replacing DOL with NMP, only a small fraction of capacity (~ 13%) is sacrificed (Figure 4c). Because of limited solubility of LiF in water, LiF coating further improves stability of Li_xSi NPs in humid air. After being stored in humid air (~ 40% RH) for 1 day, the capacity of LiF-coated Li_xSi NPs is 2328.9 mAh/g, showing a high capacity retention of 85.9% (Figure 4d). The capacity decay is slow, compared with Li_2O -coated Li_xSi NPs, as shown Figure 4d-inset. Without LiF coating, Li_xSi primarily reacts with O_2 and H_2O to form LiOH (PDF#00–032-0564) after exposure to humid air. In contrast, no peaks belonging to LiOH are present in the X-ray diffraction (XRD) pattern of LiF-coated Li_xSi NPs exposed to the same conditions. The crystalline and dense LiF coating eliminates side reactions in NMP and humid air, increasing feasibility of incorporating LiF-coated Li_xSi NPs in the commercial electrodes fabrication process.

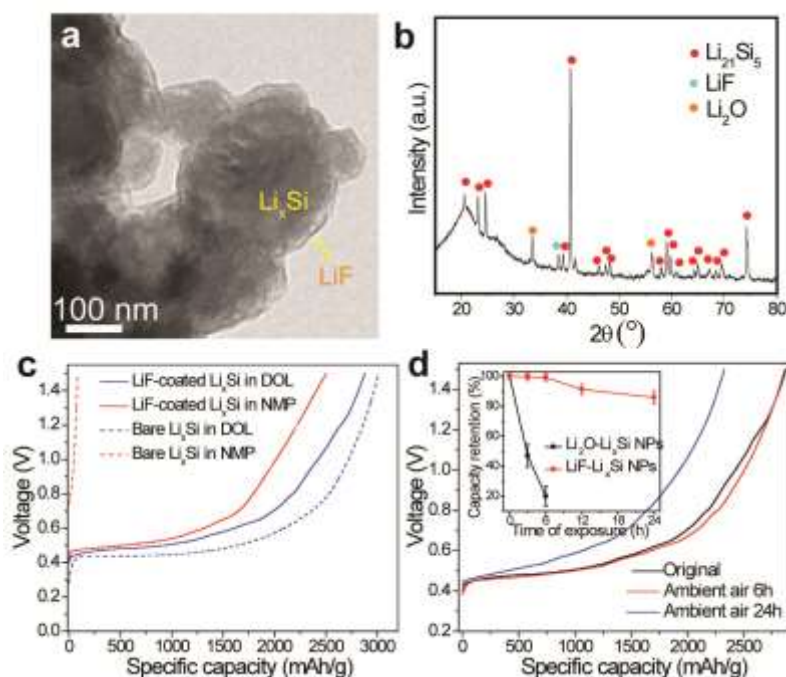


Figure 4. Characterization and stability of LiF-coated Li_xSi nanoparticles (NPs). (a) Transmission electron microscopy image and (b) X-ray diffraction pattern of LiF-coated Li_xSi NPs. (c) First-cycle delithiation capacities of LiF-coated Li_xSi NPs (solid line) and bare Li_xSi NPs (dashed line) using different solvents to form the slurry. (d) The extraction capacities of LiF-coated Li_xSi NPs exposed to ambient air (~ 40% RH) with varying durations. The inset shows the trend of capacity decay of LiF-coated Li_xSi NPs (red) and Li_2O -coated Li_xSi NPs (black) with varying durations.

Patents/Publications/Presentations

Publication

- Zhao, Jie, and Lei Liao, Feifei Shi, Ting Lei, Guangxu Chen, Allen Pei, Jie Sun, Kai Yan, Guangmin Zhou, Jin Xie, Chong Liu, Yuzhang Li, Zheng Liang, Zhenan Bao, and Yi Cui.* “Surface Fluorination of Reactive Battery Anode Materials for Enhanced Stability.” *JACS*. Accepted.

Task 1.3 – Electrode Architecture-Assembly of Battery Materials and Electrodes (Karim Zaghib, Hydro-Quebec)

Project Objective. The project goal is to develop an electrode architecture based on nano-Si materials and to design a full cell having high energy density and long cycle life. To achieve the objective, this project investigates the structure of nano-Si materials that provide acceptable volume change to achieve long cycle life, while still maintaining the high-capacity performance of silicon. The project scope includes control of the particle size distribution of nano-Si materials, crystallinity, silicon composition, and the surface chemistry of nano-Si materials. The focus is to develop electrode formulations and electrode architectures based on nano-Si materials, which require optimized nano-Si/C composites and functional binders, as well as a controlled pore distribution in the electrode and the related process conditions to fabricate the electrode.

Project Impact. Silicon is a promising alternative anode material with a capacity of ~4200 mAh/g, which is more than a magnitude higher than that of graphite. However, many challenges remain unresolved, inhibiting commercialization of silicon; this is mainly due to the large volume variations of silicon during charge/discharge cycles that result in pulverization of the particle and poor cycling stability. Successful development of highly reversible silicon electrodes with acceptable cost will lead to higher-energy-density and lower-cost batteries that are in high demand, especially for expanding the market penetration for EVs.

Approach. The project approach will encompass the following:

- Explore synthesis methods for low-cost, nano-Si materials with controlled purity and particle morphology.
- Develop an appropriate silicon anode architecture that can tolerate volumetric expansion and provide an acceptable cycle life with low capacity fade.
- Identify a binder and electrode composition by investigating parameters that define the electrode structure, such as porosity, loading, and electrode density. The optimized Si-anode will be matched with a high-voltage NMC cathode to fabricate large format Li-ion cells.
- Use *in situ* techniques such as SEM and impedance spectroscopy to monitor the particle and electrode environment changes during cycling.
- Achieve reduced cost by moving from silicon (> \$50/kg) to metallurgical silicon, projected to be \$3~\$5/kg.

Out-Year Goals. Conduct failure mode analysis of nano-Si anodes before and after cycling. Use dual-beam (electron + ion) microscopy and TOF-SIMS (time-of-flight secondary ion mass spectrometry) techniques to analyze residual lithium contents in the structure of delithiated anodes. This analysis will help in understanding the failure mode of the anode and help guide efforts to improve particle morphology and electrode architecture.

Collaborations. This project collaborates with BMR PIs: V. Battaglia and G. Liu (LBNL), C. Wong and Jason Zhang (Pacific Northwest National Laboratory, PNNL), and J. Goodenough (University of Texas, UT).

Milestones

1. Failure mode analysis of the nano-Si/C composite electrode before and after cycling. Improve the structure of the nano-Si/C composite based on the result of failure mode analysis. (Q1 – Completed December 2016)
2. Explore new binder system with nano-Si/C composite; make composite with electrospinning process. (Complete)
3. Optimize electrode composition with nano-Si/C composite; evaluate electrochemical performance. (Complete)
4. Verify performance in pouch-type full cell. *Deliverable:* 20g of nano-Si/C composite powder. (September 2017)

Progress Report

This quarter, efforts focused on improving the electrochemical performance of a nano-Si/C composite by producing the material using electrospraying. Previously, capacity and cyclability were improved by heat treatment. That work resulted in an electrode of nano-Si/C composite secondary particles held together with a polyimide binder.

A syringe was charged with slurry at a high electric potential of 20 kV; the distance from the grounded electrode plate was set at 10 cm. Powders were formed via a bath 5-mm deep of deionized water and an injection speed of 50 $\mu\text{l}/\text{min}$. The samples were filtered and heat treated at 600°C for 3 h in a N₂ flow furnace. As seen in Figure 5a, the powder is composed of two different shapes: small and flaky (< 100 μm) and larger and spherical (< 400 μm). The electrochemical performance was tested in a coin-type half-cell, and the result is shown in Figure 5b. The loading of total anode was around 1.05 mg/cm², and the electrode density was around 1.0g/cc. Water-based acrylic resin was used as a binder with no incidence of gas generation. The measured capacity was around 3500 mAh/g at C/24, and the first-cycle efficiency was 76%. The cycle life is being tested.

The anode thickness change was monitored by electrochemical dilatometer, Figure 6. Thickness increased after the solid electrolyte interphase (SEI) formation step and finished at 3.7 μm at the end of the first discharge. This thickness increase is equivalent to 12% of the fresh electrode. For the following charge step, thickness decreased by about 2.7 μm , and the electrode was

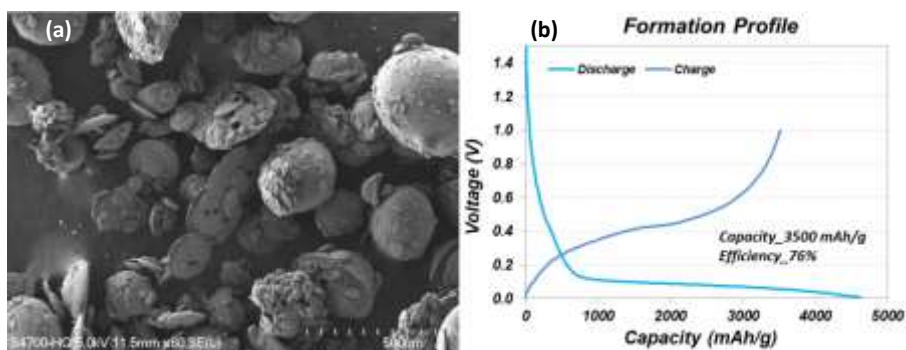


Figure 5. (a) Scanning electron microscopy image of nano-Si/C composite made by electrospray process and (b) first discharge/charge voltage profile of this.

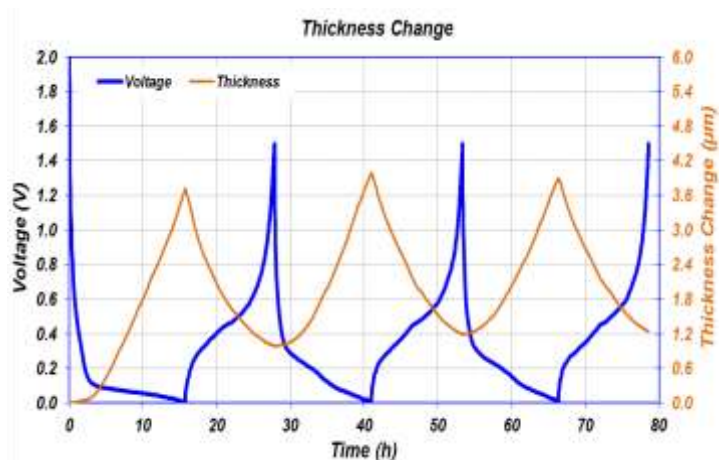


Figure 6. Cell thickness monitoring during cycling with C/24 rate between 1.5 V and 0.005 V at room temperature.

1 μm thicker than that of the fresh electrode due to the irreversible changes that occurred during the first cycle.

Going forward, the focus will be on understanding variation of thickness during cycling and modifying the binder and the electrolyte to address it.

Deliverable. SBR/CMC binder materials and 1.5 m of anode electrode made by water-based CMC/SBR binder to LBNL.

Task 2 – Silicon Anode Research

Summary and Highlights

Most Li-ion batteries used in state-of-the-art EVs contain graphite as their anode material. Limited capacity of graphite (LiC_6 , 372 mAh/g) is one barrier that prevents the long-range operation of EVs required by the EV Everywhere Grand Challenge proposed by the DOE Office of Energy Efficiency & Renewable Energy (EERE). In this regard, silicon is one of the most promising candidates as an alternative anode for Li-ion battery applications. Silicon is environmentally benign and ubiquitous. The theoretical specific capacity of silicon is 4212 mAh/g ($\text{Li}_{21}\text{Si}_5$), which is 10 times greater than the specific capacity of graphite. However, the high specific capacity of silicon is associated with large volume changes (more than 300 percent) when alloyed with lithium. These extreme volume changes can cause severe cracking and disintegration of the electrode and can lead to significant capacity loss.

Significant scientific research has been conducted to circumvent the deterioration of Si-based anode materials during cycling. Various strategies, such as reduction of particle size, generation of active/inactive composites, fabrication of Si-based thin films, use of alternative binders, and synthesis of one-dimensional silicon nanostructures, have been implemented by several research groups. Fundamental mechanistic research also has been performed to better understand the electrochemical lithiation and delithiation processes during cycling in terms of crystal structure, phase transitions, morphological changes, and reaction kinetics. Although significant progress has been made on developing Si-based anodes, many obstacles still prevent their practical application. Long-term cycling stability remains the foremost challenge for Si-based anode, especially for the high loading electrode ($> 3\text{mAh/cm}^2$) required for many practical applications. The cyclability of full cells using Si-based anodes is also complicated by multiple factors, such as diffusion-induced stress and fracture, loss of electrical contact among silicon particles and between silicon and current collector, and the breakdown of SEI layers during volume expansion/contraction processes. The design and engineering of a full cell with a Si-based anode still needs to be optimized. Critical research remaining in this area includes, but is not limited to, the following:

- Low-cost manufacturing processes must be found to produce nano-structured silicon with the desired properties.
- The effects of SEI formation and stability on the cyclability of Si-based anodes need to be further investigated. Electrolytes and additives that can produce a stable SEI layer need to be developed.
- A better binder and a conductive matrix need to be developed. They should provide flexible but stable electrical contacts among silicon particles and between particles and the current collector under repeated volume changes during charge/discharge processes.
- The performances of full cells using Si-based anode need to be investigated and optimized.

The main goal is to have a fundamental understanding on the failure mechanism on Si-based anode and improve its long-term stability, especially for thick electrode operated at full-cell conditions. Success of this project will enable Li-ion batteries with a specific energy of $> 350\text{ Wh/kg}$ (in cell level), 1000 deep-discharge cycles, 15-year calendar life, and less than 20% capacity fade over a 10-year period to meet the goal of the EV Everywhere Grand Challenge.

Highlight. The PNNL group developed a low-temperature (210°C) thermic reduction method to prepare porous silicon with a specific capacity of $\sim 2100\text{ mAh g}^{-1}$ and a capacity retention of $\sim 80\%$ after 200 cycles.

Task 2.1 –High-Capacity and Long Cycle Life Silicon Carbon Composite Materials and Electrodes (Gao Liu, Lawrence Berkeley National Laboratory)

Project Objective. This project will synthesize Si/C anode composite materials at 1,000 mAh/g capacity at a cost less than \$10/kg and fabricate a long-cycle-life electrode similar to a graphite electrode for high-energy-density Li-ion batteries.

Project Impact. Low energy density and limited lifetime are two major drawbacks of the automobile Li-ion batteries for EV and plug-in hybrid electric vehicle (PHEV) applications. The project will develop high-capacity and long-life Si/C composite anodes to prolong battery cycling and storage lifetime, and to provide an in-depth understanding of silicon electrode design strategies to stabilize silicon material volume change and to prevent surface side reactions. This research effort will generate new intellectual properties based on the fundamental discovery of novel materials and new synthesis processes, and will bridge the research and development (R&D) gaps between the fundamental research and the applied materials discovery, to pave the way for the successful commercialization of silicon materials in the United States.

Approach. This work combines novel materials design and innovative synthesis process to synthesize mechanically robust and dimensionally stable Si/C composite materials. In addition, it will use low-cost Si/C precursor materials and a scalable process to generate low-cost Si/C product.

Out-Year Goals. The work progresses toward study of the physical and chemical properties and of electrochemical properties of the low-cost precursor materials. Novel synthesis strategy will be developed and used to fabricate materials to tailor the morphology, structure, composite component, and electrochemical properties of the Si/C composite materials. The morphologic and structural features and electrochemical properties will be characterized for the as-prepared Si/C composited with functional binder during electrochemical testing. The goal is to achieve a high-capacity, long-life Li-ion battery using this Si/C composite anode.

Collaborations. This project is a single investigator project. However, the proposed work requires extensive collaboration with DOE user facilities at national laboratories and industries. These include the National Center for Electron Microscopy (NCEM) and the Advanced Light Sources (ALS) program at LBNL, *in situ* electrochemical TEM facilities at the Environmental Molecular Sciences Laboratory (EMSL), the national user facility at PNNL, HQ's Research Institute (IREQ), General Motors (GM) R&D Center, and LBNL BMR laboratories. The project will also involve collaboration with BMR participants at LBNL, including Dr. Marca Doeff's group and Dr. Vince Battaglia's group.

Milestones

1. Set up the silicon materials and carbon precursors library, and finish characterizing the starting materials. (Q1 – Completed December 2016)
2. Conduct preliminary tests to generate Si/C composite particles with the spray methods. (Q2 – Completed March 2017)
3. Electron microscopy image analyses of the Si/C samples, and development of functional binders based on Si/C composite structures. (Q3 – Completed June 2017)
4. Electrochemical analysis to demonstrate > 1000 mAh/g and > 3 mAh/cm² of the Si/C composite electrodes. (Q4 – September 2017; Initiated July 1, 2017)

Progress Report

The coating on Si-based materials can potentially decrease the side reactions, improving CE. This can lead to significantly improved cycling performance of the silicon materials. A carbon-based coating using poly (1-pyrenemethyl methacrylate) (PPy) precursor is developed, as shown in Figure 7. One of the major limitations with carbon precursor coating and sintering for Si-based materials is the relatively low temperature (below 800°C) required to carbonize the precursors. The low-temperature sintering leads to incomplete carbonization of the carbon precursor, which tends to induce a high degree of side reactions during battery cycling. The PPy polymer forms layered structure between the pyrene moieties, due to the π - π stacking interaction of the pyrene units. This preferred layered-structure of PPy polymer in the pre-carbonized structure results in much improved carbonization and graphitization structure at a lower sintering temperature. By sintering PPy polymer on SiO material at a low-temperature range between 400°C and 600°C, a conformal carbon coating is formed on the surface of SiO materials, as shown in Figure 8.

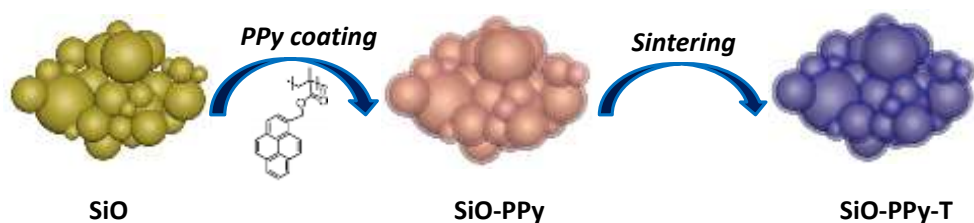


Figure 7. Schematic illustrating the synthesis process of the SiO-PPy composite material.

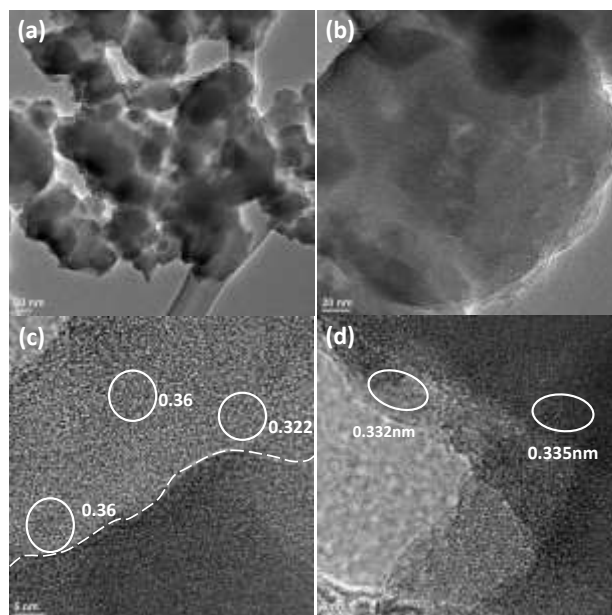


Figure 8. Transmission electron microscopy (TEM) images of the SiO-PPy composite sintering at 500°C. (a, b) Low magnification TEM images of the SiO-PPy-500 composites. (c, d) High-resolution TEM image displaying details of the SiO submicron particles coated with sintered PPy.

Patents/Publications/Presentations

Publication

- Ling, Min, and Liang Zhang, Tianyue Zheng, Jun Feng, Jinghua Guo, Liqiang Mai, and Gao Liu. “Nucleophilic Substitution between Polysulfides and Binders Unexpectedly Stabilizing Lithium Sulfur Battery.” *Nano Energy* 38 (2017): 82–90.

Task 2.2 – Stable Operation of Silicon-Based Anode for Lithium-Ion Batteries (Ji-Guang Zhang and Jun Liu, Pacific Northwest National Laboratory; Prashant Kumta, University of Pittsburgh)

Project Objective. The project objective is to develop a low-cost approach to prepare high-capacity Si-carbon composite anodes with good cycle stability and rate capability to replace graphite anode used in Li-ion batteries. In one approach, low-cost Si-graphite-carbon composite will be developed to improve the long-term cycling performance while maintaining a reasonably high capacity. Si-based secondary particles with a nano-Si content of ~10 to 15 wt% will be embedded in the matrix of active graphite and inactive conductive carbon materials. Controlled void space will be pre-created to accommodate the volume change of silicon. A layer of highly graphitized carbon coating on the outside will be developed to minimize the contact between silicon and electrolyte and hence minimize the electrolyte decomposition. New electrolyte additives will be investigated to improve stability of the SEI layer. In another approach, nanoscale silicon and Li-ion conducting lithium oxide composites will be prepared by *in situ* chemical reduction methods. The stability of Si-based anode will be improved by generating the desired nanocomposites containing nanostructured amorphous or nanocrystalline silicon as well as amorphous or crystalline lithium oxide (Si+Li₂O) by the direct chemical reduction of a mixture and variety of silicon sub oxides (SiO and SiO_x) and/or dioxides. Different synthesis approaches comprising direct chemical reduction using solution, solid-state, and liquid-vapor phase methods will be utilized to generate the Si+Li₂O nanocomposites. The electrode structures will be modified to enable high utilization of thick electrode.

Project Impact. Si-based anodes have much larger specific capacities compared with conventional graphite anodes. However, the cyclability of Si-based anodes is limited because of the large volume expansion that is characteristic of these anodes. This work will develop a low-cost approach to extend the cycle life of high-capacity, Si-based anodes. The success of this work will further increase the energy density of Li-ion batteries and accelerate market acceptance of EVs, especially for PHEVs required by the EV Everywhere Grand Challenge.

Out-Year Goals. The main goal of the proposed work is to enable Li-ion batteries with a specific energy of > 200 Wh/kg (in cell level for PHEVs), 5000 deep-discharge cycles, 15-year calendar life, improved abuse tolerance, and less than 20% capacity fade over a 10-year period.

Collaborations. This project collaborates with Xingcheng Xiao (GM): *In situ* measurement of thickness swelling silicon anode.

Milestones

1. Synthesize micron-sized silicon with the desired porosity and *in situ* grown graphene coating. (Q1 – Completed December 2016)
2. Synthesize low-cost Si-based nanocomposite anode materials using high-energy mechanical milling (HEMM) and other economical template derived methods. (Q2 – Completed March 2017)
3. Identify new electrolyte additive to improve the stable operation of Si-based anode. (Q3 – Completed June 2017)
4. Fabricate and characterize Si-based anode with desired electrode capacity (~ 3 mAh/cm²). (Q4 – Initiated June 2017)

Progress Report

The third milestone was completed this quarter. Electrolyte and binders were optimized to improve the performance of nano Si-based anode. High mass loading electrodes were prepared with different binder compositions. The silicon NP with conventional poly(acrylic acid) (PAA) binder was used as a control electrode. The anode with 20 wt% PAA delivered stable cyclic performance for only ~40-50 cycles. The mixed PAA and carboxymethyl cellulose (CMC) binder (15:5) leads to relatively slower capacity fade. In contrast, the anode consisting of silicon nano powders, 20 wt% PAA, and 2 wt% sodium calcinate alginate (SCA) binders was able to deliver ~1.43 mAh/cm² after 140 cycles. The mass loading of the total electrode was 1.17 mg/cm² corresponding to the areal capacity of ~2.3 mAh/cm². In addition, porous silicon (P-Si) was synthesized by a low-temperature (210°C) aluminothermic reduction of porous silica (3-5 μm) in the presence of eutectic salt mixture of AlCl₃ and ZnCl₂ (mp. ~116°C). The residual silica was removed by hydrofluoric (HF) etching. P-Si exhibited a specific capacity of ~2100 mAh g⁻¹ at the current density of 1.2 A/g (Figure 10) and a capacity retention of ~80% after 200 cycles. The areal capacity of the electrodes was ~1 mAh/cm².

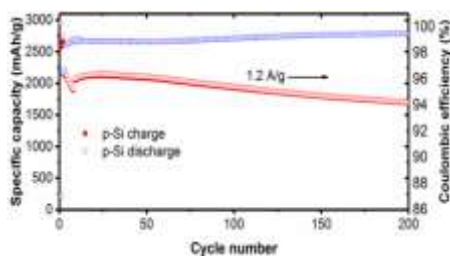


Figure 10. The cycling performance and Coulombic efficiency of the porous silicon obtained from aluminum reduction.

Additionally, during this quarter, high-energy mechano chemical reduction (HEMR) of silicon monoxide (SiO) was carried out for 20 h, 40 h, and 60 h using a stoichiometric amount of inorganic reducing agent. The formation of silicon from SiO after 20 h and 60 h of HEMR has been confirmed from the XRD analysis. Additionally, peaks of silicene/siloxene are also observed due to partial oxidation of the products during HEMR process. The composite material obtained after 40 h of HEMR was heat treated (~600°C) for 6 h to achieve complete reduction of SiO to form silicon without increasing the crystallinity of silicon or crystallization of the oxide matrix. Subsequently, the undesired oxide matrix was dissolved in HCl to obtain pure nano-Si. The nano-Si was slurry casted (80% active material, 10% binder, 10% conductive C) on copper foils and tested in Li/Li⁺ coin cells as an anode material. The loading density of nano-Si in the electrodes was ~3.5-4.0 mg/cm².

The electrodes made from the nano-Si generated show a first-cycle discharge and charge capacity of ~2430 mAh/g and ~1870 mAh/g, respectively, with a first-cycle irreversible (FIR) loss of ~30-40% (Figure 11) at a charge/discharge current rate of ~100 mA/g. The obtained nano-Si also shows an excellent capacity retention with a stable capacity of ~1050 mAh/g at the end of 80 cycles at a charge/discharge rate of 500 mA/g (Figure 10). However, there is an initial capacity loss in the first 10 cycles, which may be caused by delamination of the nano-Si particles from the binder and the electrodes. Efforts are under way to embed the nano-Si in carbon nanofiber matrix (CNF) and/or graphite to prevent the initial capacity fade. Furthermore, in-depth characterization of nano-Si and nano-Si/CNF such as Raman spectroscopy, XRD, SEM, and TEM at various processing steps are planned to be executed to study evolution of the phases and nanostructures.

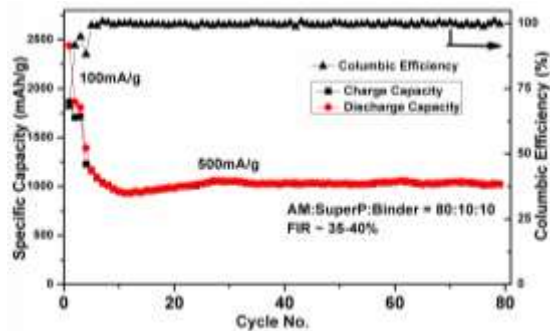


Figure 11. Long-term cycling data of nano-Si obtained from high-energy mechano chemical reduction using silicide reductant, tested at 0.1A/g for initial 3 cycles followed by 0.5A/g in Li/Li⁺ system.

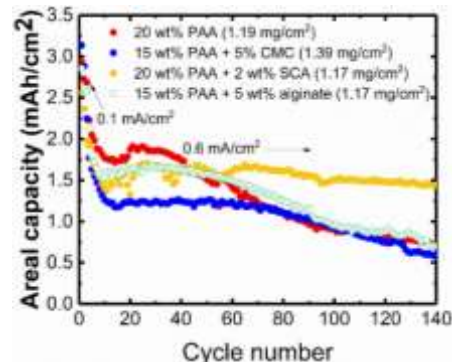


Figure 9. Cycling stability of anode prepared using silicon nano powder and different binders.

Patents/Publications/Presentations

Publications

- Gattu, B., and R. Epur, P. H. Jampani, R. Kuruba, M. K. Datta, and P. N. Kumta. “Silicon-Carbon Core-Shell (C@Si@C) Hollow Nanotubular Configuration – High Performance Lithium-Ion Anodes.” *Journal of Physical Chemistry - C* 121, no. 18 (2017): 9662–9671.
- Gattu, B., and P. H. Jampani, M. K. Datta, and P. N. Kumta. “Water-Soluble Template Derived Nanoscale Silicon Nano-Flakes and Nano-Rods Morphologies: Stable Architectures for Lithium Ion Anodes.” *Nanoresearch* (2017). Accepted.
- Gattu, B., and R. Epur, P. Shanti, P. H. Jampani, R. Kuruba, M. K. Datta, A. Manivannan, and P. N. Kumta. “Pulsed Current Electrodeposition of Silicon Thin Film Anodes for Lithium-Ion Battery Applications.” *Inorganics* 5, no. 2 (2017): 27.

TASK 3 – HIGH-ENERGY-DENSITY CATHODES FOR ADVANCED LITHIUM-ION BATTERIES

Summary and Highlights

Development of high-energy-density, low-cost, thermally stable, and environmentally safe electrode materials is one of the key enablers for advanced batteries for transportation. High energy density is synonymous with reducing cost per unit weight or volume. Currently, one major technical barrier toward development of high-energy-density Li-ion batteries is the lack of robust, high-capacity cathodes. As an example, the most commonly used anode material for Li-ion batteries is graphitic carbon, which has a specific capacity of 372 mAh/g, while even the most advanced cathodes such as NMC or NCA have a maximum capacity of ~180 mAh/g. This indicates an immediate need to develop high-capacity (and high-voltage) cathodes that have stable reversible capacities > 250 mAh/g. High volumetric energy density is also critical for transportation application. Alternative high-capacity cathodes such as those based on conversion compounds, Li-S, and metal-air chemistries still have fundamental issues that need to be addressed. Among oxide cathodes, Li-excess NMC and other cation disorder compositions provide a practical route toward high capacity at high redox voltage. Successful demonstration of practical high-energy cathodes will enable devices that meet or exceed the DOE cell level targets of 400 Wh/kg and 750 Wh/L with a system-level cost target of \$125/kWh.

During the last decade, many high-voltage cathode chemistries were developed under the BATT (now BMR) program including Li-rich NMC and Ni-Mn spinels. Current efforts are directed toward new synthesis methods and modifications for high-capacity, Ni-rich NMC to improve their structural and oxidative stability at higher voltage [Zhang, PNNL; Doeff & Tong, LBNL; Wang, Brookhaven National Laboratory (BNL)]. Thackeray and Croy's effort at Argonne National Laboratory (ANL) is focused on synthesis of composite layered-layered (LL) and layered-spinel (LS) high-voltage cathodes including Co- and Ni-based spinel phases. Nanda's effort at Oak Ridge National Laboratory (ORNL) is directed toward synthesis and stabilization of Li-excess disordered cathodes based on nickel, copper, molybdenum, chromium, and manganese. Whittingham's efforts at State University of New York (SUNY) at Binghamton are directed at high volumetric energy density Sn/Li_xVOPO₄ full cells and performance optimization.

Highlights. The highlights for this quarter are as follows:

- **Task 3.1.** Synthesized and characterized NMC doped with 5% molybdenum to improve oxygen stability.
- **Task 3.2.** Optimized full cell of Sn_yFe/Li_xVOPO₄ electrochemical couple by improving the Li_xVOPO₄ cathode design.
- **Task 3.3.** Developed lithium phosphate (LPO) solid electrolyte coatings and thermal infusion technology to improve the structural integrity/stability of Ni-rich NMC cathode (LiNi_{0.76}Mn_{0.14}Co_{0.10}O₂).
- **Task 3.4.** Reported synthesis procedures for kinetic control of the structural ordering in NMC layered oxides utilizing combined *in situ/ex situ* synchrotron X-ray and neutron studies.
- **Task 3.5.** Reported electrochemical results for 0.33Li₂MnO₃•0.67LiMn_{0.365}Ni_{0.365}Co_{0.244}M_{0.02}O₂ cathode (versus lithium metal). M represents iron, zinc, and copper as a 2% substituent.
- **Task 3.6.** Reported transmission X-ray microscopy (TXM) (nickel X-ray absorption near-edge spectroscopy, or XANES, 3D mapping) analysis for 50% and 100% delithiated NMC-622 cathodes for studying nickel redox in bulk and at the surface.
- **Task 3.7.** Reported synthesis and electrochemical performance testing of series of Li-metal oxides, Li_{2-x-y}Ni_xTM_yO₂ (0 < x, y < 1), with transition metals (TMs, where TM = Mn, Ru, Sn, Mo, Nb, Ti, V).
- **Task 3.8.** Reported synthesis and characterization of composite Li₂MnO₃•LiMn_{1.5}Ni_{0.5}O₄ (spinel) cathodes using a sol-gel method.

Task 3.1 – Studies on High-Capacity Cathodes for Advanced Lithium-Ion Systems (Jagjit Nanda, Oak Ridge National Laboratory)

Project Objective. The project goal is to develop high-energy-density, Li-ion battery electrodes for EV and PHEV applications that meet and/or exceed DOE energy-density and life-cycle targets based on the USDRIVE/USABC roadmap. This project aims to mitigate technical barriers associated with high-voltage, high-capacity cathodes, including lithium-excess TM oxides and multi-lithium compositions such as $\text{Li}_2\text{M}_x^{\text{I}}\text{M}_{1-x}^{\text{II}}\text{O}_2$ and $\text{Li}_2\text{M}_x^{\text{I}}\text{M}_{1-x}^{\text{II}}\text{O}_3$, where M^{I} and M^{II} are TMs that could include manganese or cobalt. Emphasis is on developing new materials and synthesis methods to stabilize high-voltage cathodes to enable reversible capacities in the range of 250 mAh/g at an average voltage > 3.7 V versus Li/Li^+ . Major barriers to be addressed include the following: (i) preventing structural transformations during repeated electrochemical cycling, (ii) improving oxidative stability at higher redox potential by addressing interfacial stability, and (iii) reducing voltage hysteresis by facilitating reaction kinetics and mass transport at the materials level. Cathode synthesis and optimization will utilize advanced characterization and diagnostic methods to study cell and/or electrode degradation under abuse conditions. Techniques include electrochemical impedance spectroscopy (EIS), micro-Raman spectroscopy, mass spectrometry (MS), aberration corrected electron microscopy combined with electron energy loss spectroscopy (EELS), X-ray photoelectron spectroscopy (XPS), inductively coupled plasma atomic emission spectroscopy (ICP-AES), XANES, and X-ray and neutron diffraction.

Project Impact. Short-term and long-term deliverables are directed toward VTO Energy Storage 2015 and 2022 goals. Work involves advanced electrode couples that have cell-level energy density targets exceeding 400 Wh/kg and 700 Wh/l for 5000 cycles. Increasing energy density per unit mass or volume ultimately reduces the cost of battery packs consistent with the DOE 2022 EV Everywhere Grand Challenge goal of \$125/kWh.

Out-Year Goals. The goal is to develop cathode materials that have high capacity, use low-cost materials, and meet the DOE roadmap in terms of safety and cycle life. Over the last few years, the PI has worked to improve performance of high-capacity, high-voltage cathodes by utilizing new synthesis and interfacial approaches such as surface modification. The cathode chemistries include Li-Mn-rich NMC, multi-lithium TM oxides such as nickel-copper and manganese. In the coming years, the PI plans to improve anionic (oxidative) stability of cathode compositions and develop new synthesis approaches to create disordered cathodes with improved structural and electrochemical stability. The tasks also include working in collaboration with researchers at Stanford Synchrotron Research Laboratory (SSRL) and Advanced Photon Source (APS) at LBNL to understand local changes in morphology, microstructure, and chemical composition under *in situ* and *ex situ* conditions.

Collaborations. This project collaborates with Johanna Weker at SSRL/SLAC on X-ray imaging and XANES; Pengfei Yan and Chongmin Wang at PNNL on electron microscopy; Feng Wang at BNL on X-ray synchrotron spectroscopy and microscopy; and Jason Croy at ANL.

Milestones

1. Synthesize Ni-rich $\text{Li}_2\text{Cu}_x\text{Ni}_{1-x}\text{O}_2$ cathodes with $x = 0.2$ and 0.3 and evaluate their high-voltage capacity and oxidative stability (> 225 mAh/g, 25 cycles). (Q1 – Completed December 2016)
2. Complete *in situ* and *ex situ* X-ray, neutron, and spectroscopic studies of Ni-rich $\text{Li}_2\text{Cu}_x\text{Ni}_{1-x}\text{O}_2$ and related high-voltage cathode compositions. (Q2 – Completed March 2017)
3. Synthesis of one particular class and composition of disordered cathodes such as Cr-substituted Li_2MoO_3 and Mo-doped NMC. (Q3 – On track)
4. Complete structural and electrochemical performance analysis of disordered cathodes— Li_2MoO_3 and Cr-substituted Li_2MoO_3 and Mo-doped NMC. (Q4 – On track)

Progress Report

As described last quarter, Li_2MoO_3 cathodes exhibited stable reversible capacities ~ 160 mAh/g with an operating potential ~ 2.5 V versus Li/Li^+ . *In situ* MS studies indicated that the Li_2MoO_3 did not evolve oxygen even when charged to 4.8 V versus Li/Li^+ (results not shown). The excellent oxidative stability of Li_2MoO_3 makes it an ideal candidate to improve performance of traditional LiMO_2 ($M = \text{Ni}, \text{Mn}, \text{and/or Co}$) cathodes, which show severe capacity and voltage fade when charged beyond ~ 4.4 V versus Li/Li^+ . This quarter, a sol-gel synthesis route was developed to produce composite cathodes with the general formula $x\text{Li}_2\text{MoO}_3 \cdot (1-x)\text{LiNi}_{1/3}\text{Mn}_{1/3}\text{Co}_{1/3}\text{O}_2$ in which the Li_2MoO_3 acts as a structural stabilizing unit. This synthesis approach potentially allows for production of a wide range of compositions by appropriately tuning the TM ratio in the precursors. As a first step, the project tried lower molybdenum substitution ($\sim 5\%$) in NMC. If successful, the project will move toward Li_2MoO_3 -stabilized NMC composite cathodes. Figure 12a shows XRD patterns of the two end-member compositions (that is, Li_2MoO_3 and $\text{LiNi}_{1/3}\text{Mn}_{1/3}\text{Co}_{1/3}\text{O}_2$, referred to as NMC-111), and NMC-111 with 5% molybdenum doping. The structure of all three compounds is described by the $R\bar{3}m$ space group. For the NMC-111 compounds, the most intense reflections ($2\theta = 18$ and 44°) are shifted to higher 2θ values compared to Li_2MoO_3 due to the presence of smaller TMs (that is, the ionic radii of Ni^{3+} , Mn^{3+} , and Co^{3+} ranges from $0.54 - 0.64$ Å, whereas that of Mo^{4+} is 0.65 Å). The diffractogram for Mo-doped NMC-111 contained additional peaks at $2\theta = 30, 35, 53^\circ$, which are being investigated.

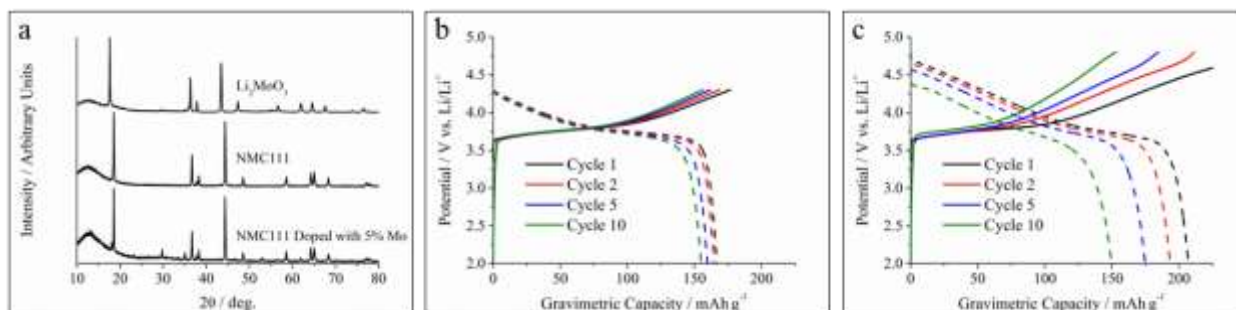


Figure 12. (a) X-ray diffraction patterns of Li_2MoO_3 , NMC-111, and NMC-111 doped with 5% molybdenum. Galvanostatic charge/discharge curves collected at 10 mA/g for undoped NMC-111 cathodes cycled between 2.0 – 4.3 V (b) and 2.0 – 4.8 V (c).

Preliminary coin cell experiments were conducted on a sol-gel derived NMC-111 cathode. As shown in Figure 12b, the NMC-111 delivered a stable reversible capacity of ~ 160 mAh/g with an operating potential ~ 3.9 V versus Li/Li^+ when cycled between 2.0 – 4.3 V. When the upper cutoff voltage was changed to 4.8 V versus Li/Li^+ , the initial capacity increased to 210 mAh/g; however, significant capacity and voltage fade occurred during cycling (see Figure 12b), presumably due to irreversible structural changes and oxygen evolution. Composite cathodes containing Li_2MoO_3 structure stabilizing units are expected to have significantly improved cycle life and oxidative stability. As such, electrochemical evaluation of a composite cathode containing 5% molybdenum doping is under way. Various cathode compositions with x ranging from 0.05 – 0.75 will be screened next quarter, and the best performing cathodes will be selected for detailed studies utilizing a suite of advanced characterization methods to correlate changes in electronic structure with electrochemical performance and oxygen stability.

Patents/Publications/Presentations

Publication

- Kan, Wang Hay, and Saravanan Kuppan, Lei Cheng, Marca Doeff, Jagjit Nanda, Ashfia Huq, and Guoying Chen. “Crystal Chemistry and Electrochemistry of $\text{Li}_x\text{Mn}_{1.5}\text{Ni}_{0.5}\text{O}_4$ Solid Solution Cathode Materials.” *Chemistry of Materials* (2017). doi: 10.1021/acs.chemmater.7b 01898.

Presentations

- Materials Research Society (MRS) Spring Meeting, Phoenix, Arizona (April 2017): “Meso and Micron Scale Chemical and Morphological Heterogeneities in High-Energy-Density Lithium-ion Electrodes.”
- DOE Annual Merit Review, Washington, D. C. (June 7, 2017): “High Capacity Multi-Lithium Oxide Cathodes and Oxygen Stability”; Jagjit Nanda.

Task 3.2 – High-Energy-Density Lithium Battery (Stanley Whittingham, SUNY Binghamton)

Project Objective. The project objective is to develop the anode and cathode materials for high-energy-density cells for use in PHEVs and EVs that offer substantially enhanced performance over current batteries used in PHEVs and with reduced cost. Specifically, the primary objectives are to:

- Increase the volumetric capacity of the anode by a factor of 1.5 over today’s carbons
 - Using a SnFeC composite conversion reaction anode.
- Increase the capacity of the cathode
 - Using a high-capacity conversion reaction cathode, CuF₂, and/or
 - Using a high-capacity 2 lithium intercalation reaction cathode, VOPO₄.
- Enable cells with an energy density exceeding 1 kWh/liter.

Project Impact. The volumetric energy density of today’s Li-ion batteries is limited primarily by the low volumetric capacity of the carbon anode. If the volume of the anode could be cut in half, and the capacity of the cathode to over 200 Ah/kg, then the cell energy density can be increased by over 50% to approach 1 kWh/liter (actual cell). This will increase the driving range of vehicles.

Moreover, smaller cells using lower cost manufacturing will lower the cost of tomorrow’s batteries.

Out-Year Goals. The long-term goal is to enable cells with an energy density of 1 kWh/liter. This will be accomplished by replacing both the present carbon used in Li-ion batteries with anodes that approach double the volumetric capacity of carbon, and the present intercalation cathodes with materials that significantly exceed 200 Ah/kg. By the end of this project, it is anticipated that cells will be available that can exceed the volumetric energy density of today’s Li-ion batteries by 50%.

Collaborations. The APS at ANL and, when available, the National Synchrotron Light Source II at BNL will be used to determine the phases formed in both *ex situ* and *operando* electrochemical cells. The University of Colorado at Boulder and University of Michigan will provide some of the electrolytes to be used.

Milestones

1. Determine cyclability of Sn/Li_xVOPO₄. (Q1 – Completed December 2016)
5. Demonstrate cyclability of Sn/CuF₂. (Q2, March 2017 – In progress)
6. Choose optimum couple. (Q3 – Complete)
7. Supply cells to the DOE. (Q4)

Progress Report

The project goal is to synthesize tin-based anodes that have 1.5 times the volumetric capacity of the present carbons, and conversion and intercalation cathodes with capacities over 200 Ah/kg.

Milestone 3 – “Choose Optimum Cell Couple for Optimization. The Cells will be Cycled until Failure.”

Major efforts this quarter were to compare and select the optimum cathode among suggested intercalation Li_xVOPO_4 cathode and conversion CuF_2 cathode to couple with the Sn_yFe anode for the full cell and to optimize performance. Due to challenges of Cu^+ transport in the electrolyte, which is detrimental to the cyclability of CuF_2 , and further improved performance of the Li_xVOPO_4 cathode, a $\text{Sn}_y\text{Fe}/\text{Li}_x\text{VOPO}_4$ electrochemical couple was selected as the focus of the full-cell study

Different lithiation methods have been verified that can incorporate lithium into either the Li_xVOPO_4 cathode or the Sn_yFe anode. Presently, the project mainly incorporates lithium into the Sn_yFe anode through electrochemical lithiation because the large irreversible capacity in initial cycles for Sn_yFe can be removed and also the amount of incorporated lithium can be readily and accurately controlled. Preliminary results obtained on the $\text{Sn}_y\text{Fe}/\text{Li}_x\text{VOPO}_4$ full cell have been shown in the last quarterly report, where the goal of 4 mAh was achieved. However, the capacity fading is fast for the initial cell (Figure 13a), which is mainly caused by the decay of Li_xVOPO_4 cathode and in part because of a mismatch in capacity between the two electrodes. Recently, with the optimization for Li_xVOPO_4 cathode, especially the introduction of graphene as the conductive additive for electrode preparation, the cathode performance was significantly improved; the theoretical capacity of the material can be achieved ($\sim 320 \text{ mAh/g}$) at a current density of $C/20$ (Figure 13b). Using the optimized Li_xVOPO_4 cathode and adjusted match of the two electrodes (excess capacity of Sn_yFe anode), the full cell gives much improved performance (Figure 13c): 80% capacity can be maintained after 20 cycles. Most interesting is the good reversibility and maintenance of the high-voltage plateau reaction, which remains unchanged on discharge.

In the final quarter, this project will optimize the couple to improve cyclability and rate over full-voltage range.

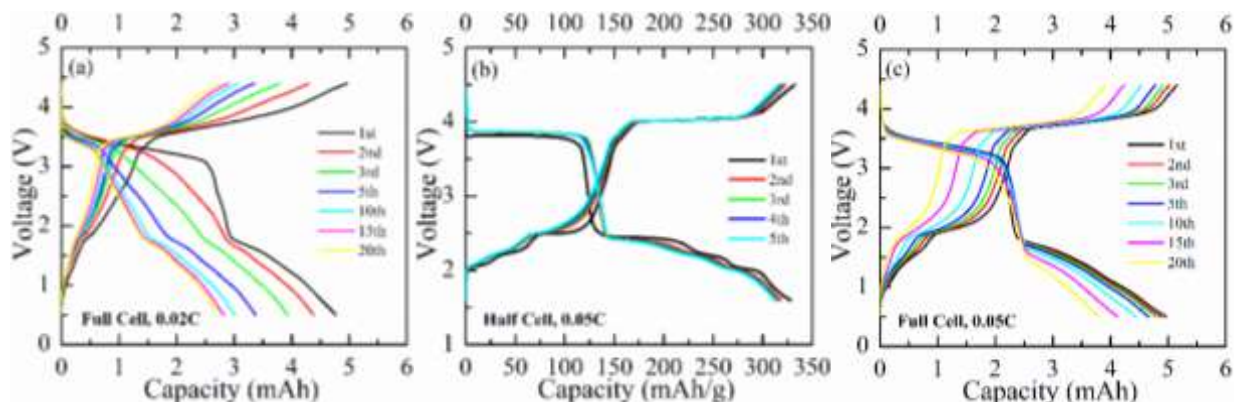


Figure 13. The cycling behavior of the (a) former full cell of the $\text{Sn}_y\text{Fe}/\text{Li}_x\text{VOPO}_4$ electrochemical couple, (b) optimized Li_xVOPO_4 half-cell, and (c) presently optimized full cell of $\text{Sn}_y\text{Fe}/\text{Li}_x\text{VOPO}_4$ electrochemical couple.

Patents/Publications/Presentations

Presentations

- American Chemical Society (ACS) National Meeting, San Francisco (April 4, 2017): “Storing Energy in Lithium Batteries for a Sustainable Energy Future”; Presidential Session, Science for a Sustainable Energy Future; M. Stanley Whittingham.
- MRS Spring Meeting, Phoenix, Arizona (April 13, 2017): “Synthesis and Electrochemistry of High Energy Cathode Material LiVOPO_4 with Enhanced Electronic and Ionic Conductivity”; Dong Shi et al.
- Corning, Inc., Corning, New York (May 2, 2017): “Storing Energy in Lithium Batteries for a Sustainable Energy Future”; M. Stanley Whittingham.
- DOE Review at Binghamton, New York, (June 4, 2017): “High Energy Density Lithium Battery”; M. Stanley Whittingham. In addition, held three in-depth discussions on the components CuF_2 , LiVOPO_4 , and SnFe_y (Fred Omenya, Hui Zhou, and Fenxia Xin).
- DOE Annual Merit Review, Washington, D. C. (June 7, 2017): “High Energy Density Lithium Battery”; M. Stanley Whittingham.

Task 3.3 – Development of High-Energy Cathode Materials (Ji-Guang Zhang and Jianming Zheng, Pacific Northwest National Laboratory)

Project Objective. The project objective is to develop high-energy-density, low-cost, cathode materials with long cycle life. The previous investigation demonstrates that synthesis condition, synthesis approach, and surface modification have significant effects on performances of high-voltage spinel and LMR-NCM cathodes. These valuable understandings will be used to guide development of high-energy-density, enhanced long-term cycling stability of Ni-rich $\text{LiNi}_x\text{Mn}_y\text{Co}_z\text{O}_2$ (NMC) cathode materials that can deliver a high discharge capacity with long-term cycling stability.

Project Impact. Although state-of-the-art layered structure cathode materials such as $\text{LiNi}_{1/3}\text{Mn}_{1/3}\text{Co}_{1/3}\text{O}_2$ and $\text{LiNi}_{0.4}\text{Mn}_{0.4}\text{Co}_{0.2}\text{O}_2$, have relatively good cycling stability at charge to 4.3 V, their energy densities need to be further improved to meet the requirements of EVs. This work focuses on the two closely integrated parts: (1) develop the high-energy-density NMC layered cathode materials for Li-ion batteries; and (2) characterize the structural properties of the NMC materials by various diagnostic techniques including scanning transmission electron microscopy (STEM)/EELS, EDX mapping and SIMS, and correlate with the first part. The success of this work will increase energy density of Li-ion batteries and accelerate market acceptance of EVs, especially for PHEVs required by the EV Everywhere Grand Challenge.

Approach. In fiscal year (FY) 2016, the compositions of NMC cathode materials and the charge cutoff voltage were optimized. Ni-rich NMC cathode materials with initial discharge capacity higher than 200 mAh g^{-1} and capacity retention of 90% after 100 cycles were successfully achieved. However, the long-term cycling stability is still unsatisfactory and requires further improvement. In FY 2017, several strategies will be carried out to further enhance the long-term cycling stability as well as the thermal stability of NMC cathode materials, including (1) cationic/anionic lattice doping; (2) surface modification; and/or (3) introduction of effective electrolyte formulas/additives.

Out-Year Goals. The long-term goal of the proposed work is to enable Li-ion batteries with a specific energy of $> 96 \text{ Wh kg}^{-1}$ (for PHEVs), 5000 deep-discharge cycles, 15-year calendar life, improved abuse tolerance, and less than 20% capacity fade over a 10-year period.

Collaborations. This project engages with the following collaborators:

- Prof. Andy Sun (Western University) – ALD coating,
- Dr. Bryant Polzin (ANL) – NMC electrode supply,
- Dr. X. Q. Yang (BNL) – *in situ* XRD characterization during cycling, and
- Dr. Kang Xu (U.S. Army Research Laboratory, ARL) – new electrolyte.

Milestones

1. Complete lattice doping to enhance cycling stability of NMC at high charge cutoff voltages, and identify the effect of dopants in NMC during cycling using quantitative atomic level mapping. (Q1 – Completed December 2016)
2. Identify appropriate solvents for surface modification of NMC, and reveal the structural changes of different NMC materials after wash with water. (Q2 – Completed March 2017)
3. Complete surface modification to enhance the cycling stability of NMC at high charge cutoff voltages. (Q3 – Completed June 2017)
4. Achieve NMC performance improvement of 200 mAh g^{-1} and 80% capacity retention after 200 cycles. (Q4 – Initiated June 2017)

Progress Report

The third quarter milestone was completed. LPO solid electrolyte coating and thermal infusion technology were developed to improve structural integrity/stability of Ni-rich NMC cathodes (for example, $\text{LiNi}_{0.76}\text{Mn}_{0.14}\text{Co}_{0.10}\text{O}_2$) and hence enhance their electrochemical performances.

The lithium phosphate was coated on the Ni-rich $\text{LiNi}_{0.76}\text{Mn}_{0.14}\text{Co}_{0.10}\text{O}_2$ using atomic layer deposition (ALD). The pristine sample contains secondary particles of 10~15 μm composed of primary particles of 100~300 nm (Figure 14a). After ALD coating, a thin layer of LPO was coated on the surface of secondary particles (Figure 14b). After thermal treatment at 600°C, the thin-film LPO infused into the interior grain boundaries of secondary particles, which was confirmed by TEM EDS mapping. Electrochemical data (Figure 14d) demonstrated that the LPO-as-coated material delivered lower discharge capacity because the coating layer blocked the fast Li-ion diffusion. With thermal treatment, the LPO-infused $\text{LiNi}_{0.76}\text{Mn}_{0.14}\text{Co}_{0.10}\text{O}_2$ was able to deliver similar initial discharge capacity as compared to the pristine material. Importantly, the long-term cycling stability of Ni-rich $\text{LiNi}_{0.76}\text{Mn}_{0.14}\text{Co}_{0.10}\text{O}_2$ was significantly improved. The LPO-infused material showed 91.6% capacity retention after 200 cycles, which is much higher than 79.0% retained by pristine material.

The functioning mechanism of LPO solid electrolyte coating was systematically investigated using focused ion beam (FIB) SEM, TEM, EIS analysis, etc. The pristine material showed substantial crack formation after cycling (Figure 15a/c), indicating a poor capability to accommodate the micro strain generated during deep Li-ion extraction processes. Accompanied with the crack formation, the electrolyte then penetrated the interior of secondary particles along the cracks, leading to formation of a resistive SEI layer at the grain boundaries. Therefore, the pristine material showed fast capacity fading. In contrast, the LPO-infused material exhibited greatly improved structural integrity upon cycling (Figure 15b/d), with no obvious crack being observed. This result suggests that the LPO solid electrolyte formed along the particle boundaries could effectively eliminate micro strain generated during deep delithiation process, contributing to superior long-term cycle life. The results indicate that formation of solid electrolyte along the grain boundaries is a promising technology to enhance the cycling stability of Ni-rich cathode materials for high-energy-density Li-ion batteries.

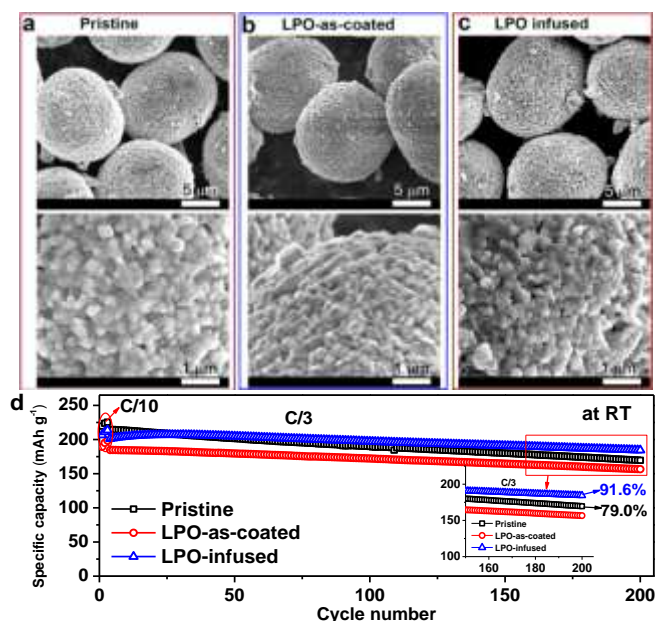


Figure 14. (a-c) Scanning electron microscopy images of (a) pristine, (b) LPO-as-coated, and (c) LPO-infused $\text{LiNi}_{0.76}\text{Mn}_{0.14}\text{Co}_{0.10}\text{O}_2$ cathode materials, and (d) the corresponding cycling performance at C/3 between 2.7~4.5 V.

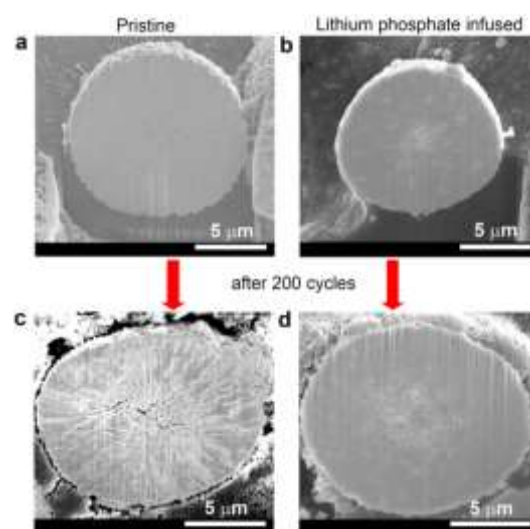


Figure 15. Cross-section scanning electron microscopy images of pristine (a, c) and LPO-infused (b, d) $\text{LiNi}_{0.76}\text{Mn}_{0.14}\text{Co}_{0.10}\text{O}_2$ before (a, b) and after (c, d) 200 cycles at C/3 between 2.7~4.5 V.

Patents/Publications/Presentations

Publication

- Yan, Pengfei, and Jianming Zheng, Ji-Guang Zhang, and Chongmin Wang. “Atomic Resolution Structural and Chemical Imaging Revealing the Sequential Migration of Ni, Co, and Mn upon the Battery Cycling of Layered Cathode.” *Nano Letters* 17, no. 6 (2017): 3946–3951.

Presentation

- DOE Annual Merit Review Meeting, Washington, D. C. (June 5 - 9, 2017): “Development of High-Energy Cathode Materials”; Ji-Guang Zhang and Jianming Zheng.

Task 3.4 – *In Situ* Solvothermal Synthesis of Novel High-Capacity Cathodes (Feng Wang and Jianming Bai, Brookhaven National Laboratory)

Project Objective. The goal is to develop novel high-capacity cathodes with precise control of the phase, stoichiometry, and morphology. Despite considerable interest in developing low-cost, high-energy cathodes for Li-ion batteries, designing and synthesizing new cathode materials with the desired phases and properties have proven difficult, due to complexity of the reactions involved in chemical synthesis. Building on established *in situ* capabilities/techniques for synthesizing and characterizing electrode materials, this project will undertake *in situ* studies of synthesis reactions under real conditions to identify the intermediates and to quantify the thermodynamic and kinetic parameters governing the reaction pathways. The results of such studies will enable strategies to “dial in” desired phases and properties, opening a new avenue for synthetic control of the phase, stoichiometry, and morphology during preparation of novel high-capacity cathodes.

Project Impact. Present-day Li-ion batteries are incapable of meeting the targeted miles of all-electric-range within the weight and volume constraints, as defined by the DOE in the EV Everywhere Grand Challenge. New cathodes with higher energy density are needed for Li-ion batteries so that they can be widely commercialized for plug-in electric vehicle (PEV) applications. The effort will focus on increasing energy density (while maintaining the other performance characteristics of current cathodes) using synthesis methods that have the potential to lower cost.

Out-Year Goals. This project is directed toward developing novel high-capacity cathodes, with a focus on Ni-rich layered oxides. Specifically, synthesis procedures will be developed for making LiNiO_2 and a series of Co/Mn substituted solid solutions, $\text{LiNi}_{1-x}\text{M}_x\text{O}_2$ (M=Co, Mn); through *in situ* studies, this project undertakes systematic investigations of the impact of synthesis conditions on the reaction pathways and cationic ordering processes toward the final layered phases. The structural and electrochemical properties of the synthesized materials will be characterized using scanning XRD, neutron scattering, TEM, EELS, and various electrochemical techniques. The primary goal is to develop a reversible cathode with an energy density of 660 Wh/kg or higher.

Collaborations. This project engages with the following collaborators: Lijun Wu and Yimei Zhu at BNL; Khalil Amine, Zonghai Chen, Yang Ren, and Chengjun Sun at ANL; Jagjit Nanda and Ashfia Huq at ORNL; Nitash Balsara, Wei Tong, and Gerbrand Ceder at LBNL; Peter Ko at Cornell High Energy Synchrotron Source, Scott Misture at Alfred University; Peter Khalifha at SUNY; and Kirsuk Kang at Seoul National University.

Milestones

1. Identify the synthesis reactions and involved structural ordering in both Ni-rich and Co-rich layered oxides through *in situ* synchrotron X-ray studies. (Q1 – Completed December 2016)
2. Develop neutron scattering-based techniques for *in situ* probing cation ordering in Ni-rich NMC layered oxides during synthesis under controlled atmosphere. (Q2 – Completed March 2017)
3. Identify synthesis procedures for kinetic control of the structural ordering in NMC layered oxides through combined *in situ/ex situ* synchrotron X-ray and neutron studies. (Q3 – Completed June 2017)
4. Complete the evaluation of synthesis conditions, specifically identifying the effect of temperature and time on the structural ordering and electrode performance of Ni-rich NMC layered cathodes. (Q4, September 2017 – On schedule)

Progress Report

This quarter, synthesis procedures for kinetic control of the structural ordering in NMC layered oxides were identified through combined *in situ/ex situ* synchrotron X-ray and neutron studies.

Previously, synchrotron and neutron scattering based techniques were developed for *in situ* probing and synthetic control of structural ordering in various NMC layered oxides. This quarter, these *in situ* techniques were further applied to kinetic control of the cationic ordering in Ni-rich layered oxides subjected to heat treatment at high temperatures. Representative time-resolved synchrotron XRD patterns from $\text{LiNi}_{0.7}\text{Mn}_{0.15}\text{Co}_{0.15}\text{O}_2$ (NMC71515) are shown in Figure 16a. The evolution of diffraction peaks, such as fast rise of (003) peak, indicates rapid improvement of cationic ordering during the heat treatment, with a strong dependence on temperature (Figure 16b-d).

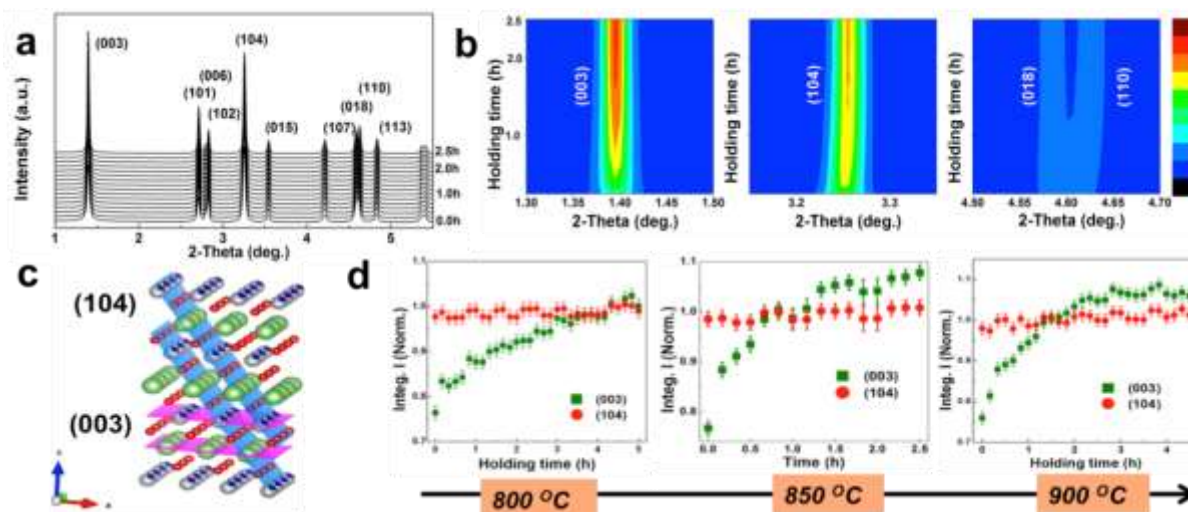


Figure 16. (a) Representative time-resolved X-ray diffraction patterns from $\text{LiNi}_{0.7}\text{Mn}_{0.15}\text{Co}_{0.15}\text{O}_2$ during heat treatment. (b) Evolution of the reflections characteristic of layered structure. (c) Illustration of the atomic configuration and reflection planes of (104) and (003) in the layered structure. (d) Evolution of the integrated intensity of the (003) and (104) peaks.

Details on structural ordering processes, such as the evolution of slab distance and Li/Ni disordering with holding time, were obtained through quantitative analysis of XRD data (Figure 17). The results from this study revealed a complex synthesis process, involving competition between cationic ordering and disordering processes (largely due to Li/O loss) that concomitantly occur during heat treatment. Treatment at elevated temperature would always facilitate the ordering process, but the ordering kinetics did not increase monotonically with temperature—being compromised by accelerated disordering with an increase of temperature. Kinetic control of the cationic ordering, via finely tuning heating temperature and holding time, was found to be crucial to optimizing structural ordering of the final products. The findings from this *in situ* study, in combination with *ex situ* structural/electrochemical characterization, enabled identification of optimal conditions (that is, 850 °C for ~ 3 h) for synthesizing NMC-71515 with low cationic disordering and high electrochemical activities.

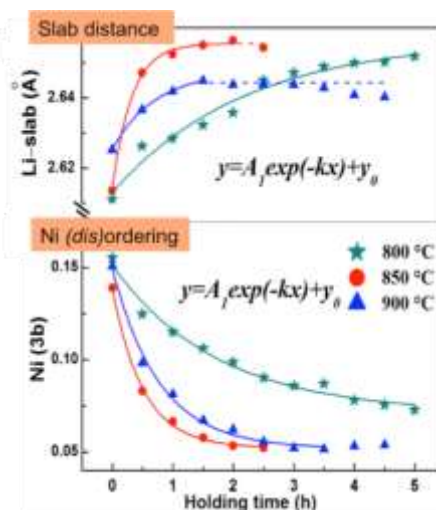


Figure 17. Evolution of Li-slab distance and cationic disordering (that is, nickel ions at 3b sites) with holding. (Lines: fittings to $y = A_1 \exp(-kx) + y_0$).

Patents/Publications/Presentations

Presentations

- MRS Spring Meeting (April 17 – 21, 2017): “*In Situ* Tracking of the Structural Chemistry during Synthesis of Ni-Rich Layered Oxides as High-Energy Cathodes for Li-Ion Batteries”; J. Bai, J. Zhao, D. Wang, J. Y. P. Ko, A. Huq, and F. Wang.
- DOE Annual Merit Review, Washington, D. C. (June 5 – 9, 2017): “*In Situ* Solvothermal Synthesis of Novel High-Capacity Cathodes”; F. Wang and J. Bai.

Task 3.5 – Novel Cathode Materials and Processing Methods (Michael M. Thackeray and Jason R. Croy, Argonne National Laboratory)

Project Objective. The project goal is to develop low-cost, high-energy, and high-power Mn-oxide-based cathodes for Li-ion batteries that will meet the performance requirements of PHEVs and EVs. Improving the design, composition, and performance of advanced electrodes with stable architectures and surfaces, facilitated by an atomic-scale understanding of electrochemical and degradation processes, is a key objective.

Project Impact. Standard Li-ion battery technologies are unable to meet the demands of the next-generation EVs and PHEVs. Battery developers and scientists will take advantage of both the applied and fundamental knowledge generated from this project to advance the field. This knowledge should enable progress toward meeting DOE goals for 40-mile, all-electric range PHEVs.

Approach. Exploit the concept and optimize performance of structurally integrated “composite” electrode structures with a primary focus on “layered-layered-spinel” materials. Alternative processing routes will be investigated; ANL’s comprehensive characterization facilities will be used to explore novel surface and bulk structures by both *in situ* and *ex situ* techniques in pursuit of advancing properties of state-of-the-art cathode materials. A theoretical component will complement the project’s experimental work.

Out-Year Goals. The out-year goals are as follows:

- Identify high-capacity (LL and LS) composite electrode structures and compositions that are stable to electrochemical cycling at high potentials (~ 4.5 V).
- Identify and characterize surface chemistries and architectures that allow fast Li-ion transport and mitigate or eliminate TM dissolution.
- Use complementary theoretical approaches to further understanding of electrode structures and electrochemical processes to accelerate progress of materials development.
- Scale-up, evaluate, and verify promising cathode materials in conjunction with scale-up and cell fabrication facilities at ANL.

Collaborators. This project engages with the following collaborators: Eungje Lee, Roy Benedek, Arturo Gutierrez, and Meinan He in Chemical Sciences and Engineering (CSE) at ANL.

Milestones

1. Explore the energy content, and stabilization thereof, of moderate Li_2MnO_3 -content ($25\% < x < 50\%$) $y[\text{xLi}_2\text{MnO}_3 \cdot (1-x)\text{LiMO}_2] \cdot (1-y)\text{LiM}_2\text{O}_4$ (M=Mn, Ni, Co), LL and LLS electrodes; target capacity ≥ 220 mAh/g. (Q4 – Completed March 2017; Ongoing)
2. Identify surface-treatment strategies that enable LLS electrodes to maintain high capacities (≥ 220 mAh/g) and high rate performance (~ 200 mAh/g at 1C). (Q4 – Completed June 2017; Ongoing)
3. Demonstrate oxide energy densities ≥ 750 Wh/kg_{oxide} in full-cell testing of surface-modified, LLS electrodes. (Q4, September 2017 – In progress)

Progress Report

Mn-rich, LLS cathodes have shown potential as alternatives to their more Ni-rich, NMC counterparts (for example, $\text{LiNi}_{0.5}\text{Mn}_{0.3}\text{Co}_{0.2}$). As nickel content is continuously pushed to higher levels, concerns over both cost and safety warrant further exploration of these promising LLS materials. Major challenges that remain with respect to the performance of LLS cathodes are related to improvement of bulk and surface instabilities. Recent reports have shown that it is possible to enhance surface stability, where targeted materials and carefully chosen processing conditions are likely to yield further improvements. A more daunting challenge, perhaps, is the stabilization of bulk structures. Integration of a spinel component, along with optimized compositions and voltage windows, can go a long way in improving electrode performance. However, further improvements are necessary, and ongoing studies have been focusing on bulk stabilization of LLS materials through theory and experiment. Because it is well-known that local structures, due to the presence of excess lithium and manganese, are directly involved in the mechanisms of bulk structural degradation, compositions with high lithium and manganese contents were chosen for these studies.

Figure 18a shows differential capacity plots (dQ/dV) of a “baseline,” Li- and Mn-rich, layered-layered, $0.33\text{Li}_2\text{MnO}_3 \bullet 0.67\text{LiMn}_{0.365}\text{Ni}_{0.365}\text{Co}_{0.244}\text{M}_{0.02}\text{O}_2$ cathode (versus lithium metal). Herein, M represents iron, zinc, and copper as a 2% substituent. As shown in Figure 18a, and more clearly seen in the magnified view of Figure 18b, substitution of these elements does influence both the high (~ 4.5 V) and low (~ 3.5 V) voltage charge processes, where the lower voltage process at ~ 3.5 V is known to correlate with structural changes and the corresponding voltage fade. Though characterization work is ongoing, it is interesting to note that each “dopant” influences the energetics of charge/discharge in slightly different ways, with zinc, expected to be electrochemically inactive, pushing potentials to somewhat higher values, followed by copper, the baseline sample, and finally iron substitution showing the most capacity in the low-voltage region. Figure 18c shows first-cycle charge (uppermost closed symbols) and discharge (lowermost open symbols) capacities as a function of integrated spinel (quantified by the total Li:TM ratio, x-axis) to form corresponding, “doped” LLS materials. Here, a Li:TM ratio represents 0% spinel and a ratio of 1.23 represents $\sim 10\%$ spinel. As expected, first-cycle efficiencies and discharge capacities increase with spinel integration. Cycling studies are in process to determine long-term effects of dopants on charge and discharge processes of LLS materials. These studies are being used to gain insights into the role of “active” versus “inactive” substituents as a function of LLS composition and spinel content. Future studies will also focus on how such elements can influence the stability of LLS materials when specifically targeted as dopants in the surface and near-surface regions of these integrated structures.

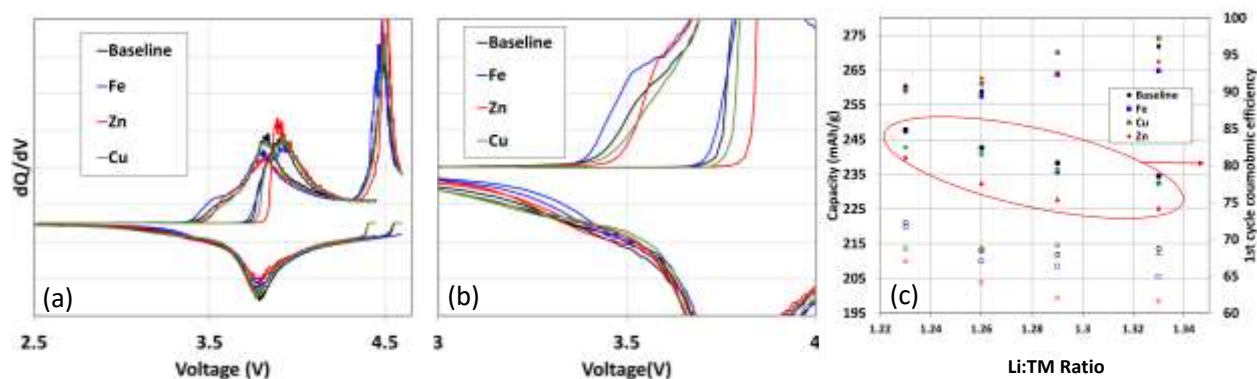


Figure 18. (a) Differential capacity plots (dQ/dV) for a $0.33\text{Li}_2\text{MnO}_3 \bullet 0.67\text{LiMn}_{0.365}\text{Ni}_{0.365}\text{Co}_{0.244}\text{M}_{0.02}\text{O}_2$ material with and without substituent $M = \text{Fe}, \text{Zn},$ and Cu . (b) Magnified view of the low-voltage processes in the dQ/dV shown in (a) associated with voltage fade. (c) First-cycle charge (uppermost closed symbols) and discharge (lowermost open symbols) capacities (left y axis) along with first-cycle Coulombic efficiencies (circled in red, right y axis) as a function of overall lithium to transition metal ratio in the tested compositions (x axis). Cycling was conducted between 4.6-2.0V in lithium half-cells at 15 mA/g and 30°C.

Patents/Publications/Presentations

Presentations

- Advanced Photon Source User Meeting, Lemont, Illinois (May 9, 2017): “Advancement of Li- and Mn-Rich High Energy Cathodes for Lithium-Ion Batteries”; A. Gutierrez, B. Yonemoto, M. He, E. Lee, R. Benedek, Y. Ren, H. M. Meyer III, J. R. Croy, and M. M. Thackeray.
- DOE Annual Merit Review, Washington, D. C. (June 5 – 9, 2017): “Tailoring Integrated Layered and Spinel Electrode Structures for High Capacity Lithium-Ion Cells” ES049; M. M. Thackeray and J. R. Croy.
- ANL Battery Industry Day, Lemont, Illinois (June 14, 2017): “Development of Cathode Materials for Lithium-Ion Applications at Argonne National Laboratory”; J. R. Croy.

Task 3.6 – Advanced Cathode Materials for High-Energy Lithium-Ion Batteries (Marca Doeff, Lawrence Berkeley National Laboratory)

Project Objective. Microscopy and synchrotron X-ray absorption and photoemission techniques will be used to study the phenomenon of surface reconstruction to rock salt on NMC particle surfaces as a function of composition, synthesis method, surface chemistry, and electrochemical history. Because the surface reconstruction is implicated in capacity fading and impedance rise during high-voltage cycling, a thorough understanding of this phenomenon is expected to lead to principles that can be used to design robust, high-capacity NMC materials for Li-ion cells. The emphasis will be on stoichiometric NMCs with high nickel content such as 622 and 523 compositions.

Project Impact. To increase the energy density of Li-ion batteries, cathode materials with higher voltages and/or higher capacities are required, but safety and cycle life cannot be compromised. Ni-rich NMCs can provide higher capacities and lower cost in comparison with low nickel content NMCs, but surface reactivity is an issue. A systematic evaluation of the effects of synthesis method, composition, and cell history on the surface reconstruction phenomenon will lead to higher capacity, robust, and structurally stable positive electrode materials that result in higher-energy-density Li-ion cells than are currently available.

Out-Year Goals. The information generated by the in-depth characterization will be used to design robust NMC materials that can withstand cycling to high potentials and deliver > 200 mAh/g.

Collaborations. TXM is done in collaboration with Yijin Liu (SSRL). Synchrotron hard and soft X-ray absorption spectroscopy (XAS) efforts are in collaboration with Dr. Dennis Nordlund, Dr. Yijin Liu, and Dr. Dimosthenis Sokaras (SSRL).

Milestones

1. Complete thermal characterization of Ni-rich NMC materials by TXM and X-ray Raman. (Q1 – Completed December 31, 2016)
2. Synthesize Ti-substituted Ni-rich NMCs by conventional and spray pyrolysis methods. (Q2 – Completed March 31, 2017)
3. Complete electrochemical characterization of Ti-substituted, Ni-rich NMCs. (Q3 – Completed June 30, 2017)
4. *Go/No Go:* Core-shell composites made by infiltration and re-firing of spray-pyrolyzed hollow spherical particles. (September 30, 2016 – No-go decision made)

Progress Report

A substantial amount of data has been collected on pristine and chemically delithiated samples of NMC-622 over the past year, using laboratory XRD (hot stage), synchrotron hard and soft XAS, X-ray Raman, and TXM at SSRL. Samples at several states-of-charge were examined at room temperature, 170°C, or 350°C using the synchrotron techniques listed above, some of which probe surfaces and others which probe bulk. The project is now analyzing the data in preparation for writing a paper, which should present a comprehensive picture of the phase behavior of delithiated samples during thermal treatment. While the full analysis of this data is not yet available, some results from the TXM (nickel XANES 3D mapping) experiments for the 100% delithiated sample are shown below and illustrate some interesting differences.

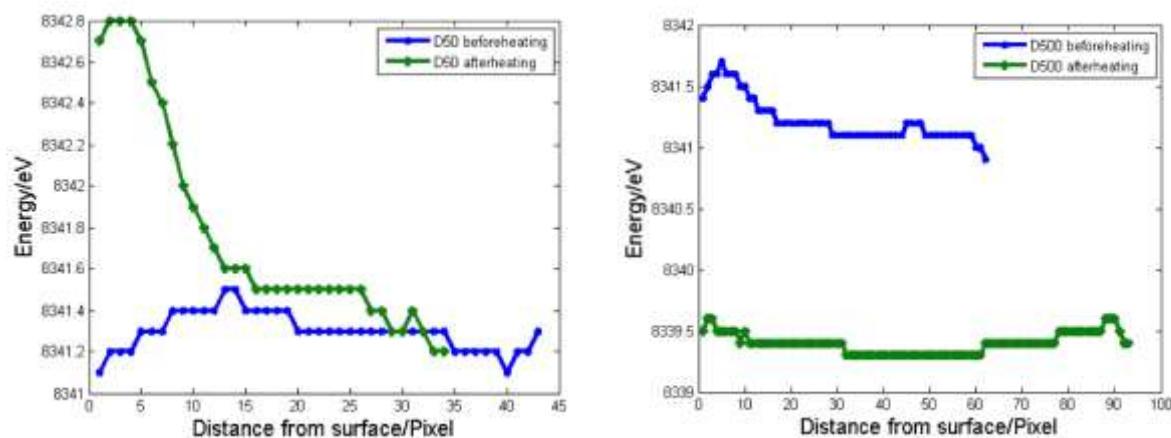


Figure 19. Statistical data from 3D nickel X-ray absorption near edge spectroscopy mapping transmission X-ray microscopy experiments, showing nickel K-edge energy as a function of distance from the surface. Results from a 50% delithiated NMC-622 sample are shown on the left, and a 100% delithiated sample on the right. Blue symbols are for data obtained on samples at room temperature, and green are for samples after heating to 350°C.

These data show that nickel is oxidized (shift to a higher energy) at the surface for the heat-treated 50% delithiated sample compared to the unheated sample, but slightly reduced in the bulk. The hot stage XRD results suggest that conversion to a spinel-type phase similar to $\text{Li}_{0.5}\text{M}_2\text{O}_4$ occurs below 300°C for this material. This does not require loss of oxygen, and significant reduction of nickel does not need to occur. For the 100% delithiated sample, heating to 350° results in a more uniform reduction of nickel from the surface to the bulk. This sample is considerably more thermally unstable than the 50% delithiated sample. The XRD patterns show substantial peak broadening as low as 150°C, suggestive of amorphization. Near 300°C, the pattern changes to something reminiscent of a cubic spinel M_3O_4 phase, with possibly some rock salt (MO) phase as well. Loss of oxygen is required to form these phases, resulting in reduction of nickel.

Next quarter, the project will further analyze the thermal data and write a paper summarizing the results.

Patents/Publications/Presentations

Publication

- Ludwig, J., and C. Alarcón-Suesca, S. Geprägs, D. Nordlund, M. M. Doeff, I. Puente Orench, and T. Nilges. “Direct Synthesis and Characterization of Mixed-Valent $\text{Li}_{0.5-\delta}\text{CoPO}_4$, a Li-Deficient Derivative of the *Cmcm* Polymorph of LiCoPO_4 .” *RSC Advances* 7 (2017): 28069.

Presentations

- 12th Pacific Rim Conference on Ceramic and Glass Technology, Waikoloa, Hawaii (May 21 – 26, 2017): “The Road to Solid State Batteries for Vehicle Applications.” Invited talk.
- Society of Vacuum Coaters (SVC) TechCon, Providence, Rhode Island (April 29 – May 4, 2017): “The Future of Energy Storage for Vehicle Applications”; Marca M. Doeff. Invited talk.

Task 3.7 – Discovery of High-Energy Lithium-Ion Battery Materials (Wei Tong, Lawrence Berkeley National Laboratory)

Project Objective. This project aims to develop a cathode that can cycle > 200 mAh/g while exhibiting minimal capacity and voltage fade. The emphasis will be on oxides with high nickel contents. This task focuses on the compositions in the Li-Ni-O phase space, which will be explored using a combinatorial materials approach to search for new high-capacity cathodes. The specific objectives of this project are to: (1) investigate and understand the correlation between the synthesis and electrochemical performance of Ni-based compounds, and (2) design, synthesize, and evaluate the potential new high-capacity cathodes within Li-Ni-O composition space using the percolation theory as a guideline.

Project Impact. Energy density needs to be at least doubled to meet the performance requirements of EVs (300 to 400 mile). Although capacities approaching 300 mAh/g have been reported in Li-, Mn-rich layered oxide compounds, capacity decay and voltage fading in the long-term cycling are always observed. Therefore, new materials are urgently needed to make the breakthrough in Li-ion battery technology.

Approach. Recent discovery of high-capacity Li-excess cathodes provides new insights into material design principle. According to percolation theory, lithium excess is required to access 1 lithium exchange capacity in LiTmO_2 compounds. This seems to be independent of TM species, and therefore, could open a composition space for the search of new materials with high capacity. The interesting $\text{Ni}^{2+}/\text{Ni}^{4+}$ redox is selected as the electrochemically active component, and combinatorial materials design concept will be used to discover the potential cathode material candidates in the Li-Ni-O phase space.

Out-Year Goals. The long-term goal is to search new high-energy cathodes that can potentially meet the performance requirements of EVs with a 300- to 400-mile range in terms of cost, energy density, and performance. Work will progress from understanding of the known compounds, LiNiO_2 and Li_2NiO_2 , toward development of new Ni-based, high-energy cathode oxides.

Collaborations. The PI closely collaborates with M. Doeff (LBNL) on soft XAS, C. Ban (National Renewable Energy Laboratory, NREL) on ALD coating, B. McCloskey (LBNL) for differential electrochemical mass spectrometry, and R. Kostecki (LBNL) for Raman spectroscopy. In addition, collaboration with other BMR PIs (X.-Q. Yang and F. Wang at BNL; K. Persson at LBNL) for crystal structure evolution upon cycling and material computation is in progress.

Milestones

1. Use Li-, Mn-rich oxide as the baseline material; develop synthesis that can be used to screen second TMs for Li-rich, Ni-based oxides. (Q1 – Completed December 2016)
2. Design Li-rich, Ni-based oxide compositions; perform synthesis of designed compositions. (Q2 – Completed March 2017)
3. Complete electrochemical tests on synthesized Li-rich, Ni-based oxides; down select one composition that shows promising electrochemical performance with an initial capacity > 200 mAh/g. (Q3 – Completed June 2017)
4. Complete structural characterization of selected composition; compare performance with Li-, Mn-rich oxide baseline. (Q4 – Initiated July 2017)

Progress Report

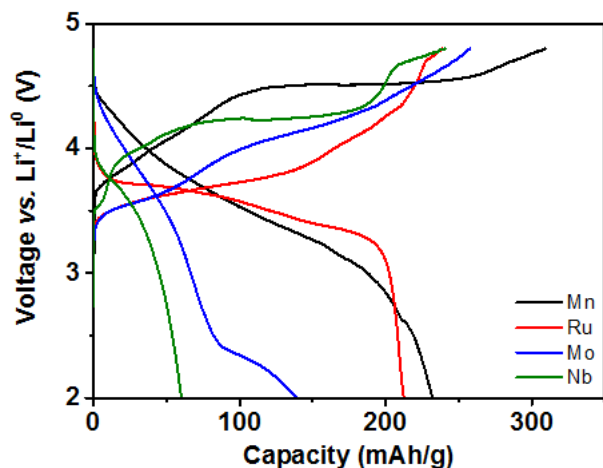


Figure 20. The first-cycle voltage profiles of $\text{Li}_{2-x-y}\text{Ni}_x\text{TMyO}_2$ (TM = Mn, Ru, Mo and Nb). Cells were cycled between 4.8 and 2.0 V at 5 mA/g at room temperature.

As shown in Figure 20, the Mn-based sample produced by a solid-state reaction exhibited a charge capacity of 310 mAh/g and a discharge capacity of 232 mAh/g, with a CE of 75%. Of the other samples, the Ru-based one demonstrated the best electrochemical performance, characterized by a charge capacity of 239 mAh/g and a discharge capacity of 213 mAh/g, leading to a CE of 88.9%. The other two compounds demonstrated a reasonably high charge capacity, 258 and 241 mAh/g for TM = Mo and Nb, respectively, which was comparable to that of Ru-based sample. However, a lower discharge capacity was obtained, 139 and 60 mAh/g for Mo and Nb, respectively.

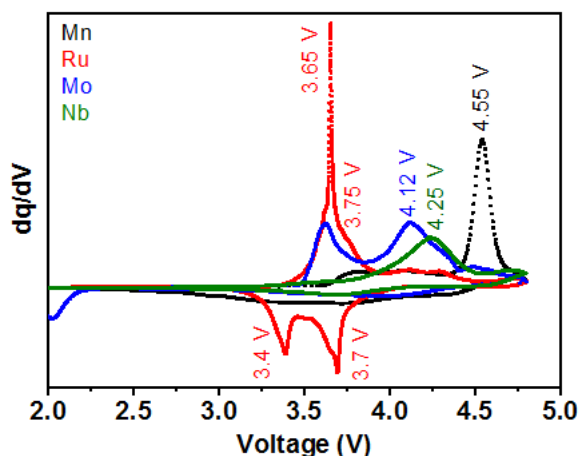


Figure 21. The first dq/dV plots of $\text{Li}_{2-x-y}\text{Ni}_x\text{TMyO}_2$ (TM = Mn, Ru, Mo and Nb). Cells were cycled between 4.8 and 2.0 V at 5 mA/g at room temperature.

Beyond the achievable capacity, it was noticed that a second TM also substantially influenced the shape of the voltage profiles; the effect was more pronounced on charge. For example, an extended voltage plateau was most distinguishable in the charge profile of Mn-based sample, corresponding to the strong oxidation peak around 4.55 V in the dq/dV plot (Figure 21). In comparison, the most distinct difference was observed in the dq/dV plots of Ru-based sample, characterized by a strong oxidation peak at 3.65 V on charge. For Mo-based sample, an initial oxidation peak at a voltage of 3.65 V was also observed, followed by a second oxidation peak at 4.12 V upon charging. The oxidation peak for Nb-based sample appeared at 4.25 V. During the discharge, the reduction peaks were much less pronounced for TM = Mn, Mo, Nb, as opposed to those at 3.4 and 3.7 V for TM = Ru. It was clearly observed that TM drastically affected the electrochemical characteristics, suggesting the possibly different reaction mechanism for each composition. Particularly, it is well acknowledged that the extended high-voltage plateau for Mn-based sample is associated with oxygen activation. Therefore, Ru-based sample will be used as a model to study oxygen activity in these Li-rich metal oxides, given the sharp contrast in charge profile but similar structure between Mn- and Ru-based compounds.

Patents/Publications/Presentations

Publication

- Xu, J., and S. Renfrew, M. A. Marcus, M. Sun, B. D. McCloskey, and W. Tong. “Investigating Li_2NiO_2 - Li_2CuO_2 Solid Solutions as High-Capacity Cathode Materials for Li-Ion Batteries.” *Journal of Physical Chemistry C* 121 (2017): 11100–11107.

Presentations

- DOE Annual Merit Review, Washington, D. C. (June 2017): “Discovery of High-Energy Lithium-Ion Battery Materials”; W. Tong.
- University of California, Berkeley Mechanical Engineering / LBNL Energy Technology Area Seminar Series, Berkeley, California (April 2017): “Combinatorial Materials Approach: Accelerating Material Discovery for Energy Storage”; W. Tong.

Task 3.8 – Exploiting Cobalt and Nickel Spinel in Structurally Integrated Composite Electrodes (Michael M. Thackeray and Jason R. Croy, Argonne National Laboratory)

Project Objective. The project goal is to stabilize high-capacity, composite ‘layered-layered’ electrode structures with lithium-cobalt-oxide and lithium-nickel-oxide spinel components (referred to as LCO-S and LNO-S, respectively), or solid solutions thereof (LCNO-S), which can accommodate lithium at approximately 3.5 V versus Li/Li⁺. This approach and the motivation to exploit the electrochemical and structural LCO-S and LNO-S spinel structures, about which relatively little is known, is unique.

Project Impact. State-of-the-art Li-ion batteries are currently unable to satisfy the performance goals for PHEVs and EVs. If successful, this project will impact the advance of energy storage for electrified transportation as well as other applications, such as portable electronic devices and the electrical grid.

Approach. This work will focus on the design and synthesis of new spinel compositions and structures that operate above 3 V and below 4 V and on determining their structural and electrochemical properties through advanced characterization. This information will be subsequently used to select the most promising spinel materials as stabilizers in high-capacity composite electrode structures.

Out-Year Goals. The electrochemical capacity of most high-potential, Li-metal oxide insertion electrodes is generally severely compromised by structural instability and surface reactivity with the electrolyte at low lithium loadings (that is, at highly charged states). Although progress has been made by cation substitution and structural modification, the practical capacity of these electrodes is still restricted to approximately 160-170 mAh/g. This project proposes a new structural and compositional approach with the goal of producing electrode materials that can provide 200-220 mAh/g without significant structural or voltage decay for 500 cycles. If successful, the materials processing technology will be transferred to the ANL Materials Engineering and Research Facility for scale up and further evaluation.

Collaborations. This project collaborates with Eungje Lee, Christopher Johnson, Wenquan Lu, and Roy Benedek (CSE, ANL).

Milestones

1. Explore solution-based synthesis routes to optimize the structure and performance of Co-based spinel and structurally integrated LS electrodes. (Q4 – In progress; see text)
2. Determine structure/electrochemical property relationships of Co-based spinel materials and composite LS electrodes. (Q4 – In progress)
3. Investigate bulk and surface modifications of Co-based spinel and LS electrodes. (Q4 – In progress; see text)

Progress Report

Previous reports have focused on the synthesis of composite, layered-spinel $\text{Li}_2\text{MnO}_3 \cdot \text{LiMn}_2\text{O}_4$ cathode materials, the resulting structures, and their electrochemical behavior. For these lithium-manganese-oxide materials with relatively simple elemental components, the formation of structurally-integrated layered and spinel domains is readily achieved by high-temperature firing of homogeneously-mixed precursors. However, such simple synthesis routes rely on the thermodynamic phase segregation into composite structures and, therefore, have limitations in preparing multi-element samples. As such, alternative synthesis routes that enable more precise control over compositional and structural arrangements at the nano-scale are desired. Herein, a continuing investigation of new synthesis approaches is reported whereby a modified sol-gel process is used to synthesize a layered-spinel $\text{Li}_2\text{MnO}_3 \cdot \text{LiNi}_{0.5}\text{Mn}_{1.5}\text{O}_4$ composite structure in which a heterogeneous distribution of nickel and manganese in the component phases is required.

Single-phase powder samples of layered Li_2MnO_3 and spinel $\text{LiNi}_{0.5}\text{Mn}_{1.5}\text{O}_4$ were prepared by a sol-gel method. An aqueous solution of metal acetates (manganese or manganese/nickel) was added to a glycolic acid or citric acid solution at 70°C , and ammonium hydroxide was used to adjust the pH values to between 7-9. The final solutions were dried under stirring until a gel was formed. The gel products were fired at 400°C to remove the polymer precursors and subsequently heat-treated at 800°C , for 12 h, to produce well-crystallized powder samples of Li_2MnO_3 and $\text{LiNi}_{0.5}\text{Mn}_{1.5}\text{O}_4$. To produce a LS $\text{Li}_2\text{MnO}_3 \cdot \text{LiNi}_{0.5}\text{Mn}_{1.5}\text{O}_4$ composite structure, the Li_2MnO_3 and $\text{LiNi}_{0.5}\text{Mn}_{1.5}\text{O}_4$ sols were mixed together prior to gel formation. With continued stirring and heating, the mixed sol quickly formed a gel. The gel product was then decomposed at 400°C and heat-treated under the same conditions as those used for the single-phase powder samples (800°C , 12 h). For comparison, a physical blend of the Li_2MnO_3 and $\text{LiNi}_{0.5}\text{Mn}_{1.5}\text{O}_4$ powders, in a 1:1 molar ratio, was also prepared.

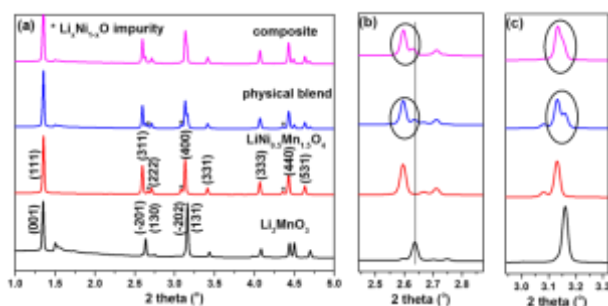


Figure 22. (a) Synchrotron X-ray diffraction of Li_2MnO_3 , $\text{LiNi}_{0.5}\text{Mn}_{1.5}\text{O}_4$, a 1:1 physical blend of the two, and a $\text{Li}_2\text{MnO}_3 \cdot \text{LiNi}_{0.5}\text{Mn}_{1.5}\text{O}_4$ composite. (b) and (c) Enlarged regions ranging from 2.5° to 2.8° 2-theta and from 3.0° to 3.3° 2-theta, respectively.

The synchrotron XRD patterns for the composite material in Figure 22a-c show a merging of the peaks for each single-phase component together with some peak broadening. This merging effect is noticeably different in the corresponding XRD patterns of the physical blend, indicating a more complex structure than the simple mixture. In Figure 23c, the electrochemical profiles for the composite material display the characteristics of both, Li_2MnO_3 (Figure 23b) and $\text{LiNi}_{0.5}\text{Mn}_{1.5}\text{O}_4$ (Figure 23a), but with much improved electrochemical performance relative to a physical blend of the individual components (Figure 23d). These X-ray and electrochemical data indicate that the modified sol-gel method provides an effective route to produce structurally-integrated electrode materials. Studies are in progress to use this method to synthesize more complex, structurally-integrated electrode compositions.

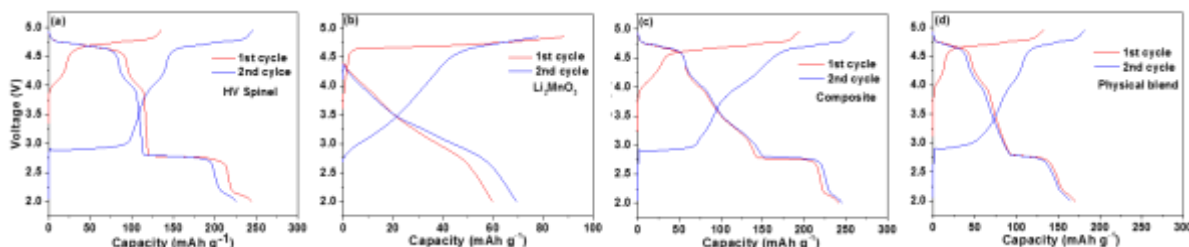


Figure 23. (a) Initial voltage profiles of spinel $\text{LiNi}_{0.5}\text{Mn}_{1.5}\text{O}_4$, (b) layered Li_2MnO_3 , (c) a $\text{Li}_2\text{MnO}_3 \cdot \text{LiNi}_{0.5}\text{Mn}_{1.5}\text{O}_4$ composite, and (d) a 1:1 physical blend of the two components. 4.8-2.0V at $\sim\text{C}/15$ and 30°C against lithium metal.

Patents/Publications/Presentations

Presentations

- DOE Annual Merit Review, Washington, D. C. (June 5 – 9, 2017): “Tailoring Integrated Layered and Spinel Electrode Structures for High Capacity Lithium-Ion Cells” ES049; M. M. Thackeray and J. R. Croy.
- ANL Battery Industry Day, Lemont, Illinois (June 14, 2017): “Development of Cathode Materials for Lithium-Ion Applications at Argonne National Laboratory”; R. Croy.

TASK 4 – ELECTROLYTES

Summary and Highlights

The BMR Program goal is to develop long-life batteries superior to commercial Li-ion systems in terms of cost, vehicle range, and safety. The BMR Program addresses the fundamental problems of electrode chemical and mechanical instabilities that have slowed development of affordable, high performance, automotive batteries. The aim is to identify electrode/electrolyte materials that yield enhanced battery performance and lead to greater acceptance of EVs. Currently, the VTO supports seven projects in the BMR Program under the Electrolytes area. These projects can be categorized into three general topics:

- **Liquid.** The projects for liquid electrolyte aim to develop an atomic/molecular level understanding of the stability of electrochemical interfaces during charge-discharge cycling to stabilize solid/liquid interfaces in Li-ion batteries. In addition, electrolyte formulations, based on fluoro-chemistries, will be developed to achieve significantly improved operating voltage, increased durability, and increased energy density of Li-ion batteries at a reasonable cost.
- **Polymer.** The target of polymer electrolyte projects is mainly for use in Li-S batteries. Inorganic/polymer and polymer/gel hybrid electrolytes that have flexibility, mechanical strength, thermal stability, high ionic conductivity, stable interfaces against lithium metal, and polysulfide-trapping capability will be developed to enable energy densities twice that of the state-of-the-art Li-ion batteries, with comparable cycle life.
- **Self-Forming & Self-Healing.** The self-forming and self-healing electrolyte projects focus on developing and implementing Li-metal-based metal fluorite and metal iodide batteries, capable of energy densities > 400-500 Wh/kg and 1000 Wh/L.

Highlights. This quarter, the group at ANL finished benchmarking the newly developed high-precision electrochemical measuring system for stability studies by applying it to the anodic dissolution of aluminum foils in nonaqueous electrolytes. By measuring potential dependence on the static parasitic current for aluminum foil with surface coatings of carbon, graphene, and AlPO_4 , they have concluded that the corrosion reaction of aluminum foil at a relatively high potential is a coupled electrochemical–chemical reaction.

At the Daikin group, additional baseline experiments are being completed to characterize all starting materials in the project. These starting materials include components of the electrolyte as well as characterization of battery electrodes before battery fabrication.

The University of Maryland (UMD) group performed molecular dynamics simulations of Li^+ diffusion in garnet nanofibers and the effect of mechanical deformation on Li^+ diffusion, which provide insights into the Li^+ diffusion mechanisms in garnet nanofibers.

At the University of Washington (UW), using PENDI-C6 and Py linker, a self-healing film with the ability to clearly heal a total fracture in 4 hours at the moderate temperature of 40°C was demonstrated. By contrast, a previous film made using PENDI-C3 was not able to self-heal at this temperature even after 16 hours, instead requiring 60°C before the onset of self-healing. MH00 carbon/sulfur composites containing thiophenol surface modifiers were cycled at C/10, producing mixed results: specific capacity underwent a sharp decrease as compared to unmodified samples; however, capacity retention over 20+ cycles dramatically improved. Investigation continues into these materials and improved modifiers.

The West Virginia University (WVU) group successfully improved the ionic conductivity of $\text{Li}_{0.33}\text{La}_{0.56}\text{TiO}_3$ (LLTO) nanofibers from 7.7×10^{-4} S/cm to 1.08×10^{-3} S/cm through 0.5% aluminum doping. Highly ionic-conductive Garnet-type $\text{Li}_{6.4}\text{La}_3\text{Al}_{0.2}\text{Zr}_2\text{O}_{12}$ (LLAZO) nanofibers with desirable cubic phase structure were

obtained at a lower heating rate. For the polymer matrix, they have completed the synthesis of Li[PSTFSI-b-MPEGA-b-PSTFSI] triblock copolymer and cross-linked polyethylene/polyethylene oxide (PE/PEO) polymer. The ionic conductivity of PE/PEO cross-linked polymer reached up to 1.15×10^{-4} at room temperature. They have also fabricated and investigated the ionic conductivity of composite electrolytes based on the synthesized nanofibers and polymers.

The Stony Brook University (SBU) group measured conductivity of LiI with various percentages of AgI, and with AgI+Al₂O₃. They demonstrated that reduction of resistance at the interface shows significant benefit for more highly conductive electrolytes; thus, this is an area of investigation planned for future cell designs.

At Rutgers University, the focus this quarter has been on systematic improvement of both: (1) the chemistry related to the composition and phase of reactive current collectors, and (2) electrode architectures of full cells. This combined approach has effectively increased the stack energy density of the second quarter examples by an order of magnitude. The stack energy density of current cells provide amount to 70% of the go/no-go goal.

Task 4.1 – Understanding and Mitigating Interfacial Reactivity between Electrode and Electrolyte (Khalil Amine, Larry A. Curtiss, and Nenad Markovic, Argonne National Laboratory)

Project Objective. This project aims to develop an understanding, at atomic/molecular levels, of the stability of electrochemical interfaces during charge-discharge cycling and to use the knowledge for stabilizing solid/liquid interfaces in Li-ion batteries. The goal is to improve stability of solid/liquid interfaces using insights into the atomic/molecular processes that limit stability during cycling. The core objective is to identify, rationalize, and understand the dynamics of the dissolution processes of 3D-TM cations in the cathode materials, stability of various commercial and highly purified electrolytes comprised of organic solvents, salts, and additives, and evolution of O₂ and other gaseous products formed from the electrode material or the electrolyte during the charging-discharging of the Li-ion battery.

Project Impact. The instability of the solid-liquid interfaces during cycling limits use of novel cathodes such as 6:2:2 and 8:1:1 NMC cathodes with higher voltage and higher power densities. Stabilization of solid/liquid interfaces in Li-ion batteries can lead to enhanced performance and increased safety.

Approach. This project follows an integrated program focused on solid-liquid interfaces in Li-ion batteries using state-of-the-art *in situ* characterization tools and computational modeling to understand and design interfaces with enhanced stability. The range of high-end analytical tools includes the following: (1) a three-electrode rotating disk electrode (RDE) setup; (2) ICP-MS; (3) GC with Triple Quadrupole MS (GC-QqQ) in Headspace sampling mode; and (4) differential electrochemical MS (DEMS). High-precision electrochemical measurements in combination with *in situ* measurements and characterization are highly suitable to investigate correlation of stability with various electrochemical, structural, and compositional properties of interfaces. Computational methods that provide reaction energies and barriers as well as structural information at the atomic level will be used to predict and test possible reactions that affect stability of solid-liquid interfaces.

Out-Year Goals. Work will progress toward more comprehensive *in situ* characterization and integrated modeling capabilities with applications to solid-liquid interfaces of electrolytes and 6:2:2 NMC cathodes. If the project can harness the complexity that governs interface instability, it should be able to move far beyond current state-of-the-art Li-ion systems and create new avenues to design and deploy cathode materials and electrolytes.

Collaborations. This project collaborates with Jun Liu at PNNL and X. He at Tsinghua University. At ANL, Zonghai Chen, Sanja Tepavcevic, Pietro Papa Lopes, and Peter Zapol contribute to the project.

Milestones

1. Perform first *ex situ* measurements of electrode/electrolyte decomposition products using ICP-MS and GC-MS. (Q1 – Complete)
2. Develop protocol for calculating electrochemical reactions at electrolyte-electrode interfaces. (Q1 – Complete)
3. Build a new 16-channel high-precision electrochemical measurement system dedicated to this project. (Q2 – Complete)
4. Benchmark the kinetics of direct electrochemical oxidation of baseline electrolyte at different potentials. (Q3 – Complete)
5. Couple ICP-MS with electrochemical cell for direct *in situ* investigation of metal dissolution from the cathode. (Q4 – In progress)

Progress Report

The project finished benchmarking the newly developed high-precision electrochemical measuring system for stability studies by applying it to the anodic dissolution of aluminum foils in nonaqueous electrolytes. It found that the measured static leakage current grows roughly exponentially with the applied potential, indicating an ongoing electrochemical oxidation of electrolyte on the carbon-coated aluminum foil. From analysis of data along with theoretical calculations, the project derived a hypothesis for corrosion of aluminum used in current collectors.

Previously, it had found that measured static leakage current grows roughly exponentially with the applied potential, indicating an ongoing electrochemical oxidation of electrolyte on the carbon-coated aluminum foil. The measured parasitic current increased exponentially with the holding potential, indicating an electrochemical oxidation of a certain species on the aluminum foil. The role of carbon was further investigated given that carbon is mostly resistive to chemical corrosion in an acidic environment. A layer of carbon black was deposited on the surface of the aluminum foil. The electrochemical characterization showed that the static parasitic current measured increased almost 10-fold (see Figure 24a), compared to previous findings for non-coated aluminum foil. This increase of parasitic current could be a result of either an increase in the active electrochemical surface area or a decrease of charge transfer impedance at the interface of the aluminum foil. Considering the high loading of carbon black physically cast on the sample, the high parasitic current shown in Figure 24a must be dominated by the reduction of charge transfer impedance across the interface due to the carbon coating, which

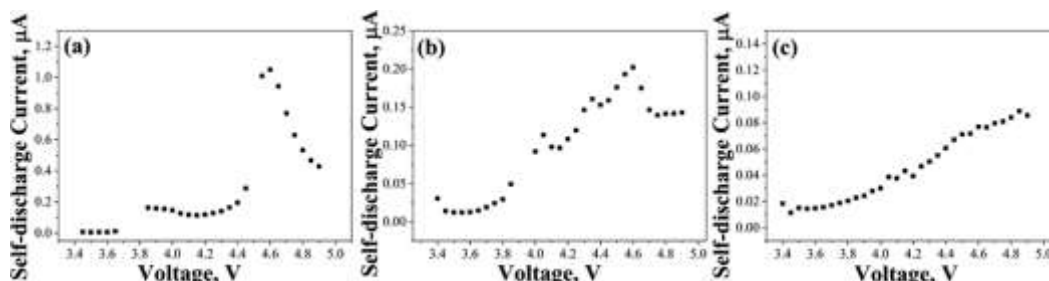


Figure 24. Potential dependence on the static parasitic current for aluminum foil with surface coating of (a) carbon, (b) graphene, and (c) AlPO_4 .

is intended to protect the aluminum foil from the chemical corrosion in an acidic environment. In addition, graphene with a low out-of-plane electronic conductivity was also deposited on the aluminum foil. The results showed that the measured parasitic current was substantially lower than that for the carbon-coated samples, but not better than that for the uncoated sample (see Figure 24b). Finally, AlPO_4 , which is an electronic insulator and also resistive to corrosion in an acidic environment, was coated on the surface of aluminum foil, and a dramatic change in the parasitic current was observed with the AlPO_4 coating (see Figure 24c). First, the corrosion window shown at about 3.9 V completely disappeared because the coating layer is resistive toward reaction with protons, resulting in a constant charge transfer impedance throughout the whole course of the potential sweep. In addition, the maximum parasitic current measured for the AlPO_4 -coated sample was about 50% that of the non-coated sample, implying that a significantly smaller amount of proton is expected at similar operation conditions. Thus, these results further confirm the hypothesis that the corrosion reaction of aluminum foil at a relatively high potential is a coupled electrochemical–chemical reaction, as illustrated in the schematic shown in Figure 25.

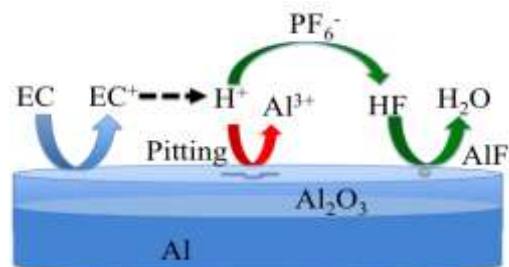


Figure 25. Schematic showing the proposed coupled electrochemical chemical reaction on the aluminum surface at a relatively high potential.

Task 4.2 – Advanced Lithium-Ion Battery Technology: High-Voltage Electrolyte (Joe Sunstrom and Ron Hendershot, Daikin)

Project Objective. The overall project objective is to identify electrolyte formulations, based on fluoro-chemistries, that will allow significantly improved operating voltage, increased durability, and increased energy density of Li-ion batteries at a reasonable cost. The project objective is to understand the conditions under which the electrolyte degrades, the effect on battery performance, and solutions that can overcome current limitations of the electrolyte. The strategy is to select from a range of available fluorinated chemistries those combinations that provide the highest possible battery voltages, greater than 4.5 V, while keeping incremental battery cost increase as low as possible.

Project Impact. An understanding of the failure mechanisms for both state-of-the-art hydrocarbon and fluorocarbon electrolytes as they pertain to various cell chemistries is ultimately valuable in the design of future high-performance batteries. Electrolyte degradation has been a key limiting factor in development of new Li-ion technology. The ability to stop or significantly slow this degradation opens a whole new level of design for rechargeable batteries.

Approach. The evolving composition of the electrolyte in the battery will be examined by a variety of analytical instrumentation to study the gas (GC/MS), liquid chromatography (LC/MS), and solid (TOF-SIMS, thermogravimetric analysis (TGA)/MS, XRD) electrolyte decomposition products during battery operation. In the first year, the team will address the gas composition and kinetics for both hydrocarbon and fluorocarbon as a function of several charge/discharge conditions that include (but are not limited to) electrode composition, operational voltage and current, temperature, and cycle number.

Out-Year Goals. Work will progress toward formulating rough mass balances of both the fluorinated and hydrocarbon electrolytes under the performance parameters suggested. Specifically, analysis of the liquid and solid decomposition products will be pursued. Understanding how the mass balance and kinetics change will give information on decomposition pathways and allow for solutions to be formulated to increase battery performance.

Milestones

1. Determination of gas composition. Failure mechanisms are understood, and mitigation strategies/additives are selected for interim cells. (Initiated December 2016 – Delayed)
2. Gassing kinetics of FEC. (Delayed start until August 2017)

Progress Report

This quarter, there have been delays in milestones due to the shipping/handling schedule for two pieces of key equipment. This equipment includes a new Arbin battery tester and additional glove box, which are necessary for sample preparation to complete the project. The battery tester will increase the testing capability from 20 channels to 104 channels. The glovebox is needed for additional battery fabrication. Delivery of both pieces of equipment was taken in June 2017, with installation and training to be completed in July 2017. Currently, sample preparation/testing is in a bottle neck. A set of 8 samples for chromatography analysis takes approximately 6 weeks to prepare.

In the interim period, additional baseline experiments are being completed to characterize all starting materials in the project. These starting materials include components of the electrolyte as well as characterization of the battery electrodes before battery fabrication.

GC-MS of the Daikin fluoroether is shown in Figure 26. Due to the methods used in the synthesis of the ether, purification of the ether and quantification of side products are important. Any side products contained in the ether may interrupt film formation on the battery electrodes and lead to non-reproducible results. The GC-MS results show a highly pure (> 99.99 percent) of the target fluoroether.

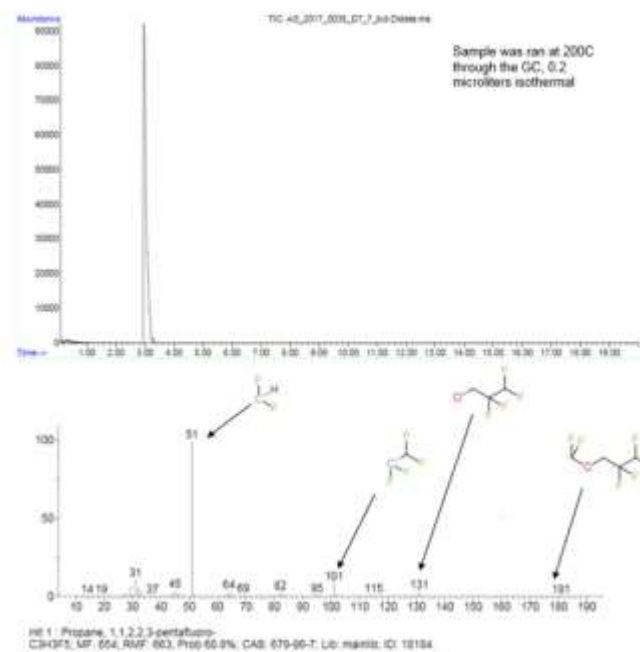


Figure 26. Gas chromatography (top) and mass spectrometry (bottom) of the native D7 fluoroether used in Daikin electrolytes.

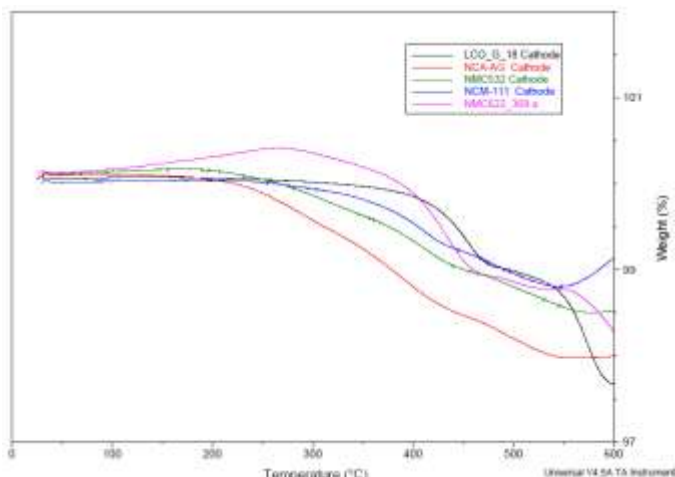


Figure 27. Thermogravimetric analysis traces for all cathodes used in this project (LCO, NMC-111, NMC-532, NMC-622, and NCA).

In addition, baseline scans for all the electrodes for thermal analysis have been completed. An example of this is found in Figure 27, which shows TGA of all cathode chemistries used in this project. These baselines will be used as comparison for later experiments on the same electrodes after cycling. The post-cycling electrodes will be examined by TGA analysis with GC-MS detection of species to understand trapped/intercalated species.

A review of this project was given at the DOE Annual Merit Review in June. Additional personnel (two co-ops and a post-doctoral student) are in the process of being hired.

Patents/Publications/Presentations

Presentation

- DOE Annual Merit Review, Washington, D. C. (June 5–8, 2017): “Daikin Advanced Lithium-Ion Battery Technology – High Voltage Electrolyte”; Joseph Sunstrom, Abundio Sandoval, Michael Gilmore, and Ron Hendershot.

Task 4.3 – Multi-Functional, Self-Healing Polyelectrolyte Gels for Long-Cycle-Life, High-Capacity Sulfur Cathodes in Lithium-Sulfur Batteries (Alex Jen and Jihui Yang, University of Washington)

Project Objective. The project objective is to develop self-healing and polysulfide-trapping polyelectrolyte gels containing room-temperature ionic liquid (RTIL) for the Li-S battery system. The battery design will be capable of achieving gravimetric and volumetric energy densities of ≥ 800 Wh/kg and ≥ 1000 Wh/L, respectively.

Project Impact. The Li-S battery system is currently hampered by poor capacity retention, primarily caused by dissolution of polysulfide reaction intermediates in typical organic electrolytes, as well as poor electrical contact between insulating sulfur and the conductive carbon matrix. This project aims to produce a high-capacity, long-cycle-life Li-S battery system by using rational molecular design strategies to address each capacity loss mechanism directly. A long-cycle-life Li-S battery system with the capability of doubling Li-ion energy density would enable production of lighter, longer range EVs at a cost that is affordable to the average U.S. household.

Approach. The team will develop Li-S coin cells that utilize self-healing, interpenetrated ionomer gel electrolytes in both the cathode and separator. The team will synthesize necessary starting materials and fabricate components of these gels while testing their relevant electrochemical and mechanical properties. All components will be combined into interpenetrating structures, which will be tested both alone and in cell configurations. Device performance data will be collected and used to further optimize designs of both material and cell, culminating in an optimized Li-S battery design capable of doubling the energy density of traditional Li-ion batteries. During the first year, the team is focusing on (1) synthesis of a variety of precursors for gel electrolytes, (2) fabrication and testing of both baseline materials and novel materials made from these precursors, and (3) iterative validation and improvement of design principles through both materials and device testing.

Out-Year Goals. Work will progress toward developing structure-property relationships for the self-healing, interpenetrated gel ionomer electrolyte and its individual components, as well as successful incorporation of such an electrolyte into a working Li-S cell. The team plans to demonstrate significant improvements in both capacity and retention when using the project's novel materials, as compared to state-of-the-art baseline systems.

Collaborations. This project funds work at UW. Dr. Alex Jen (PI) focuses on the design, synthesis, and testing of novel materials, as well as device-based verification of design principles. Dr. Jihui Yang (Co-PI) focuses on optimization of device fabrication and testing, as well as investigation of failure mechanisms in devices using novel materials. Facilities at PNNL will be used for detailed study of device operation.

Milestones

1. Synthesize organic starting materials, and demonstrate both an ionomer gel electrolyte and a self-healing film based on these materials. (Q3 – Completed June 2017)
2. Integrate S/C composites into Li-S coin cells, and cycle them both with an organic electrolyte system and with several novel gel electrolyte systems. (Q4 – Initiated in January 2017)

Progress Report

Ionomer Gel Fabrication. Several polyelectrolyte gel formulations of varying composition were tested for their ability to form free-standing films. The films were fabricated by mixing ionic liquid and monomer components in air, and transferring into an argon filled glovebox where the precursor solution was loaded into molds of 0.1mm thickness. These molds were sealed using rare-earth magnets and loaded into an oven at 80°C to cure over 4 hours. While the project was successful at producing free-standing polyelectrolyte gel films this way (Figure 28), the gels produced were too mechanically fragile for reliable property testing. Further optimization of precursor composition and fabrication conditions is under way.



Figure 28. A polyelectrolyte gel prepared using ionic liquid, cross-linkable poly(ethylene glycol) chains, and ionic-liquid-like monomer.

Self-Healing Materials. A second-generation self-healing system was developed by changing the length of the carbon tail on PENDI (Figure 29). The differences in physical properties of the polymers are summarized in Table 1 below. The purpose of this change was to modulate self-healing properties and conditions by controlling the strength of interactions between naphthalene diimide (NDI) and pyrene (Py) groups. Ultraviolet-visible (UV-Vis) dilution analysis indeed showed that changing the carbon tail decreased PENDI/Py linker binding strength from -12.44 kJ/mol in PENDI-C3 to -9.43 kJ/mol in PENDI-C6. The project postulates that this is due to increased steric repulsion between the NDI pendants and Py linker arms. Differential scanning calorimetry (DSC) data showed a decrease in T_g between the polymers of 55°C, suggesting decreased interchain interactions and higher chain mobility.



Figure 29. Structures of PENDI-C3 and PENDI-C6.

Table 1. Gen 1/2 polymer properties.

Property (Measurement)	PENDI-C3	PENDI-C6
M_n (GPC)	34.6 kDa	102.4 kDa
PDI (GPC)	1.09	1.30
T_g (DSC)	168°C	113°C

Using PENDI-C6 and Py linker, a self-healing film with the ability to clearly heal a total fracture in 4 h at the moderate temperature of 40°C was demonstrated (Figure 30a-b). By contrast, a film made using PENDI-C3 was not able to self-heal at this temperature even after 16 h (Figure 30c-d), instead requiring 60°C before the onset of self-healing. Work is ongoing to demonstrate self-healing at room temperature, as well as quantitatively evaluating the film's mechanical properties and self-healing efficiency.

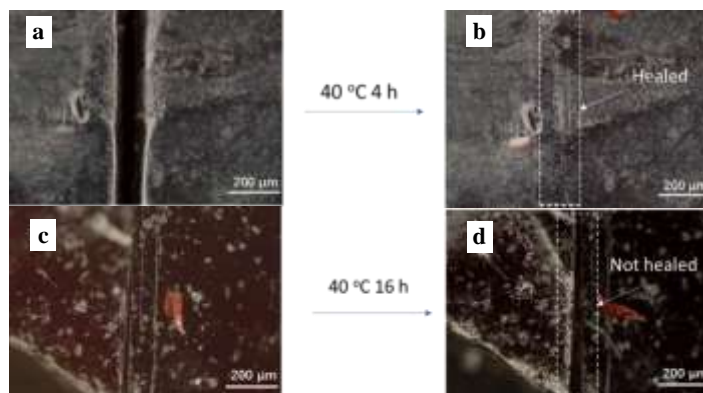


Figure 30. (a, b) A film made of PENDI-C6 and pyrene (Py) Linker (1:1 naphthalene diimide [NDI]/Py molar ratio) self-healed after 4 hours at 40°C. (c, d) A film made of PENDI-C3 and Py Linker (1:1 NDI/Py molar ratio) was not self-healed at 40°C, even after 16 hours.

Mesoporous Carbon Functionalization and C/S Composite Synthesis. A thiophenol-based organic modifier group was introduced onto mesoporous carbon surfaces by the previously reported diazonium-chemistry. The thiol (-SH) group is known to be capable of forming reversible sulfur-sulfur covalent bonds with other sulfur species, mediated by electron exchange with different substrates. This makes them potentially well-suited as chemical trapping agents for lithium polysulfides, capable of forming covalent bonds with them to prevent their escape from the conductive carbon matrix. Successful functionalization of thiophenol onto MH00, a mesoporous carbon from Toyo Tanso with 4-nm average pore size, was confirmed via TGA and XPS analysis. Thiophenol was also functionalized onto the surfaces of carbons containing larger pore sizes—MJ410 (10-nm pores), MJ430 (30-nm pores), and MJ150 (150-nm pores)—to study the interplay between modifier chemistry and pore size on overall cell performance. All four of these carbons, both functionalized and as-received, were infiltrated with elemental sulfur (60 wt%) using melt-diffusion at 155°C. C/S composite formation was confirmed using XRD and TGA.

Li-S Concept Cell Test. MH00 C/S composites containing thiophenol modifiers were cycled at C/10 (Figure 31a), producing mixed results: on one hand, specific capacity underwent a sharp decrease as compared to unmodified samples, primarily due to a significant increase in overpotential (Figure 32a) that caused the cathode to reach its voltage cutoffs prematurely. However, capacity retention over 20+ cycles dramatically improved; in fact, by 40 cycles, capacities of modified and unmodified samples had nearly converged. The project theorizes that thiophenol groups can indeed bond to polysulfides covalently, removing them from the liquid phase as intended, which improves capacity retention; on the other hand, this process forces the redox chemistry of the cell to proceed largely through solid-state reactions in confined spaces, producing the observed overpotential increase due to inhibited diffusion of lithium. This is exacerbated by the significant shrinkage of average pore size (4 nm \rightarrow 2 nm) induced by modification in MH00.

The hypothesis on modifier behavior is supported by data from carbons with larger pore sizes (Figure 31b-d and Figure 32b-d), which show that increasing pore size generally decreases overpotential and increases overall capacity, while retention behavior is retained. This is likely due to the lessening of diffusion overpotentials. In fact, when cells are cycled at C/20 instead of C/10, the lower discharge plateau in modified samples recovers to its original, flatter shape. Investigation continues into these materials and improved modifiers.

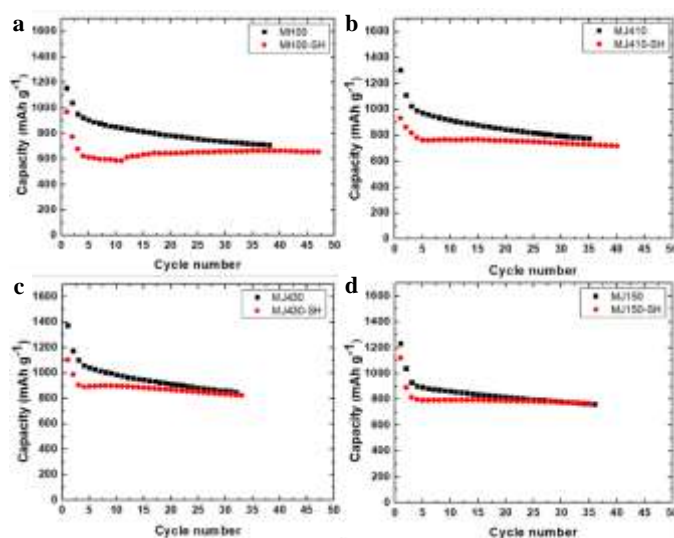


Figure 31. Cycling data (C/10) of as-received and phenylthiol-modified mesoporous carbons with majority pore sizes of (a) 4 nm, (b) 10 nm, (c) 30 nm, and (d) 150 nm.

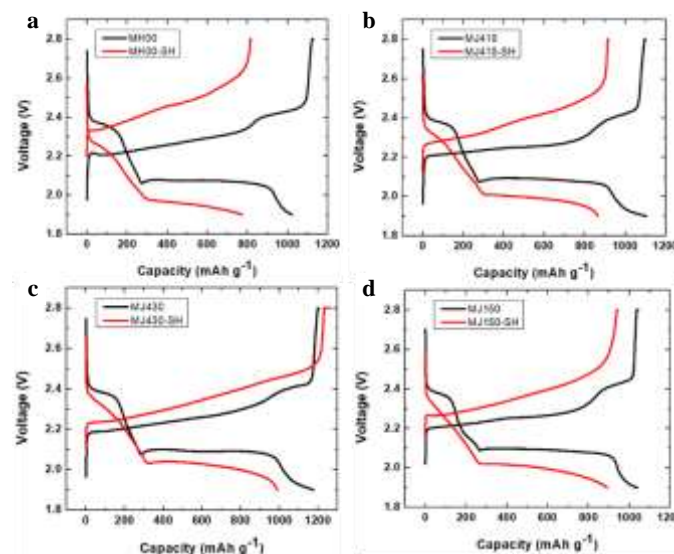


Figure 32. Second-cycle voltage profile (C/10) of as-received and thiophenol-modified mesoporous carbons with majority pore sizes of (a) 4 nm, (b) 10 nm, (c) 30 nm, and (d) 150 nm.

Task 4.4 – Development of Ion-Conducting Inorganic Nanofibers and Polymers (Nianqiang (Nick) Wu, West Virginia University; Xiangwu Zhang, North Carolina State University)

Project Objective. The project objective is to develop solid-state electrolytes (SSEs) based on the highly-conductive inorganic nanofibrous network in the polymer matrix for lithium batteries.

Project Impact. The research team will conduct R&D on solid-state inorganic nanofiber-polymer composite electrolytes that will not only provide higher ionic conductivity, improved mechanical strength, and better stability than the polyethylene oxide polymer electrolyte, but also exhibit better mechanical integrity, easier incorporation, and better compatibility with the Li-metal anode than the planar ceramic membrane counterparts. The proposed inorganic nanofiber-polymer composite electrolytes will enable practical use of high-energy-density, high-power-density Li-metal batteries and Li-S batteries.

Approach. Integration of the highly Li⁺-conductive inorganic nanofiber network into the polymer matrix not only provides the continuous Li⁺ transport channels, but also kinetically inhibits the crystallization from the amorphous state of polymer electrolyte. The inorganic nanofibers will be fabricated with an electrospinning technique; and the ionic conductivity of inorganic nanofibers will be improved by chemical substitution or doping. Highly ionic-conductive polymers will be developed by cross-linking and/or creation of a block-copolymer structure; the composition and microstructure of the composite electrolyte will be designed to suppress the lithium dendrite formation.

Out-Year Goals. Work will progress toward synthesis of the inorganic nanofibers and the polymer matrix. The goal is to find the optimal synthetic route to achieve the desirable conductivity.

Collaborations. This project funds work at WVU and North Carolina State University (NCSU). Dr. Nianqiang (Nick) Wu at WVU serves as PI, and Dr. Xiangwu Zhang at NCSU acts as Co-PI. Sujan Kasani (Ph.D. student at WVU), Hui Yang (Postdoctoral Fellow at WVU), Botong Liu (Ph.D. student at WVU), Chaoyi Yan (Ph.D. student at NCSU) and Mahmut Dirican (Postdoctoral Fellow at NCSU) contributed to the project.

Milestones

1. **Subtask 1.1.4.** Test the temperature-dependence ionic conductivity of inorganic nanofibers, and the bulk and grain-boundary conductivity. (Q3 – April 2017; In progress, 90%)
2. **Subtask 1.1.5.** Dope the lithium lanthanum zirconium oxide (LLZO) with aluminum, and study the effects of aluminum on the ionic conductivity as well as the thermal, mechanical, and electrochemical stability. (Q3 – April 2017; In progress, 80%)
3. **Subtask 1.2.2.** Synthesize the ion-conducting polymers. (Q3 – April 2017; Completed, 90%)
4. **Subtask 1.2.3.** Characterize the chemical composition, the phase, and the structure of ion-conducting polymers. (Q3 – April 2017; Completed, 80%)
5. **Subtask 1.2.4.** Test the temperature-dependence ionic conductivity of polymers and other properties. (Q3 – April 2017; In progress, 75%)

Progress Report

This quarter, the project improved the ionic conductivity of inorganic Perovskite-type LLTO nanofibers from 7.7×10^{-4} S/cm to 1.08×10^{-3} S/cm through 0.5% aluminum doping. Highly ionic-conductive Garnet-type LLZO nanofibers with desirable cubic phase structure were obtained at a lower heating rate. For the polymer matrix, the project completed synthesis of Li[PSTFSI-*b*-MPEGA-*b*-PSTFSI] triblock copolymer and cross-linked PE/PEO polymer. The ionic conductivity of PE/PEO cross-linked polymer reached up to 1.15×10^{-4} at room temperature. The project fabricated and investigated the ionic conductivity of composite electrolytes based on the synthesized nanofibers and polymers.

Task 1.1.2 - Synthesis of Inorganic Nanofibers

LLZO Nanofibers

The highly ionic-conductive LLZO nanofibers with desirable cubic phase structure and fibrous morphology were successfully obtained after calcination of electrospun LLZO precursor nanofibers at a lower heating rate of $1^\circ\text{C}/\text{min}$. The PEO/LiTFSI/LLZO solid composite electrolytes were prepared by dispersing LLZO nanofibers in PEO/LiTFSI salt/acetonitrile solution. At room temperature, the calculated ionic conductivity of the PEO/LiTFSI/LLZO composite electrolyte, with 15 wt% LLZO nanofibers based on total PEO and LiTFSI amount, was 2.95×10^{-4} S/cm.

LLTO Nanofibers

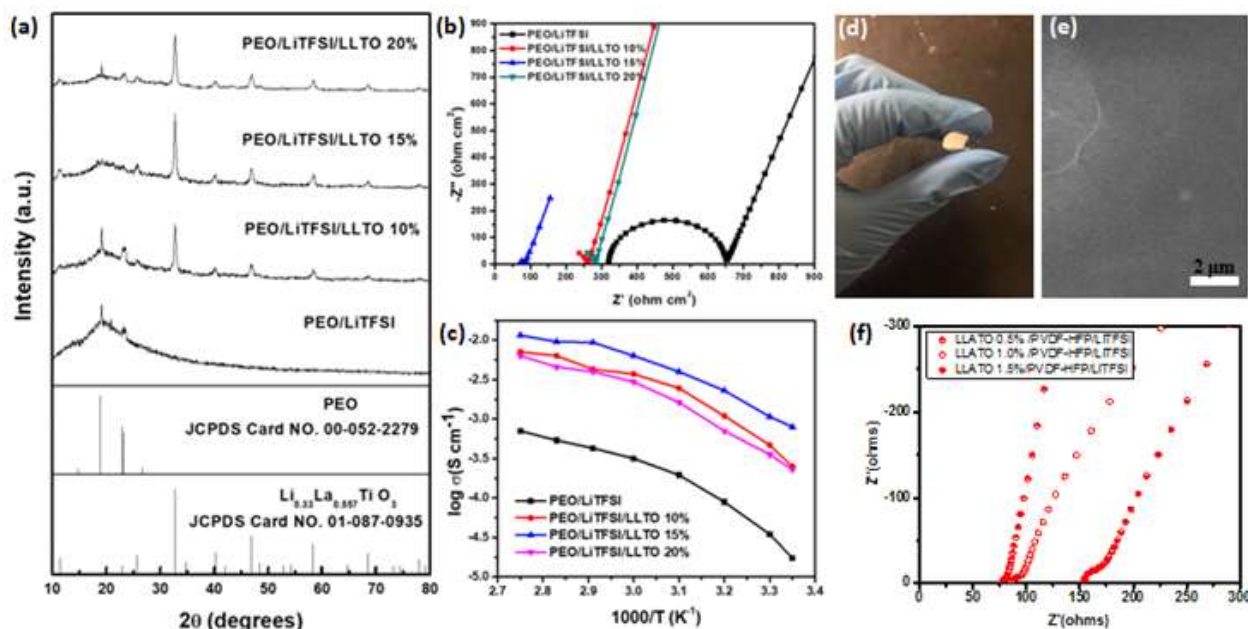


Figure 33. (a) X-ray diffraction patterns. (b) Electrochemical impedance spectroscopy (EIS) curves of the PEO/LiTFSI/LLTO solid composite electrolytes with different LLTO nanofiber contents. (c) Arrhenius plots of PEO/LiTFSI and PEO/LiTFSI/LLTO. (d-e) Photograph and top scanning electron microscopy of flexible and bendable PVDF-HFP/LiTFSI/LLATO 0.5% membrane. (f) EIS curves of the PVDF-HFP/LiTFSI/LLATO solid composite electrolytes with different aluminum doping percentage.

Perovskite-type LLTO nanofibers were successfully synthesized; the LLTO pellet exhibited an ionic conductivity of 7.7×10^{-4} S/cm. The ionic conductivity can be improved to 1.08×10^{-3} S/cm through 0.5% aluminum doping.

The composite electrolyte based on the LLTO or the aluminum-doped LLATO nanofibers has been fabricated. The PEO/LiTFSI/LLTO composite electrolyte (Figure 33a), with 15 wt% of LLTO nanofibers based on total PEO and LiTFSI amount, showed ionic conductivity of 3.31×10^{-4} S/cm at room temperature, as shown in Figure 33b. The PVDF-HFP/LiTFSI/LLATO composite electrolyte membrane was fabricated by dropping LiTFSI and PVDF-HFP acetone solution onto the calcinated nanofiber membrane, which displayed high ionic conductivity of 3.98×10^{-4} S/cm and yet retained its excellent mechanical stability (Figure 33d). This was higher than that of the reported LLZO based 2.5×10^{-4} S/cm.

Task 1.2.2 - Synthesis of Polymer Matrix

Li[PSTFSI-*b*-MPEGA-*b*-PSTFSI] Triblock Copolymer

The Li[PSTFSI-co-MPEGA] random copolymer and the Li[PSTFSI-*b*-MPEGA-*b*-PSTFSI] block copolymer were synthesized using (4-styrenesulfonyl) (trifluoromethanesulfonyl)imide (STFSI) and methoxy-polyethylene glycol acrylate (MPEGA) monomers through free radical polymerization and nitroxide-mediated polymerization (NMP), exhibiting ionic conductivity of 3.03×10^{-5} S/cm and 1.75×10^{-5} S/cm, respectively.

Cross-Linked PE/PEO Polymer with LiTFSI Salt

The cross-linked PE/PEO polymers were synthesized using butyl acrylate (BA) as the PE monomer and poly(ethylene glycol) dimethacrylate (PEGDMA) as the cross-linker. The cross-linked polymer with concentration of lithium salt to triblock copolymer $[\text{EO}]/[\text{Li}^+] = 24$ showed the highest ionic conductivity of 1.15×10^{-4} S cm^{-1} at room temperature.

Task 2.1 - Development of Inorganic Nanofibers-Polymer Composites

Inorganic Nanofibers/Li[PSTFSI-co-MPEGA] Copolymer Composite Electrolytes

The Li[PSTFSI-co-MPEGA] random copolymer/inorganic nanofiber composite solid electrolytes with 15 wt% LLTO and 15 wt% LLZO nanofiber fillers were prepared. At room temperature, the ionic conductivities of Li[PSTFSI-co-MPEGA]/LLTO (15 wt%) and Li[PSTFSI-co-MPEGA]/LLAZO (15 wt%) were 1.56×10^{-4} S/cm and 1.01×10^{-4} S/cm, respectively.

Inorganic Nanofibers/Cross-Linked PE/PEO Polymer Composite Electrolytes

Introducing the LLTO nanofibers in cross-linked PE/PEO polymers resulted in huge improvements on the ionic conductivity. The ionic conductivity of 15 wt% LLTO nanofiber dispersed cross-linked PE/PEO polymers composite solid electrolytes reached 6.25×10^{-4} S/cm at room temperature.

Task 4.5 – High Conductivity and Flexible Hybrid Solid-State Electrolyte (Eric Wachsmann, Liangbing Hu, and Yifei Mo, University of Maryland)

Project Objective. The project objective is to develop flexible hybrid electrolyte with garnet nanofibers to achieve the following: (1) flexible, with greater mechanical strength (~ 10 MPa) and thermal stability than polymer electrolytes; (2) high room-temperature ionic conductivity, ~ 0.5 mS/cm; (3) stable interface with lithium metal and effective blocking of lithium dendrites at current densities up to 3 mA/cm²; and (4) battery performance with Li-S chemistry with an energy density of ≥ 450 Wh/kg and (≥ 1000 Wh/L) and maintaining $\geq 80\%$ of capacity up to 500 cycles.

Project Impact. Instability and/or high resistance at the interface of lithium metal with various solid electrolytes limit the use of the metallic anode for batteries with high energy density, such as Li-air and Li-S batteries. The critical impact of this endeavor will be focused on developing a new type of SSE that is highly conductive, highly flexible, and electrochemically stable. The new SSE will enable Li-metal anodes with excellent interfacial impedance and blocking of lithium dendrite formation.

Approach. The project will synthesize garnet nanofibers, fill the porous region with polymer electrolyte, and characterize the flexible hybrid membrane properties. The flexible hybrid SSE microstructure will be determined using FIB/SEM and integrated with electrochemical methods to investigate the properties and stability with Li-metal anode.

Out-Year Goals. The project will develop a fundamental understanding of the mechanism of Li-ionic diffusion in garnet nanofibers and their mechanical properties, as well as these properties for hybrid garnet-fiber/polymer hybrids. Work will progress toward the study of the electrode assembly during electrochemical cycling of the anode.

Collaborations. This project funds work at UMD, College Park. Dr. Eric D. Wachsmann (PI) will focus on optimizing the garnet network to achieve high ionic conductivity and flexibility using FIB/SEM and EIS characterization. Dr. Liangbing Hu (Co-PI) focuses on synthesis of the hybrid electrolyte and test for Li-metal anode with the hybrid electrolyte. Dr. Yifei Mo (Co-PI) will lead efforts on computational modeling of the garnet nanofiber hybrid electrolytes for fundamental mechanistic understanding.

Milestones

1. Fabricate 4-cm by 4-cm garnet nanofiber membrane. (Q1 – Completed December 2016)
2. Synthesize ion-conductive polymers, synthesize ion-insulation polymers, and *in situ* synthesize polymer electrolyte coated garnet nanofibers. (Q2 – Completed March 2017)
3. Understand Li-ionic diffusion in garnet nanofibers and its response to mechanical deformation. (Q3 – Completed June 2017)
4. Achieve hybrid SSE with high ionic conductivity ($\sim 0.5 \times 10^{-3}$ S/cm), high electrochemical stability (~ 4.5 V), and high mechanical property. (Q4 – Initiated March 2017)

Progress Report

To perform molecular dynamics (MD) simulations for garnet nanofibers, the project implemented and tested force fields for lithium garnet $\text{Li}_7\text{La}_3\text{Zr}_2\text{O}_{12}$ (LLZO). Using the newly tested force field, the lattice parameters in tetragonal and cubic phases of LLZO were calculated using MD simulations as a function of temperature, in good agreement with experimental values. Li^+ diffusion in LLZO was also modeled using MD simulations. The calculated Li^+ conductivity and activation energy of LLZO are in good agreement with *ab initio* calculations and experimental measured values.

Atomistic model of garnet nanofibers was constructed and equilibrated in MD simulations (Figure 34). The Li^+ transport in single garnet nanofiber was modeled using MD simulations at different temperatures. The Li^+ conductivities at different temperatures and the activation energies for Li^+ diffusion are calculated in single garnet nanofibers. The Li^+ diffusion properties from MD simulations were compared to the bulk phase of LLZO and show faster Li^+ diffusion in single garnet nanofibers. In addition, Li^+ migration mechanism was analyzed for Li^+ transport along and perpendicular to the nanofiber direction, and at surface and core regions of the nanofiber. Insight into Li^+ diffusion in garnet nanofiber was obtained.

Mechanical deformation on garnet bulk and nanofiber was performed under MD simulations. The elastic modulus from these calculations are in good agreement with experiments and previous studies. The Li^+ diffusion under mechanical deformation was studied using MD simulations (Figure 35). The project simulated the garnet at both tensile and compressive stress with different strain (1% and 3%). It found the mechanical deformation has significant impact on Li^+ diffusion. Li conductivity decreases and activation energy increases in both stressed states. This change is in good agreement with experiments. The MD simulations in both bulk and nanofiber show similar results. Mechanical deformation decreases Li^+ conductivity in garnet. Both tensile and compressive deformation drives garnet toward slow-conducting tetragonal phase. In summary, MD simulations were performed to understand Li^+ diffusion in garnet nanofibers and the effect of mechanical deformation.

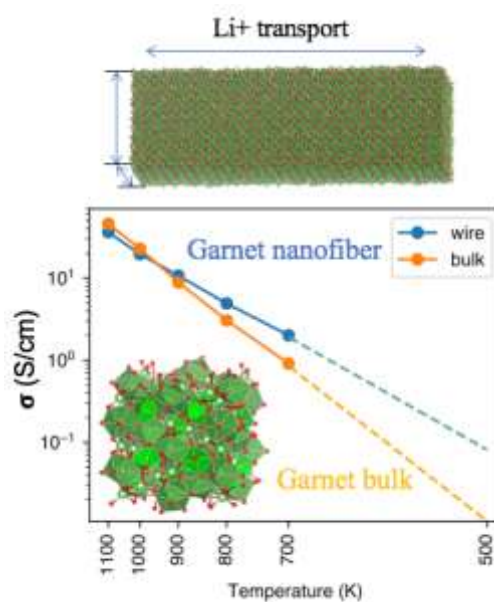


Figure 34. Computer modeling of Li^+ transport in garnet nanofibers.

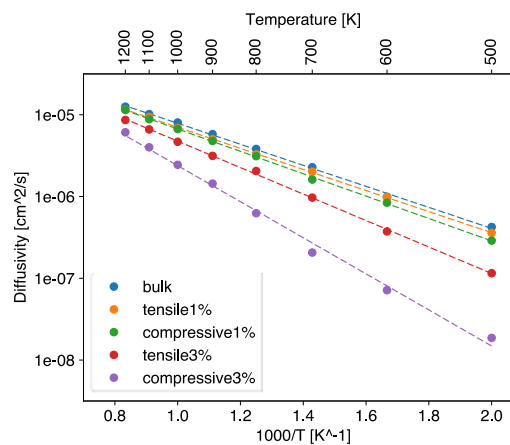


Figure 35. Lithium diffusion of garnet under strain.

Patents/Publications/Presentations

Presentations

- 21st International Conference on Solid State Ionics, Padua, Italy (June 23 – 29, 2017): “All-Solid-State Li-Ion Batteries for Transformational Energy Storage”; Eric Wachsman. Invited.
- Beyond Lithium Ion Symposium-10 (BLI-X), IBM, Almaden, California (June 27 – 29, 2017): “Enabling All-Solid-State Li-Ion Batteries through Computation-Guided Design of Materials and Interfaces”; Yifei Mo. Invited.
- 17th Annual Advanced Automotive Battery Conference, San Francisco, California (June 2017): “Computation-Guided Understanding and Design of Interfaces in All-Solid-State Li-ion Batteries”; Yifei Mo. Invited.
- University of California, Berkeley, California (April 6, 2017): “All-Solid-State Li-ion Batteries for Transformational Energy Storage”; Eric Wachsman. Invited.

Task 4.6 – Self-Forming Thin Interphases and Electrodes Enabling 3D Structured High-Energy-Density Batteries (Glenn Amatucci, Rutgers University)

Project Objective. The project objective is to develop and implement a novel *in situ* formed lithium-metal-based metal fluoride battery that will enable packaged 10 mAh batteries of energy densities > 1000 Wh/L and > 400 Wh/kg at 12 V.

Approach. The project focuses on the coalescence of three main aspects of the baseline technology, corresponding to the three sub-tasks of the project: the self-forming chemistry comprised of electrodes and electrolyte, electrode and electrolyte fabrication, and cell design.

Impact. Successful realization of 3D batteries formed *in situ* with a practical approach to large-scale fabrication would address some of the DOE EV performance goals, including: (1) areal capacity increase, (2) improved rates, and (3) designs to enable high-voltage unit cells.

Milestones

6. Establish positive reactive current collector compositions that achieve 50% of the theoretical energy density. (June 2017 – In progress; *Note:* On schedule for completion by Q4 end. Compositions achieved 20% of theoretical energy density)
7. Establish negative reactive current collector compositions with uniform Li-plating after *in situ* formation showing $< 30\%$ variation of the plated-Li thickness. (June 2017 – In progress; *Note:* This milestone was initially set to characterize reactions at negative reactive current collector. Although there is still interest in characterizing Li-plating reaction at the negative electrode, it is not critical to achieve the *Go/No-Go* goal. Resources initially associated here would have a more significant impact if redirected to optimize cell chemistry and architecture, which can be achieved faster. This milestone could be revisited in FY 2018/2019 if the DOE deems this milestone important for project success.
8. Establish a bi-ion solid-state conducting glass composition with ionic conductivity $> 1 \times 10^{-4}$ S/cm prior to *in situ* formation. (June 2017 – Concluded in Q1; *Note:* Greater than 1×10^{-5} S/cm achieved pre-formation, and $> 1 \times 10^{-4}$ S/cm achieved post formation. No additional focus this year, as sufficient results achieved.
9. Establish cell-stack design to achieve the first *Go/No-Go* point with 50% utilization of the positive reactive current collector. (June 2017 – In progress; *Note:* The stack energy density in Wh/L is the electrochemical characterization metric primarily focused on during full cell evaluation and optimization. As such, project progress was assessed based on advance in stack energy density. Significant improvement was achieved, from 5% of the 500 Wh/L goal in Q2 to 70% in Q3. Milestone #1 statements are directly related to use of the positive current collector addressed by this milestone.
10. *Go/No Go:* Achieve self-formed cell-stack with > 500 Wh/L and 200 Wh/kg at a rate of C/10, and $> 80\%$ capacity retention after 25 cycles. *Note:* The project has been progressing rapidly toward year-end goals and has achieved 70% of the 500 Wh/L goal in Q3, although at lower rate. It is anticipated that the energy density goal of > 500 Wh/L will be achieved along with 200 Wh/kg by the end of Q4, as scheduled. Since the project is establishing a potential new paradigm in energy storage technology, it has focused effort on achievement of energy density goals rather than capacity retention, which it proposes to address in FY 2018.

Progress Report

Full Cell Performance Optimization. Following the conclusion late last quarter, the project has transferred exclusively to the maskless, scalable manufacturing process for all R&D work, well ahead of schedule. The focus this quarter was on the systematic improvement of: (1) the chemistry related to both the composition and phase of the reactive current collectors, and (2) electrode architectures of full cells. Both efforts were conducted in parallel and at similar level, as they both have an important impact on the electrochemical performance of the fabricated cells. This combined approach has effectively increased the stack energy density of the second quarter examples by an order of magnitude. The stack energy density of the current cells provides amount to 70% of the *Go/No-Go* goal.

Task 4.7 – Dual Function Solid-State Battery with Self-Forming, Self-Healing Electrolyte and Separator (Esther Takeuchi, Stony Brook University)

Project Objective. The project objective is to demonstrate a solid-state rechargeable battery based on a Li-metal anode and iodine cathode with a self-forming, self-healing electrolyte and separator. The resulting rechargeable self-assembled metal/iodine solid state battery will provide an energy density of ≥ 560 Wh/kg and ≥ 1536 Wh/kg.

Project Impact. This program will enable demonstration of the proposed rechargeable battery with improved power capability, high energy density, and a self-forming, self-healing SSE/separator. Technical insight will be gained regarding improved conductivity of the solid lithium iodide (LiI) based electrolyte, power capability of the proposed system, the self-healing nature of the LiI layer, the nature of the electrode-electrolyte interfaces, and feasibility of the system to reach the EV Everywhere Grand Challenge targets.

Approach. The proposed concept is a dual function rechargeable solid-state battery utilizing LiI combined with silver iodide (AgI) as the electrolyte, with lithium metal (and small quantities of silver metal) as the anode and iodine as the cathode with a self-forming, self-healing separator/electrolyte. The battery will be assembled in the discharged state where the anode and cathode will be created during the first formation (charge) step. Initially, silver ion (Ag^+) will diffuse toward the negative electrode and be reduced to silver metal (Ag^0), and iodine ion (I^-) will be oxidized to elemental iodine (I_2) at the cathode side. As the formation of the battery continues, lithium ion (Li^+) will form a Li-metal layer at the anode, with generation of iodine at the cathode. LiI will remain and serve as both the separator and electrolyte.

Out-Year Goals. This is a multiyear program where the effort is divided into three major tasks.

- Year 1 involves electrolyte preparation and characterization including preparation of SSEs and conductivity measurements.
- Year 2 will focus on cell construction and testing including both *in situ* and *ex situ* analysis.
- Year 3 will focus on cell characterization. Under the program, cycle life, efficiency, energy density, and the functional capacity of cells will be determined.

Collaborations. This project collaborates with Amy Marschilok and Kenneth Takeuchi of SBU.

Milestones

1. Reagents procured; composition, purity, and water content verified. (Q1 – Complete)
2. Develop methodology for AC impedance measurement as a function of temperature. (Q2 – Complete)
3. Identify the four most conductive silver-containing LiI solid electrolytes for further study. (Q3 – Complete)
4. At least one electrolyte with conductivity $\geq 10^{-3}$ S/cm. (Q4 – In progress)

Progress Report

Measurement of LiI Composite Solid Electrolytes

The milestone this quarter was identification of four conductive Ag-containing LiI solid electrolytes for further study with additional additives and polymers. The project used the previously demonstrated method of measuring AC EIS methodology of solid electrolytes to measure AC impedance of three sets of LiI composites: (a) LiI + $x\%$ AgI, (b) LiI + $x\%$ AgI + 20% Al_2O_3 additive, and (c) LiI + synthesized KAg_4I_5 . The measurement method was validated by repeating measurements of the same material over a range of temperatures with a minimum of triplicate measurements of each material.

Method validation was confirmed previously by comparison of collected data of pure materials with previous reports. Resistance values collected as a function of temperature were analyzed quantitatively by equivalent circuit modeling. The same circuit model was used both in analysis of all LiI + x ($x = \text{AgI}$, AgI 20% Al_2O_3 , or KAg_4I_5). KAg_4I_5 was synthesized and determined to be phase pure (Figure 38). Figure 38 includes a comparison for the conductivity of previously synthesized ion conductor RbAg_4I_5 . Note that the conductivities of both RbAg_4I_5 and KAg_4I_5 are $\geq 10^{-2}$ S/cm.

Identification of the Ag-Containing LiI Solid Electrolytes as Initial Group for Further Study

Samples of LiI with AgI with and without the inclusion of 20% Al_2O_3 additive were identified as Ag-containing LiI solid electrolytes for further study next quarter. The resistance of the electrolyte samples over a range of compositions was measured and analyzed. The next stage involves exploration of polymers as part of the electrolyte and as interface modifiers. Planned studies include the addition of polymers, 3-hydroxypropionitrile (LiHPN_2) and iodine containing poly-2-vinylpyridine (P2VP). (Task 1.2) Further, modification of the interfaces in contact with the solid electrolyte is under exploration. The project has demonstrated that reduction of resistance at the interface shows significant benefit for more highly conductive electrolytes; thus, this is an area of investigation planned for future cell designs.

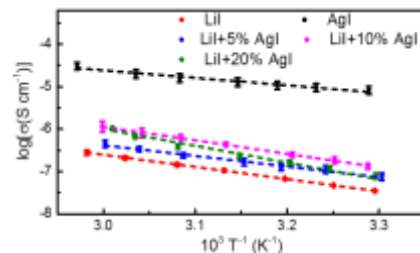


Figure 36. Conductivity of LiI with $x\%$ AgI additive including error bars.

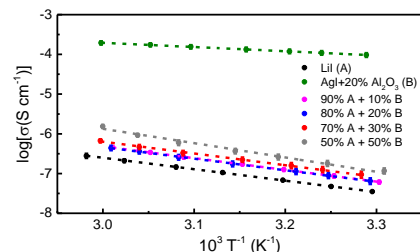


Figure 37. Conductivity of LiI with $x\%$ AgI + 20% Al_2O_3 additive including error bars.

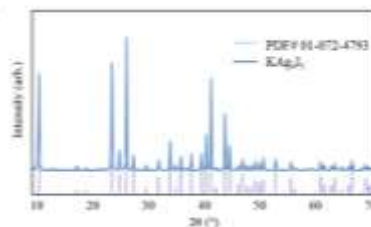


Figure 38. X-ray diffraction of KAg_4I_5 .

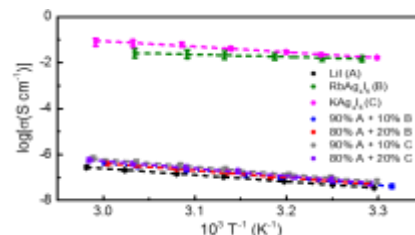


Figure 39. Conductivity as a function of temperature for $\text{LiI}_x\%\text{MAg}_4\text{I}_5$ ($x = 10, 20$, $M = \text{K, Rb}$).

Patents/Publications/Presentations

Presentations

- BMR/ABR/Battery 500 Research Information Exchange, Berkeley, California (January 17 – 19, 2017): “Dual Function Solid State Battery with Self-Forming Self-Healing Electrolyte and Separator”; E. Takeuchi, A. Marschilok, and K. Takeuchi.
- Program Officer Site Visit, Stony Brook University, Stony Brook, New York (May 3, 2017): “Dual Function Solid State Battery with Self-Forming Self-Healing Electrolyte and Separator” 11794; E. Takeuchi, A. Marschilok, and K. Takeuchi.
- DOE Annual Merit Review, Washington, D. C. (June 5 – 9, 2017): “Dual Function Solid State Battery with Self-Forming Self-Healing Electrolyte and Separator”; E. Takeuchi, A. Marschilok, and K. Takeuchi. Poster.

TASK 5 – DIAGNOSTICS

Summary and Highlights

To meet the goals of the VTO Multi-Year Program Plan and develop lower-cost, abuse-tolerant batteries with higher energy density, higher power, better low-temperature operation and longer lifetimes suitable for the next-generation of HEVs, PHEVs and EVs, there is a strong need to identify and understand structure-property-electrochemical performance relationships in materials, life-limiting and performance-limiting processes, and various failure modes to guide battery development activities and scale-up efforts. In the pursuit of batteries with high energy density, high cell operating voltages and demanding cycling requirements lead to unprecedented chemical and mechanical instabilities in cell components. Successful implementation of newer materials such as silicon anode and high-voltage cathodes also requires better understanding of fundamental processes, especially those at the solid/electrolyte interface of both anode and cathode.

This Task takes on these challenges by combining model system, *ex situ*, *in situ*, and *operando* approaches with an array of state-of-the-art analytical and computational tools. Four subtasks are tackling the chemical processes and reactions at the electrode/electrolyte interface. Researchers at LBNL use *in situ* and *ex situ* vibrational spectroscopy, far- and near-field scanning probe spectroscopy and laser-induced breakdown spectroscopy (LIBS) to understand the composition, structure, and formation/degradation mechanisms of the SEI at silicon anode and high-voltage cathodes. The University of California at San Diego (UCSD) combines STEM/EELS, XPS and *ab initio* computation for surface and interface characterization and identification of instability causes at both electrodes. At the University of Cambridge, nuclear magnetic resonance (NMR) is being used to identify major SEI components, their spatial proximity, and how they change with cycling. Subtasks at BNL and PNNL focus on the understanding of fading mechanisms in electrode materials, with the help of synchrotron-based X-ray techniques (diffraction and hard/soft X-ray absorption) at BNL and high-resolution transmission electron microscopy (HRTEM) and spectroscopy techniques at PNNL. At LBNL, model systems of electrode materials with well-defined physical attributes are being developed and used for advanced diagnostic and mechanistic studies at both bulk and single-crystal levels. These controlled studies remove the ambiguity in correlating material's physical properties and reaction mechanisms to performance and stability, which is critical for further optimization. The final subtask takes advantage of the user facilities at ANL that bring together X-ray and neutron diffraction, X-ray absorption, emission and scattering, HRTEM, Raman spectroscopy, and theory to investigate the structural, electrochemical, and chemical mechanisms in the complex electrode/electrolyte systems. The diagnostics team not only produces a wealth of knowledge key to developing next-generation batteries, it also advances analytical techniques and instrumentation that have a far-reaching effect on material and device development in a variety of fields.

Task 5.1 – Model System Diagnostics for High-Energy Cathode Development (Guoying Chen, Lawrence Berkeley National Laboratory)

Project Objective. This project will use a rational, non-empirical approach to design and synthesize next-generation high-energy, high-voltage cathode materials. Combining a suite of advanced diagnostic techniques with model cathode materials and model electrode/electrolyte interfaces, the project will perform systematic studies to achieve the following goals: (1) obtain new insights into solid-state chemistry, particularly cationic and/or anionic redox activities during charge and discharge of high-capacity Li-TM oxides, (2) gain fundamental understanding on cathode/electrolyte interfacial chemistry and charge transfer process as a function of operating voltage, (3) reveal performance- and stability-limiting properties and processes in high-energy, high-voltage cathodes, and (4) develop strategies to mitigate the structural and interfacial instabilities.

Project Impact. The project will improve the commercial viability of next-generation high-energy cathode materials. The findings will enable more stable high-voltage cycling of existing Li-TM oxides as well as development of novel high-capacity cathode materials for advanced Li-ion batteries.

Approach. Prepare crystal samples of Li-stoichiometric and Li-excess TM oxides with well-defined physical attributes. Perform advanced diagnostic and mechanistic studies at both bulk and single-crystal levels. Global properties and performance of the samples will be established from the bulk analyses, while the single-crystal-based studies will utilize time- and spatial-resolved analytical techniques to probe the material redox transformation process and failure mechanisms under battery operating conditions.

Out-Year Goals. Obtain fundamental knowledge on performance-limiting physical properties, phase transition mechanisms, parasitic reactions, and transport processes that prevent cathode materials from delivering higher capacities and achieving more stable cycling at high voltages. Develop approaches to mitigate cathode structural and interfacial instabilities during high-voltage operation. Design and synthesize optimized Li-TM oxide cathodes as well as novel high-energy electrode materials.

Collaborations. This project collaborates with the following: G. Ceder, K. Persson, M. Doeff and P. Ross (LBNL); V. Srinivasan (ANL); Simon Mun (Gwangju Institute of Science and Technology, GIST); Y. Liu (SSRL); J. Guo (ALS); C. Wang (PNNL); C. Grey (Cambridge); and A. Huq and J. Nanda (ORNL).

Milestones

1. Synthesize model Li-TM oxide cathode materials with several different chemical compositions and/or morphologies. (Q1 – Completed December 2016)
2. Investigate the bulk activities of TM and oxygen redox centers in Li-TM oxides as a function of state of charge and temperature. (Q2 – Completed March 2017)
3. *Go/No-Go*: Investigate synthesis methods for preparing single crystals of Li-excess TM oxides with previously reported reversible oxygen redox activities. *No-Go* if high-quality crystals of the oxide cannot be made. (Q3 – Completed June 2017)
4. Determine the activities of lattice oxygen and TM on particle surface and the impact of cathode chemistry and surface facet. (Q4 – On schedule; September 2017)

Progress Report

This quarter, studies on first-cycle redox activities occurring in the bulk of high-capacity Li-excess oxides continued. Figure 40a-c shows the manganese K-edge hard X-ray absorption spectra (hXAS) collected on pristine and chemically delithiated $\text{Li}_x\text{Nb}_{0.3}\text{Mn}_{0.4}\text{O}_2$ ($0 \leq x < 1.3$) crystal samples. In the manganese pre-edge region (Figure 40b), there is a clear division in peak intensity below and above Li0.9, suggesting a change in manganese local environment. Figure 40c shows the expanded view of the XANES region. Above Li0.9, manganese K-edge energy continuously shifts to a higher value in a near linear fashion, which then becomes constant below 0.9. This trend is further revealed in Figure 40d where the relationship between lithium content and manganese XANES edge position, defined by the interception of the spectrum at half of the normalized intensity, is shown. Combined hXAS and XRD results confirm that cation redox involving $\text{Mn}^{3+}/\text{Mn}^{4+}$ only occurs in the single-phase region above Li0.9. Below Li0.9, lithium extraction occurs with the complex oxygen redox activities that involve two rock-salt phases.

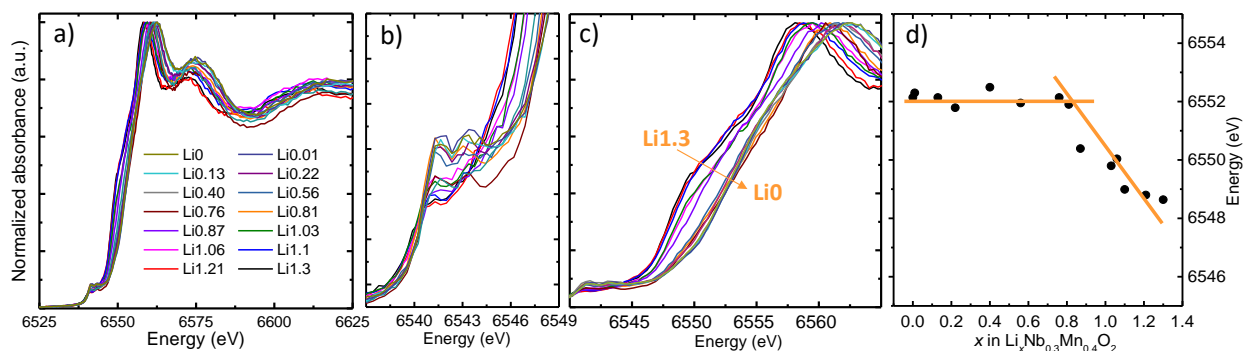


Figure 40. Manganese K-edge hard X-ray absorption spectroscopy (hXAS) measurements of $\text{Li}_x\text{Nb}_{0.3}\text{Mn}_{0.4}\text{O}_2$ crystals: (a) hXAS spectra, (b) expanded view of the pre-edge region, (c) expanded view of the X-ray absorption near-edge spectroscopy (XANES) region, and (d) relationship between manganese XANES edge position and lithium content in the samples.

The molten-salt method previously developed was modified to synthesize single crystal samples of newer Li-excess TM oxides. A series of samples with a formula of $\text{Li}_{1.4-x}\text{M}_{0.4-x}\text{Mn}_{0.2+2x}\text{O}_2$ ($x = 0, 0.1$ and 0.2 , $\text{M} = \text{Nb}, \text{Nb}_{0.5}\text{Ta}_{0.5}$ and Ta) was prepared. The typical procedure involves ball-milling a stoichiometric amount of Mn_2O_3 and Nb_2O_5 (and/or Ta_2O_5) with Li_2CO_3 in 10-15% excess. KCl flux, in a KCl/total TM mole ratio of 2.5-5, was added to the mixture, which was then heated at 950°C under an argon atmosphere to produce the crystalline product. Figure 41 shows powder XRD patterns of the synthesized crystal samples. Rietveld refinements confirmed that all samples were phase pure with a rock-salt crystal structure (space group of $Fm\bar{3}m$). The morphology of the crystals was largely immune to Li/Mn/Nb ratio, as uniform spherical particles with an average size of $\sim 5 \mu\text{m}$ were obtained in all cases. Detailed analysis using selected area (electron) diffraction, high-angle annular dark-field imaging (HAADF) STEM and EDX confirms that samples are composed of single crystals with uniform distribution of the TMs and oxygen. This completes the third milestone with a go decision.

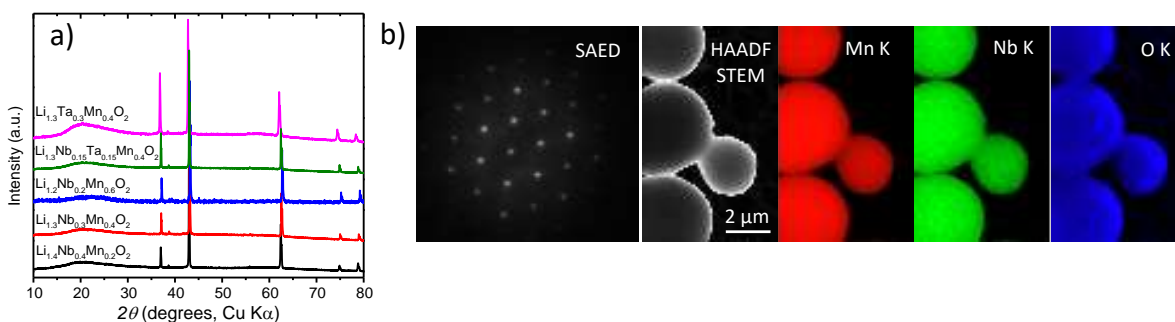


Figure 41. (a) Powder X-ray diffraction patterns of $\text{Li}_{1.4-x}\text{Nb}_{0.4-x}\text{Mn}_{0.2+2x}\text{O}_2$ ($x = 0, 0.1$ and 0.2) and $\text{Li}_{1.3}\text{MMnO}_2$ ($\text{M} = \text{Nb}_{0.5}\text{Ta}_{0.5}$ and Ta) crystal samples. (b) Selected area (electron) diffraction pattern, high-angle annular dark field scanning transmission electron microscopy image, and elemental distributions on $\text{Li}_{1.3}\text{Nb}_{0.3}\text{Mn}_{0.4}\text{O}_2$ crystals.

Patents/Publications/Presentations

Publication

- Kan, W. H., and S. Kuppan, L. Cheng, M. Doeff, J. Nanda, A. Huq, and G. Chen. “Crystal Chemistry and Electrochemistry of $\text{Li}_x\text{Mn}_{1.5}\text{Ni}_{0.5}\text{O}_4$ Solid Solution Cathode Materials.” *Chemistry of Materials* (2017). In press.

Task 5.2 – Interfacial Processes – Diagnostics (Robert Kostecki, Lawrence Berkeley National Laboratory)

Project Objective. This collaborative project involves developing and applying advanced experimental methodologies to study and understand the mechanism of operation and degradation of high-capacity NMC materials for Li-ion cells for PHEV and EV applications. The main objective is to apply *in situ* and *ex situ* far- and near-field optical multi-functional probes to obtain detailed insight into the active material structure and the physicochemical phenomena at electrode/electrolyte interfaces of stoichiometric NMCs with high nickel contents such as 622 and 523 composition materials at a spatial resolution that corresponds to the size of basic chemical or structural building blocks. The primary goal of these studies is to unveil the structure and reactivity at hidden or buried interfaces and interphases that determine material, composite electrode, and full-cell electrochemical performance and failure modes.

Project Impact. Instability and/or high resistance at the interface of high-voltage Li-ion cathodes limits electrochemical performance of high-energy density batteries. A better understanding of the underlying principles that govern these phenomena is inextricably linked with successful implementation of high-energy-density materials such as silicon and high-voltage cathodes in Li-ion cells for PHEVs and EVs. The proposed work constitutes an integral part of the concerted effort within the BMR Program, and it supports development of new cathode materials for high-energy Li-ion cells.

Approach. The pristine and cycled NMC powders and electrodes will be probed using a variety of surface- and bulk-sensitive techniques, including Fourier transform infrared (FTIR), attenuated total reflection (ATR)-FTIR, near-field infrared and Raman spectroscopy and microscopy, and scanning probe microscopy to identify and characterize changes in materials structure and composition. Novel *in situ/ex situ* far- and near-field optical multi-functional probes in combination with standard electrochemical and analytical techniques are developed to unveil the structure and reactivity at interfaces and interphases that determine materials electrochemical performance and failure modes.

Out-Year Goals. Determine the degradation mechanism(s) of high-voltage cathodes; propose and test effective remedies to intrinsic interfacial instability of these materials and composite electrodes.

Collaborations. NMC materials and composite electrodes tested under different cycling regimes by M. Doeff (LBNL) and C. Ban (NREL) will be studied. The diagnostic studies will be carried out in sync with differential electrochemical MS analysis by B. McCloskey (LBNL) and other diagnosticians in the BMR program. This project will also work closely with V. Battaglia (LBNL) to obtain samples from full-cell cycling experiments.

Milestones

1. Determine relationship between surface reconstruction and aging/cycling of NMC powders/electrodes. (Q1– Completed December 2016)
2. Complete *in situ* atomic force microscopy (AFM) characterization of interfacial activity of the model NMC material in organic carbonate electrolytes. (Q3 – Completed June 2017)
3. Determine composition of surface film and its effect on electrochemical performance of NMC electrodes. (Q3 – Completed June 2017)
4. Determine relationship between surface reconstruction, film formation, and metal dissolution in NMC electrodes. (Q4 – On schedule)

Progress Report

This quarter, the project studied changes in the surface morphology of model NMC cathodes during operation at potentials above 4 V in 1M LiPF₆ in ethylene carbonate/diethyl carbonate (EC/DEC; 1:2 vol.). To enable a high-resolution surface analysis by *in situ* AFM, a nominally flat, binder-free, and conductive-additive-free NMC thin-film electrode was produced by pulsed laser deposition (PLD) directly on an aluminum substrate, using NMC (Ni:Co:Mn = 5:3:2) target. A Raman spectrum (Figure 42a) of the model NMC/Al electrode shows vibrational modes typical for layered hexagonal structure (R $\bar{3}m$)^[1] which is consistent with the spectrum of standard NMC-532 powder. The electrochemical performance of the thin-film NMC/Al electrode was evaluated in a coin cell against Li-foil counter electrode in 1M LiPF₆ in EC/DEC (1:2 vol.). The cyclic voltammogram (Figure 42b) of the model electrode displays similar redox features as a typical NMC composite electrode. The *in situ* three-electrode AFM cell with the NMC/Al working, Li-foil counter, and reference electrodes is shown in Figure 42c. The cell was operated in He-filled environmental chamber under saturated DEC partial vapor pressure to prevent drying of the electrolyte during the experiment. NMC electrode was charged at constant potential steps from OCV (~3.4 V) to 4.7 V (Figure 42c) for 30 minutes at each step before AFM imaging.

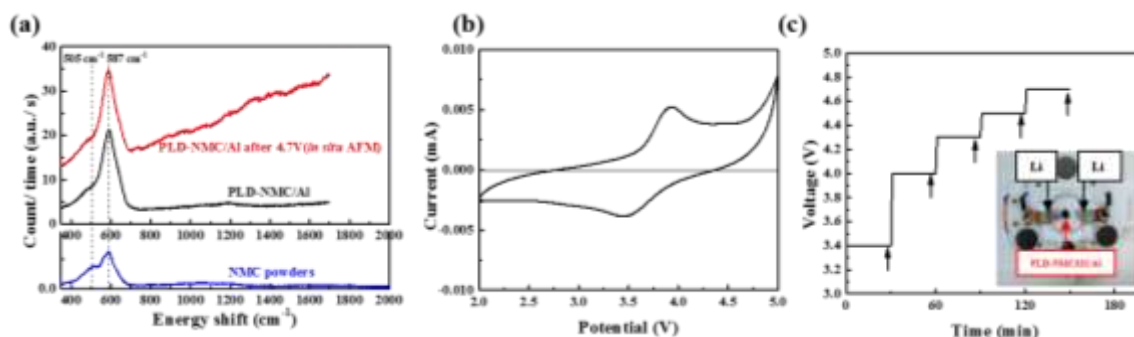


Figure 42. (a) Raman spectra of NMC powder (blue), pulsed laser deposition (PLD)-NMC/Al electrode (black), and PLD-NMC/Al electrode after 4.7 V charged (red). (b) Cyclic voltammogram of PLD-NMC/Al electrode at the 3rd cycle. (c) The voltage-time profile of electrode during *in situ* atomic force microscopy (AFM) experiment. The arrows point at the time when AFM images were acquired. Inset: *in situ* AFM cell.

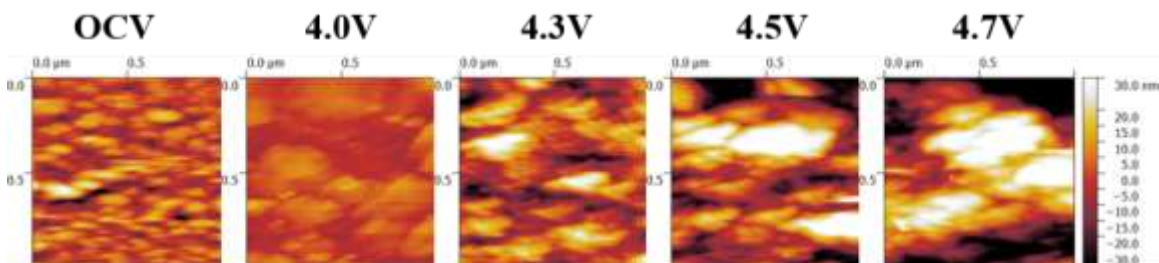


Figure 43. Atomic force microscopy images of pulsed laser deposition (PLD)-NMC/Al electrode in 1 x 1 μm scale after staying in each target voltage for 30 minutes.

The AFM images of the NMC surface at OCV (~ 3.4 V), 4.0, 4.3, 4.5, 4.7 V are shown in Figure 43. The pristine electrode is composed of tightly packed 100- to 150-nm NMC grains. After charging to 4.0 and 4.3 V, the NMC particles tend to agglomerate and form ~300-nm clusters, and larger 500-nm aggregates at 4.5 V and 4.7 V. At potentials < 4.3 V, the cluster surface morphology still shows individual 100-nm grains of NMC. However, at higher potentials (> 4.5 V), the observed changes in surface morphology also can be assigned to a surface film formation. The NMC/Al electrode was removed from the AFM cell after polarization at 4.7 V, washed in DEC, and probed by *ex situ* Raman spectroscopy (Figure 43a). The spectrum shows a strong fluorescence background and weak features in a range of 800-1600 cm^{-1} , which indicates possible formation of β -keton coordination complexes similar to LMNO.^[2] These results provide direct insight into the surface film

formation process, which otherwise is difficult to observe by other diagnostic methods, especially in NMC composite cathodes. At the end of anodic polarization, the film is ca. 10-nm thick; it may give rise to formation of electronic and ionic barriers, which can contribute to the commonly observed degradation modes of NMC cathodes in Li-ion batteries. This report completes milestone 3.

- [1] Ruther, R. E., and A. F. Callender, H. Zhou, S. K. Martha, and J. Nanda. *J Electrochem Soc* 162 (2015): A98.
- [2] Jarry, A., and S. Gottis, Y. S. Yu, J. Roque-Rosell, C. Kim, J. Cabana, J. Kerr, and R. Kostecki. *J Am Chem Soc* 137 (2015): 3533.

Task 5.3 – Advanced *In Situ* Diagnostic Techniques for Battery Materials (Xiao-Qing Yang and Seongmin Bak, Brookhaven National Laboratory)

Project Objective. The primary project objective is to develop new advanced *in situ* material characterization techniques and to apply these techniques to support development of new cathode and anode materials for the next generation of Li-ion batteries for PHEVs. To meet the challenges of powering the PHEV, Li-ion batteries with high energy and power density, low cost, good abuse tolerance, and long calendar and cycle life must be developed.

Project Impact. The VTO Multi-Year Program Plan describes the goals for battery: “Specifically, lower-cost, abuse-tolerant batteries with higher energy density, higher power, better low-temperature operation, and longer lifetimes are needed for development of the next-generation of HEVs, PHEVs, and EVs.” The knowledge gained from diagnostic studies through this project will help U.S. industries develop new materials and processes for new generation Li-ion batteries in the effort to reach these VTO goals.

Approach. This project will use the combined synchrotron-based *in situ* X-ray techniques (XRD, and hard and soft XAS) with other imaging and spectroscopic tools such as HRTEM and MS to study the mechanisms governing the performance of electrode materials.

Out-Year Goals. Complete the first-stage development of diagnostic technique to study effects of microstructural defects on performance fading of high-energy-density LMR cathode materials for Li-ion batteries using pair distribution function (PDF), XRD, and XAS combined with STEM imaging and TXM. Apply these techniques to study the structural changes of various new cathode materials.

Collaborations. The BNL team will work closely with material synthesis groups at ANL (Drs. Thackeray and Amine) for the high-energy composite; and at PNNL for the Si-based anode materials. The project will also collaborate with industrial partners at GM and Johnson Controls, as well as with international collaborators.

Milestones

1. Complete the structure studies of $\text{Li}_2\text{Ru}_{0.5}\text{Mn}_{0.5}\text{O}_3$, as a model compound for Li- and Mn- rich (LMR) high-energy-density cathode materials using PDF to correlate the voltage and capacity fading with microstructural defects in this type of material. (Q1 – Completed December 2016)
2. Complete the structure studies $\text{Li}_2\text{Ru}_{0.5}\text{Mn}_{0.5}\text{O}_3$, as a model compound for LMR high-energy-density cathode materials using STEM to correlate the voltage and capacity fading with microstructural defects in this type of material. (Q2 – Completed March 2017)
3. Complete the XRD and XAS studies of $\text{Li}_2\text{Ru}_{0.5}\text{Mn}_{0.5}\text{O}_3$ cathode material samples with different cycle history (charge and discharge limit and cycle numbers). (Q3 – Completed June 2017)
4. Complete the structure studies of $\text{Li}_{1.2}\text{Ni}_{0.15}\text{Co}_{0.1}\text{Mn}_{0.55}\text{O}_2$ for LMR high-energy-density cathode materials using STEM to correlate the voltage and capacity fading with microstructural defects in this type of material. (Q4 – In progress; September 2017)

Progress Report

This quarter, the third milestones was completed. BNL focused on the structure studies of $\text{Li}_2\text{Ru}_{0.5}\text{Mn}_{0.5}\text{O}_3$, as a model compound for Li- and Mn-rich (LMR) high-energy-density cathode materials using synchrotron-based XRD and absorption (XAS) to correlate the voltage and capacity fading with microstructural defects in this type of material. The prelithiated sample experiences more reduction. Figure 44a indicates that TM cations in both “OCV-1V-(4.6V-2V)20Cy” sample and “OCV-(4.6V-2V)20Cy” sample experience reduction during cycling. This is true both for manganese and ruthenium, as seen from the edges shifting to the lower energy in both manganese K-edge and ruthenium K-edge spectra. Oxygen release is not only exacerbated by the microstructural defects, but also promotes formation of defects. Evidence comes from *ex situ* XRD studies shown in Figure 44b. The figure is separated by a dash line in the middle. The upper part corresponds to the prelithiated case and the lower one to the normally cycled case. Compared with the normally cycled case, samples in the prelithiated case show much greater peak broadening; this broadening effect increases as the cycle number increases. Oxygen release and microstructural defects also accelerate spinel formation. This can be seen from Figure 44c, which gives the evolution of lattice parameter c to lattice parameter a ratio during cycling.

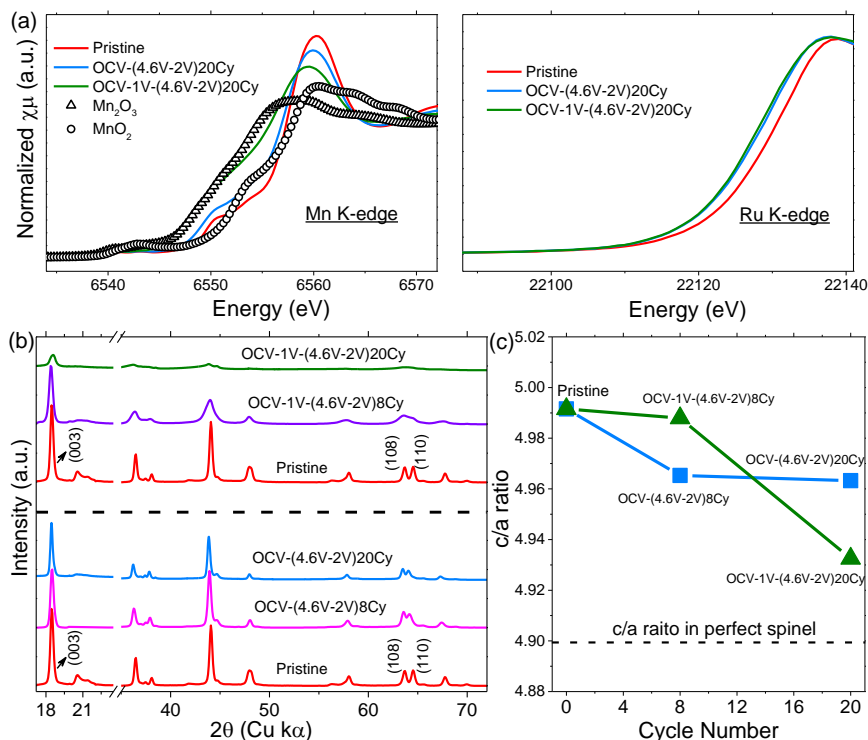


Figure 44. (a) *Ex situ* manganese K-edge and ruthenium K-edge X-ray absorption spectroscopy data of pristine $\text{Li}_2\text{Ru}_{0.5}\text{Mn}_{0.5}\text{O}_3$ sample, sample normally cycled 20 times, and sample cycled 20 times but first prelithiated, with references of Mn_2O_3 and MnO_2 shown. (b) *Ex situ* X-ray diffraction patterns of two cases (with [003], [108] and [110] peaks indexed according to the space group $R\bar{3}m$): pristine sample, cycled 8 times and cycled 20 times for the normally cycled case (the part below the dash line); and pristine sample, cycled 8 times and cycled 20 times for the prelithiated case (the part above the dash line). (c) The ratio between lattice parameter c and lattice parameter a as a function of cycle numbers. The dash line shows the c/a ratio in perfect spinel.

Patents/Publications/Presentations

Publication

- Xu, Yahong, and Enyuan Hu, Kai Zhang, Xuelong Wang, Valery Borzenets, Zhihong Sun, Piero Pianetta, Xiqian Yu,* Yijin Liu,* Xiao-Qing Yang,* and Hong Li. “*In Situ* Visualization of State-of-Charge Heterogeneity within a LiCoO₂ Particle that Evolves upon Cycling at Different Rates.” *ACS Energy Lett.* 2, no. 5 (2017): 1240–1245. doi: 10.1021/acsenerylett.7b00263; publication date (Web), May 5, 2017.

Presentation

- Third International Forum on Cathode & Anode Materials for Advanced Batteries, Ningbo, China (April 12 – 14, 2017): “Studies of New Electrode Materials for Next Generation of Batteries Using Synchrotron Based *In Situ* X-Ray Diffraction and Absorption as well as TXM Techniques”; Enyuan Hu, Xiqian Yu, Yongning Zhou, Yingchun Lyu, Yahong Xu, Xiao-Qing Yang,* Seong-Min Bak, Hung-Sui Lee, Xuelong Wang, Yijin Liu, Zhaoxiang Wang, Lin Gu, Hong Li, Xuejie Huang, and Liquan Chen. Invited.

Task 5.4 – Nuclear Magnetic Resonance and Magnetic Resonance Imaging Studies of Solid Electrolyte Interphase, Dendrites, and Electrode Structure (Clare Grey, University of Cambridge)

Project Objective. The growth of a stable SEI on most electrode materials is key to long-term capacity retention of a working Li-ion battery. On anodes such as silicon, this is particularly critical because the continual expansion and contraction of this intermetallic upon alloying with lithium exposes fresh, reactive surfaces that result in further electrolyte decomposition and SEI growth. This project will perform a detailed multinuclear NMR study of the SEI that forms on silicon, where thick SEIs typically grow and where SEI stability is a key aspect hindering commercialization of this technology. The focus will be to determine how additives (for example, fluoroethylene carbonate, or FEC) and charging parameters (for example, voltage) influence the composition and stability of the SEI. Fundamental studies of SEI structure *in operando* will be complemented by a synthetic program aimed at preparing new silicon coatings based on phosphazene (P-N) elastomeric polymers to increase CE. Further, the nature of the SEI is one factor that appears to control the type of lithium microstructures that form on lithium metal during cycling. To test this hypothesis, the project will use magnetic resonance imaging (MRI) to investigate lithium dendrite versus moss formation in different electrolytes as a function of salt concentration and with different additives. Finally, it will compare lithium and sodium metal anode chemistries to determine the composition, morphology, and stability of local structures that form on sodiating anodes such as tin and hard carbons.

Project Impact. The first impact of this project will be a molecular-level understanding of how factors such as applied voltage and electrolyte additives modify the SEI that forms on silicon anodes. The insight gained from these studies will guide the design of new P-N coatings for silicon. A rationally designed surface coating has the potential to improve SEI stability, and thus increase CE for silicon and beyond. A description of how SEI composition influences lithium microstructures will provide the foundation to mitigate dendrite formation during cycling that currently limits the safety of many promising electrode materials. These approaches will be extended to study Na-ion battery electrodes to provide an understanding of how to chemically manipulate both electrodes as well as the electrolyte to avoid adverse failure mechanisms in next-generation batteries.

Out-Year Goals. The project goals are as follows: (a) determine the effect of voltage and additives (for example, FEC) on the composition of the silicon SEI; (b) synthesize and test new inorganic coatings to increase the CE seen on cycling silicon; (c) identify correlations between SEI structure and thickness and Li-metal dendrite formation; and (d) determine the local and long-range structures formed on cycling sodium anode materials and compare with lithium. To facilitate these goals, the project will prepare ^{13}C -enriched FEC for ^{13}C NMR multinuclear studies to investigate the SEI that forms on silicon during cycling. It will synthesize new P-N polymers for coating silicon nanoparticles and probe changes in performance in the presence of these coatings. In addition, the project will use MRI to correlate lithium dendrite formation with the nature of the SEI. Finally, it will apply the methods developed to study lithium chemistries to investigate sodium electrodes.

Collaborations. This project collaborates with B. Lucht (University of Rhode Island); J. Cabana, (University of Illinois – Chicago); Y. Shirley Meng (UCSD), S. Whittingham (SUNY – Binghamton); P. Bruce (St. Andrews); S. Hoffman and A. Morris (Cambridge); and P. Shearing (University College London).

Milestones

1. Synthesis of ^{13}C FEC. (Q1 – Complete)
2. Preparation of P-N coatings on silicon; Develop *in situ* ^{19}F NMR studies of FEC. (Q2 – Complete)
3. Multinuclear NMR studies of SEI coatings on silicon with FEC. (Q3 – Complete; paper submitted)
4. Testing of P-N coatings; MRI/dendrite studies of two ionic liquids. (Q4 – In progress; focus on additives)

Progress Report

The primary aim of this study was to understand how the electrolyte additive FEC enhances stability of the SEI formed on silicon anodes. The organic species formed on silicon nanowires (SiNWs) in both the standard carbonate-only electrolyte (LP30) as well as LP30 and additive FEC were characterized with solution and solid-state NMR techniques, including dynamic nuclear polarization (DNP). SiNWs were used here as model systems, since they can be prepared as binder-free anodes that cycle for multiple cycles without losing electrical contact.

After long-term cycling, ^1H NMR shows that LP30 decomposes and forms various soluble oligomers in addition to the transient species lithium ethylene decarbonate (LEDC, yellow shading, Figure 45a). Addition of 10 vol% FEC into the electrolyte results in suppression of the decomposition of EC/dimethyl carbonate (DMC), shown in Figure 45b-c, that is correlated with an increased CE in the electrochemical cycling data after the first few cycles. To facilitate more in-depth characterization of electrolyte products in the presence of FEC via 1D and 2D NMR (for example, ^{13}C - ^{13}C COSY, ^1H - ^{13}C HMBC, ^1H - ^{13}C HSQC to assign red shaded peaks x, y, and z), the project synthesized ^{13}C -enriched FEC, which ultimately allowed detailed structural assignment of the organic SEI. The ^1H and ^{13}C NMR spectra provide

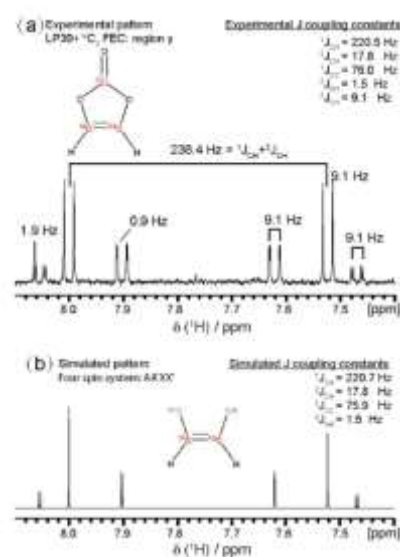


Figure 46. Multiplet pattern of LP30 + $^{13}\text{C}_3$ -FEC in region y of Figure 45c, (a) experimental pattern and (b) simulated pattern of a four-spin system AA'XX' (cis-H-CR=CR-H).

similar cross-linking groups (Figure 47b, peak at 103 ppm). Neither these cross-linking units nor the vinoxyl species are observed in the absence of the FEC additive (Figure 47a). The vinoxyl species are signatures for the formation of the vinoxyl radicals that are believed to initiate the polymerization that eventually results in a highly cross-linked network. The project hypothesizes that highly cross-linked polymeric networks are key to increased stability of SEI formed on silicon that is observed in the presence of FEC, motivating studies with additives that may promote cross-linking. Further insight into the molecular nature of the SEI and the parameters that impart stability offers the opportunity to tailor the SEI chemistry to maximize performance in LIBs.

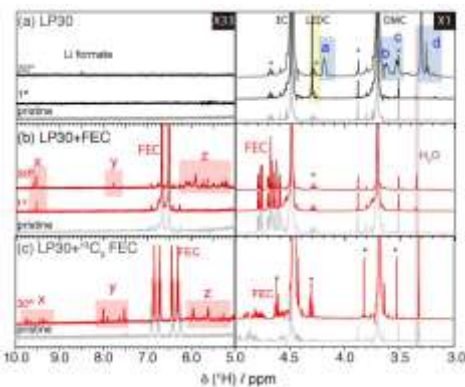


Figure 45. ^1H solution NMR of (a) LP30, (b) LP30 + FEC, and (c) LP30 + 10 vol% $^{13}\text{C}_3$ -FEC before cycling (pristine), and after the 1st and 30th cycles.

compelling evidence for the defluorination of FEC to form soluble vinoxyl species (HCOCH_2OR) and vinylene carbonate (VC). The formation of VC, rather than LVDC, was unambiguously determined, with the assignment being based on the J coupling pattern that arises as a result of the uniform ^{13}C labeling of FEC and the subsequent breakdown products (Figure 46). Oligomers with characteristic peaks due to protonated carbons that bonded to two adjacent oxygen groups from cross-linking units were also identified. These oligomeric precursors presumably react further to form insoluble polymeric species in the SEI, with

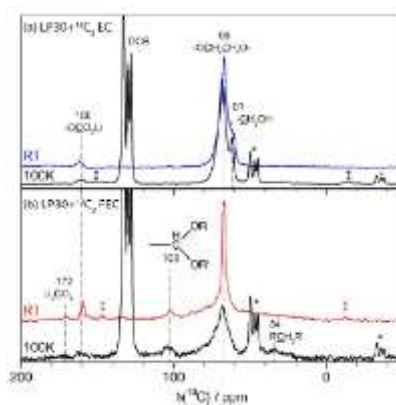


Figure 47. ^1H - ^{13}C CP nuclear magnetic resonance (NMR) spectra of silicon nanowires after 30 cycles in (a) LP30 + 25 vol% $^{13}\text{C}_3$ -EC and (b) LP30 + 10 vol% $^{13}\text{C}_3$ -FEC electrolytes. The room-temperature spectra were measured by conventional solid-state NMR, whereas the 100 K spectra were measured with dynamic nuclear polarization (DNP) NMR. The dicyanobenzene was used as the radical solvent for DNP.

Patents/Publications/Presentations

Publications

- Stratford, J. M., and M. Mayo, P. K. Allan, O. Pecher, O. J. Borkiewicz, K. M. Wiaderek, K. W. Chapman, C. J. Pickard, A. J. Morris, and C. P. Grey. “Investigating Sodium Storage Mechanisms in Tin Anodes: A Combined Pair Distribution Function Analysis, Density Functional Theory, and Solid-State NMR Approach.” *J. Am. Chem. Soc.* 139 (2017): 7273.
- Pell, A. J., and K. J. Sanders, S. Wegner, G. Pintcuda, and C. P. Grey. “Low-Power Broadband Solid State MAS NMR of N-14.” *J. Chem. Phys.* 146 (2017): 194202. doi: 10.1063/1.4983220.

Presentations

- Experimental NMR Conference, Pacific Grove, California (March 2017).
- ACS Meeting, San Francisco, California (April 2017).
- 21st International Conference on Solid State Ionics, Padua, Italy (June 2017).

Task 5.5 – Advanced Microscopy and Spectroscopy for Probing and Optimizing Electrode-Electrolyte Interphases in High-Energy Lithium Batteries (Shirley Meng, University of California – San Diego)

Project Objective. The proposed research aims to develop advanced microscopy and spectroscopy tools to probe, understand, and optimize the anion activities that govern the performance limitations such as capacity and voltage stabilities in high-energy Li-excess TM (such as nickel, cobalt, manganese) oxides cathode materials. The approach uniquely combines atomic resolution STEM, EELS, *operando* Bragg Coherent Diffraction Imaging (BCDI), and first principles computation to probe anion redox and oxygen evolutions in Li-excess NMC materials. Furthermore, the project will track the lithium and oxygen dynamics under electrochemical testing via *operando* neutron diffraction which will enhance the understanding of the overall structural changes due to anion activities. Ultimately, this will hone in on the synthesis efforts to produce the modified materials with the optimum bulk compositions and surface characteristics at large scale for consistently good performance. The above-mentioned characterization tools will be extended to diagnose various anode types, such as Li-metal anode.

Project Impact. If successful, this research will enable *operando* imaging at the single particle level by advanced microscopy imaging and high energy resolution O K-edge EELS. This work will provide an in-depth understanding of anion activities in high-voltage electrode materials, which can lead to significant improvement in stabilizing operation voltage and electrode-electrolyte interface for future generation high-energy-density electrodes.

Approach. This unique approach combines STEM/EELS, *operando* BCDI, and *ab initio* computation as diagnostic tools for probing anion redox and oxygen evolutions in Li-excess NMC materials. This allows for pinning down the atomistic/molecular mechanism of anion oxidation and determining the speciation compositions and surface characteristics for enabling high rate and long life in the proposed materials. Neutron enables the characterization of bulk material properties to enhance and further optimize high-energy electrode materials.

Out-Year Goals. The goal is to probe and control oxygen activity in the high-energy composite cathodes and to characterize electrode/electrolyte interface in lithium anodes so that their cycle life and efficiency can be significantly enhanced.

Collaborations. This work funds collaborations on EELS (Miaofang Chi, ORNL); neutron diffraction (Ken An, ORNL); soft XAS (Marca Doeff, LBNL). It supports collaborative work with Zhaoping Liu and Yonggao Xia at Ningbo Institute of Materials Technology and Engineering in China.

Milestones

1. Structure recovery demonstration of Li-rich layered oxide after cycling. (Q3 – Completed June 17)
2. BCDI Characterization on single particle of Li-rich layered oxide after cycling. (Q4 – On track, September 2017)
3. STEM/ EELS characterization of Li-rich layered oxide after structure recovery. (On track – December 2017)
4. Chemical composition and structure of electrochemically deposited lithium metal at nano scale. (On track – December 2017)

Progress Report

Structure Recovery Demonstration of Li-Rich Layered Oxide (LRLO) After Electrochemical Cycling

Last quarter, the project demonstrated that anion (oxygen) redox in LRLO materials is the main reason for the high reversible capacity over 300 mAh g^{-1} at room temperature. Unfortunately, these composites suffer from a poor structural stability and limited cycle life. A large fraction of the TM ions is in under-coordinated octahedral sites due to oxygen vacancies formation, which are not stable and spontaneously migrate to the fully coordinated octahedral sites nearby. Lithium ions in the TM layer migrate to the shared tetrahedral site in the lithium layer. These migrations dramatically alter the cation ordering in the TM layer as well as local lithium environment, and thus lead to the structure disorder. The cycled material will be trapped in a metastable state with energetically unfavorable local lithium environment, which finally contributes to the voltage fade during the cycling process. As shown in Figure 48a, the superstructure peak between 20° and 25° disappears after 50 cycles, which indicates the material becomes partially disordered. The project designs a path to re-order the superstructure by high-temperature annealing of the cycled electrode ($> 150^\circ\text{C}$). After heat treatment, the superstructure peak is recovered, which indicates the bulk structure is reordered. Based on the mechanism described above, the superstructure recovery is decisive in restoring the original voltage output of LRLO cathode (see Figure 48b). The project will combine STEM/EELS, *operando* BCDI, and *ab initio* computation as diagnostic tools for probing the structure transformation during the heat treatment process to ultimately identify and mitigate obstacles for improved cycling performance of LRLO cathode material.

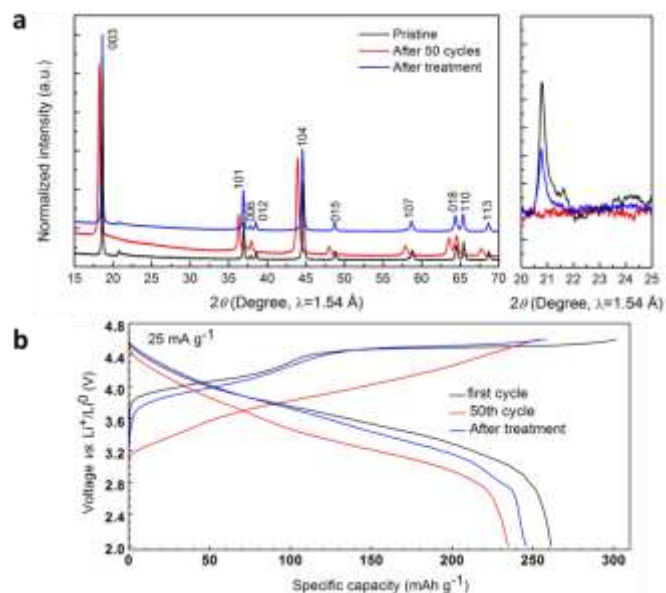


Figure 48. (a) The evolution of the superstructure peak intensity in the pristine state, after 50 cycles, and after the heat treatment. (b) Charge-discharge voltage curves of Li-rich layered oxide cathode with Li-metal as anode for the voltage range of 2.0-4.6 V versus Li^+/Li .

Feasibility of Cryo-TEM to Characterize Li-Metal Dendrite Formation

Understanding the physical/chemical property of the deposited lithium metal and its nanostructure evolution in different electrolytes is crucial to prevent its detrimental dendritic growth and enhance the cycling reversibility. It is difficult to properly characterize lithium metal without damaging or contaminating due to its intrinsic high chemical reactivity and low thermal stability. Inspired from the biology community, cryo protection is applied to reduce the beam damage and stabilize the lithium metal for TEM imaging. The lithium metal was directly deposited on the copper foil of the TEM grid below 0.0 V at 0.5 mA cm^{-2} (Figure 49a-b). The electrolyte is 1 mol/L LiPF_6 in EC/ethylmethyl carbonate (EC/EMC, 50/50 wt%) and its H_2O content is 22 ppm. A 5-minute deposition was chosen to highlight the nucleation process and avoid the lithium full coverage on the grid (Figure 49c). After deposition, the cell was disassembled in the glovebox where the grid was taken out and slightly rinsed with DMC to remove trace lithium salt. The grids were then loaded in a covered cryogenic dewar with continuous argon flow. The holder was pumped down to 10^{-5} bar and quickly loaded into a vacuum transfer chamber, where it remained under vacuum to be cooled to 100 K before introducing it to the microscope for imaging. It was demonstrated last quarter that lithium metal was quite unstable and quickly drifted once the beam focused on the sample even at a low magnification (19 kX) at room temperature (300 K). In contrast, lithium metal is very stable at 100 K (Figure 49d-f); no visible changes are observed with the same magnification as the room temperature. Therefore, development of the cryo-TEM allows detection of the lithium metal at the nano scale while avoiding beam damage of the sample.

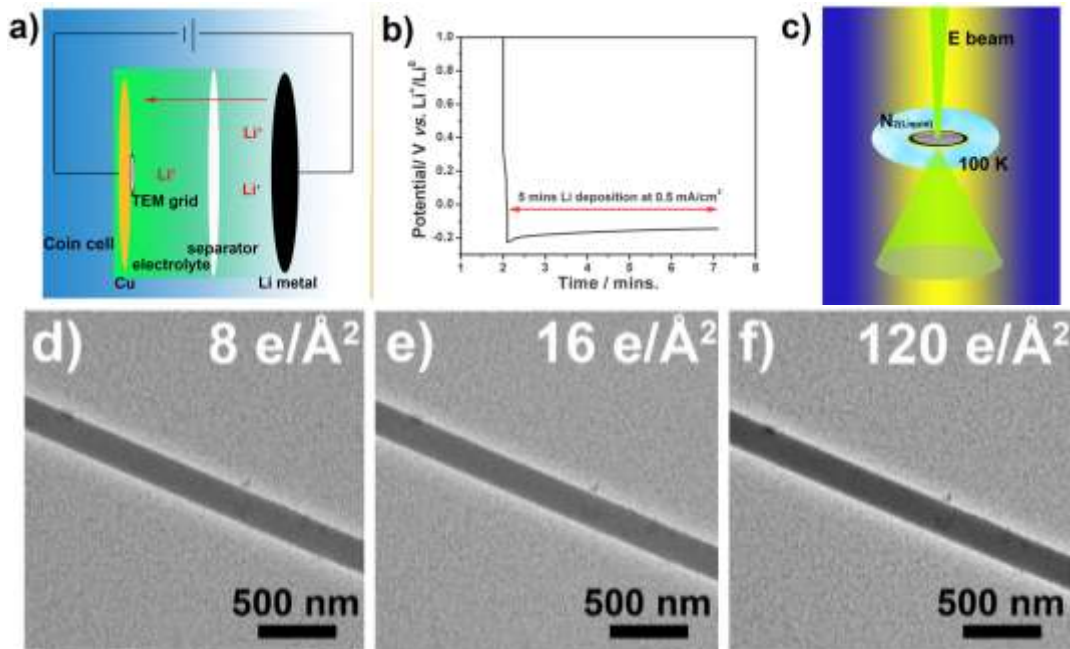


Figure 49. Schematic cell configuration: (a) potential curve, (b) schematic cryo transmission electron microscopy (TEM) imaging of the EDLi for TEM observation, and (c) TEM images of the EDLi as a function of the electron radiation dose at 100 K (d-f at 19 kX magnification).

Patents/Publications/Presentations

Publication

- Singer, A., and M. Zhang, Y. S. Meng, O. G. Shpyrko, et al. “Nucleation of Dislocations and Their Dynamics in Layered Oxides Cathode Materials during Battery Charging.” Under review.

Presentations

- MRS Meeting, Phoenix, Arizona (2017): “Morphological and Surface Structural Changes during Electrochemical Cycling in Li-rich Layered Oxides for Next Generation Li-Ion Batteries”; M. Zhang, H. D. Liu, C. Fang, and Y. S. Meng.
- MRS Meeting, Phoenix, Arizona (2017): “Diagnostic Comparison between Lithium-Rich Layered Oxides and Classical Layered Oxides”; Y. S. Meng. Invited.

Task 5.6 – *In Situ* Diagnostics of Coupled Electrochemical-Mechanical Properties of Solid Electrolyte Interphases on Lithium Metal Rechargeable Batteries
(Xingcheng Xiao, General Motors; Brian W. Sheldon, Brown University; Yue Qi, Michigan State University; and Y. T. Cheng, University of Kentucky)

Project Objective. The project objective is to develop a comprehensive set of *in situ* diagnostic techniques combined with atomic/continuum modeling schemes to investigate and understand the coupled mechanical/chemical degradation of the SEI layer/lithium system during lithium cycling. The goal of this understanding is to develop a new coating design strategy to achieve high cycle efficiency/dendrite free and extend the cycle life of high-energy-density batteries with lithium as the anode for EV application.

Project Impact. The fundamental understanding of the coupled mechanical/chemical degradation of the SEI layer during lithium cycling will enable the project to identify the desirable mechanical properties on SEI/lithium as a system and the specific transport properties that enable the homogenous lithium stripping/plating while avoiding the mossy structure. Furthermore, it will allow the project to develop a highly impactful strategy to protect lithium metal and achieve dendrite-free high cycle efficiency, which can dramatically increase the energy density of lithium batteries for EV applications.

Approach. Different *in situ* techniques, including AFM, nanoindenter, dilatometer, and stress-sensor, will be developed to investigate the mechanical compatibility between SEI and soft lithium and the relationship between surface morphology and current density distribution that results in an inhomogeneous lithium plating/stripping process. Multiple strategies will be developed to tailor the mechanical and transport properties of SEI and to properly engineer the protective coating/lithium interface.

Out-Year Goals. The project will first develop a lithium film model-system with well-controlled thickness, roughness, and textures for different *in situ* diagnostic tools and cycle performance tests. Then, a comprehensive set of *in situ* diagnostic tools will be adapted from the previous work to characterize the mechanical behavior of both SEI and lithium electrodes. In parallel, the advanced electrochemical characterization and postmortem analysis will be used to characterize the electrochemical performance, composition, and microstructure of the SEI and lithium.

Collaborations. Prof. Huajian Gao (Brown University) and Dr. Peng Lu (GM) will be the key researchers involved in continuum simulation and postmortem analysis. Dr. Chongmin Wang (PNNL), Dr. Wangli Yang (LBNL), and Dr. Jie Xiao will be collaborators on advanced *in situ* analysis and electrolyte additives.

Milestones

1. Li-film electrodes with controlled thickness and roughness developed. (Q1 – Completed December 2016)
2. Composition map of representative SEI as a function of current density and capacity established. (Q2 – Completed March 2017)
3. The results from different tools correlated with SEI microstructure, transport properties, and cycle performance. (Q3 – Completed June 2017)
4. *Go/No-Go*: Decision based on information obtained from *in situ* and *ex situ* experiments demonstrated to be complementary and coherent. (September 2017)

Progress Report

The coupled electrochemical-mechanical properties of the SEI on lithium metal for rechargeable batteries were investigated. The work function, band gap, and tunneling barrier with stress/strain for different SEI components were computed via density functional theory (DFT) – generalized gradient approximation (GGA) and hybrid (HSE06) functionals. The SEI components studied were Li_2O , LiF , Li_2CO_3 (major components of dense layer of SEI) and another excellent solid electrolyte, Li_3PO_4 . The tunneling probability was plotted as a function of SEI thickness for different components (Figure 50). From the HSE06 data it was seen that, for a given SEI thickness, an electron would tunnel more easily through the SEI components in the following order: $\text{Li}_2\text{CO}_3 > \text{Li}_2\text{O} > \text{Li}_3\text{PO}_4 > \text{LiF}$. This implies that higher HF volume fraction in SEI can improve the CE.

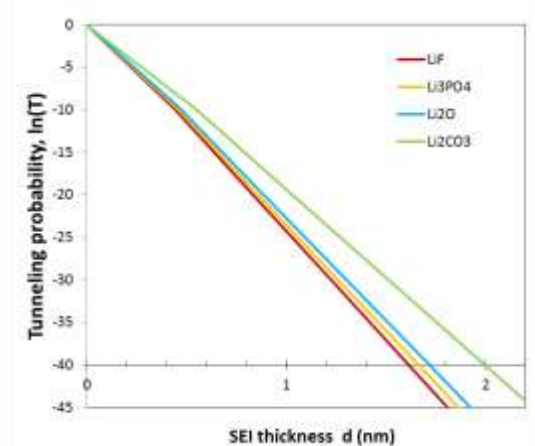


Figure 50. Tunneling probability for SEI components.

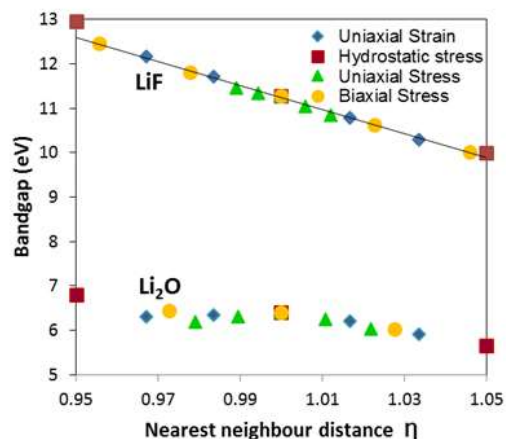


Figure 51. Bandgap change with anion distance.

For LiF (and Li_2O) as the SEI component, the bandgaps were calculated under different loading conditions. The bandgap (and tunneling barrier) decreases under tension and increases under compression for LiF . In the case of Li_2O , the bandgap decreases under tension, but mainly remains a constant under compression. For LiF , different loading conditions can be unified by the normalized average anion distance, η , and the band gap scale linearly with η . Such scaling relationship has not been found for Li_2O yet. This will be further investigated.

Mechanical properties of lithium metal in the electrolyte environment have been investigated using the nanoindentation system in a glovebox. An *in situ* fluid cell for nanoindentation has been developed to investigate the coupled mechanical/chemical properties of lithium in the electrolyte environment (1M LiPF_6 in EC:DEC=1:1 solution, the wet condition). There is no difference in the load-displacement curves of lithium metal under dry and wet conditions (shown in Figure 52). Therefore, the influence of the electrolyte on the mechanical properties of bulk lithium metal may be neglected.

The microstructure-dependent mechanical behavior of porous lithium has been investigated using the same nanoindentation system. The microstructure of porous lithium is controlled by regulating the current density during electroplating. As shown in Figure 53, the lithium cluster under high current density (2.4 mA/cm^2) is more compact than that under low current density (0.4 mA/cm^2). In addition, the average size of individual lithium dendrite under high current density is larger than low current density. Nanoindentation tests of porous lithium were conducted under the wet condition. The indentation depth of the

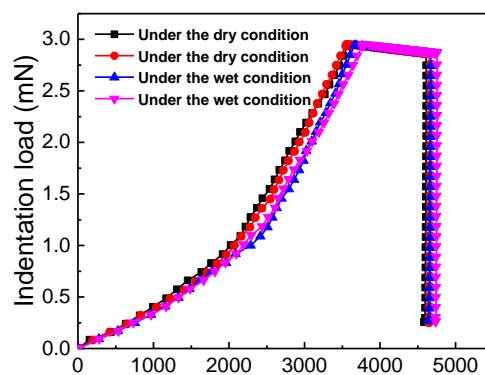


Figure 52. The load-displacement curves of lithium metal in dry and wet conditions.

denser porous lithium is 22% smaller of that of the bulk lithium, while the indentation depth of highly porous lithium is 1 time larger than the bulk lithium. The indentation deformation resistant sequence is, therefore, microstructure (a) > bulk lithium > microstructure (b). The difference in nanoindentation response of lithium metal stems from the microstructure, that is, the porosity of porous lithium and the morphology of lithium dendrites. Further study will focus on uncovering the quantitative relationship between microstructure and mechanical properties of porous and dendritic lithium.

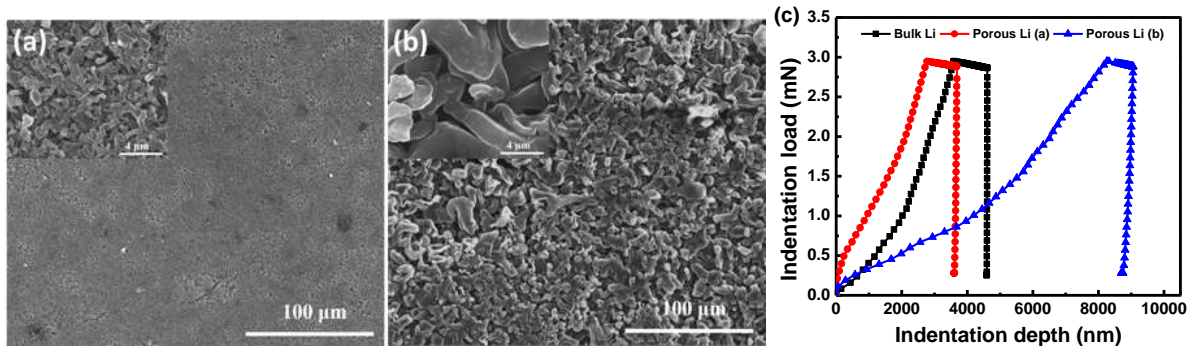


Figure 53. Microstructure of porous lithium obtained under current density (a) 2.4 mA/cm² and (b) 0.4 mA/cm². (c) Typical load-displacement curves of bulk and porous lithium under the wet condition.

An Analytical Model of Pop-Up Delamination of Electrodes in Solid-State Li-Metal Batteries. The analytical solution predicts a delamination mode transition from single-blistering to multi-blistering as the delaminated region spreads along the interface, as well as a threshold lithium concentration below which the pop-up delamination is fully suppressed (Figure 54). The analytical solutions have been validated by finite element simulations. While delamination buckling with a single blister is predicted to occur in an electrode with a liquid electrolyte, multi-blistering often occurs in solid-state batteries. This can be much more difficult to detect during cell operation, but still detrimental to the contact between the electrode and the current collector. The energy release rate calculation shows that the pop-up delamination can be suppressed by stiffening or thinning the solid electrolyte. This work may provide a guideline for the design of delamination resistant electrode system in solid-state, Li-metal batteries.

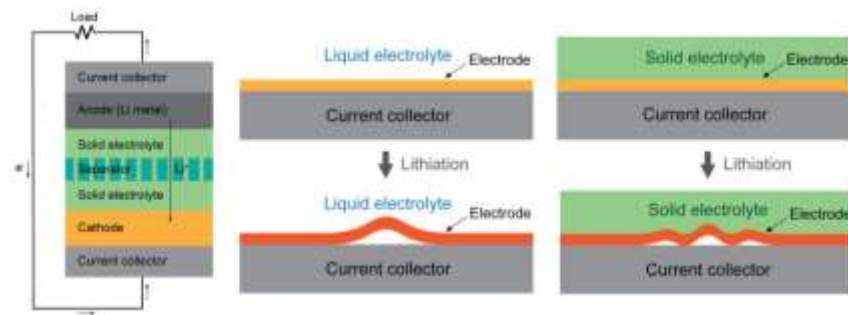


Figure 54. Schematic of a solid-state battery and pop-up modes of an electrode with a liquid electrolyte or a solid electrolyte.

Patents/Publications/Presentations

Publications

- Kim, K. J., and J. Wortman, S. Y. Kim, and Y. Qi. “Atomistic Simulation Derived Insight on the Irreversible Structural Changes of Si Electrode during Fast and Slow Delithiation.” *Nano Letters* 17 (2017): 4330–4338.
- Su, X., and K. Guo, T. Ma, P. A. Tamirisa, H. Ye, H. Gao, and B. W. Sheldon. “Deformation and Chemomechanical Degradation at Solid Electrolyte–Electrode Interfaces.” *ACS Energy Letters* 2 (2017): 1729–1733.
- Guo, K., and P. A. Tamirisa, B. W. Sheldon, X. Xiao, and H. Gao. “Pop-Up Delamination of Electrodes in Solid-State Batteries.” To be submitted to *J. Power Sources*.

Presentations

- Advanced Automotive Battery Conference, San Francisco, California (June 20, 2017): “Towards High Cycle Efficiency of High Energy Density Lithium Ion Batteries”; X. Xiao.
- MRS Spring Meeting, Phoenix, Arizona (April 2017): “Multi-Component and Multi-Functional Protection Coating for High Capacity Anodes (Li and Si)”; Yue Qi.
- 21st International Conference on Solid State Ionics, Padua, Italy (June 2017): “DFT and DFTB Simulations of Lithium Ion Transport through the Complex Electrode/SEI/Electrolyte Interface”; Yue Qi.

Task 5.7 – Microscopy Investigation on the Fading Mechanism of Electrode Materials (Chongmin Wang, Pacific Northwest National Laboratory)

Project Objective. The objective will be using a combination of *ex situ*, *in situ*, and *operando* HRTEM and spectroscopy to probe the fading mechanism of layer structured cathode under high-voltage operating condition. To complement the HRTEM study, *in situ* liquid cell SIMS and atom probe tomography (APT) will also be used to gain structural and chemical evolution of electrodes and correlate the structural and chemical evolution with battery performance.

Project Impact. The proposed characterization work focused on atomic level structural and chemical analysis and direct correlation with battery fading properties. The work can be directly used to guide the designing of electrode materials with tailored microstructure and chemistry for enhanced properties of increasing the energy density of Li-ion batteries and to accelerate market acceptance of EV, especially for PHEV required by the EV Everywhere Grand Challenge.

Approach. This project will use the unique *ex situ* and *in situ* TEM methods to probe the structure of Li-ion batteries, especially a biasing liquid electrochemical cell that uses a real electrolyte in a nano-battery configuration. It will also use various microscopic techniques, including *ex situ*, *in situ*, and especially the *operando* TEM system, to study the fading mechanism of electrode materials in batteries. This project will be closely integrated with other R&D efforts on high-capacity cathode and anode projects in the BMR Program to: (1) discover the origins of voltage and capacity fading in high-capacity layered cathodes, and (2) provide guidance for overcoming barriers to long cycle stability of electrode materials.

Out-Year-Goals. This project has the following out-year goals:

- Multi-scale (ranging from atomic-scale to meso-scale) *ex situ/in situ* and *operando* TEM investigation of failure mechanisms for energy-storage materials and devices. Atomic-level *in situ* TEM and STEM imaging to help develop fundamental understanding of electrochemical energy-storage processes and kinetics of electrodes.
- Extend the *in situ* TEM capability for energy storage technology beyond lithium ions, such as Li-S, Li-air, Li-metal, sodium ions, and multi-valence ions.

Collaborations. This project collaborates with Michael M. Thackeray and Jason Croy (ANL); Guoying Chen (LBNL); Jagjit Nanda (ORNL); Chunmei Ban (NREL); Khalil Amine (ANL); Donghai Wang (Pennsylvania State University), Arumugam Manthiram (UT Austin), Wei Tong (LBNL), Gao Liu (LBNL); Yi Cui (Stanford University); Jason Zhang (PNNL); Jun Liu (PNNL); Xingcheng Xiao (GM), Shirley Meng (UCSD), and Stan Whittingham (SUNY –Binghamton).

Milestones

1. Void formation mechanism and its correlation with ionic mobility in the lattice upon high-voltage cycling; exploring lattice stability with dopant such as tin, silicon, and phosphorous. (Q2 – Completed March 2017)
2. Atomic-level identification of behavior of nickel, manganese, cobalt, and aluminum in the NCM and NCA when cycled at high voltage; correlate with fading mechanism. (Q3 – Completed June 2017)
3. Environmental TEM (ETEM) studies of the nickel segregation characteristics, and correlation with materials processing temperature. (Q4 September 2017 – Initiated June 2017)

Progress Report

Layered lithium TM oxides (LTMO) are promising cathode materials for next generation high-energy-density Li-ion batteries. The challenges for using this category of cathode are capacity and voltage fading; these are believed to be associated with the layered structure disordering, a process initiated from the surface or SEI and facilitated by TM reduction and oxygen vacancy formation. However, the atomic level dynamic mechanism of such a layered structure disordering remains unclear.

Intensive studies reveal that such phase transformation is initiated by local chemistry change, including TM reduction and aggregation, lithium depletion, and oxygen loss. Lattice transformation, from layered to either spinel-like structure or rock-salt structure, is realized through TM migration, noting that the oxygen sub-lattice adopts the same stacking sequence during the phase transformation. Therefore, suppression of TM migration is the key to stabilize the layered structure during cycling.

It was proposed that, among nickel, cobalt, and manganese, nickel ions are prone to migrate to initialize the lattice transformation. However, direct evidence for this claim is still lacking. Based on high-energy electron irradiation, it has been reported that nickel ions, as contrasted with manganese ions, are prone to migrate into Li-layer in the Li-rich LTMO. However, migration behavior of nickel, cobalt, and manganese during electrochemical cycling is still not well characterized.

In recent work, the spatial evolution of nickel, cobalt, and manganese in a cycled $\text{LiNi}_{1/3}\text{Mn}_{1/3}\text{Co}_{1/3}\text{O}_2$ (NMC-333) layered cathode was mapped using atomic resolution EELS. In combination with atomic level structural imaging, a direct correlation of TM ions migration behavior with lattice disordering has been established. Specifically, the surface layer structural and chemical evolution of NMC-333 following the high-cutoff voltages cycling at 4.2 V and 4.8 V were studied. It was noticed that 4.8 V cycling can introduce a much thicker surface phase transformation layer. STEM-annular bright field (STEM-ABF) imaging directly reveals the residing of TM-ions at the tetrahedral site in the heavily disordered region. A sequential migration of nickel, cobalt, and manganese upon the increased lattice disordering of the layered structure has been noticed (Figure 55). This observation indicates that nickel ions, though acting as the dominant redox species in many LTMO, are labile to migrate to cause lattice disordering upon battery cycling; the manganese ions are more stable as compared with nickel and cobalt, and can act as a pillar to stabilize layered structure.

The present observations provide key insights on the lattice degradation mechanism of layered LTMO at atomic level, shedding new light on material selection and composition optimization for NMC-based LTMO in countering lattice degradation and correspondingly mitigating capacity and voltage fading.

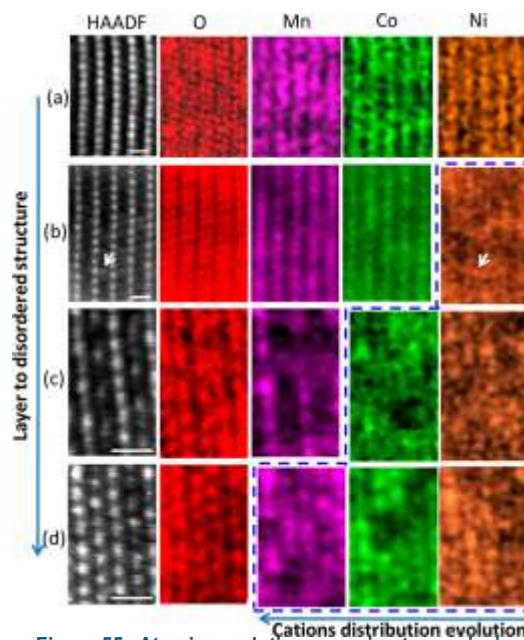


Figure 55. Atomic resolution scanning transmission electron microscopy – electron energy loss spectroscopy (STEM-EELS) mapping of NMC-333. (a) From the pristine NMC-333 without cycling. (b–d) From NMC-333 after 100 cycles with a high cutoff voltage of 4.8 V. (b) From the well-preserved layered region. (c) From the disordered region. (d) From the heavily disordered region. The dashed blue frame at bottom right highlights transition metal maps with disordered structure. The white arrows in row b indicate a correspondence between the STEM – high-angle annular dark-field (HAADF) image and EELS map for identifying the nickel that migrates to the lithium layer. The scale bars in HAADF images are 0.5 nm.

Patents/Publications/Presentations

Publication

- Yan, Pengfei, and Jianming Zheng, Ji-Guang Zhang, and Chongmin Wang. “Atomic Resolution Structural and Chemical Imaging Revealing the Sequential Migration of Ni, Co, and Mn upon the Battery Cycling of Layered Cathode.” *Nano Lett.* 17 (2017): 3946–3951.

Presentation

- MRS Spring Meeting, Phoenix, Arizona (April 4, 2017): “Advanced Electron Microscopy Probing of Functioning Mechanisms of Nanoscale Surface Coating Layer for Mitigating Capacity Fading of Lithium Ion Battery”; Chongmin Wang. Invited.

Task 5.8 – Characterization and Computational Modeling of Structurally Integrated Electrodes (Michael M. Thackeray and Jason R. Croy, Argonne National Laboratory)

Project Objective. The primary project objective is to explore the fundamental, atomic-scale processes that are most relevant to the challenges of next-generation, energy-storage technologies, in particular, high-capacity, structurally integrated electrode materials. A deeper understanding of these materials relies on novel and challenging experiments that are only possible through unique facilities and resources. The goal is to capitalize on a broad range of facilities to advance the field through cutting-edge science, collaborations, and multi-disciplinary efforts to characterize and model structurally integrated electrode systems, notably those with both layered and spinel character.

Project Impact. This project capitalizes on and exploits DOE user facilities and other accessible national and international facilities (including skilled and trained personnel) to produce knowledge to advance Li-ion battery materials. Specifically, furthering the understanding of structure-electrochemical property relationships and degradation mechanisms will contribute significantly to meeting the near- to long-term goals of PHEV and EV battery technologies.

Approach. A wide array of characterization techniques including X-ray and neutron diffraction, X-ray absorption, emission and scattering, HRTEM, Raman spectroscopy, and theory will be brought together to focus on challenging experimental problems. Combined, these resources promise an unparalleled look into the structural, electrochemical, and chemical mechanisms at play in novel, complex electrode/electrolyte systems being explored at ANL.

Out-Year Goals. The out-year goals are as follows:

- Gain new, fundamental insights into complex structures and degradation mechanisms of high-capacity composite cathode materials from novel, probing experiments carried out at user facilities and beyond.
- Investigate structure-property relationships that will provide insight into the design of improved cathode materials.
- Use knowledge and understanding gained from this project to develop and scale up advanced cathode materials in practical Li-ion prototype cells.

Collaborators. This project collaborates with the following: J. R. Croy, A. Gutierrez, R. Benedek, Meinan He, Jie Wang (ANL).

Milestones

1. Characterize bulk and surface properties of structurally integrated electrode materials using the DOE User Facilities at ANL, including the APS, Electron Microscopy Center, and Argonne Leadership Computing Facility (ALCF), along with facilities elsewhere (for example, SNS), EMSL at PNNL, and the Northwestern University's Atomic and Nanoscale Characterization Experimental Center (NUANCE). (Q4 – In progress, September 2017; see text)
2. Use complementary theoretical approaches to further the understanding of structural and electrochemical properties of LS electrodes and protective surface layers. (Q4 – In progress, September 2017)
3. Analysis, interpretation, and dissemination of collected data for publication and presentation. (Q4 – In progress, September 2017)

Progress Report

Efforts to integrate spinel components into lithium- and manganese-rich, layered-layered (LL) electrode materials to create complex LLS materials has generated significant interest due to their resultant, promising electrochemical properties. In particular, the spinel framework, being more robust to TM migration, could be a viable route to structural stabilization and the mitigation of phenomena such as voltage fade. However, controlling the content and composition of spinel domains is a challenge with respect to practical synthesis methods. Furthermore, controlling the distribution of spinel domains within integrated cathode structures may also be a very important consideration. For example, LL materials are known to undergo severe surface damage upon activation and high-voltage cycling. If a stabilizing spinel component could be concentrated at the surface of LL particles, it is possible that additional stability could be imparted, thereby extending the useful cycle life of such LLS electrodes. Recent reports have shown that certain surface treatments can positively influence the electrochemical performance of LLS cathode materials. In particular, exposure of LLS particles to an aqueous, acidic solution of Al, followed by a low-temperature heat treatment ($\sim 110^{\circ}\text{C}$), resulted in an unexpected improvement in capacity retention and rate capability as well as mitigated impedance rise relative to untreated particles. The improvements were unexpected in that the low-temperature treatment produced a distorted, Al-oxy-hydroxide film on the particle surface, whereas higher temperatures drove aluminum into the lattice and consequently degraded electrochemical performance. To gain more insight into the mechanisms of improvement for the low-temperature, Al-treated materials, microscopy studies were conducted.

Figure 56a shows a SEM image of an Al-treated, LLS particle after undergoing a focused ion beam (FIB) lift-out procedure to allow for elemental mapping studies. Figure 56b shows a high resolution transmission electron microscopy image (HRTEM) of particles including two regions included for Fast Fourier Transform (FFT) analysis. This figure, and similar images, suggest that the Al-treated, LLS particles may have preferentially formed spinel domains at the surface of particles, possibly due to lithium leaching in an acidic environment. Figure 56c shows energy-dispersive X-ray spectroscopy (STEM-EDX) of an Al-treated, LLS particle. It was found that a thin (~ 2 nm) aluminum layer covered the particles in a uniform manner, verifying the efficacy of the treatment conditions. However, some images showed indications of increased concentrations of both aluminum and nickel on the same surfaces, for example, top left and bottom right in Figure 56c. Whether this “segregation” is a consequence of the surface treatment itself, or other mechanisms related to the pristine particles is unclear. Additional imaging is under way for both treated and untreated particles to obtain better statistics on the relative formation of surface spinel and any possible tendencies of segregation (for example, preferential location of Ni/Al) between treated and untreated particles. This information is expected to provide further insight into the structure-property relationships of LLS materials and the dependence of their electrochemical properties on processing conditions.

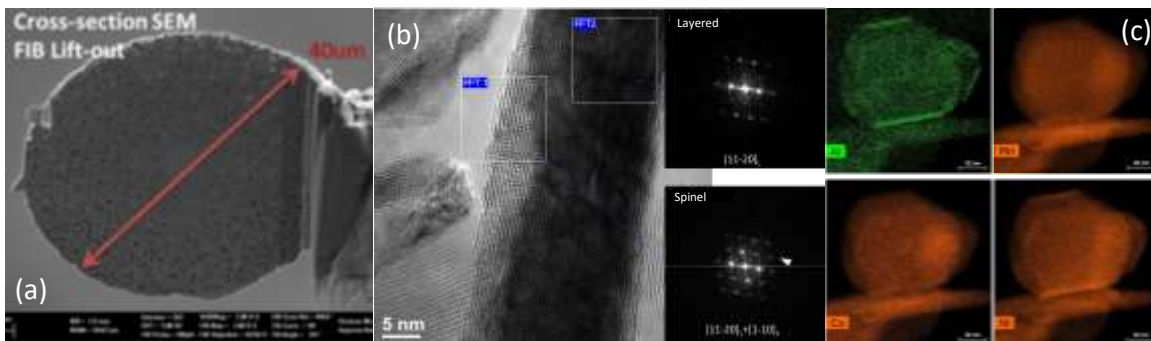


Figure 56. (a) Cross-sectional scanning electron microscopy image of Al-treated, layered-layered-spinel (LLS) particle. (b) Transmission electron microscopy image and fast Fourier transform (FFT) of surface and bulk regions showing spinel integration at the surface of the particle. (c). STEM-EDX analysis of Al-treated LLS particle showing distribution of Al (top left), Mn (top right), Co (bottom left), and Ni (bottom right).

Patents/Publications/Presentations

Publication

- Benedek, R., and H. Iddir. “Simulation of First-Charge Oxygen-Dimerization and Mn-Migration in Li-Rich Layered Oxides $x\text{Li}_2\text{MnO}_3 \cdot (1-x)\text{LiMO}_2$ and Implications for Voltage Fade.” *J. Phys. Chem. C* 121 (2017): 6492.

Publication

- DOE Annual Merit Review, Washington, D. C. (June 5 – 9, 2017): “Characterization and Modeling of High-Capacity Composite Electrode Structures” ES235; J. R. Croy and M. M. Thackeray.

TASK 6 – MODELING ADVANCED ELECTRODE MATERIALS

Summary and Highlights

Achieving the performance, life, and cost targets outlined in the EV Everywhere Grand Challenge will require moving to next generation chemistries, such as higher capacity Li-ion intercalation cathodes, silicon and other alloy-based anodes, Li-metal anode, and sulfur cathodes. However, numerous problems plague development of these systems, from material-level challenges in ensuring reversibility to electrode-level issues in accommodating volume changes, to cell-level challenges in preventing cross talk between the electrodes. In this task, a mathematical perspective is applied to these challenges to provide an understanding of the underlying phenomenon and to suggest solutions that can be implemented by the material synthesis and electrode architecture groups.

The effort spans multiple length scales from *ab initio* methods to continuum-scale techniques. Models are combined with experiments, and extensive collaborations are established with experimental groups to ensure that the predictions match reality. Efforts are also focused on obtaining the parameters needed for the models, either from lower-length scale methods or from experiments. Projects also emphasize pushing the boundaries of the modeling techniques used to ensure that the task stays at the cutting edge.

In the area of intercalation cathodes, the effort is focused on understanding the working principles of the high nickel layered materials with an aim of understanding structural changes and the associated changes in transport properties. Coatings, an effective strategy for high-voltage operation, are being explored with the aim of providing a rational design approach for new coating materials. In addition, focus is paid to the assembling of porous electrodes with particles to predict the conduction behavior and developing tools to measure electronic conduction. In the area of silicon anodes, the effort is in trying to understand the interfacial instability and suggest ways to improve the cyclability of the system.

In the area of Li-metal anodes, the focus is on understanding how materials can be designed to prevent dendrite growth at high current densities using continuum modeling approaches. The results are used to guide materials development by providing the properties needed to prevent dendrites while also achieving the energy and power goals. Models are also starting to examine the role of the SEI on the morphology of the dendrite.

Highlight. This quarter significant progress was achieved on modeling dendrite growth conditions. The model was revised to include the effect of current density on the propensity for dendrite growth. The model is expected to provide insights into material properties needed for dendrite prevention.

Task 6.1 – Predicting and Understanding Novel Electrode Materials from First Principles (Kristin Persson, Lawrence Berkeley National Laboratory)

Project Objective. This project supports VTO programmatic goals by developing next-generation, high-energy cathode materials and enabling stable cathode operation at high voltages through target particle morphology design, functional coatings, and rational design of electrolytes. The end-of-project goals include: (1) novel disordered, high-rate Li-excess cathodes, (2) new fundamental understanding of the cathode/electrolyte interface and the factors that control the interfacial chemistry and interfacial impedance, (3) critical surface and coating design and optimization strategies that will improve cycling of Li-ion battery cathodes, and finally (4) understanding of the factors that govern stability in nonaqueous electrolytes for Li-ion and Li-S systems.

Project Impact. To enhance the performance of Li-ion systems, improvements on the cathode and the electrolyte side are needed. This project is aimed to result in an improved understanding of the atomistic mechanisms underlying the surface behavior and performance of the Li-ion cathode materials with the ultimate goal being to suggest strategies, such as coatings, surface protection, and particle morphology design. Furthermore, fundamental studies of electrolyte stability, as a function of solvent and salt concentrations, and components will be conducted.

Out-Year Goals. Stable interfaces will be determined by focusing initially on degradation mechanisms related to the release of surface oxygen at high charge. Tuning particle morphology and coating materials—both of crystalline as well as amorphous structure—will be explored using the Materials Project. For the electrolyte development, work will be aimed toward understanding the atomistic interactions underlying the performance of lithium electrolytes specifically elucidating the solvation structure (as a function of salt concentration) and its impact on the stability of different liquid constituent species.

Collaborations. This project is highly collaborative between BMR PIs G. Chen (LBNL), G. Ceder (LBNL) and V. Srinivasan (ANL). Cathode design and synthesis will be performed by Chen and Ceder, surface design by Persson, and electrolyte design and testing by Persson and Srinivasan.

Milestones

1. Provide matrix of surface candidate dopants based on literature search and practical considerations. (December 2016 – Complete)
2. Benchmark calculations of amorphous coating materials, that is, $\text{Al}_2\text{O}_3/\text{SiO}_2$. (March 2017 – Complete)
3. Present first screening of surface dopants. (May 2017 – In progress)
4. *Go/No-Go*: New strategies are identified. Stop this approach if facet stabilization cannot be achieved. (May 2017 – In progress)
5. Evaluate two electrolyte benchmark formulations for Li-S and Li-ion for stability and diffusion. (September 2017 – In progress)

Progress Report

The current BMR project is aimed toward the study of surface stabilization strategies of the Li-excess layered materials using the first-principles calculations. This project is examining the end member of the Li-excess, Mn-rich layered cathodes (Li_xMnO_3). Continuing the previous investigation, the project has been focused on computational screening strategy for finding best candidate surface dopant elements for all five low Miller index surfaces which are (001), (010), (100), (110), and (111). The project aims to identify optimal candidate dopants to increase oxygen retention at the surface of Li-excess materials. Last quarter, the team investigated the dopant segregation tendency, between bulk and surface.

In addition to investigating the dopant segregation toward the surface, the dopant defect formation energy is examined to screen for optimal candidate surface doping elements. The project defines the defect formation energy as;

$$E_{\text{def}}^{\text{surf}} = (\Delta E_{\text{def}}^{\text{surf}} + E_{\text{bulk}}^{\text{Li}_2\text{MnO}_3} - E_{\text{convex hull}}^{\text{Li}_2\text{MnO}_3})$$

where $\Delta E_{\text{def}}^{\text{surf}}$ represents the energy difference between the doped and undoped target system, $E_{\text{bulk}}^{\text{Li}_2\text{MnO}_3}$ the bulk energy of Li_2MnO_3 , and $E_{\text{convex hull}}^{\text{Li}_2\text{MnO}_3}$ the energy above the convex hull of the composite system. The $E_{\text{def}}^{\text{surf}}$ values are listed in the public open database (MaterialsProject.org). Here, this project investigated EDS for all five surfaces as well as the bulk for the stoichiometric compound. All surface defect formation energies are positive numbers which indicates a metastable surface doping process. Consistently, most surface defect formation energies are lower than the comparative bulk (green dashed line in Figure 57). Hence, the dopant elements are relatively more stable on the surfaces, particularly for the (110) surface. In the screening for optimal dopant elements, it is necessary to consider both dopant preference for the surface (as compared to the bulk) as well as the surface defect formation energy. Furthermore, the defect formation energy of the two majority surfaces (001) and (010) facets, are relatively higher than the minority facets (100), (110) and (111). The results are being incorporated into the screening for optimal surface dopants to mitigate surface oxygen release in the Li-excess materials.

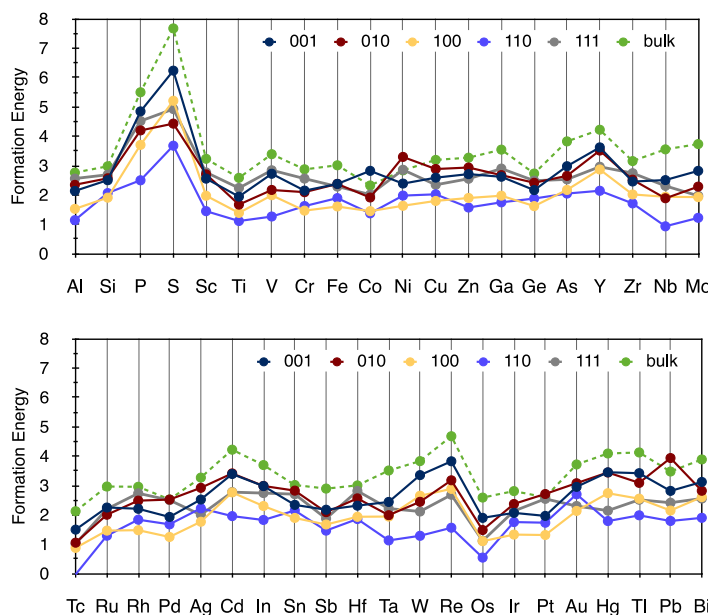


Figure 57. The defect formation energy of each stable surface facet as compared to the bulk, covering defect transition metal, post-transition metal, and metalloid elements.

Patents/Publications/Presentations

Presentation

- DOE Annual Merit Review, Washington, D. C. (June 2017): “Predicting and Understanding Novel Electrode Materials from First Principles”; Yongwoo Shin and Kristin A. Persson.

Task 6.2 – Addressing Heterogeneity in Electrode Fabrication Processes (Dean Wheeler and Brian Mazzeo, Brigham Young University)

Project Objective. The project goal is to better understand connections between fabrication conditions and undesired heterogeneity of thin-film electrodes by means of new nondestructive inspection techniques and computer models. Two nondestructive inspection techniques will be developed or improved to characterize electrochemical and mechanical uniformity of the electrodes. The first tool will be a flexible contact probe on a polymer substrate for rapidly measuring local electrical conductivity across electrodes of any geometry. The second tool will be a new acoustic probe that measures local elasticity and density of the composite film. These two prototyping efforts will be tied together by a particle-based microstructure model that allows prediction and correlation of electrode conductive and mechanical properties with fabrication conditions.

Project Impact. This work will result in new diagnostic and modeling tools for rapidly and conveniently interrogating how well homogeneity has been maintained in electrodes during fabrication and in subsequent cycling. Real-time measurement of heterogeneity will enable manufacturer quality control improvements. The measurement and modeling tools will further enable researchers to compare different electrodes, improve formulations and processes, and anticipate cell performance of new designs.

Out-Year Goals. This project was initiated October 2016 and concludes September 2018. Overall goals by fiscal year are as follows:

- **2017.** Fabricate first-generation flexible conductivity probe and proof-of-concept of acoustic probe; and improve microstructure model to match experiment.
- **2018.** Integrate flex probe with test fixtures suitable for assessment of large or continuous samples; and demonstrate measurement of localized ionic conductivity.

Collaborations. Ram Subbaraman (Bosch), Daniel Abraham (ANL), Steve Harris (LBNL), Bryant Polzin (ANL), and Karim Zaghib (HQ) have provided battery materials for analysis. Other collaborations and the transfer of this technology to interested parties are being pursued.

Milestones

1. Complete flex probe prototype and demonstrate that measurements match those for the previous rigid probe. (Q1 – Complete)
2. Integrate the flex probe with existing high-precision positioning system and make measurements on 3 different electrode materials. (Q2 – Complete)
3. Demonstrate that the dynamic particle packing (DPP) model can predict effective conductivities that match experiment for 3 different electrode materials. (Q3 – Complete)
4. Complete prototype of localized acoustic probe and associated model. *Go/No-Go:* Determine whether to continue developing the acoustic method by assessing sensitivity to film stiffness. (Q4 – On track)

Progress Report

A significant part of VTO-funded efforts at BYU has been to develop a versatile and accurate electrode microstructure prediction model. The model uses fundamental forces and interactions to determine particle dynamics and packing during all electrode-fabrication steps: mixing, coating, drying, and calendaring. The third milestone of FY 2017 was to make improvements to the DPP microstructural model and validate that it can match experimental values of conductivity for one anode and two cathode films. The previous iteration of the model (FY 2015-2016) was reasonably successful at predicting microstructure and transport and mechanical properties of dried films, but exhibited a few physical deficiencies. Thus, a major overhaul was begun during the last year to incorporate smoothed-particle hydrodynamics (SPH) into the model to better describe slurry and solid bulk behavior and interfaces.

The model uses spheres with a diameter of $\sim 2 \mu\text{m}$ to represent the carbon-binder domain and solvent. Active material particles were constructed from overlapping combinations of spheres; the technique allows different shapes such as bumpy spheroids and flattened discs that approximate the observed shapes of active-material particles. For this milestone, there was an emphasis on the drying and calendaring steps with the new SPH framework because these steps lead to substantial particle rearrangements that directly affect the electrode structure and therefore conductivity. Ionic conductive properties are compared in Table 1, in which tortuosity can be considered a dimensionless resistance to ion movement. The results show that the model is semi-quantitatively correct for three different active materials (each having different particle shapes). Further refinement of the model parameters will be undertaken to achieve quantitative agreement with experiment for a range of physical properties.

Work toward Milestone 4, namely proof of concept of acoustic interrogation of electrode films, is on track. Work is also under way on improvements to N-line conductivity probes for FY 2018 milestones.

Table 2. Simulated and experimental effective ionic transport results, following drying and calendaring steps.

Electrode	Simulation		Experiment	
	Porosity (%)	Tortuosity	Porosity (%)	Tortuosity
CPG-A12	43.9	4.3	36.1	3.4
Toda 523	44.3	5.4	30.0	3.1
Toda HE5050	49.4	3.6	36.1	2.9

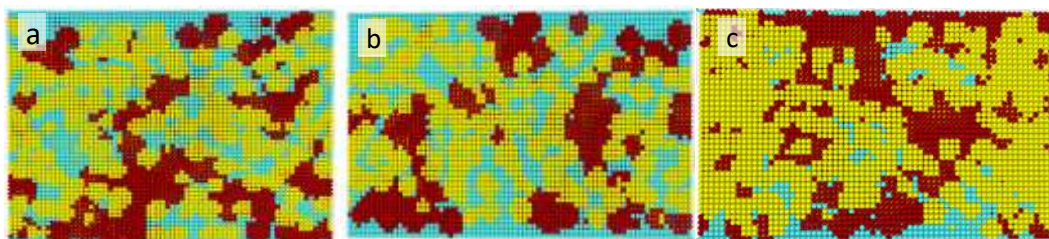


Figure 58. Cross-section images from models of (a) CPG-A12, (b) Toda 523 (B), and (c) Toda HE5050; carbon-binder domain is red, active material is yellow, and larger pores are blue.

Patents/Publications/Presentations

Publications

- Four manuscripts being prepared this quarter, with completion expected next quarter.

Presentations

- DOE Annual Merit Review, Washington, D. C. (June 2017): “Addressing Heterogeneity in Electrode Fabrication Processes”; D. R. Wheeler and B. A. Mazzeo.
- 231st Meeting of the Electrochemical Society (ECS), New Orleans, Louisiana (2017): “Quantifying Tortuosity of Porous Li-Ion Battery Electrodes: Comparing Polarization-Interrupt and AC Impedance (Blocking-Electrolyte) Methods”; F. Pouraghajan, H. Knight, B. A. Mazzeo, and D. R. Wheeler.
- 231st ECS Meeting, New Orleans, Louisiana (2017): “Determination of Mechanical Properties of Battery Films from Acoustic Measurements”; K. L. Dallon, M. Wray, D. R. Wheeler, and B. A. Mazzeo.
- 231st ECS Meeting, New Orleans, Louisiana (2017): “The Effects of Aging on the Tortuosity of Li-Ion Battery Electrodes”; H. Knight, F. Pouraghajan, M. Wray, D. R. Wheeler, and B. A. Mazzeo.
- 231st ECS Meeting, New Orleans, Louisiana (2017): “Flexible Probe for Measuring Local Conductivity Variations in Li-Ion Electrode Films”; E. E. Hardy, J. E. Vogel, D. V. Clement, D. R. Wheeler, and B. A. Mazzeo.
- 231st ECS Meeting, New Orleans, Louisiana (2017): “Local Variation in Microstructure Causes Heterogeneity in the Conductivity of Commercial Lithium-Ion Cathode Films”; J. E. Vogel, D. V. Clement, E. Hardy, B. A. Mazzeo, and D. R. Wheeler.

Task 6.3 – Understanding and Strategies for Controlled Interfacial Phenomena in Lithium-Ion Batteries and Beyond (Perla Balbuena, Jorge Seminario, and Partha Mukherjee, Texas A&M University)

Project Objective. The project objective is to evaluate and characterize interfacial phenomena in lithiated silicon and Li-metal anodes and to develop guidelines for potential solutions leading to controlled reactivity at electrode/electrolyte interfaces of rechargeable batteries using advanced modeling techniques based on first-principles.

Project Impact. Understanding SEI growth on constantly evolving silicon surfaces and on highly reactive Li-metal surfaces is expected to define the electrolyte properties required in high performance cells. Strategies to control the silicon anode instability and pulverization issues and the well-known safety and short effective lifetimes of Li-metal anodes will be developed by tuning the electrolyte composition, structure, dynamic, and stability, as well as that of the electrode morphology and interactions with the electrolyte, based on multiple characterizations of interfacial phenomena.

Approach. A comprehensive multiscale modeling approach including first-principles *ab initio* static and dynamics, classical molecular dynamics, and coarse-grained mesoscopic models will focus on the roles of the electrolyte chemical, structural, and dynamical properties and of the electrode micro- and nanostructure on the formation and evolution of the SEI layer and associated electrochemical performance on silicon and on Li-metal anodes.

Out-Year Goals. Work will progress toward characterizing lithiation and SEI formation at silicon surfaces as well as the subsequent cracking and reforming events under the most realistic modeling conditions. Similarly, the project will investigate electrolyte effects on reactivity and dendrite formation in Li-metal surfaces. The project aims to capture how the chemistry of the various components of the electrolyte (mainly liquids, but also solid polymers and gels) affects the main issues that influence the electrode performance.

Collaborations. This project funds work at Texas A&M University (TAMU). Dr. Chunmei Ban (NREL), Dr. Xiaolin Li (PNNL), and Dr. Kevin Leung (Sandia National Laboratories, SNL) may also contribute.

Milestones

1. Characterize SEI nucleation and modes of cracking as functions of SEI composition on lithiated silicon nanoparticles. (Q1 – Completed December 2016)
2. Identify and quantify Li-ion transport mechanisms through SEI blocks. (Q2 – Completed March 2017)
3. Evaluate and quantify the relative influence of mechanical and chemical degradation interplay in silicon active particles. (Q3 – Completed June 2017)
4. Characterize SEI growth as a function of SEI composition. Compare the SEI rate growth with experimental trends in the literature and from collaborators; if there is any disagreement, revise respective modeling approach. (Q4 – In progress)

Progress Report

Relative Influence of Mechanical and Chemical Degradation Interplay in Silicon Active Particles.

Crystalline silicon showing two-phase behavior converts into amorphous silicon with single-phase behavior after initial lithiation-delithiation cycles. This project investigated the effect of the surface SEI film on

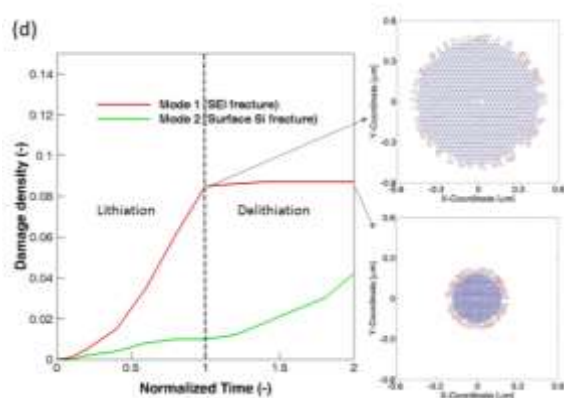


Figure 59. Evolution of damage during lithiation-delithiation of an amorphous silicon particle for one cycle.

amorphous silicon. Higher damage is obtained in the brittle SEI layer as well as active material, with increase in SEI Young's modulus due to faster accumulation of strain energy. Thus, modifying the SEI to decrease its Young's modulus can help mitigate fracture inside both silicon particle and film. The coupled chemical and mechanical degradation is analyzed (Mukherjee) by quantifying the area exposed to electrolyte due to SEI fracture and surface silicon fracture. One type of damage affects diffusion inside the silicon active material and formation of new electrochemically active surface sites for SEI formation, while another type of damage strips the SEI layer leading to its chemical reformation with cycling. Figure 59 shows the damage evolution during one lithiation-delithiation cycle. Rupture of SEI film (fracture due to diffusion-induced stress and volumetric expansion inside active silicon material)

occurs mainly during the lithiation stage because of the SEI film being unable to accommodate the large volumetric expansion of the silicon particle. Silicon particle surface damage (SEI film breakage) is observed predominantly during delithiation because of formation of surface tensile stresses. Clearly, the first mode of damage supersedes the second, and capacity fading with cycling can be predominantly attributed to SEI layer reformation for silicon particle size < 500 nm.

An analysis of the cracking mechanism studied with classical molecular dynamics simulations (Seminario) follows the morphology change of the LiF coating structure upon cracking. The initial LiF crystal structure evolves forming rings and then a monolayer structure as cracking continues. The radial distribution function (RDF) analysis (Figure 60, left)

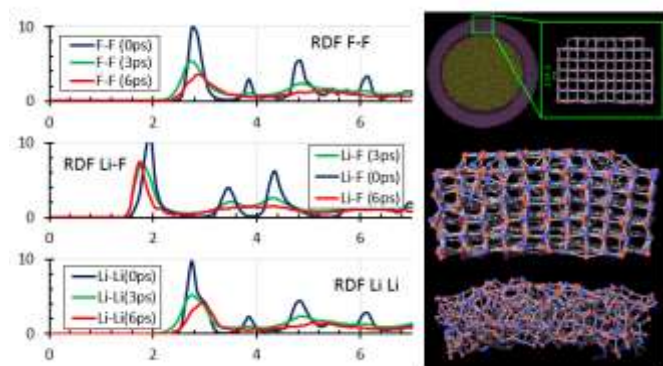


Figure 60. Morphology change of a model LiF coating during cracking of a silicon nanoparticle.

shows shortening of Li–F bonds (1st peak in the Li–F RDF) during particle expansion after several bonds are broken upon cracking. Nonbonded Li–Li and F–F distances tend to increase as the particle expands and cracking propagates.

DFT and *ab initio* molecular dynamics (AIMD) simulations are used to characterize various coatings on the reactivity of silicon nanoparticles (Balbuena). Graphene, reduced graphene oxide (RGO), and self-healing polymer (SHP) films were tested. No decomposition of the electrolyte was

observed in any system during the duration of the simulation (~ 10 ps), whereas severe decompositions were found in absence of the coating. The RGO film did experience some morphological changes (defect formation). In the SHP film, lithium was inserted around it. No decompositions of the polymer were observed, but there was notable disruption of the hydrogen-bonding sites, which are what make the polymer “self-healing.” This was the only system that experienced decomposition of the salt.

Patents/Publications/Presentations

Publications

- Hankins, Kie, and Fernando A. Soto, and Perla B. Balbuena. “Insights into the Li Intercalation and SEI Formation on LiSi Nanoclusters.” *J. Electrochem. Soc.* 164, no. 11 (2017): E3457–E3464.
- Benitez, L., and J. M. Seminario. “Ion Diffusivity through the Solid Electrolyte Interphase in Lithium-Ion Batteries.” *J. Electrochem. Soc.* 164, no. 11 (2017): E3159–E3170.
- Ponce, V., and D. E. Galvez-Aranda, and J. M. Seminario. “Analysis of a Li-Ion Nanobattery with Graphite Anode Using Molecular Dynamics Simulations.” *J. Phys. Chem. C* 121 (2017): 12959–12971.
- Gomez–Ballesteros, Jose L., and Perla B. Balbuena. “Reduction of Electrolyte Components on a Coated Si Anode of Lithium-Ion Batteries.” *J. Phys. Chem. Lett.* In press.
- Horowitz, Yonatan, and Hui-Ling Han, Fernando A. Soto, Walter T. Ralston, Perla B. Balbuena, and Gabor A. Somorjai. “Key to High Performance Silicon Anodes: Fluorine as a Directing Agent for Stable Solid Electrolyte Interphase Formation.” Submitted to *JACS*, May 10, 2017.

Task 6.4 – First Principles Modeling of SEI Formation on Bare and Surface/Additive Modified Silicon Anode (Perla Balbuena, Texas A&M University)

Project Objective. This project aims to develop fundamental understanding of the molecular processes that lead to formation of an SEI layer due to electrolyte decomposition on silicon anodes, and to use such new knowledge in a rational selection of additives and/or coatings. The focus is on SEI layer formation and evolution during cycling and subsequent effects on capacity fade through two concatenated problems: (1) SEI layers formed on lithiated silicon surfaces, and (2) SEI layers formed on coated surfaces. Key issues being addressed include the dynamic evolution of the system and electron transfer through solid-liquid interfaces.

Project Impact. Finding the correspondence between electrolyte molecular properties and SEI formation mechanism, structure, and properties will allow identification of new/improved additives. Studies of SEI layer formation on modified surfaces will allow identification of effective coatings able to overcome the intrinsic deficiencies of SEI layers on bare surfaces.

Approach. Investigating the SEI layer formed on modified silicon surfaces involves the following: (1) analysis of the interfacial structure and properties of specific coating(s) deposited over the silicon anode surface, (2) characterization of the corresponding surface properties before and after lithiation, especially how such modified surfaces may interact with electrolyte systems (solvent/salt/additive), and (3) what SEI layer structure, composition, and properties may result from such interaction. This study will allow identification of effective additives and coatings able to overcome the intrinsic deficiencies of SEI layers on bare surfaces. Once the SEI layer is formed on bare or modified surfaces, it is exposed to cycling effects that influence its overall structure (including the anode), chemical, and mechanical stability.

Out-Year Goals. Elucidating SEI nucleation and electron transfer mechanisms leading to growth processes using a molecular-level approach will help establish their relationship with capacity fading, which will lead to revisiting additive and/or coating design.

Collaborations. Work with Chunmei Ban (NREL) consists in modeling the deposition-reaction of alucone coating on silicon surfaces and their reactivity. Reduction of solvents and additives on silicon surfaces was studied in collaboration with K. Leung and S. Rempe from SNL. This project collaborates with Professor Jorge Seminario (TAMU) on electron and ion transfer reactions and with Dr. Partha Mukherjee (TAMU) focusing on development of a multi-scale model to describe SEI growth on silicon anodes.

Milestones

1. Determining matching and chemistry of solid-solid interfaces including possible cracking effects. Further force-field development and test for solid-liquid interfaces. (Complete)
2. Perform further computational studies on SEI formed in alucone coating including some experimental tests by Chunmei Ban and Clare Grey. (In progress)

Progress Report

Ion Transport from the Cathode through the Electrolyte to the Anode. This project investigated Li-ion transport in a model nanobattery containing all the main elements: from the cathode through the electrolyte to a graphite anode, using classical molecular dynamics simulations. Figure 61 illustrates the interaction energy experienced by one lithium ion traveling under an applied potential through all the phases.

Region 1 (cathode) shows the lithium ion in the LiCoO_2 crystal with a potential energy average of -255 kcal/mol. After 4.62 ps, the lithium ion has moved to the interface between regions 1 and 2 (electrolyte). An average energy of -36.7 kcal/mol is calculated in region 2, which represents the binding of the lithium ion with the electrolyte solution. The energy for the lithium ion to leave the cathode-electrolyte interface is 218.3 kcal/mol; this energy is supplied by the applied electric field. After the lithium ion has gone through the electrolyte, entered the anode, and been reduced, its potential energy average in region 3 is 2.1 kcal/mol and the binding energy of the lithium ion at the anode-electrolyte interface at 38.8 kcal/mol. Notice that this is the energetics for a particular lithium ion; these energies are not representative averages, as they simply allow the project to obtain typical geometric structures of the Li-ion local environment.

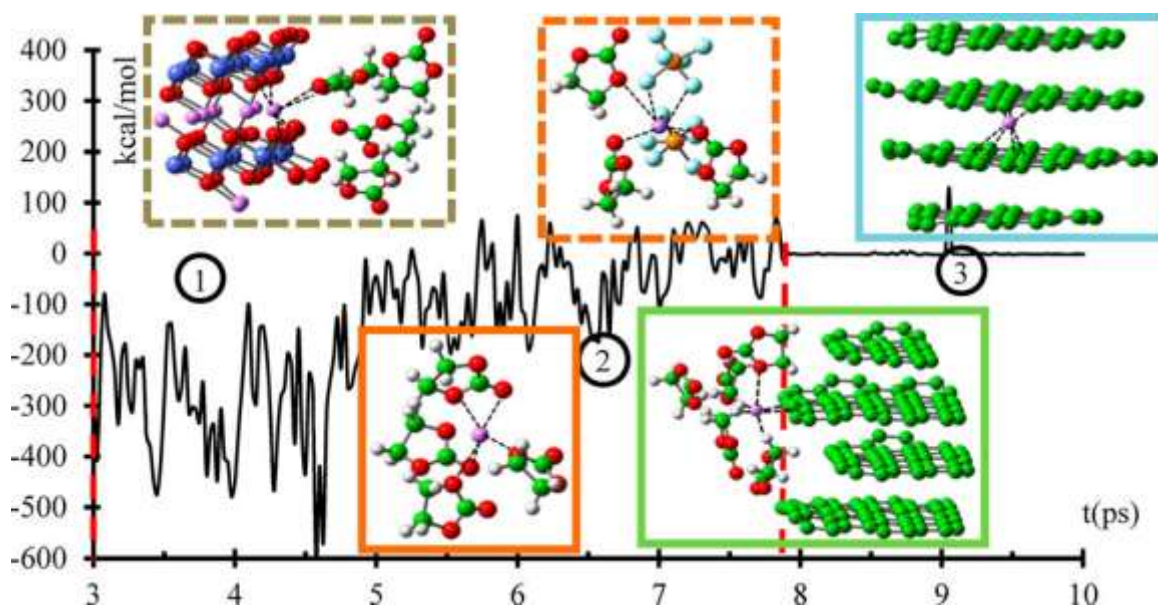


Figure 61. Interaction energy (E) of one lithium ion with its nearest neighbors within a sphere of 6 \AA radius during charging with $E = 1.0 \text{ V/\AA}$. This is a particular trajectory of a lithium ion from the cathode (1) through the electrolyte (2) to the anode (3). [Ponce et al. *JPC* 121 (2017): 12959.]

Reactivity of Alucone Coating. Current work in collaboration with NREL focuses on the reactivity behavior of an alucone coating deposited on a silicon anode. The project studied the reactivity of the film using AIMD simulations and were able to detect changes in the oxidation state of aluminum in the film, as well as changes in its coordination number, and structural changes inside the film. These properties are also being studied experimentally at NREL. The project is preparing a full report of findings to be submitted for publication in an invited issue.

Dissolution of Manganese Cations from the Cathode and Travelling to Anode Side. To better understand cross-talk effects between cathode and anode chemistries, the project has carried out AIMD simulations of a model manganese cation surrounded by a model environment, and has followed its trajectory through bulk electrolyte and then near the anode/electrolyte interface. It was found that the manganese cation travels with its solvation shell through the electrolyte; it is reduced at the anode surface, and incorporated into the SEI layer at the anode. More details will be reported in a new publication.

Patents/Publications/Presentations

Publications

- Benitez, L., and J. M. Seminario. “Ion Diffusivity through the Solid Electrolyte Interphase in Lithium-Ion Batteries.” *J. Electrochem. Soc.* 164, no. 11 (2017): E3159–E3170.
- Ponce, V., and D. E. Galvez-Aranda, and J. M. Seminario. “Analysis of a Li-Ion Nanobattery with Graphite Anode Using Molecular Dynamics Simulations.” *J. Phys. Chem. C* 121 (2017): 12959–12971.

Task 6.5 – Electrode Materials Design and Failure Prediction (Venkat Srinivasan, Argonne National Laboratory)

Project Objective. The project goal is to develop a continuum-based mathematical model to (1) investigate the impact of mechanical stress on growth of dendritic protrusions and (2) elucidate competition between transport and mechanical means for preventing dendrite growth. Effectiveness of protective layers in preventing growth of dendritic protrusions will also be studied. The focus will be to develop a microscale model that can capture the mechanical stresses and transport processes within lithium metal and adjacent electrolyte/protective layer. Impact of surface energy on growth of dendrites will be investigated. Possibility of plastic deformation within lithium metal and/or solid electrolyte material will also be elucidated along with its effect on propagation of dendrites. Propensity of fracture within the SEI layer (or the protective layer) and its impact on dendrite growth will be explored.

Project Impact. The next-generation Li-ion batteries are expected to use Li-metal based anodes, which offer low reduction potential and superior specific capacity. The biggest drawback preventing widespread usage of Li-metal anodes is formation of dendrites over multiple cycles during operation at higher current densities. Insight gained from this project will provide guidance in designing solid polymer electrolytes (or protective layers) that prevent growth of dendrites on lithium metal.

Out-Year Goals. At the end of this project, a mathematical model will be developed that can capture the mechanical stress field, concentration, and potential profiles around a dendritic protrusion. This model will allow estimation of the propensity for growth of such a protrusion and provide guidance in design of solid polymer electrolytes (or protective layers) for prevention of lithium dendrites.

Highlight. This quarter, significant progress was achieved on modeling dendrite growth conditions. The model was revised to include the effect of current density on the propensity for dendrite growth. The model is expected to provide insights into material properties needed for dendrite prevention.

Milestones

1. Develop mathematical model to understand the proper stress state that exists within lithium metal and adjacent electrolyte during electrochemical deposition of lithium. (Q1 – Complete)
2. Develop mathematical models to investigate and capture possibility of plastic deformation within lithium metal. Impact of plasticity on effective exchange current density will also be explored. (Q2 – Complete)
3. Combine the impact of elasto-plastic stress evolution with transport of lithium within the electrode-electrolyte system. If unsuccessful in combining both elastic and plastic deformation with the transport process, consider only elastic deformation of lithium and electrolyte. (Q3 – In progress)
4. Report on the electrolyte shear modulus required for successful prevention of dendrites. The coupled mechanics and transport framework will be used to analyze the Li-electrolyte system. (Q4 – In progress)

Progress Report

Combine the Impact of Elasto-Plastic Stress Evolution with Transport of Lithium within the Electrode-Electrolyte System. If Unsuccessful in Combining Both Elastic and Plastic Deformation with the Transport Process, Consider Only Elastic Deformation of Lithium and Electrolyte. In a Li-ion battery, formation of lithium dendrites depends significantly on distribution of potential and salt concentration within the electrolyte, which is again affected by the applied current density. The total reaction current around the dendritic protrusion should be estimated according to the Butler-Volmer equation, which has contributions from both the mechanical-stress and concentration-overpotential induced components:

$$i_{BV}(x) = \exp\left(\frac{a D m}{RT} \frac{Dm}{e}\right) \cdot F k_a^{a_c} (k_c c_e)^{a_a} \left[\exp\left(\frac{a F h}{RT}\right) - \exp\left(-\frac{a F h}{RT}\right) \right] \quad (1)$$

The first exponential term is the mechanical-stress factor, and the remaining portion is the conventional Butler-Volmer expression. Mass transport and charge balance equations have been solved in the electrolyte and the lithium metal. Figure 62a-d shows the potential and concentration contours observed at low and high current density operations within electrolyte around the dendritic protrusion.

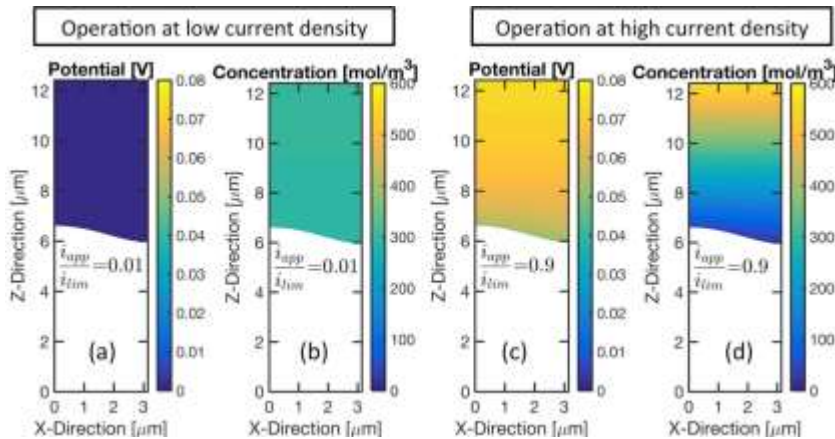


Figure 62. Concentration and potential contour within the electrolyte around the dendritic protrusion at high and low rates of current. Potential in lithium metal remains extremely close to zero. (a) Potential contour for $i_{app} = 0.01 i_{lim}$. (b) Concentration contour for $i_{app} = 0.01 i_{lim}$. (c) Potential contour for $i_{app} = 0.9 i_{lim}$. (d) Concentration contour for $i_{app} = 0.9 i_{lim}$.

Variation in reaction current density from protrusion peak to valley has been shown in Figure 63a, by the black lines, for two different applied current densities (circle – high current; square – low current). The reaction currents have been normalized with respect to current density at the protrusion peak. Relative contribution from the mechanical-stress factor (blue line) and the concentration-overpotential factor (red line) has also been demonstrated. Figure 63b depicts the reaction current ratio between protrusion peak and valley for different applied current densities. Present analysis indicates that, with polymer electrolytes, no dendrite growth should occur for applied current less than 40% of the limiting current. Model predictions are also consistent with experimental observations adopted from Brissot et al. (*Journal of Power Sources* (1999): 81–82, 925–929). Successful incorporation of the mass and charge transport with the elastic-plastic mechanical stress completes the milestone for the third quarter.

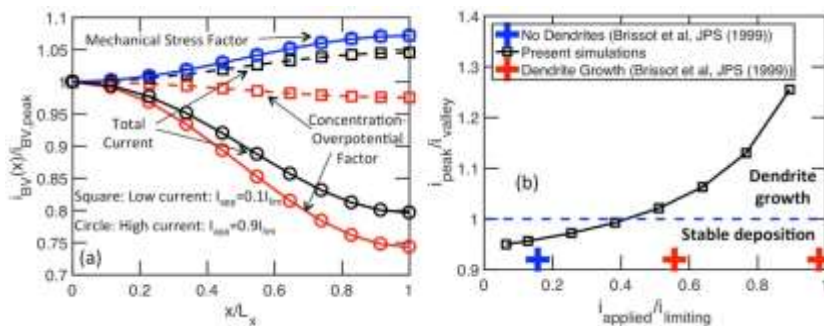


Figure 63. (a) Distribution of reaction current from the peak to the valley at two different applied current densities. (b) Reaction current ratio between protrusion peak and valley for different applied current densities. Model predictions are consistent with experiments.

Patents/Publications/Presentations

Publication

- Barai, P., and K. Higa, and V. Srinivasan. “Lithium Dendrite Growth Mechanisms in Polymer Electrolytes and Prevention Strategies.” *Physical Chemistry Chemical Physics* (2017). Accepted.

Presentation

- 231st ECS Meeting, New Orleans, Louisiana (May 28 – June 1, 2017): “Plastic Deformation of Lithium Metal and Impact on Dendrite Growth Process”; P. Barai, K. Higa, and V. Srinivasan.

Task 6.6 – First Principles Calculations of Existing and Novel Electrode Materials (Gerbrand Ceder, Lawrence Berkeley National Laboratory)

Project Objective. The main project objectives are as follows: (1) develop very high-capacity, layered cathodes with high structural stability (> 250 mAh/g) and high surface stability; (2) clarify the role that Li-excess and cation disorder play in capacity and structural stability; (3) develop predictive modeling of oxygen charge transfer and oxygen loss, and find ways to make oxygen redox beneficial in terms of increase capacity; and (4) develop materials with engineered surface passivation that does not lead to impedance increase.

Project Impact. The project will lead to insight in how Li-excess materials work and ultimately to higher capacity cathode materials for Li-ion batteries. The project will help in the design of high-capacity cathode materials that are tolerant to TM migration.

Out-Year Goals. Future goals include the following: (1) develop higher capacity Li-ion cathode materials, and novel chemistries for higher energy density storage devices, and (2) guide the field in the search for higher energy density Li-ion materials.

Collaborations. This project collaborates with K. Persson (LBNL), C. Grey (Cambridge), V. Srinivasan (ANL), and G. Chen (LBNL).

Milestones

1. Computational approach to predict cation disorder and synthesis temperature. (Q1 – Complete)
2. Comparison of electronic structure modeling with experimental spectra (for example, XAS, XPS, or EELS). (Q2 – Complete)
3. Use modeling to come up with a new cation-disordered material. (Q3 – On target)
4. Demonstrate reduced surface oxygen loss by surface modification of a disordered cathode material using DEMS or TEM. (Q4 – On target)

Progress Report

The development of percolation theory for Li-excess cation-disordered rock-salt oxides has proven to be powerful in finding novel cathode materials for lithium batteries with high capacity and energy density. Recently, the project succeeded in designing a new class of Li-excess cation disordered Li-Ni-Ti-Mo oxides that delivers up to 250 mAh/g and 750 Wh/kg at 10 mA/g. To understand the origin of this remarkable performance, the project applied a combination of *in situ* XRD, XANES, EELS, and electrochemistry to elucidate the oxidation mechanism for a representative compound of that class, the $\text{Li}_{1.2}\text{Ni}_{1/3}\text{Ti}_{1/3}\text{Mo}_{2/15}\text{O}_2$ composition. Based on this detailed characterization, the project was able to distinguish between $\text{Ni}^{2+}/\text{Ni}^{3+}$ oxidation, oxygen loss, and oxygen oxidation as separate redox processes, demonstrating the relationship of oxygen loss and capacity fading.

The project obtained $\text{Li}_{1+x/100}\text{Ni}_{1/2-x/120}\text{Ti}_{1/2-x/120}\text{Mo}_{x/150}\text{O}_2$ ($x = 0, 5, 10, 15, 20$) compounds, in the following referred to as LNTMO and LNTMO $_x$ ($x=5, 10, 15, 20$), by traditional solid-state synthesis. Figure 64 shows the cycling performance of these materials (1.5-4.5V, 20 mA/g), showing an increasing capacity with lithium content. As seen in Figure 64a, LNTMO20 delivers much higher capacity (~230 mAh/g) and energy density (~680 mAh/g) compared to LNTMO (~110 mAh/g, ~350 Wh/kg). More importantly, the project notes that the capacity of LNTMO20 significantly exceeds the theoretical $\text{Ni}^{2+}/\text{Ni}^{4+}$ capacity (=201.6 mAh/g), indicating other active redox couples in LNTMO20. The material also exhibits some capacity fading upon cycling, as shown in Figure 64b. Motivated by these observations, the project studied the oxidation mechanism and capacity fading with *in situ* XRD, XANES, and EELS.

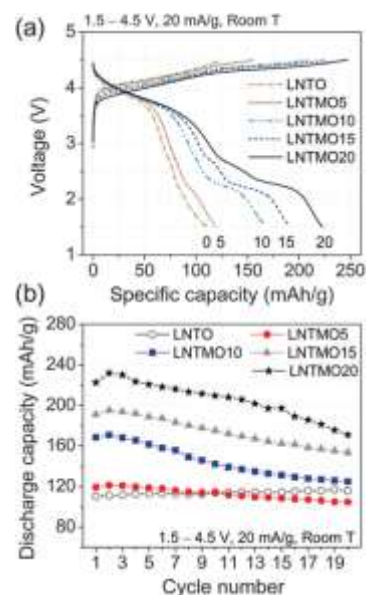


Figure 64. (a) The first-cycle voltage profiles of LNTMO compounds. (b) Capacity evolution over 20 cycles.

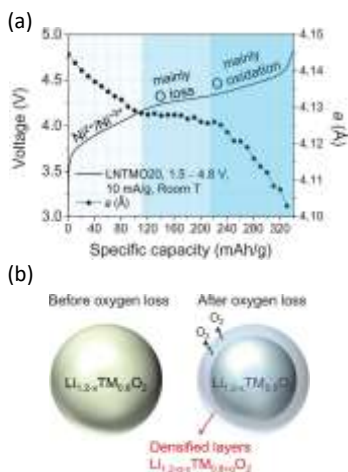


Figure 65. (a) Proposed first-charge mechanism of LNTMO20, with voltage profile and corresponding lattice constant from *in situ* X-ray diffraction. (b) Illustrations of a LNTMO20 particle before and after oxygen loss with densified surface.

Surprisingly, the XANES results show that only the $\text{Ni}^{2+}/\text{Ni}^{3+}$ redox couple is accessed, and Ni^{3+} is not oxidized further to Ni^{4+} , which accounts for around 110 mAh/g of the charge capacity. The remaining capacity must originate from oxygen activity, that is, either from oxygen loss or from reversible oxygen oxidation. As shown in Figure 65a, charged to ~215 mAh/g (that is, beyond $\text{Ni}^{2+}/\text{Ni}^{3+}$ oxidation), the lattice constant barely changes; this indicates oxygen loss from the electrode surface. Finally, charging beyond ~215 mAh/g gives rise to a decrease of the lattice parameter, as oxygen oxidation contracts the oxygen framework by reducing the size of the oxygen ions.

With this insight, the capacity fading on discharge can be attributed mainly to irreversible oxygen loss. Further evidence for oxygen loss is seen in the EELS results, which show that the O/Ti intensity decreases ~39% on the surface. When oxygen is released from the particle surface, either oxygen vacancies or under-coordinated TM ions at the surface may diffuse into the bulk, creating new surface phases rich in TM. After such surface densification, the lithium content drops below the percolation threshold (~9% excess), and lithium diffusion through the surface is no longer facile, causing the capacity fading. Currently, the project is exploring pathways to modify the surface structure so that oxygen loss can be minimized and capacity retention can be enhanced.

Task 6.7 – Dendrite Growth Morphology Modeling in Liquid and Solid Electrolytes (Yue Qi, Michigan State University)

Project Objective. The ultimate goal of this project is to develop a validated model to predict lithium dendrite morphology evolution in both liquid and solid electrolytes during electrodeposition and stripping, in order to accelerate the adoption of Li-metal electrodes in current and emerging battery technologies. To achieve this goal, the project has four objects: (1) formulate a general framework that captures the electrochemical-mechanical driving forces for lithium morphology evolution; (2) consider the role of the nm-thin SEI in liquid-electrolytes as well as the microstructures of mm-thick solid-electrolytes for lithium morphology evolution; (3) connect micron-scale phase-field models and atomic-scale DFT-based simulations via parameter- and relationship-passing to predict lithium dendrite nucleation and growth kinetics and morphology; and (4) validate the key input parameters and main conclusions of the multi-scale model as new capabilities being developed step-by-step.

Project Impact. This atomically informed, fully coupled, electrochemical-mechanical dendrite morphology evolution model will allow us to design the desired properties of artificial SEI coatings, the microstructure of solid electrolyte materials, and the corresponding battery operating conditions, so as to avoid dendrite growth during cycling. It will accelerate design of durable and safe lithium anodes for Li-S, Li-air, and all-solid Li-ion batteries. Thus, it directly impacts emerging technologies, such as Li-S, Li-air, and all-solid Li-ion batteries, which aim to meet the DOE target of the high-energy-density battery cells ($> 350 \text{ Wh/kg}$) for EV applications and to push the cost below $\$100/\text{kWh}_{\text{use}}$.

Out-Year Goals. The goal this year is to illuminate the role of SEI kinetics on lithium dendrite growth in liquid electrolytes. To achieve this goal, a phase-field model will be developed to capture the electrochemical driven dendrite morphology evolution in a liquid electrolyte. The role of SEI will be modeled both implicitly and explicitly. The kinetic properties, as well as lithium diffusion coefficient along the Li/SEI interface will first be computed from DFT- and density functional tight binding (DFTB)- based atomic simulations. The validation of the model will come from experiments to correlate the distinctively different transport properties of artificial SEI layers with their impact on lithium dendrite morphology.

Collaborations. This project collaborates with the University of Maryland, SNL–Albuquerque, PNNL, and the University of Arkansas.

Milestones

1. Computational approach to predict cation disorder and synthesis temperature. (Q1 – Complete)
2. Comparison of electronic structure modeling with experimental spectra (for example, XAS, XPS, or EELS). (Q2 – Complete)
3. Use modeling to come up with a new cation-disordered material. (Q3 – On target)
4. Demonstrate reduced surface oxygen loss by surface modification of a disordered cathode material using DEMS or TEM. (Q4 – On target)

Progress Report

Liquid Electrolyte. The implicit SEI phase-field dendrite growth model along with parametric studies revealed that the charge transfer reaction rate plays a key role in determining the lithium dendrite growth morphology in liquid electrolyte, as higher reaction rate leads to faster growth rate, sharper tip fronts, and finer dendritic patterns. This reaction rate is controlled by lithium de-solvation and diffusion barriers. The detailed DFTB simulations of this reaction at Li_2CO_3 covered Li-electrode surface (Figure 66a) showed Li^+ de-solvation barrier from the EC electrolyte increased with lower applied potential (Figure 66b). At the potential of -0.18V , the EC molecules were randomly oriented, and two out of five EC in the Li^+ solvation sheath were removed, forming $\text{Li}^+(\text{EC})_3$, upon de-solvation (Figure 66c). Lower potential (-0.54V) induced stronger electric field to orient the C=O carbonyl groups away from the interface, forming an increased barrier for Li^+ ion to approach the Li_2CO_3 surface. At the de-solvated state, the solvation sheath became $\text{Li}^+(\text{EC})_2$, requiring higher de-solvation energy. The diffusion energy barrier of Li^+ ion in Li_2CO_3 decreased with the applied potential due to Coulombic interaction. This is the first energy landscape of the charge transfer reaction of $\text{Li}^+ + e^- \leftrightarrow \text{Li}^0$ at an SEI covered Li-electrode/electrolyte interface.

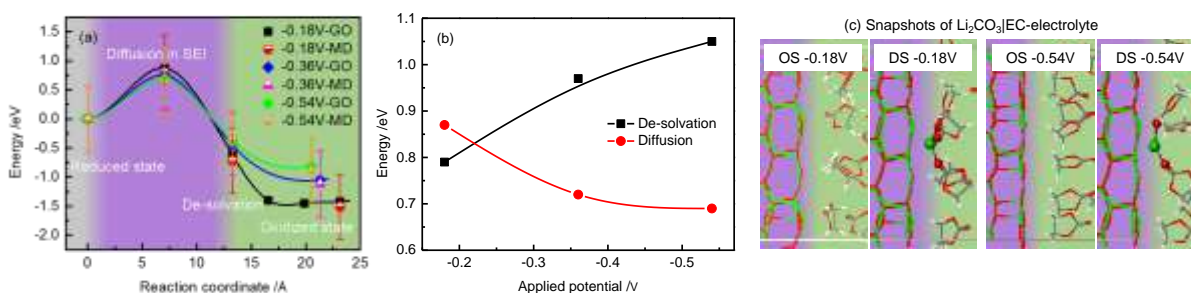


Figure 66. (a) Energy profile for Li^+ ion at the $\text{Li}|\text{Li}_2\text{CO}_3|\text{EC}$ -electrolyte interface and (b) de-solvation barriers and diffusion barrier under the applied potential. (c) Snapshots of $\text{Li}_2\text{CO}_3|\text{EC}$ -electrolyte interface when lithium is away or at the interface under the different applied potentials.

Solid Electrolyte. A general non-linear phase-field model for lithium dendrite growth in solid electrolyte (for example, LLZO, LLZTO, etc.) were formulated and implemented. It was reported that lithium dendrites tend to grow into pores and along the grain boundaries of the solid electrolytes. Therefore, the microstructure of LLZO was resolved, and a three-phase system was defined as: Li-metal, solid-electrolyte (grains), and pores/cracks/grain boundaries. Currently, the solid-electrolyte phase is considered to be non-evolving during electrodeposition, and the lithium diffusion coefficients were assumed to be: $D_{\text{GB}} > D_{\text{Grain}} \gg D_{\text{pore}}$. Numerically, phase field governing equations were solved together with diffusion and charge conservation equations via finite element method. An intergranular lithium dendrite growth has been simulated in 2D, as shown in Figure 67. The electrodeposited Li-metal morphology is in agreement with the SEM images of dendrite morphology from cycled LLZO all-solid-state batteries. The driving force for lithium dendrite growth at the grain boundaries in LLZO will be addressed by DFT calculations.

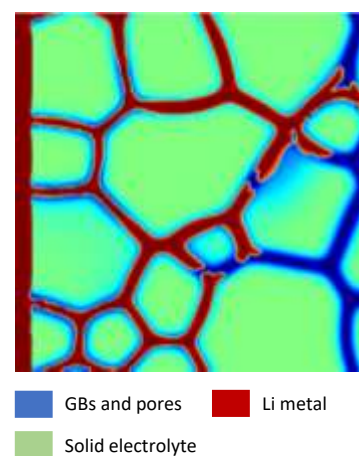


Figure 67. Modeling of lithium dendrite growth in LLZO microstructure.

Patents/Publications/Presentations

Presentations

- MRS Spring Meeting, Phoenix, Arizona (April 2017): “Multi-Component and Multi-Functional Protection Coating for High Capacity Anodes (Li and Si)”; Y. Qi. Invited.
- MRS Spring Meeting, Phoenix, Arizona (April 2017): “Computational Insights to Charge Transfer Reactions at Electrode|SEI|Electrolyte Interface”; Y. Li and Y. Qi.
- 231st ECS Meeting, New Orleans, Louisiana (May 2017): “A Non-Linear Multi-Phase Field Model for Li Plating and Dendrite Growth at Li Metal Anode Incorporating Solid Electrolyte Interphase (SEI) Layer”; Z. Liu, L. Chen, Y. Qi, P. Lu, and L-Q. Chen.
- 231st ECS Meeting, New Orleans, Louisiana (June 2017): “Approaching In-Situ Investigation of SEI Growth Dynamics by Isotope-Assisted TOF-SIMS”; Z. Liu, P. Lu, Q. Zhang, X. Xiao, and L-Q. Chen.
- Advanced Automotive Battery Conference (AABC), San Francisco, California (June 2017): “Towards High Cycle Efficiency of High Energy Density Lithium Ion Batteries”; X. Xiao. Invited.
- 21st International Conference on Solid State Ionics, Padua, Italy (June 2017): “DFT and DFTB Simulations of Lithium Ion Transport through the Complex Electrode|SEI|Electrolyte Interface”; Y. Qi. Invited.

Task 6.8 – First Principles Modeling and Design of Solid-State Interfaces for the Protection and Use of Li-Metal Anodes (Gerbrand Ceder, UC Berkeley)

Project Objective. The project objective is to determine the design principles that control the solid electrolyte/lithium electrode interfaces by determining the reaction products stemming from pairing solid electrolytes and lithium metal. The project will conduct rigorous analysis based on computing electrolyte phase-diagrams closed and open to lithium. Li-ion transport properties in bulk electrolytes and interfacial products will be assessed through AIMD and nudged elastic band calculations. Simultaneously, a robust framework will be developed to identify factors controlling Li-dendrite propagation within solid electrolytes and interfacial products by accounting for irregularities, defects, and grain boundaries, through a model that includes elements of fracture mechanics, thermodynamics, and electrochemistry.

Project Impact. The project will lead to understanding of the complex evolution of lithium metal/SEI during electrochemical cycling. The understanding of such process is necessary to determine design principles to develop reliable all solid-state batteries.

Out-Year Goals. The out-year goals include the following: (1) obtain design criteria for solid electrolytes that can resist unstable lithium propagation by computing elastic properties surface energies and decohesion energies, and (2) adapt fracture mechanics models describing crack propagation to lithium dendrite propagation in different scenarios.

Milestones

1. Chemistry selection of solid electrolytes through large-scale material recognition based on the Inorganic Crystal Structure Database (ICSD) and materials prediction. (Q1/Q2 – In Progress)
2. Stability screening of solid electrolyte materials using phase diagrams to assess chemical and electrochemical stability. (Q3/Q4 – On target)

Progress Report

The use of bulk reactive metals, such as lithium, as negative electrodes in batteries, is a promising way to increase energy density of Li-ion batteries. Furthermore, the use of ceramic and/or glass solid electrolytes to create all solid-state batteries can enable the use of lithium metal by preventing unstable propagation of lithium dendrites, therefore enhancing safety and decreasing capacity fade. Interface chemistry and stability between lithium metal and solid electrolytes remains elusive; however, the formation of unstable interface products has been identified as the main contribution to limited cycle lifetime and dendrite propagation.

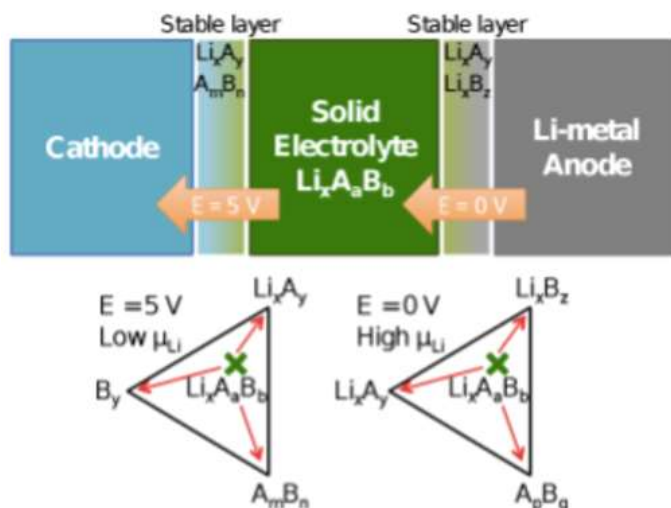


Figure 68. Schematic for the reverse design strategy overlaid on a Li-ion all-solid-state cell. Arrows show the lithium chemical potentials, which favor lithium percolation from the lithium anode (gray) toward the cathode (blue). The interfacial products, originating from the contact of electrodes and the ionic conductor, are identified by the ternary phase diagrams (triangular shapes) at the bottom.

The stability window of electrode, solid electrolyte, and interface products requires construction of multicomponent phase diagrams. The project has already developed theory to construct such diagrams using data available from the ICSD or data from *ab initio* calculations. Furthermore, a framework for stability analysis was previously developed to determine electrode/electrolyte interface materials for systems closed and open to Li-ion transport. The stability window of materials is determined by the voltage at which lithium is extracted or inserted to the electrolyte. Lithium deposition at Li-metal electrodes can occur with the reduction of other species, forming a decomposition layer. Figure 69 shows stability ranges of common binary lithium compounds.

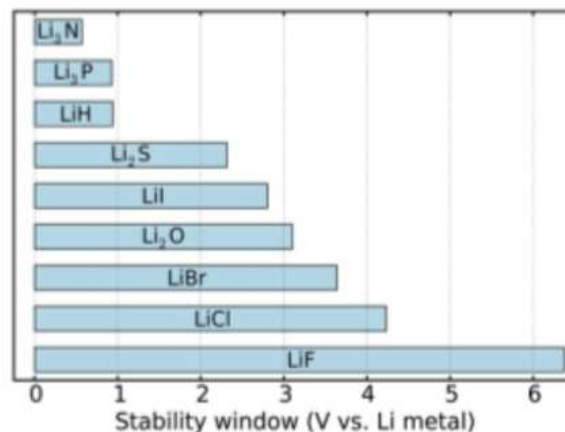


Figure 69. Electrochemical stability ranges of binary lithium decomposition products.

TASK 7 – METALLIC LITHIUM AND SOLID ELECTROLYTES

Summary and Highlights

The use of a metallic lithium anode is required for advanced battery chemistries like Li-air and Li-S to realize dramatic improvements in energy density, vehicle range, cost requirements, and safety. However, the use of metallic lithium with liquid and polymer electrolytes has so far been limited due to parasitic SEI reactions and dendrite formation. Adding excess lithium to compensate for such losses effectively negates the high-energy density for lithium in the first place. For a long lifetime and safe anode, it is essential that no lithium capacity is lost either (1) to physical isolation from roughening, dendrites, or delamination processes, or (2) to chemical isolation from side reactions. The key risk and current limitation for this technology is the gradual loss of lithium over the cycle life of the battery.

To date there are no examples of battery materials and architectures that realize such highly efficient cycling of metallic lithium anodes for a lifetime of 1000 cycles due to degradation of the Li-electrolyte interface. A much deeper analysis of the degradation processes is needed, so that materials can be engineered to fulfill the target level of performance for EV, namely 1000 cycles and a 15-year lifetime, with adequate pulse power. When projecting the performance required in terms of just the lithium anode, this requires a high rate of lithium deposition and stripping reactions, specifically about 40 μm of lithium per cycle, with pulse rates up to 10 and 20 nm/s (15mA/cm²) charge and discharge, respectively. This is a conservative estimate, yet daunting in the total mass and rate of material transport. While such cycling has been achieved for state-of-the-art batteries using *molten* sodium in Na-S and zebra cells, solid sodium and lithium anodes are proving more difficult.

The efficient and safe use of metallic lithium for rechargeable batteries is then a great challenge, and one that has eluded R&D efforts for years. This Task takes a broad look at this challenge for both solid-state batteries and batteries continuing to use liquid electrolytes. For the liquid electrolyte batteries, PNNL researchers are examining the use of dual lithium salts and organic additives to the typical organic carbonate electrolytes to impede lithium corrosion and dendrite formation at both the lithium and graphite anodes. If successful, this is the simplest approach to implement. At Stanford, novel coatings and 3D structures are applied to the lithium surface and appear to suppress roughening and lengthen cycle life. A relatively new family of solid electrolytes with a garnet crystal structure shows super-ionic conductivity and good electrochemical stability. Four programs chose this family of solid electrolytes for investigation. Aspects of processing this ceramic garnet electrolyte are addressed at UMD and at the University of Michigan, with attention to effect of flaws and the critical current density (CCD). Computational models will complement their experiments to better understand interfaces and guide reduction of the lithium and cathode ASR. At ORNL, composite electrolytes composed of ceramic and polymer phases are being investigated, anticipating that the mixed phase structures may provide additional means to adjust the mechanical and transport properties. The last project takes on the challenge to use nano-indentation methods to measure the mechanical properties of the solid electrolyte, the Li-metal anode, and the interface of an active electrode. Each of these projects involves a collaborative team of experts with the skills needed to address the challenging materials studies of this dynamic electrochemical system.

Highlights. The highlights for this quarter are as follows:

- Tensile tests revealed the adhesive strength of the lithium electrode with an LLZO ceramic electrolyte. The adhesive strength exceeds the tensile strength of the Li-metal foil, ~ 8 MPa, for samples with very low interfacial ASR.
- Electron backscatter diffraction provided maps of the grain structure for LLZO ceramic electrolyte. Larger grains, from extended annealing, allow for a 2-fold higher ionic current density without lithium shorts.
- Acid/base treatment of Ohara ceramic powders (pH of 3.3 to 12.7) did not substantially reduce the interface resistance for Li-ion motion between the polymer and ceramic electrolytes.

- Interface reactions of LLZO ceramic electrolyte with sulfur and with NMC cathodes were evaluated with model and experiment. The main reaction products (for example, Li_2SO_4 and Li_6ZrO_7) provide protection for the LLZO with reasonable Li-ion conduction.
- A Freon gas reaction was used to prepare thin and conformal LiF passivation layers on 3D Li-metal anodes.
- In liquid electrolyte batteries, various electrolyte additives improved the extended cycling stability of Li / LiPF_6 , PC / NMC cells. The SEI thickness at the lithium anode of Li / LiTFSI+LiBOB, EC-EMC / NMC batteries varied linearly for a 5-fold variation in the areal capacity of the NMC.
- Solid-state lithium batteries were constructed with a cross-linked poly (ethylene glycol) methyl ether acrylate + LiTFSI electrolyte. Cycling with Cu//Li electrodes results in a Cu^+/Cu^0 redox reaction and the dissolution of Cu^+ ions.
- Sputter deposition of lithium onto Nb-doped SrTiO_3 leads to reduction of both Ti^{+4} and Nb^{+5} as observed by XPS. For lithium deposition onto LiCoO_2 thin films, the reaction depends on the LiCoO_2 (003) versus (104) texture.
- An asymmetric cell, Li (thick) / liquid electrolyte / Li (thin on Cu) was used to distinguish dendritic from non-dendritic lithium morphology. The approach is based on cumulative cycling until the thin lithium is depleted; this was tested for four different electrolyte solutions.

Task 7.1 – Mechanical Properties at the Protected Lithium Interface

(Nancy Dudney, Oak Ridge National Laboratory; Erik Herbert, Michigan Technological University; Jeff Sakamoto, University of Michigan)

Project Objective. This project will develop understanding of the Li-metal SEI through state-of-the-art mechanical nanoindentation methods coupled with solid electrolyte fabrication and electrochemical cycling. The goal is to provide the critical information that will enable transformative insights into the complex coupling between the microstructure, its defects, and the mechanical behavior of Li-metal anodes.

Project Impact. Instability and/or high resistance at the interface of lithium metal with various solid electrolytes limit the use of the metallic anode for high-energy-density batteries, such as Li-air and Li-S. The critical impact of this endeavor will be a much deeper analysis of the degradation so that materials can be engineered to fulfill the target level of performance for EV batteries, namely 1000 cycles and 15-year lifetime, with adequate pulse power.

Approach. Mechanical properties studies through state-of-the-art nanoindentation techniques will be used to probe the surface properties of the solid electrolyte and the changes to the lithium that result from prolonged electrodeposition and dissolution at the interface. An understanding of the degradation processes will guide future electrolyte and anode designs for robust performance. In the first year, the team will address the two critical and poorly understood aspects of the protected Li-metal anode assembly: (1) the mechanical properties of the solid electrolyte, and (2) the morphology of the cycled lithium metal.

Out-Year Goals. Work will progress toward study of the electrode assembly during electrochemical cycling of the anode. The project hopes to capture the formation and annealing of vacancies and other defects in the lithium and correlate this with the properties of the solid electrolyte and the interface.

Collaborations. This project funds work at ORNL, Michigan Technological University (MTU), and University of Michigan. Steve Hackney (MTU) has contributed greatly to analysis of the creep mechanisms active for thin-film lithium. Asma Sharafi and Michael Wang (University of Michigan Ph. D. students) and Dr. Robert Schmidt (ORNL) also contribute to the project. Steve Visco (PolyPlus) will serve as a technical advisor.

Milestones

1. Characterize *in situ* changes in lithium anode from a single stripping and plating half cycle. (Q2, March 2017 – On going)
2. Measure the Li-LLZO interface strength as a function of surface treatment using the Instron and EIS capability. (Q3 – Completed June 2017)
3. Examine lithium anode *in situ* during extended electrochemical plating, stripping, and relaxation to assess defect formation and annealing. (Q4 – Completed March 2017)
4. Determine the physical properties of electrolyte failures, the nature of material reduction or lithium incursion/pileup, using indentation and X-ray tomography. Samples obtained from other Task 7 projects. (Q4, September 2017 – X-ray, tomography initiated May 2017)

Progress Report

Analysis and models have been developed to describe mechanical properties of thin-film lithium as revealed by numerous nanoindentation experiments. The complex dependence on strain rate and displacement into the film indicates several processes contribute to plastic deformation. A manuscript is being prepared to describe and map these effects. To summarize, Figure 70a shows hardness as a continuous function of indentation depth for lithium films (5- and 18- μm thick) and four indentation strain rates. This is the average of many indentation maps across the surface. The different creep mechanisms are shown in Figure 70b. At slower strain rates and smaller displacement, Nabarro-Herring creep is the primary mechanism. Here, lattice defects (vacancies) diffuse between the tip and the free surface of the lithium film. At higher strain rate, plastic flow must be accommodated by diffusion of vacancies from nearby dislocations within the plastic zone. This Harper-Dorn mechanism correctly predicts that pressure is inversely proportional to the square root of the length scale. At the inflection point in the hardness, an avalanche of dislocations occurs. The power law relationship in Figure 70c strongly suggests that the avalanche occurs only after a threshold limit of energy per unit area has been exceeded. These stresses far exceed the yield or tensile strengths reported for bulk polycrystalline lithium. After the dislocation avalanche, the deformation mechanism capitalizes on the significant increase in the dislocation density and reverts from diffusional creep mechanisms to a balance between the rate of defect anneal (recovery) and the rate of strain hardening.

Separately, new results show the relationship between electrochemical and mechanical behavior at the interface of lithium metal and $\text{Li}_7\text{La}_3\text{Zr}_2\text{O}_{12}$ (LLZO) solid electrolytes. There is clear correlation between the ASR and tensile adhesive strength of the Li/LLZO interface. The later was determined as Li/LLZO/Li cells were pulled in tension using an Instron housed in an argon glove box. Analysis of fracture surfaces showed that at high ASRs, there is a clean separation of the lithium from the LLZO surface, leaving behind negligible lithium residue. In contrast, at the lowest ASRs reported, the adhesive strength of the Li/LLZO interface clearly exceeds the tensile strength of the lithium metal. To support these results, tensile strength of lithium foil was measured to be ~ 8 MPa, which is the maximum interface strength observed in Li/LLZO/Li stacks (red-dashed line in Figure 71). The fact that the strength of the interface is stronger than the lithium metal itself at low ASRs suggests there is good surface chemistry and wettability of lithium on LLZO. From these studies, it can be concluded that both adhesive strength and ASR of the interface are governed by surface chemistry and wettability of the LLZO surface.

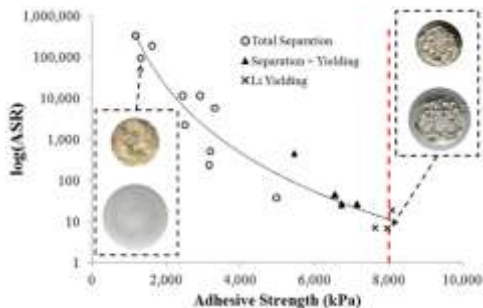


Figure 71. Area specific resistance as a function of the adhesion strength of the Li-LLZO interface. Optical microscope images show the fracture surface of the lithium and LLZO disks at low and high area specific ionic resistance. The red dashed line indicates the measured tensile strength of lithium metal.

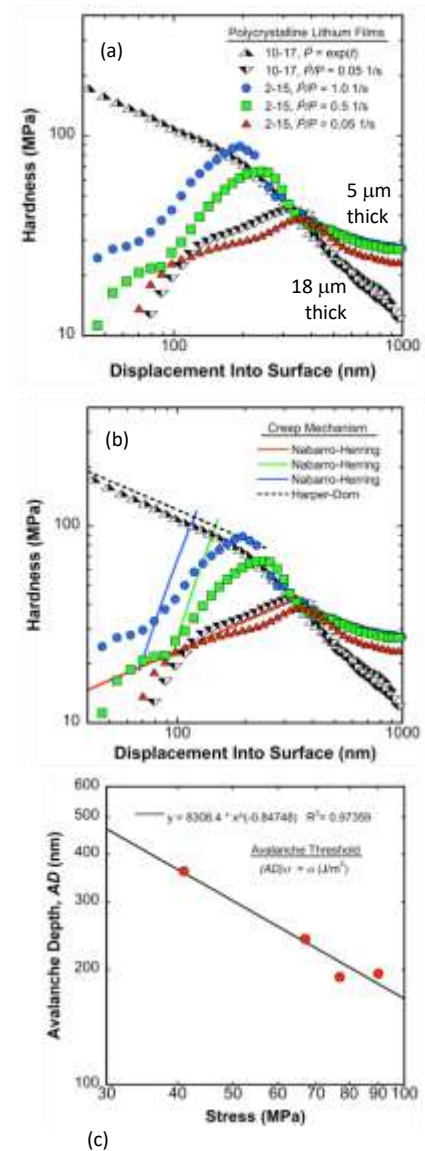


Figure 70. (a) Hardness versus depth. (b) Data and rationalizations. (c) Dislocation avalanche threshold criterion.

that at high ASRs, there is a clean separation of the lithium from the LLZO surface, leaving behind negligible lithium residue. In contrast, at the lowest ASRs reported, the adhesive strength of the Li/LLZO interface clearly exceeds the tensile strength of the lithium metal. To support these results, tensile strength of lithium foil was measured to be ~ 8 MPa, which is the maximum interface strength observed in Li/LLZO/Li stacks (red-dashed line in Figure 71). The fact that the strength of the interface is stronger than the lithium metal itself at low ASRs suggests there is good surface chemistry and wettability of lithium on LLZO. From these studies, it can be concluded that both adhesive strength and ASR of the interface are governed by surface chemistry and wettability of the LLZO surface.

Patents/Publications/Presentations

Presentations

- DOE Annual Merit Review, Washington, D. C. (June 5 – 9, 2107): “Mechanical Properties at the Protected Lithium Interface”; Nancy Dudney, Erik Herbert, and Jeff Sakamoto.
- BLI-X, IBM, Almaden, California (June 27, 2017): “The Mechanical Behavior of Vapor Deposited Lithium Films”; Erik Herbert, Nancy Dudney, and Steve Hackney. Invited.

Task 7.2 – Solid Electrolytes for Solid-State and Lithium–Sulfur Batteries (Jeff Sakamoto, University of Michigan)

Project Objective. *Enable Advanced Li-Ion Solid-State and Lithium-Sulfur EV Batteries Using LLZO Solid-Electrolyte Membrane Technology.* Owing to its combination of fast ion conductivity, stability, and high elastic modulus, LLZO exhibits promise as an advanced SSE. To demonstrate relevance in EV battery technology, several objectives must be met. First, LLZO membranes must withstand current densities approaching $\sim 1 \text{ mA/cm}^2$ (commensurate with EV battery charging and discharging rates). Second, low ASR between lithium and LLZO must be achieved to obtain cell impedance comparable to conventional Li-ion technology ($\sim 10 \text{ Ohms/cm}^2$). Third, low ASR and stability between LLZO and sulfur cathodes must be demonstrated.

Project Impact. The expected outcomes will: (1) enable Li-metal protection, (2) augment DOE access to fast ion conductors and/or hybrid electrolytes, (3) mitigate Li-polysulfide dissolution and deleterious passivation of Li-metal anodes, and (4) prevent dendrite formation. Demonstrating these aspects could enable Li-S batteries with unprecedented end-of-life, cell-level performance: $> 500 \text{ Wh/kg}$, $> 1080 \text{ Wh/l}$, > 1000 cycles, and lasting > 15 years.

Approach. This effort will focus on the promising new electrolyte known as LLZO ($\text{Li}_7\text{La}_3\text{Zr}_2\text{O}_{12}$). LLZO is the first bulk-scale ceramic electrolyte to simultaneously exhibit the favorable combination of high conductivity ($\sim 1 \text{ mS/cm}$ at 298K), high shear modulus (61 GPa) to suppress lithium dendrite penetration, and apparent electrochemical stability (0-6 V versus Li/Li⁺). While these attributes are encouraging, additional R&D is needed to demonstrate that LLZO can tolerate current densities in excess of 1 mA/cm^2 , thereby establishing its relevance for PHEV/EV applications. This project hypothesizes that defects and the polycrystalline nature of realistic LLZO membranes can limit the CCD. However, the relative importance of the many possible defect types (porosity, grain boundaries, interfaces, and surface and bulk impurities), and the mechanisms by which they impact current density, have not been identified. Using experience with the synthesis and processing of LLZO (Sakamoto and Wolfenstine), combined with sophisticated materials characterization (Nanda), this project will precisely control atomic and microstructural defects and correlate their concentration with the CCD. These data will inform multi-scale computation models (Siegel and Monroe), which will isolate and quantify the role(s) that each defect plays in controlling the current density. By bridging the knowledge gap between composition, structure, and performance, this project will determine if LLZO can achieve the current densities required for vehicle applications.

Milestones

1. Establish a process to control the microstructural defect that governs the CCD to achieve $> 1 \text{ mA/cm}^2$. (Q1 – Completed December 2016)
2. Establish a process to control the atomic-scale defect that governs the CCD to achieve $> 1 \text{ mA/cm}^2$. (Q1 – Completed December 2016)
3. Design, fabricate, and test beginning of life performance of hybrid Li-LLZO-liquid-S+carbon cells. (Q2 – Completed March 2017)
4. Design, fabricate, and test beginning of life performance of Li-LLZO-liquid-SOA Li-ion cathode cells. (Q3 – Completed June 30, 2017)
5. Experimentally evaluate the CCD, based on the dominant defects (atomic and or microstructural) identified in years 1 and 2, as a function of Q, temp, and pressure. Characterize the CE. (Q4 – Initiated in Q3)

Progress Report

Achieving current densities $\geq 1 \text{ mA}\cdot\text{cm}^{-2}$ is a necessary condition for a viable SSE to enable use of metallic lithium anodes. Toward this goal, the project examined parameters such as fracture toughness and grain size that could affect the maximum tolerable current density. It was observed that maximum current density was roughly independent of fracture toughness and strongly dependent on grain size. When the grain size increased from 5 to 600 μm , the CCD increased from 0.3 to 0.6 $\text{mA}\cdot\text{cm}^{-2}$ (Figure 72). It is believed that this increase in grain size reduced the grain boundary area and hence the number of possible failure points leading to an increase in CCD.

LLZO was densified using rapid induction hot pressing. Grains were grown either by hot pressing at high temperature or using a combination of hot pressing and annealing. New techniques to prevent lithium loss during elevated temperature were developed and are amenable to large-scale processing. Electron backscatter diffraction was used to determine grain size, and grain boundary misorientation angle to allow for determination of a grain growth exponent. Mechanical properties were analyzed using indentation. Lastly, CCD was measured at fixed stack pressure and at room temperature.

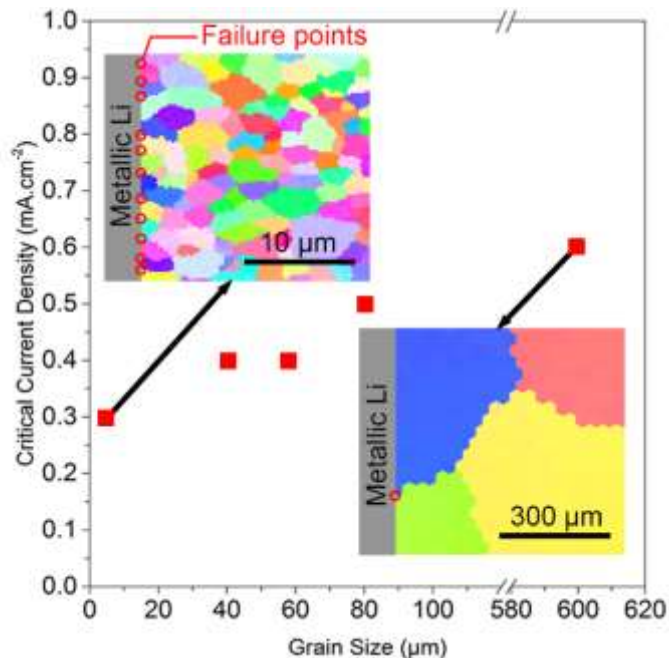


Figure 72. The critical current density increases with increasing grain size. Color maps indicate LLZO crystallographic orientations determined using electron backscatter diffraction.

Patents/Publications/Presentations

Publication

- Sharafi, A., and S. Yu, M. Naguib, M. Lee, C. Ma, H. M. Meyer, J. Nanda, M. Chi, D. J. Siegel, and J. Sakamoto. “Impact of Air Exposure and Surface Chemistry on Li / $\text{Li}_7\text{La}_3\text{Zr}_2\text{O}_{12}$ Interfacial Resistance.” *Journal of Materials Chemistry A* (2017). doi:10.1039/c7ta0316.

Presentations

- MRS 2017 Spring Meeting, Phoenix, Arizona (April 17 – 21, 2017): “Mechano-Electrochemical Aspects in Solid-State Batteries”; J. Sakamoto. Invited.
- Waterloo Institute for Nanotechnology, University of Waterloo, Waterloo, Ontario, Canada (May 8, 2017): D. J. Siegel. Invited.
- MRS 2017 Spring Meeting, Symposium on “Mechanics of Energy Storage and Conversion,” Phoenix, Arizona (April 17 – 21, 2017); D. J. Siegel. Invited.
- MRS 2017 Spring Meeting, Symposium on “Mechanical Properties of Oxide Based Li-ion Conducting Solid Electrolytes,” Phoenix, Arizona (April 17 – 21, 2017); J. Wolfenstine. Invited.
- DOE Annual Merit Review, Washington, D. C. (June 5–9, 2017): “Solid Electrolytes for Solid-State and Lithium-Sulfur Batteries”; J. Sakamoto.

Task 7.3 – Composite Electrolytes to Stabilize Metallic Lithium Anodes (Nancy Dudney and Frank Delnick, Oak Ridge National Laboratory)

Project Objective. Prepare composites of representative polymer and ceramic electrolyte materials to achieve thin membranes that have the unique combination of electrochemical and mechanical properties required to stabilize the metallic lithium anode while providing for good power performance and long cycle life. Understand the Li-ion transport at the interface between polymer and ceramic solid electrolytes, which is critical to effective conductivity of the composite membrane. Identify key features of composite composition, architecture, and fabrication that optimize performance. Fabricate thin electrolyte membranes to use with a thin metallic lithium anode to provide good power performance and long cycle life.

Project Impact. A stable lithium anode is critical to achieve high energy density with excellent safety, lifetime, and cycling efficiency. This study will identify key design strategies that should be used to prepare composite electrolytes to meet the challenging combination of physical, chemical, and manufacturing requirements to protect and stabilize the Li-metal anode for advanced batteries. By utilizing well characterized and controlled component phases, the design rules developed for composite structures will be generally applicable toward substitution of alternative and improved solid electrolyte component phases as they become available. Success in this project will enable these DOE technical targets: 500-700 Wh/kg, 3000-5000 deep discharge cycles, and robust operation.

Approach. This project seeks to develop practical solid electrolytes that will provide stable and long-lived protection for the Li-metal anode. Current electrolytes have serious challenges when used alone: oxide ceramics are brittle, sulfide ceramics are air sensitive, polymers are too resistive and soft, and many electrolytes react with lithium. Composites provide a clear route to address these issues. This project does not seek discovery of new electrolytes; rather, the goal is to study combinations of current well-known electrolytes. The project emphasizes investigation of polymer-ceramic interfaces formed as bilayers and as simple composite mixtures where the effects of the interface properties can be readily isolated. In general, the ceramic phase is several orders of magnitude more conductive than the polymer electrolyte, and interfaces can contribute an additional source of resistance. Using finite element simulations as a guide, composites with promising compositions and architectures are fabricated and evaluated for Li-transport properties using AC impedance and DC cycling with lithium in symmetric or half cells. General design rules will be determined that can be widely applied to other combinations of solid electrolytes.

Out-Year Goal. The out-year goal is to use advanced manufacturing processes where the architecture of the composite membrane can be developed and tailored to maximize performance and cost-effective manufacturing.

Collaborations. Work is conducted by Dr. A. Samuthira Pandian and Dr. Xi Chen. Dr. Jihua Chen (ORNL) assisted with electron microscopic characterization and Dr. Rose Ruther (ORNL) with Raman spectroscopy. Electrolyte powders are obtained from Ohara corporation and Prof. Sakamoto (University of Michigan). Dr. Sergiy Kalnaus has provided finite element simulations.

Milestones

1. For spray-coated composites with high ceramic loading, vary the salt, plasticizer, and ceramic content to achieve facile ion transport across phase boundaries and 10^{-5} S/cm. (Q2 – Completed March 2017, still shy of 10^{-5} S/cm)
2. Assess lithium/electrolyte interface resistance. Adjust composition or add barrier coating to reduce ASR and passivate interface. (Q3 – Completed June 2017)
3. Fabricate full battery using aqueous spray coating for both the composite electrolyte and cathode incorporating a protected Li-metal anode. Demonstrate lithium cyclability. (Q4 – Stretch goal)

Progress Report

Li/electrolyte/Li symmetrical cell was constructed to obtain the lithium transference number (t_{Li^+}) as well as to check stability of the composite polymer electrolyte (CPE) with lithium. The thin CPE of 50 vol% ceramic with PEO + Li triflate + tetraglyme was spray-coated and hot-pressed as described earlier. A transference number of 0.79 is obtained upon polarization at 10mV with EIS evaluation of bulk and interface resistance (Figure 73, left) following the literature^[1]. The compatibility of the CPE with lithium was tested by extended DC cycling of lithium at different applied currents (Figure 73, center). The current was reversed at 5-minute intervals, followed by 1-hour intervals. In all cases, the observed voltage was flat and symmetric and did not change with time. The EIS response also does not change upon DC cycling (Figure 73, right). Upon disassembly, the composite electrolyte with Ohara ceramic is still white, suggesting that the polymer suffices to prevent titanium reduction. The lithium, however, was dark; this interface reaction will be investigated.

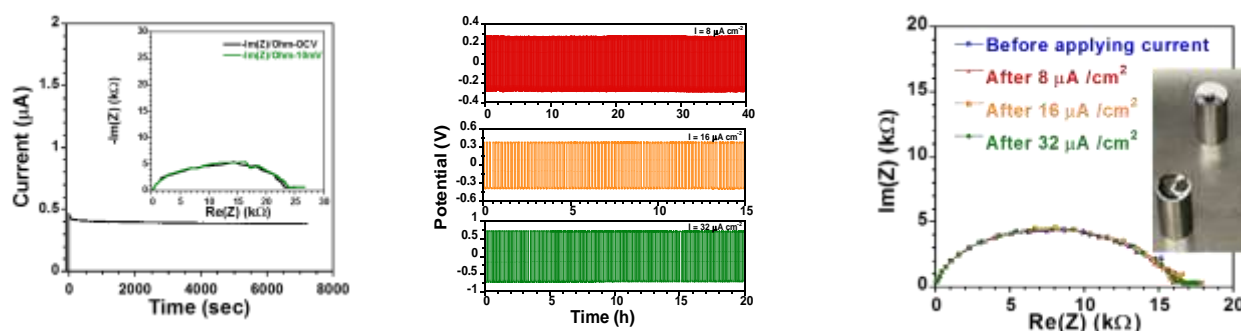


Figure 73. Results for symmetrical cell Li/composite polymer electrolyte (CPE)/Li. At left, DC polarization and electrochemical impedance spectroscopy (EIS) response as inset. At center, voltage measured for +/- DC current of 8, 16, 32 $\mu\text{A}/\text{cm}^2$ at 5 min steps. At right, EIS response after each DC cycling test, and appearance of CPE and lithium when cell was disassembled.

To continue to address the interface resistance between the Ohara powder and the polymer electrolyte, the project studied the effects of acid and base treatment of the Ohara LiCGC powders. Previous studies^[2, 3] have shown moderate change in the ion conductivity of PEO-LiX-alumina composites by using alumina with acidic, neutral, and basic surfaces. The project treated LiCGC powder with HNO_3 and NaOH aqueous solutions with 4 pH values, 1.4, 3.3, 10.6, and 12.7. XRD revealed change in the LiCGC structure after treatment in pH = 12.7 solution; infrared spectra did not show significant differences in treated and untreated LiCGC powders. With a composition of 74 wt% LiCGC and salt concentration of $[\text{Li}^+]:[\text{EO}] = 1:16$, results in Figure 74 show that treating LiCGC with mild acid (pH = 3.3) and base (pH = 10.6) led to a 2- to 3- fold reduction of conductivity, whereas the composite containing LiCGC treated with strong base (pH = 12.7) showed conductivity similar to composite containing untreated LiCGC. These composites were formed by spray coating of an aqueous slurry, and will be repeated for composites formed by dry milling and melt pressing.

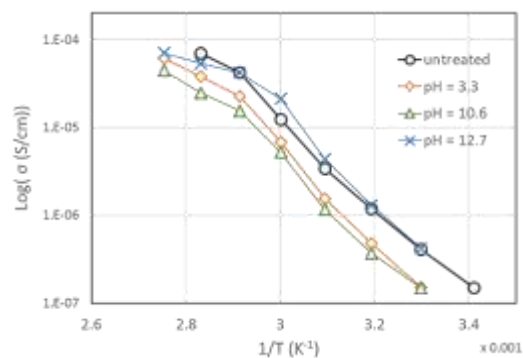


Figure 74. Arrhenius plot of composite polymer electrolyte with Ohara acid/base treated.

[1] Chintapalli M., et al., *Macromolecules* 49 (2016): 3508–3515.

[2] Croce, F., et al., *Electrochimica Acta* 46, no. 16 (2001): 2457–2461.

[3] Marcinek, M., et al., *The Journal of Physical Chemistry B* 104, no. 47 (2000): 11088–11093.

Patents/Publications/Presentations/Presentations

Presentation

- DOE Annual Merit Review, Washington, D. C. (June 5 – 9, 2017): “Composite Electrolyte to Stabilize Metallic Lithium Anodes”; Nancy Dudney, Amaresh Samuthira Pandian, and Frank Delnick.

Task 7.4 – Overcoming Interfacial Impedance in Solid-State Batteries (Eric Wachsman, Liangbing Hu, and Yifei Mo, University of Maryland College Park)

Project Objective. The project objective is to develop a multifaceted and integrated (experimental and computational) approach to solve the key issue in solid-state, Li-ion batteries (SSLiBs), interfacial impedance, with a focus on garnet-based SSEs, the knowledge of which can be applied to other SSE chemistries. The focus is to develop methods to decrease impedance across interfaces with the solid electrolyte, and ultimately demonstrate a high power/energy density battery employing the best of these methods.

Project Impact. Garnet electrolytes have shown great promise for intrinsically safer batteries with high energy density. The success of the proposed research can lead to dramatic progress on development of SSLiBs based on garnet electrolytes. The methodology of combining computational and experimental methods can lead to an understanding of the thermodynamics, kinetics, and structural stability of SSLiBs with garnet electrolytes. Garnet electrolyte particles are naturally brittle and hard due to their ceramic nature, and thus typically have poor contact between electrolyte particles and with electrode materials. A fundamental understanding of the particle interfaces at the nanoscale and through computational methods, especially with interface layers, can guide improvements to the SSE and battery design and eventually lead to commercial use of SSLiB technology.

Approach. Electrode/electrolyte interfaces in SSLiBs are typically planar, resulting in high impedance due to low specific surface area. Attempts to make high surface area 3D interfaces (for example, porous structure) can also result in high impedance due to poor contact at the electrode-electrolyte interface that hinders ion transport or degrades due to expansion/contraction with voltage cycling. This project will experimentally and computationally determine the interfacial structure-impedance relationship in SSLiBs to obtain fundamental insight into design parameters to overcome this issue. Furthermore, it will investigate interfacial modification (layers between SSE and electrode) to extend these structure-property relationships to demonstrate higher performance SSLiBs.

Collaborations. This project collaborates with Dr. Venkataraman Thangadurai on garnet synthesis. It will collaborate with Dr. Leonid A. Bendersky (Leader, Materials for Energy Storage Program at NIST) and use neutron scattering to investigate the lithium profile across the bilayer interface with different charge-discharge rates. The project is in collaboration with Dr. Kang Xu, ARL, with preparation of perfluoropolyether (PFPE) electrolyte.

Milestones

1. Fabricate and test SSLiBs with Li-NMC Chemistry. (Q1 – Completed December 2016)
2. Fabricate and test SSLiBs with Li-S Chemistry. (Q2 – Completed March 2017)
3. Develop models to investigate interfacial transport for Li-S and Li-NMC SSLiBs. (Q3 – Completed June 2017)
4. Achieve full cell (Li-S or Li-NMC) performance of 350-450 Wh/kg and 200 cycles. (Q4 – Initiated April 2017)

Progress Report

Computation Modeling Study for Interface for Li-S and Li-NMC SSLiBs

Thermodynamic computation predicted potential reaction and interphase formation between LLZO and lithium polysulfides in solid-state Li-S battery. Li_2SO_4 is identified as a dominant reaction product, which is confirmed in the XPS spectra. The formed interphase layer may serve as a protection layer between garnet solid electrolyte and sulfur cathode. The Li-ion transport in these interphase layers would be crucial for interfacial ion transport. First-principles computation based on nudged-elastic-band methods were performed to identify the Li^+ transport pathway (Figure 75c) and migration energy barrier (Figure 75d) of $\sim 0.6\text{--}0.8\text{eV}$, showing reasonable Li^+ interfacial transport across the formed interphase layers in Li-S solid-state battery.

Thermodynamic computation also predicted potential reaction and interphase formation between LLZO and NMC cathode in solid-state lithium battery, and such reaction is energetically more favorable at high applied voltages. As potential formed products, the interphase equilibria include Li_6ZrO_7 , $\text{La}_2\text{Zr}_2\text{O}_7$, and various Li/La TM oxides. The Li^+ transport is studied in Li_6ZrO_7 , a dominant interphase product, using first-principles computation. The Li^+ transport pathway (Figure 75e) and migration energy barrier (Figure 75f) of $\sim 0.2\text{--}0.8\text{eV}$ indicate decent Li^+ transport across the garnet-NMC interface. In summary, the developed computation models reveal the interphase layer formation between garnet solid electrolyte and S/NMC cathode materials in solid-state lithium batteries. The formation of such layers serves an important protection role at the electrolyte-cathode interfaces with Li^+ transport in these interphase layers crucial to battery performance. First principles calculations revealed Li^+ diffusion mechanisms and reasonable Li^+ transport across the interfaces.

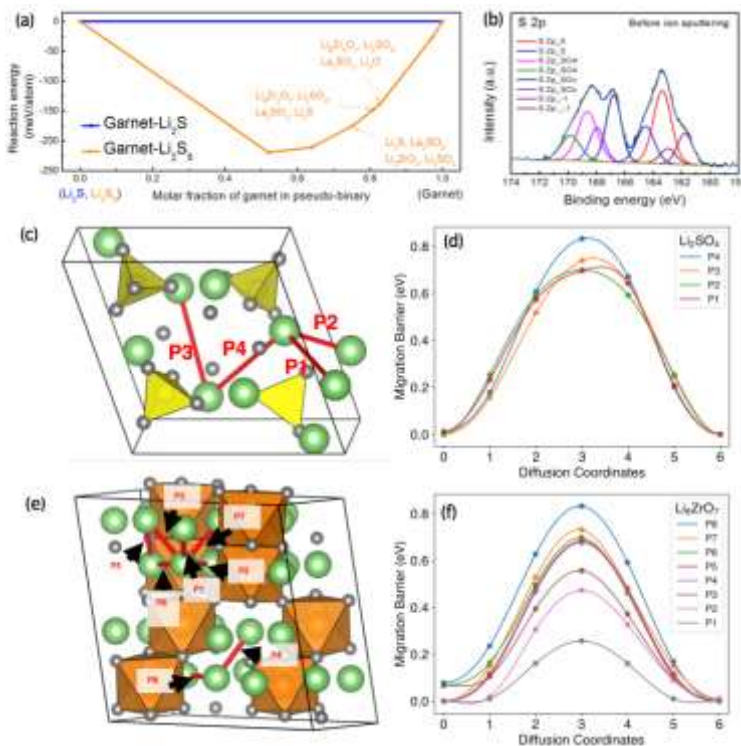


Figure 75. (a) Calculated interphase equilibria and reaction energy between LLZO and lithium polysulfides. (b) X-ray photoelectron spectroscopy spectra of garnet interface in Li-S battery. Calculated Li^+ transport pathway (c) and energy barriers (d) of Li_2SO_4 . Calculated Li^+ transport pathway (e) and energy barriers (f) of Li_6ZrO_7 .

Patents/Publications/Presentations/Presentations

Presentations

- 21st International Conference on Solid-State Ionics, Padua, Italy (June 23 – 29, 2017): “All-Solid-State Li-Ion Batteries for Transformational Energy Storage”; Eric Wachsman. Invited.
- BLI-X, IBM, Almaden, California (June 27 – 29, 2017): “Enabling All-Solid-State Li-ion Batteries through Computation-Guided Design of Materials and Interfaces”; Yifei Mo. Invited.
- 17th Annual Advanced Automotive Battery Conference, San Francisco, California (June 2017): “Computation-Guided Understanding and Design of Interfaces in All-Solid-State Li-Ion Batteries”; Yifei Mo. Invited.
- University of California at Berkeley, Berkeley, California (April 6, 2017): “All-Solid-State Li-ion Batteries for Transformational Energy Storage”; Eric Wachsman. Invited.

Task 7.5 – Nanoscale Interfacial Engineering for Stable Lithium-Metal Anodes (Yi Cui, Stanford University)

Project Objective. This study aims to render Li-metal anode with high capacity and reliability by developing chemically and mechanically stable interfacial layers between lithium metal and electrolytes, which is essential to couple with sulfur cathode for high-energy, Li-S batteries. With the nanoscale interfacial engineering approach, various kinds of advanced thin films will be introduced to overcome issues related to dendritic growth, reactive surface, and virtually “infinite” volume expansion of Li-metal anode.

Project Impact. Cycling life and stability of Li-metal anode will be dramatically increased. The success of this project, together with breakthroughs of sulfur cathode, will significantly increase the specific capacity of lithium batteries and also decrease cost, thereby stimulating the popularity of EVs.

Out-Year Goals. Along with suppressing dendrite growth, the cycle life, CE, and current density of Li-metal anode will be greatly improved (that is, no dendrite growth for current density up to 3.0 mA/cm², with CE greater than 99.5%) by choosing the appropriate interfacial nanomaterial along with rational electrode material design.

Milestones

1. Rational design of composite artificial SEI for the stabilization of 3D nanoporous Li-metal anode. (Q1 – Completed December 2016)
2. Explore novel materials and their properties as artificial SEI layer on lithium metal. (Q2 – Completed March 2017)
3. Explore surface coating techniques and materials for Li-metal stabilization. (Q3 – Completed June 2017)
4. Stabilizing 3D Li-metal anode with solid electrolytes. (Q4 – In progress)

Progress Report

Previously, the project developed 3D Li-anode composites, which realized minimum volumetric change at the electrode level during cycling, more uniform Li-deposition behavior, and better electrochemical performance. To further improve the 3D Li-metal anode design toward practical applications, effective protective surface coatings are essential. Among the surface protection materials, lithium fluoride (LiF) has gained special attention due to its wide electrochemical stability window with negligible solubility in most electrolytes as well as its capability of regulating surface tension. In the early stage, it was found that addition of HF or fluorinated compounds into electrolyte would help form LiF in SEI and enable more uniform lithium deposition. However, these methods are unlikely to produce high-quality continuous and conformal LiF coating on lithium metal. Instead, dispersive LiF domains would form with many weakly linked grain boundaries, which would easily fracture during Li-metal plating and stripping. Moreover, HF and other fluorinated compounds are highly hazardous reagents, which might impose extra challenges in either industrial processing or battery packaging. Herein, this project explores the possibility of gas phase reaction (using Freon R134a, 1,1,1,2-tetrafluoroethane, as the reagent) in attempt to produce high-quality LiF passivation layers conformally on 3D Li-metal anode.

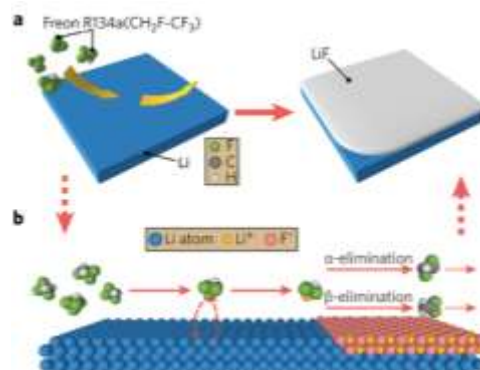


Figure 76. (a) Schematic showing surface treatment of lithium metal with Freon R134a. (b) Proposed major chemical reactions at the early stage of surface treatment.

The idea is illustrated schematically in Figure 76. By exposing lithium metal to Freon R134a gas, assisted with controlled gas pressure, and reaction temperature, the project was able to coat a dense and uniform LiF layer with tunable thickness directly onto metallic lithium.

It was found that at a fixed temperature, increasing gas pressure would accelerate the reaction and afford rougher surface; when gas pressure was fixed, the reactivity increased with temperature. At temperature below 150°C, the surface was smooth without visible domains; however, once the temperature was increased to approaching the melting point of lithium metal, the reaction occurred in a much more vigorous fashion and formed micron-sized and porous LiF domains. Thus, to obtain high-quality LiF coating and sufficient reaction rate, 150°C and 0.5 atm is a good condition for conducting the surface coating. Figure 77 shows the SEM images of a LiF-coated lithium foil, where the top view shows smooth LiF surface, and the cross-section indicates a uniform thickness of ~40 nm.

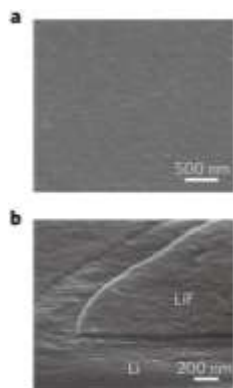


Figure 77. High-resolution scanning electron microscopy images showing (a) surface morphology and (b) cross-section of LiF-coated lithium foil.

To study the efficacy of the LiF coating for improving electrochemical stability of 3D Li-metal anode (lithium metal infused into layered graphene oxide matrix, Li-rGO), time-dependent EIS studies were carried out, as shown in Figure 78. LiF-coated Li-rGO does not show obvious increase in impedance within the tested period of time, indicating robust surface passivation that suppressed continuous side reactions and reduced initial SEI formation. In addition, more stable symmetric cell cycling with suppressed increase in polarization was also observed.

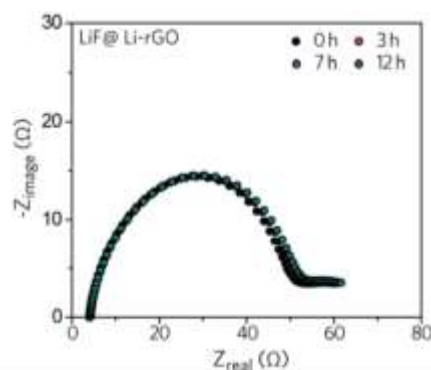


Figure 78. Time-dependent electrochemical impedance measurement on 3D Li-metal symmetric cells with LiF coating.

Patents/Publications/Presentations

Publication

- Liu, D., et al. “Conformal Lithium Fluoride Protection Layer on Three-Dimensional Lithium by Nonhazardous Gaseous Reagent Freon.” *Nano Lett.* 17 (2017): 3731–3737.

Task 7.6 – Lithium Dendrite Prevention for Lithium-Ion Batteries (Wu Xu and Ji-Guang Zhang, Pacific Northwest National Laboratory)

Project Objective. The project objective is to enable lithium metal to be used as an effective anode in rechargeable Li-metal batteries for long cycle life at a reasonably high current density. The investigation will focus on effects of various lithium salts, additives, and carbonate-based electrolyte formulations on Li-anode morphology, lithium CE, and battery performances in terms of long-term cycling stability at room temperature and elevated temperatures and at various current density conditions, rate capability, and low-temperature discharge behavior. The surface layers on lithium anode and cathode will be systematically analyzed. The properties of solvates of cation-solvent molecules will also be calculated to help explain obtained battery performances.

Project Impact. Lithium metal is an ideal anode material for rechargeable batteries. Unfortunately, dendritic lithium growth and limited CE during lithium deposition/stripping inherent in these batteries have prevented practical applications. This work will explore new electrolyte additives that can lead to dendrite-free lithium deposition with high CE. The success of this work will increase energy density of Li-metal batteries and accelerate market acceptance of EVs, especially for PHEVs required by the EV Everywhere Grand Challenge.

Out-Year Goals. The long-term goal of the proposed work is to enable lithium and Li-ion batteries with > 120 Wh/kg (for PHEVs), 1000 deep-discharge cycles, 10-year calendar life, improved abuse tolerance, and less than 20% capacity fade over a 10-year period.

Collaborations. This project collaborates with the following: Bryant Polzin (ANL) on NMC electrodes, Chongmin Wang (PNNL) on characterization by TEM/SEM, and Zihua Zhu (PNNL) on TOF-SIMS.

Milestones

1. Verify formation of a transient high Li⁺-concentration electrolyte layer during fast discharging by direct microscopic observation. (Q1 – Completed December 2016)
2. Identify effects of dual-salt electrolytes on Li-metal protection during fast charging. (Q2, March 31, 2017 – Complete)
3. Identify new electrolytes that are stable with both lithium and high-voltage cathode. (Q3, June 20, 2017 – Completed)
4. Increase the CE of lithium cycling in the new electrolyte to be more than 99%. (Q4, September 30, 2017 – In progress)

Progress Report

The effects of additives (VC, FEC, and X) in the electrolyte of 1 M LiPF₆/PC on the average CE of Li-metal anode and the long-term cycling performance of Li||NMC-333 cells were investigated, and the results are shown in Figure 79a-b. It is seen that additive X can slightly improve the lithium CE of the baseline electrolyte, but additives VC and FEC can greatly enhance the lithium CE to about 94%; the mixtures of VC+X and FEC+X can further increase lithium CE to about 96.5%. So far, the VC+X mixed additive in the LiPF₆/PC electrolyte shows the most stable long-term cycling in Li||NMC-333 cells. The FEC+X additive mixture does not give long stable cycling, although its lithium CE is just slightly lower than the VC+X mixture. Characterizations are under way.

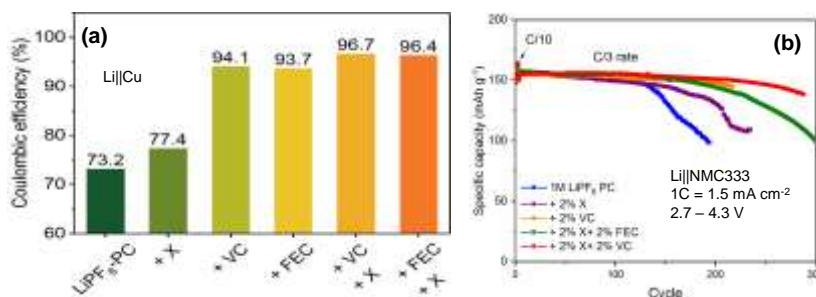


Figure 79. (a) Average lithium Coulombic efficiency in electrolytes of 1 M LiPF₆/PC with different additives (VC, FEC, and X) and additive mixtures (VC+X and FEC+X) tested in Li||Cu cells. (b) Cycling stability of these electrolytes in Li||NMC-333 cells at C/3 rate.

The effects of lithium anode areal capacity used during each deposition/stripping cycle on the stability of Li-metal anode and cycling performance of the Li-metal battery have been systematically investigated using the dual-salt electrolyte of LiTFSI-LiBOB in EC-EMC with 0.05 M LiPF₆ additive between 2.7 and 4.3 V. NMC-333 cathodes with different areal capacities (from ~ 1.0 to ~ 4.0 mAh cm⁻² with an interval of ~ 0.5 mAh cm⁻²) were used to represent the lithium areal capacity usage. Under the same charge current density at 1.0 mA cm⁻², very decent long-term cycling performance can be achieved for the NMC cathode with all areal capacity loadings or the lithium areal capacity usages, meaning that the usage of lithium amount in each cycle does not affect the cycling stability of the Li-metal cells when lithium anode is in excess. Increase of lithium capacity usage in each cycle causes variations in components of the SEI layer on lithium anode and generates more ionic conductive species from this electrolyte. Further study reveals for the first time that Li-anode degradation and SEI thickness show linear relationship with areal capacity usage. The amount of consumed lithium and ratio of SEI thickness to NMC areal loading are kept almost the same values with increasing cathode loading, respectively.

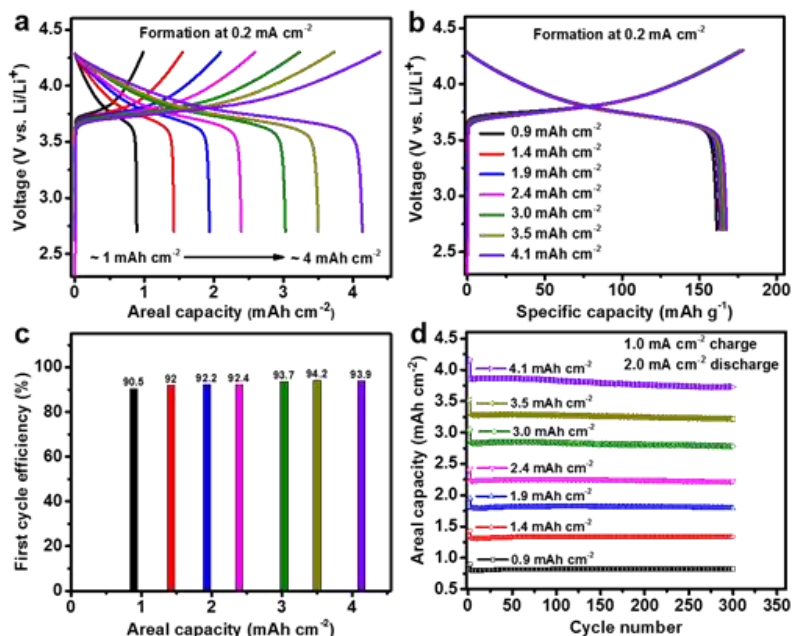


Figure 80. Performances of Li||NMC cells with different NMC areal capacity loadings. (a, b) First-cycle voltage profiles related to areal capacity (a) and specific capacity (b). (c) First-cycle efficiency. (d) Long-term cycling stability at 1.0 mA cm⁻² charge and 2.0 mA cm⁻² discharge between 2.7 and 4.3 V.

Patents/Publications/Presentations

Publication

- Jiao, S., and J. Zheng, Q. Li, M. H. Engelhard, R. Cao, J.-G. Zhang, and W. Xu. “Behavior of Lithium Metal Anode under High Lithium Capacity Utilization and High Current Density in Lithium Metal Batteries.” Submitted.

Task 7.7 – Lithium Batteries with Higher Capacity and Voltage (John B. Goodenough, University of Texas – Austin)

Project Objective. The project objective is to develop an electrochemically stable alkali-metal anode that can avoid the SEI layer formation and the alkali-metal dendrites during charge/discharge. To achieve the goal, a thin and elastic solid electrolyte membrane with a Fermi energy above that of metallic lithium and an ionic conductivity $\sigma > 10^{-4} \text{ S cm}^{-1}$ will be tested in contact with alkali-metal surface. The interface between the alkali-metal and the electrolyte membrane should be free from liquid electrolyte, have a low impedance for alkali-metal transport and plating, and keep a good mechanical contact during electrochemical reactions.

Project Impact. An alkali-metal anode (lithium or sodium) would increase the energy density for a given cathode by providing a higher cell voltage. However, lithium is not used as the anode in today's commercial Li-ion batteries because electrochemical dendrite formation can induce a cell short-circuit and critical safety hazards. This project aims to find a way to avoid the formation of alkali-metal dendrites and to develop an electrochemical cell with dendrite-free alkali-metal anode. Therefore, once realized, the project will have a significant impact through an energy-density increase and battery safety; it will enable a commercial Li-metal rechargeable battery of increased cycle life.

Approach. The project will design, make, and test cells. The key approach is to introduce a solid-solid contact between an alkali metal and a solid electrolyte membrane. Where SEI formation occurs, the creation of new anode surface at dendrites with each cycle causes capacity fade and a shortened cycle life. To avoid the SEI formation, a thin and elastic solid electrolyte membrane would be introduced, or the solid electrolyte should not be reduced by, but should be wet by, a metallic alkali-ion anode.

Out-Year Goals. The out-year goal is to develop coin cells that are safe and low-cost with a long cycle life at a voltage $V > 3.0 \text{ V}$.

Collaborations. This project collaborates with A. Manthiram at UT Austin, and Karim Zaghib at HQ.

Milestones

1. Demonstrate the cycle life and capacity of a Li-S cell. (Q1 – Complete)
2. Demonstrate a high-voltage cell containing the glass electrolyte. (Q2 – In progress)
3. Demonstrate a new battery concept. (Q3 – In progress)
4. Test energy density, cycle life, and rate of charge/discharge of the new battery concept. (Q4)

Progress Report

The Cu^+/Cu^0 redox couple in the cathode was tested in an all-solid-state lithium battery. Here, the Cu^+/Cu^0 redox couple determines the cell voltage, and a solid Li^+ electrolyte provides Li^+ ions. The project has used a cross-linked poly (ethylene glycol) methyl ether acrylate (CPMEA; Figure 81) membrane with LiTFSI salts as the solid electrolyte. The membrane was shown to be electrochemically stable up to 4.8 V versus lithium at 65°C. A battery-grade copper foil was used as a cathode current collector and a Cu^+/Cu^0 redox source. The copper foil was directly placed on one-side of the CPMEA membrane, and a Li-metal foil was placed on the other side.

Figure 82 shows initial charge/discharge voltage curves of the solid-state lithium cell at 70°C. During charging, a constant voltage plateau at ~ 3.5 V versus lithium was observed, which corresponds to the electrochemical copper dissolution via the Cu^+/Cu^0 redox reaction. Lithium plating occurs at the anode, while the dissolved Cu^+ ions keep the charge neutrality of the polymer electrolyte. During the following discharge, there are two voltage regions noticed, one at ~3.3 V and the other at ~2.1 V. The upper voltage region should be responsible for the Cu^+/Cu^0 redox couple. However, the corresponding capacity is only about a half of the charging capacity. This is partly because the initially dissolved Cu^+ ions diffuse away from the copper foil owing to the concentration gradient, and therefore, the diffusional overpotential increases as the electrochemical Cu^+ reduction proceeds at the copper surface during discharge. The results suggest that higher Li^+ and Cu^+ concentrations are necessary to increase cell capacity and reaction kinetics. For the lower voltage reaction at ~ 2.1 V, the discharge mechanism is not understood yet, and further study will be pursued.

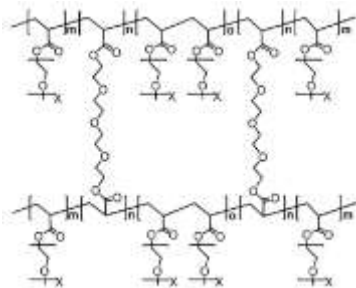


Figure 81. Structure of cross-linked poly (ethylene glycol) methyl ether acrylate (CPMEA).

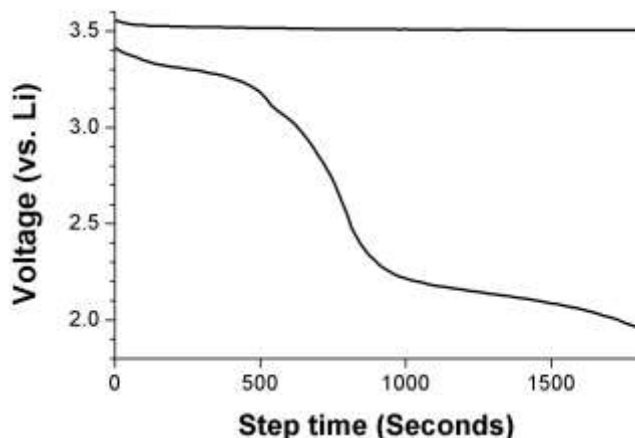


Figure 82. Charge/discharge voltage curves of all-solid-state Li/CPMEA-LiTFSI/Cu cell at 70°C.

Patents/Publications/Presentations

Publication

- Park, K., and J. B. Goodenough. “Dendrite-Suppressed Lithium Plating from a Liquid Electrolyte via Wetting of Li_3N .” *Adv. Energy Mater.* doi: 10.1002/aenm.201700732.

Task 7.8 – Advancing Solid-State Interfaces in Lithium-Ion Batteries (Nenad Markovic and Larry A. Curtiss, Argonne National Laboratory)

Project Objective. The project objectives are multifaceted, including: (1) development of a new mechanically and chemically stable Li-selective solid “membrane” capable of protecting the metal lithium anode during the discharge process in commercially available liquid electrolytes (hereafter denoted as a $S_{Li-SM-EL}$ system); and (2) development of a mechanically/chemically stable and Li-ion conductive ($\geq 2 \times 10^{-4}$ S/cm at 298K) solid electrolyte for a solid-state battery encompassing a metal lithium anode and nonflammable solid electrolyte that can operate at cathode potentials > 5 V (denoted as a $S_{Li-SEL-SC}$ system).

Project Impact. Protective organic and inorganic compounds can enhance stability of interface, improve Li-ion interfacial transport, minimize dendrite formation, and increase safety in Li-ion batteries.

Approach. The project proposes to develop and use interdisciplinary, atomic-/molecular-level insight obtained from integrating both experimental- and computational-based methodologies to define the landscape of parameters that control interfacial properties for a new generation of the Li-ion solid-solid battery systems. The strategy will involve transferring knowledge gained from well-characterized thin-film materials to real-world materials. This strategy forms a closed loop wherein the knowledge gained from model systems is used to design more complex, real-world materials and vice-versa. The work will focus on utilizing existing in-house synthesis and characterization methods to enable rapid transition from fundamental science to realistic cells.

Out-Year Goals. The out-year goals are to use and develop the physical and chemical synthesis methods for design of solid-solid interfaces with unique chemical/mechanical/conductivity properties of $S_{Li-SM-EL}$ and $S_{Li-SEL-SC}$ systems. The proposed work will develop and exploit a variety of *ex situ* and *in situ* experimental optical and surface sensitive techniques and electrochemical methods to explore and explain bulk and interfacial properties of the selected materials. The results will serve to unravel many puzzling bulk and interfacial properties of $S_{Li-SM-EL}$ and $S_{Li-SEL-SC}$ materials.

Collaborations. This project funds work at ANL and University of Illinois at Chicago (Prof. Amin Salehi). It will establish collaboration with Jeff Sakamoto at University of Michigan.

Milestones

1. Development of new synthesis and characterization methods for controlled deposition of lithium on well-defined $SrTiO_3$ single crystals. (Q1 – Initiated November 2016)
2. Use ultra high vacuum (UHV)-based experimental techniques in combination with computational methods to investigate parameters that control interaction of lithium anode with individual components of $Li_{6.5}La_3Zr_{1.5}M_{0.5}O_2$ ($M = Nb, Ta$) and Li_2CO_3 “membrane.” (Q2 – In progress)
3. Design and develop *in situ* evaluation of stability of both Li_2CO_3 “membrane” (ICP-MS) and selected organic electrolytes during charge-discharge processes (DEMS). (Q3)
4. Investigate the CE of, as well as the charge-discharge cyclability for, selected $S_{Li-SM-EL}$ and $S_{Li-SEL-SC}$ systems. (Q4)

Progress Report

Li-Oxide Interaction – The Anode Side. Conditions for controlled lithium deposition (magnetron sputtering method) on Nb-doped SrTiO₃ (Nb:STO) single crystal substrates are established (lithium sputtering ~ 30 min at 25°C). Li-coated Nb:STO samples are then transferred under UHV conditions, avoiding all air-born contamination, allowing exploration of the interaction of Li⁰ with Ti⁴⁺ and Nb⁵⁺ at atomic and molecular levels. As summarized in Figure 83, XPS data reveal that lithium reacts with both cations leading to reduction of Ti⁴⁺ to Ti³⁺ and Ti²⁺, and Nb⁵⁺ to Nb⁴⁺. The importance of these results is two-fold: (1) they demonstrate that the methodology allows for simultaneous monitoring of interaction of interfacial lithium with two cations in a model, single crystal system; and (2) it is possible to monitor interaction of the lithium anode with real solid electrolytes such as LLZO doped with niobium, aluminum, tantalum, etc., allowing monitoring of changes in interfacial dopant chemistry as well as the bulk oxide properties (see Q1 report for more details).

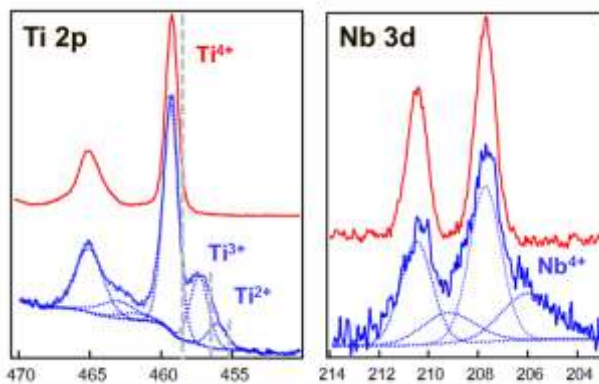


Figure 83. X-ray photoelectron spectroscopy results for Ti 2p and Nb 3d peak to establish Li-cation interactions.

Li-Oxide Interaction – The Cathode Side. Successful synthesis of single crystal LiCoO₂ cathode thin films via PLD. Films were deposited on STO (001) and STO (111), yielding LiCoO₂ (003) and LiCoO₂ (104), respectively (Figure 84a). Surface structure of the deposited films was explored by AFM (Figure 84b), revealing differences in interfacial roughness. Preliminary experiments were carried out to investigate interfacial and bulk interactions of lithium with LiCoO₂ utilizing XPS (not shown) and XAS (Figure 84c).

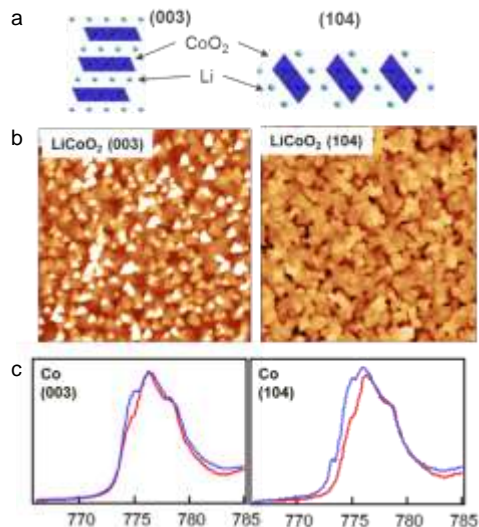


Figure 84. (a) Crystal structure of the two STO||LiCoO₂ thin films. (b) Atomic force microscopy images showing the topography of the thin films. (c) X-ray absorption spectroscopy measurements demonstrating that (003) films are unaffected by lithium deposition, whereas bulk reduction takes place on (104) films.

Such interactions are particularly relevant for understanding the stability and eventual breakdown of LiCoO₂, for example, after penetration of the electrolyte by lithium dendrites. XPS analysis reveals that orientation-specific interactions take place, with cobalt species on the surface of LiCoO₂(003) reducing completely to Co⁰, whereas LiCoO₂(104) is reduced to a mixture of Co²⁺ and Co⁰. XAS reveals that the reduction of LiCoO₂(003) is limited to the surface, whereas reduction of LiCoO₂(104) extends into the bulk. These results indicate that cathode interfacial stability is structure-sensitive, and that by tuning the orientation of the interface relative to solid electrolyte, it may be possible to create more active and stable solid-state batteries.

Task 7.9 – Engineering Approaches to Dendrite-Free Lithium Anodes (Prashant Kumta, University of Pittsburgh)

Project Objective. This project will yield Li-metal anodes with specific capacity ≥ 2000 mAh/g (≥ 10 mAh/cm²), ~ 1000 cycles, CE loss $\leq 0.01\%$, and CE $\geq 99.99\%$ with superior rate capability. The goal is to (1) systematically characterize different approaches for generation of dendrite-free Li-metal anodes while also providing understanding of the scientific underpinnings, and (2) evaluate the microstructure and electrochemical performance of dendrite-free Li-metal anodes. Generation of high-performance, dendrite-free Li-metal anodes will successfully demonstrate generation of novel sulfur cathodes, affording fabrication of Li-S batteries meeting the targeted gravimetric energy densities ≥ 350 Wh/kg and ≥ 750 Wh/l with a cost target \$125/kWh and cycle life of at least 1000 cycles for meeting the EV Everywhere Grand Challenge blueprint.

Project Impact. Dendrite formation in electrochemical systems occurs due to inhomogeneous current densities coupled with local diffusion gradients, surface roughness, and kinetic roughening. Lithium dendrite formation and growth are, however, not well understood; adding to the complexity is SEI formation. Control and elimination of Li-metal dendrite formation is a veritable challenge. If overcome, it would render universal adoption of Li-anode batteries for stationary and mobile applications. This project is a scientific study of novel approaches to address dendrite formation in Li-anode batteries, electrolyte decomposition, and associated cell failure. Development of dendrite-free, high-performance lithium anodes will enable the use of Li-free cathodes, opening myriad possibilities to push the envelope in terms of cathode capacity and battery energy density.

Out-Year Goals. This project comprises three major phases to be successfully completed in three years:

- Phase 1 (year 1) – Synthesis, characterization, and scale up of suitable PF (porous foams) for use as current collectors for lithium anodes and Li-ion conductor (LIC) materials to prepare multilayer porous foams (MPF).
- Phase 2 (year 2) – Development of Li-rich structurally isomorphous alloy (SIA) anodes; generation of composite multilayer anodes (CMAs).
- Phase 3 (year 3) – Advanced high-energy-density, high-rate, extremely cyclable cell development.

Collaborations. The project will involve collaboration with Dr. Moni Kanchan Datta (University of Pittsburgh, U Pitt) and Dr. Oleg I. Velikokhatnyi (U Pitt) as co-PIs, and Dr. Prashanth Jampani Hanumantha (U Pitt) as senior research personnel. In addition, collaboration will be undertaken with Dr. D. Krishnan Achary (U Pitt) for solid-state magic angle spinning nuclear magnetic resonance (MAS-NMR) characterization.

Milestones

1. Delegate tasks and convene the technical aspects between partners. (Q1, December 2016 – Completed)
2. Determine electrode and cell design parameters for achieving the targeted energy density. (Q1, December 2016 – Complete)
3. Identify and synthesize materials with high electronic conductivity, electrochemical stability that can be generated as porous architectures. (Q3, July 2017 – Complete)
4. Identification and synthesis of LIC materials for use as coatings on both PF and use in CMAs with room-temperature ionic conductivity (10^{-3} - 10^{-4} S/cm). (Q3 – Completed July 2017)
5. Synthesis of MPF exhibiting: specific capacity ≥ 1000 mAh/g (≥ 4 mAh/cm²), > 400 cycles without cell failure), initial CE: $\geq 95\%$ with $\leq 0.05\%$ loss per cycle. (October 2017 – In progress)
6. Perform first-principles investigations into identifying electronically and ionically conductive materials capable of acting as SIA compositions over a range of lithium compositions. (October 2017 – In progress)

Progress Report

The first phase is aimed at development of PF materials and MPF with the aim of reducing orthogonal lithium nucleation and growth.

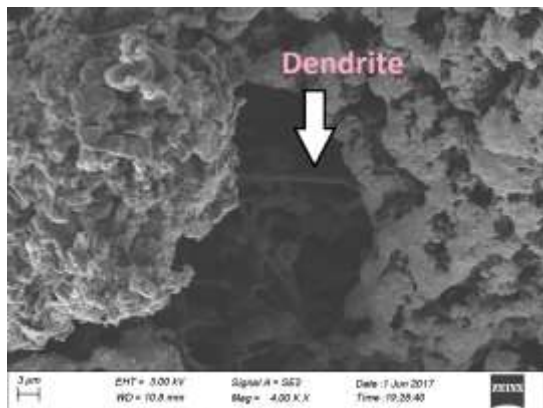


Figure 85. Very high porosity (60-80%) porous foams (PF) with hierarchical porosity. Post-cycled scanning electron microscopy images of the PF showing dendrite growth within the pores of the foam.

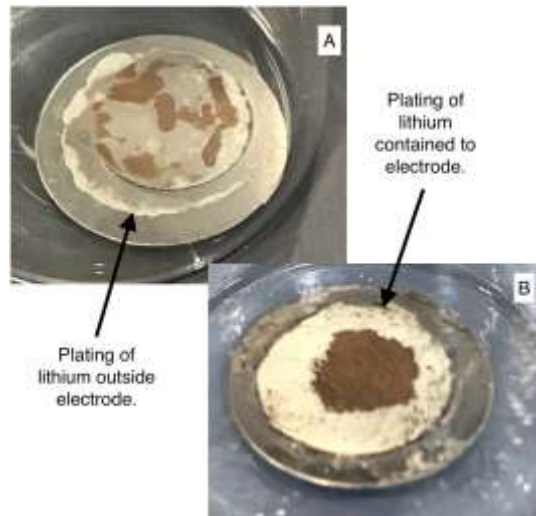


Figure 86. (a) Formation of lithium on stainless-steel spacer in coin cell tests. (b) Diffusion pathways causing plating of lithium on polymeric-coated stainless-steel spacers.

Second quarter work involved initial studies using electrochemically prepared PF. Work has now migrated to gen-2 foams with very high and easily controlled porosities of 60-80%, generated using a simple chemical method. Figure 85 shows formation of dendrites within the porous architecture after testing at a current density of $\sim 1 \text{ mA/cm}^2$ to a capacity of 1 mAh/cm^2 . It was observed post-cycling that the lithium dendrites tend to deposit around the PF materials since the separator contacts the stainless-steel spacer behind the foam structure (Figure 86a). This issue was partially resolved by use of polymeric coatings applied on the spacer (Figure 86b). An alternate cell design was also developed following these initial attempts and will be reported next quarter. Figure 87 demonstrates long-term cycling of 34 mAh/cm^2 at 1.6 mA/cm^2 using the Li-SIA electrodes. Overpotential of $\pm \sim 30\text{-}100 \text{ mV}$ is maintained for ~ 30 cycles with visible instabilities observed in the 30-60 cycles, after which the overpotential is stabilized in the range of $\sim \pm 12\text{-}15 \text{ mV}$ for over 120 cycles. The intermediate instability region is possibly due to phase segregation and compositional inhomogeneity as observed in Figure 87. Efforts are in progress to understand the same and overcome it by suitable alloying additions.

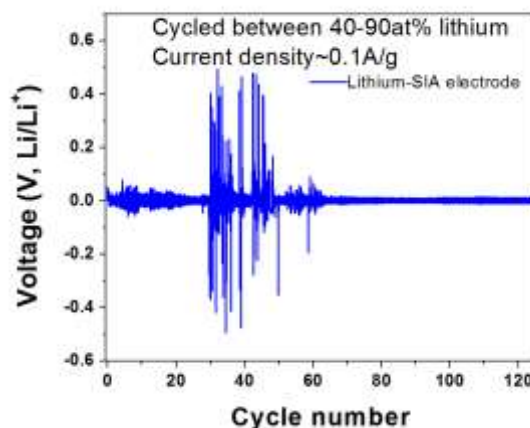


Figure 87. Lithium structurally isomorphous alloy (Li-SIA) electrodes demonstrate long-term stability, though there is a rise in overpotential due to possible phase segregation.

Patents/Publications/Presentations

Publication

- Jampani, P. H., and P. M. Shanthi, B. A. Day, B. Gattu, O. I. Velikokhatnyi, M. K. Datta, and P. N. Kumta. “Lithium Metal Anode Based Rechargeable Batteries: Recent Advances and Challenges for the Future, Progress in Materials Science.” 2017. Under review.

Presentations

- 231st ECS meeting, New Orleans, Louisiana (May 28 – June 1, 2017): “Engineering Solutions to Dendrite Formation in Lithium Anode Based Batteries”; P. H. Jampani, B. Gattu, P. M. Shanthi, M. K. Datta, and P. N. Kumta.
- DOE Annual Merit Review, Washington, D. C. (June 5 – 9, 2017): “Engineering Approaches to Dendrite-Free Lithium Metal Anodes”; P. N. Kumta. Poster.

Task 7.10 – Self-Assembling and Self-Healing Rechargeable Lithium Batteries (Yet-Ming Chiang, Massachusetts Institute of Technology; Venkat Viswanathan, Carnegie Mellon University)

Project Objective. The project objectives are as follows: (1) investigate formation of lithium halide containing SEI, (2) characterize the structure and composition of the SEI surface film and morphology of the electrochemically deposited lithium, and (3) develop combinations of electrolytes (solvents + salts) and electrolyte additives that produce a highly Li-ion conducting, mechanically robust, and self-healing SEI to suppress lithium dendrite formation and improve CE.

Project Impact. Efforts to achieve practical use of the Li-metal anode in rechargeable lithium batteries have long been plagued by lithium dendrite formation and low CE. Lithium dendrites cause battery short-circuits, leading to serious safety hazards. The low CE of Li-metal anodes demands use of excess lithium to offset the lithium loss during cycling, which lowers the overall energy density of the battery. If successful, this project will enable self-forming and self-healing SEI containing alkali and/or alkaline earth halides that can suppress dendrite formation and improve CE. This will eventually enable high-energy-density (> 400 Wh/kg) and long-cycle-life (> 500 cycles, 80% capacity retention) Li-metal batteries.

Approach. The project approach involves the following: (1) identifying suitable combinations of solvents, Li-electrolyte salts, and halide and other additives that can produce highly Li-ion conducting, mechanically robust, and self-healing SEI, (2) using integrated theory and experiment, and (3) assembling and testing symmetric and asymmetric cells and Li-metal batteries comprising a high areal-capacity cathode (> 3 mAh/cm²) and a capacity-limited Li-metal anode (< 30% lithium excess).

Out-Year Goals. The project will down-select electrolyte compositions, develop designs for prototype full cells of > 10 mAh capacity, and fabricate and deliver cells to DOE-specified laboratories for testing and evaluation.

Collaborations. This project collaborates with 24M Technologies Inc. (18 cm²/80 cm² pouch cell fabrication and tests).

Milestones

1. Complete initial computations and halide solubility studies and construct experimental matrix of halides and solvents. (Q2 – Completed April 30, 2017; initiated January 2017)
2. Demonstrate cell designs and electrochemical testing parameters that allow clear differentiation of dendritic and non-dendritic behavior of lithium electrodes. (Q3 – Completed)
3. Deliver characterization results for morphological evolution of Li-metal surface showing that halide additives diminish lithium dendrite formation. (Q4 – In progress)
4. Demonstrate Li-Li symmetric cell using halide additives that outperforms additive-free cell according to criteria in Q2 and Q3. (Q5 – Go/No-Go milestone)

Progress Report

This quarter, results are reported for the cell design and electrochemical testing parameters that allow clear differentiation of dendritic and non-dendritic behavior of lithium electrodes. On the computational side, the methodological framework used to determine trends in solubility of lithium halides was validated. Identification of solvents that trigger salt solubility and remain stable to high-voltage cathodes is under way.

Previous work has shown that lithium cycling efficiency is correlated to morphology of deposited lithium. Dendritic lithium has large surface area so that its side reactions with the liquid electrolyte are more severe compared with non-dendritic lithium. Thus, when lithium dendrite is formed, the cycling efficiency is low. To differentiate dendritic and non-dendritic behavior, an asymmetric cell design was developed to measure average lithium cycling (deposition/stripping) efficiency of different electrolytes (Figure 88a).

The asymmetric cell consists of two Li-metal electrodes that have different thickness and areal capacity. The working electrode is a 20- μm -thick lithium film coated on a copper foil (areal capacity $\sim 4.12 \text{ mAh/cm}^2$), while the counter electrode is a 750- μm -thick lithium foil. The two electrodes are assembled into a CR2032-type coin cell with a Tonen polyethylene separator and 40- μL electrolyte. The cell is cycled at a current density of 0.6 mA/cm^2 , and the cycling capacity is 3.0 mAh/cm^2 per deposition/stripping cycle. The cell is cycled until the overpotential for lithium stripping reaches 0.5 V versus Li^+/Li . The average lithium cycling efficiency is calculated using a method similar to what was previously reported by Doron Aurbach, et al.:

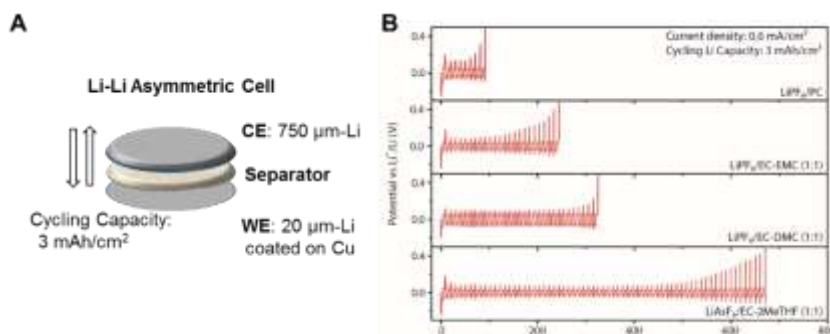


Figure 88. Li-Li asymmetric cell design and tests.

The cell is cycled at a current density of 0.6 mA/cm^2 , and the cycling capacity is 3.0 mAh/cm^2 per deposition/stripping cycle. The cell is cycled until the overpotential for lithium stripping reaches 0.5 V versus Li^+/Li . The average lithium cycling efficiency is calculated using a method similar to what was previously reported by Doron Aurbach, et al.:

$$E_{average} = 1 - \frac{Q_D}{nQ_T}$$

Q_T is cycling capacity (3 mAh/cm^2 in project tests); Q_D is total lithium capacity ($Q_D = Q_T + Q_{excess} = \sim 7.12 \text{ mAh/cm}^2$); n is number of completed deposition/stripping cycles before there is a sudden and significant increase in (over)potential for lithium stripping, indicating that no lithium on the copper substrate is available.

The effectiveness of this method was tested by measuring the lithium cycling efficiency of four different electrolytes, namely $1 \text{ M LiPF}_6/\text{PC}$, $1 \text{ M LiPF}_6/\text{EC-EMC (1:1)}$, $1 \text{ M LiPF}_6/\text{EC-DMC (1:1)}$, and $1 \text{ M LiAsF}_6/\text{EC-2MeTHF (1:1)}$ (Figure 88b). The lithium cycling efficiencies of the four electrolytes are calculated to be 73.6% (LiPF_6/PC), 90.1% ($\text{LiPF}_6/\text{EC-EMC}$), 92.6% ($\text{LiPF}_6/\text{EC-DMC}$), and 96.4% ($\text{LiAsF}_6/\text{EC-2MeTHF}$). Previous work by others has shown that lithium deposits as dendrites in the LiPF_6/PC , $\text{LiPF}_6/\text{EC-EMC}$, and $\text{LiPF}_6/\text{EC-DMC}$ electrolytes. In the $\text{LiAsF}_6/\text{EC-2MeTHF}$ electrolytes, the deposited lithium has a nodular morphology. Therefore, the trend of the lithium cycling efficiency correlates well with the morphology of the deposited lithium. In summary, the Li-Li asymmetric cell can be used to differentiate dendritic and non-dendritic behavior of the lithium electrodes. It will be used to evaluate the effect of halide and other additives in terms of dendrite suppression and improvement of lithium cycling efficiency.

Computational work is under way to identify solvents that trigger solubility of lithium halides and are stable to high voltage at the cathode. The current approach is to use the highest occupied molecular orbital (HOMO) level of the solvent to perform initial selection. Based on screening of a large dataset (900,000 solvents), initial investigations have identified several solvent classes: nitrile, fluorosulfonyl, nitro, dione, fluoroamide, and fluoroesters. Additional criterion will be used for further down selection.

Patents/Publications/Presentations

Publication

- Kerman, K., and A. Luntz, V. Viswanathan, Y.-M. Chiang, and Z. Chen. *J. Electrochem. Soc.* 164, no. 7 (2017): A1731–A1744.

TASK 8 – LITHIUM–SULFUR BATTERIES

Summary and Highlights

Advances in Li-ion technology have been stymied by challenges involved in developing high reversible capacity cathodes and stable anodes. Hence, there is a critical need for development of alternate battery technologies with superior energy densities and cycling capabilities. In this regard, Li-S batteries have been identified as the next flagship technology, holding much promise due to the attractive theoretical specific energy densities of 2,567 Wh/kg. In addition, realization of the high theoretical specific capacity of 1,675 mAh/g corresponding to formation of Li₂S using earth-abundant sulfur renders the system highly promising compared to other available cathode systems. Thus, the research focus has shifted to developing Li-S batteries. This system, however, suffers from major drawbacks, as elucidated below:

- Limited inherent electronic conductivity of sulfur-based and sulfur-compound-based cathodes;
- Volumetric expansion and contraction of both the sulfur cathode and lithium anode;
- Soluble polysulfide formation/dissolution and sluggish kinetics of subsequent conversion of polysulfides to Li₂S, resulting in poor cycling life;
- Particle fracture and delamination resulting from the repeated volumetric expansion and contraction;
- Irreversible loss of lithium at the sulfur cathode, resulting in poor CE; and
- High diffusivity of polysulfides in the electrolyte, resulting in plating at the anode and consequent loss of driving force for lithium diffusion (that is, drop in cell voltage).

These major issues cause sulfur loss from the cathode, leading to mechanical disintegration. Additionally, surface passivation of anode and cathode systems results in a decrease in the overall specific capacity and CE upon cycling. Consequently, the battery becomes inactive within the first few charge-discharge cycles. Achievement of stable high capacity in Li-S batteries requires execution of fundamental studies to understand the degradation mechanisms in conjunction with devising engineered solutions.

This Task addresses both aspects with execution of esoteric, fundamental *in situ* XAS and *in situ* electron paramagnetic resonance (EPR) studies juxtaposed with conducting innovative applied research comprising use of suitable additives, coatings, and exploration of composite morphologies as well as appropriate engineered strategies. Both ANL and LBNL use X-ray based techniques to study phase evolution and loss of CE in S-based and S-Se-based electrodes, primarily by the former during lithiation/delithiation while understanding polysulfide formation in sulfur and oligomeric PEO solvent by the latter, respectively. Work from PNNL, U Pitt, and Stanford demonstrates high areal capacity electrodes exceeding 4 mAh/cm². Following loading studies reported this quarter, PNNL performed *in situ* EPR to study reaction pathways mediated by sulfur radical formation. Coating/encapsulation approaches adopted by U Pitt and Stanford comprise flexible sulfur wire (FSW) electrodes coated with LIC by U Pitt, and TiS₂ encapsulation of Li₂S in the latter, both ensuring polysulfide retention at sulfur cathodes. BNL work, on the other hand, has focused on benchmarking of pouch cell testing by optimization of the voltage window and study of additives such as LiI and LiNO₃. *Ab initio* studies at Stanford and U Pitt involve calculation of binding energies, diffusion coefficients, ionic conductivities and reaction pathways determination, augmenting the experimental results. Similarly, AIMD simulations performed at TAMU reveal multiple details regarding electrolyte decomposition reactions and the role of soluble polysulfides on such reactions. Using kinetic Monte Carlo (KMC) simulations, electrode morphology evolution and mesostructured transport interaction studies were also executed. Studies over the last quarter at PNNL suggest that proper control of electrode porosity/thickness is essential for obtaining high-energy Li-S batteries. Porosity shows strong dependence on calendaring pressure because of low tap densities of electrode components such as sulfur and carbon. Increasing the calendaring-pressure from 0.2 to 1.5 ton (T) leads to rapid decrease of electrode porosity, resulting in improvement of electrode volumetric energy density. Measured electrode volumetric energy density increased from 650 Wh L⁻¹ for as-cast electrode (120- μ m thick)

to 1300 Wh L⁻¹ for electrode compressed to 60 μm. Additionally, Pennsylvania State University has shown use of dimethyl disulfide as a functional co-solvent, demonstrating its ability to show an alternate electrochemical reaction pathway for sulfur cathodes by formation of dimethyl polysulfides and lithium organosulfides as intermediates and reduction products. Further, University of Wisconsin has conducted high-performance liquid chromatography (HPLC)-MS studies and has determined the distribution of polysulfides at various discharge and recharge reactions. UT Austin, at the same time, has shown that by integrating polysulfide-filter-coated separators fabricated with CNF, the cells retain 50% of the initial capacity after storing for one year and exhibit a low self-discharge rate of only 0.14% per day.

Each of these projects has a collaborative team of experts with the required skill set needed to address the EV Everywhere Grand Challenge of 350 Wh/kg and 750 Wh/l and cycle life of at least 1000 cycles.

Highlights. This Task reports the following project highlights for this quarter:

- Researchers at U Pitt (Kumta) have identified a new sulfonic Complex Framework Material (CFM) that demonstrated high sulfur loading and maintained a capacity of 1051 mAh/g for over 100 cycles with 0.0011% fade at 0.2C rate.
- Work at ANL (Khalil Amine) has shown stabilization of the electrode/electrolyte interface by tuning the interactions between polysulfides/polyselenides and solvents by using advanced electrolytes.
- Using polysulfide-filter-coated separators fabricated with CNF, researchers at UT Austin (Manthiram) achieved a high sulfur loading of 11.5 mg cm⁻² and a high sulfur content of 72 wt%, including the mass of everything in the cathode region. The corresponding cells also realize a low electrolyte/sulfur (E/S) ratio of 7.5, compared to the E/S ratios of often > 20 or unknown in the literature, while still maintaining excellent cycle stability.
- Researchers working on cell design optimization at BNL (Hong Gan) have found that the sulfur loading and LiNO₃ concentration strongly impact the cell cycle life and CE, suggesting the involvement of anode SEI.

Task 8.1 – New Lamination and Doping Concepts for Enhanced Lithium–Sulfur Battery Performance (Prashant N. Kumta, University of Pittsburgh)

Project Objective. The project objective is to successfully demonstrate generation of novel sulfur cathodes for Li-S batteries meeting targeted gravimetric energy densities ≥ 350 Wh/kg and ≥ 750 Wh/l with a cost target of \$125/kWh and cycle life of at least 1000 cycles for meeting the EV Everywhere Grand Challenge blueprint. The proposed approach will yield sulfur cathodes with specific capacity ≥ 1400 mAh/g, at ≥ 2.2 V, generating ~ 460 Wh/kg energy density higher than the target. Full cells meeting required deliverables will also be made.

Project Impact. Identifying new laminated S-cathode-based systems displaying higher gravimetric and volumetric energy densities than conventional Li-ion batteries will likely result in new commercial battery systems that are more robust, capable of delivering better energy and power densities, and more lightweight than current Li-ion battery packs. Strategies and configurations based on new LIC-coated sulfur cathodes will also lead to more compact battery designs for the same energy and power density specifications as current Li-ion systems. Commercialization of these new S-cathode-based Li-ion battery packs will represent, fundamentally, a major hallmark contribution of the DOE VTO and battery community.

Out-Year Goals. This multi-year project comprises three phases to be successfully completed in three years:

- Phase 1 (year 1) – Synthesis, characterization, and scale up of suitable LIC matrix materials and multilayer composite sulfur cathodes. (Complete)
- Phase 2 (year 2) – Development of LIC-coated sulfur nanoparticles, scale up of high-capacity engineered LIC-coated multilayer composite electrodes, and doping strategies to improve electronic conductivity of sulfur.
- Phase 3 (year 3) – Advanced high-energy-density, high-rate, extremely cyclable cell development.

Collaborations. The project collaborates with the following members: Dr. Spandan Maiti (U Pitt) for mechanical stability and multi-scale modeling; Dr. A. Manivannan (NETL) for XPS for surface characterization; and Dr. D. Krishnan Achary (U Pitt) for solid-state MAS-NMR characterization.

Milestones

1. Application of ceramic filler incorporated CPEs to improve the specific capacity of commercial Sulfur to ~ 812 mAh/g for over 100 cycling. (Q1 – Completed October 2016)
2. Engineering of high-capacity LIC-coated sulfur nanoparticle. (Q2 – Completed January 2017)
3. Synthesis of VACNT and LIC-coated composite materials. (Q3 – Completed April 2017)
4. Optimize doping composition and thickness to maximize capacity, rate capability, and cycling stability. (In progress)
5. Cost analysis of the LIC-coated electrodes, electrolytes, separators, binders, and related processes and prismatic/pouch-type full cell assembly of I.E. with optimum thickness. (In progress)

Progress Report

Phase 2 concluded with improvement in the ionic conductivity of LIC by doping, altering the electronic structure of sulfur by doping with like-sized dopants and identifying effective methods for coating LIC onto sulfur cathodes. In Phase 1, commercial separator was replaced with an LIC that demonstrated complete prevention of polysulfide dissolution. The principle aims of Phase 3 are as follows: (1) generation of new integrated doped nanoparticulate based sulfur-VACNT-LIC composite electrode, (2) cost analysis of the various cell components, and (3) fabrication of 4 mAh pouch cell.

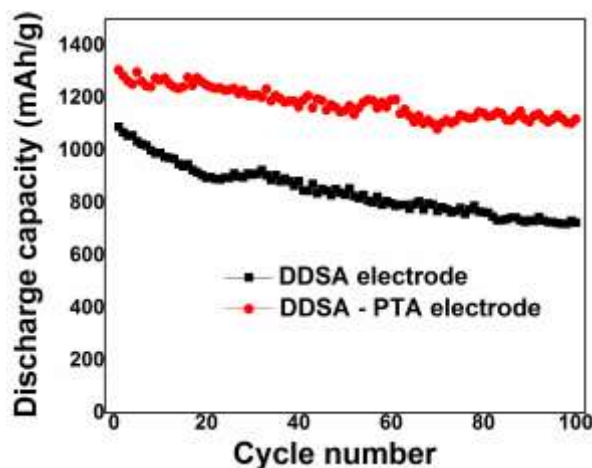


Figure 89. Electrochemical cycling performance of polysulfide trapping agent (PTA)-coated directly doped sulfur architecture electrodes.

Earlier, the project developed directly doped sulfur architecture (DDSA) electrode with very high sulfur loadings of $\sim 18 \text{ mg/cm}^2$ and developing novel polysulfide trapping agent (PTA)-coated DDSA electrodes with polysulfide trapping property. This quarter involved demonstration of extended electrochemical cycling of the PTA-coated DDSA electrode (Figure 89) with an initial capacity of 1305 mAh/g that stabilized at 1112 mAh/g for over 100 cycles with less than 0.0014% when cycled at 0.2C rate. The project also involved the design, synthesis and electrochemical characterization (Figure 90a-b) of new sulfonic CFM that demonstrated high sulfur loading and maintained a capacity of 1051 mAh/g for over 100 cycles with 0.0011% fade at 0.2C rate. A detailed study directed at understanding the mechanisms leading to superior electrochemical performance of

the sulfonic CFM is being conducted. The results will be reported.

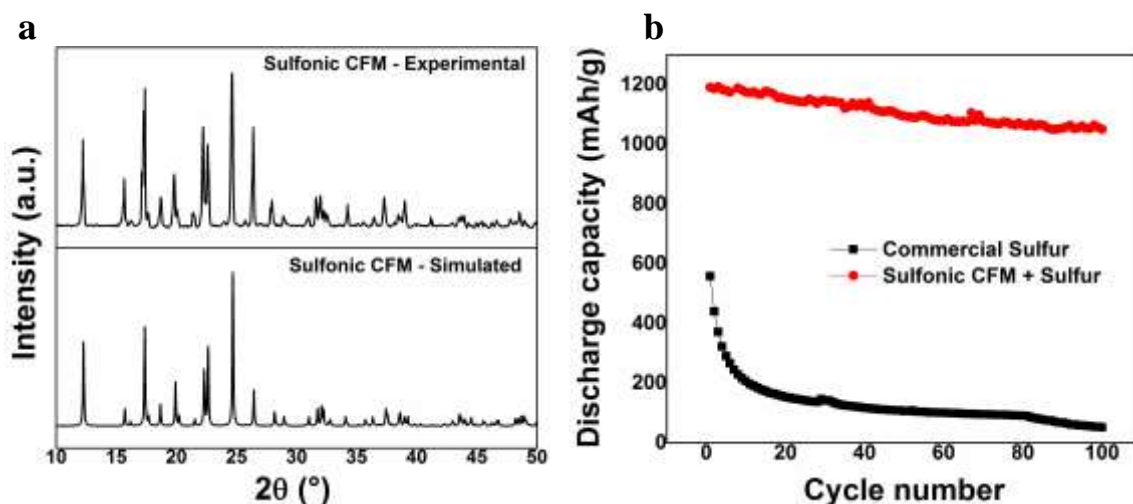


Figure 90. (a) Comparison of experimental and simulated X-ray diffraction patterns of sulfonic complex framework material (CFM). (b) Electrochemical cycling performance of the sulfonic CFM compared with commercial sulfur.

Patents/Publications/Presentations

Patent

- Jampani, P. H., and B. Gattu, P. M. Shanthi, and P. N. Kumta. Novel Electro-Spun Sulfur Wires for Fabricating Mattes of Lithium-Sulfur Batteries. International Patent Number: WO 2016/145429 A1, U.S. Provisional Patent, Application Number: PCT/US2016/022283 (Filing date: 03/14/2016).
- Shanthi, P. M, and P. H. Jampani, B. Gattu, M. K. Datta, V. Oleg, and P. N. Kumta. Electrospinning of PVdF-HFP: Novel Composite Polymer Electrolytes (CPEs) with Enhanced Ionic Conductivities for Lithium-Sulfur Batteries. U.S. Provisional Application. Serial Number 62/529,638.
- Jampani, P. H., and P. M. Shanthi, B. Gattu, M. K. Datta, V. Oleg, and P. N. Kumta. High Capacity, Air-Stable, Structurally Isomorphous Lithium Alloy (SIA), Multilayer Porous Foams (MPFs) and CMAs for Dendrite-Free Lithium Metal Anodes for Li-Ion Batteries. U.S. Provisional Patent Application Number 62/529,588.

Publications

- Jampani, P. H., and B. Gattu, P. M. Shanthi, S. S. Damle, Z. Basson, R. Bandi, M. K. Datta, S. K. Park, and P. N. Kumta. “Flexible Sulfur Wires (Flex-SWs) – A Versatile Platform for Lithium-Sulfur Batteries.” *Electrochimica Acta* 212 (2016): 286–293.
- Shanthi, P. M., and P. H. Jampani, B. Gattu, M. Sweeney, M. K. Datta, and P. N. Kumta. “Nanoporous Non-Carbonized Metal Organic Frameworks (MOFs): Effective Sulfur Hosts for High Performance Li–S Batteries.” *Electrochimica Acta* 229 (2017): 208–218.
- Shanthi, P. M., and P. H. Jampani, B. Gattu, T. Albuquerque, M. K. Datta, and P. N. Kumta. “Novel Electrospun PVdF – HFP Composite Polymer Electrolytes (CPEs) with Enhanced Ionic Conductivities for Lithium – Sulfur Batteries.” 2017. Under review.
- Shanthi, P. M., and P. H. Jampani, B. Gattu, M. K. Datta, V. Oleg, and P. N. Kumta. “The Effect of Mg, Ca and F Doping on the Ionic Conductivity of Li_4SiO_4 : Experimental and First Principle Investigation.” 2017. Under review.

Task 8.2 – Simulations and X-Ray Spectroscopy of Lithium–Sulfur Chemistry (Nitash Balsara, Lawrence Berkeley National Laboratory)

Project Objective. Li-S cells are attractive targets for energy storage applications, as their theoretical specific energy of 2600 Wh/kg is much greater than the theoretical specific energy of current Li-ion batteries. Unfortunately, the cycle-life of Li-S cells is limited due to migration of species generated at the sulfur cathode. These species, collectively known as polysulfides, can transform spontaneously, depending on the environment, and it has thus proven difficult to determine the nature of redox reactions that occur at the sulfur electrode. The project objective is to use XAS to track species formation and consumption during charge-discharge reactions in a Li-S cell. Molecular simulations will be used to obtain X-ray spectroscopy signatures of different polysulfide species, and to determine reaction pathways and diffusion in the sulfur cathode. The long-term objective is to use mechanistic information to build high specific energy lithium-sulfur cells.

Project Impact. Enabling rechargeable Li-S cells has potential to change the landscape of rechargeable batteries for large-scale applications beyond personal electronics due to: (1) high specific energy, (2) simplicity and low cost of cathode (the most expensive component of Li-ion batteries), and (3) earth abundance of sulfur. The proposed diagnostic approach also has significant potential impact, as it represents a new path for determining the species that form during charge-discharge reactions in a battery electrode.

Out-Year Goals. The out-year goals are as follows:

- **Year 1.** Simulations of sulfur and PSL in oligomeric PEO solvent. Prediction of X-ray spectroscopy signatures of PSL/PEO mixtures. Measurement of X-ray spectroscopy signatures of PSL/PEO mixtures.
- **Year 2.** Use comparisons between theory and experiment to refine simulation parameters. Determine speciation in PSL/PEO mixtures without resorting to *ad hoc* assumptions.
- **Year 3.** Build an all-solid lithium-sulfur cell that enables measurement of X-ray spectra *in situ*. Conduct simulations of reduction of sulfur cathode.
- **Year 4.** Use comparisons between theory and experiment to determine the mechanism of sulfur reduction and Li₂S oxidation in all-solid Li-S cell. Use this information to build Li-S cells with improved life-time.

Collaborations. This project collaborates with Tsu-Chien Weng, Dimosthenis Sokaras, and Dennis Nordlund at SSRL, SLAC National Accelerator Laboratory in Stanford, California.

Milestones

1. Continue *in situ* XAS and other spectroscopies to determine reaction products as a function of charge/discharge rate. (Q1 – Completed December 1, 2016)
2. Theoretical prediction of polysulfide solution composition based on thermodynamic calculations of polysulfide and disproportionation reaction Gibbs free energy. (Q2 – Completed February 15, 2017)
3. Explore the amount of effort necessary to predict theoretical polysulfide excitation spectra based on time-dependent DFT. (Q3 – Completed June 10, 2017)
4. Perform *in situ* XAS on Li-S cells containing perfluoropolyether electrolytes; determine reaction products in absence of polysulfide dissolution. (Q4, September 15, 2017 – On schedule)

Progress Report

Coupling experimental spectroscopy methods and computational predictions of electronic excited states of lithium polysulfides is important for determining the species that form in a sulfur cathode. The team recently begun to use this approach to study UV-Vis spectra of polysulfides. Theoretical interpretations of these spectra ignore the molecular structure of the solvent. The team found that including explicit solvent molecules significantly affect the calculated spectra of lithiated sulfur compounds, see Figure 91.

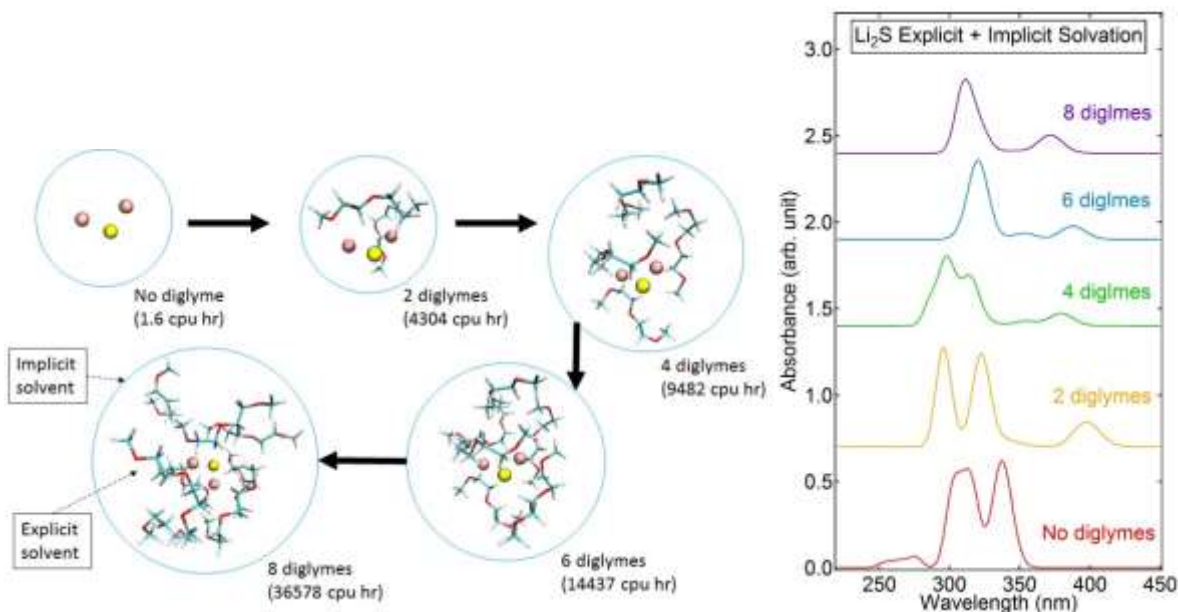


Figure 91. Schematic (left) and spectra (right) for an Li_2S complex with increasing number of diglyme solvent molecules embedded in a continuous implicit solvent medium that represents the bulk properties of diglyme.

The calculations in Figure 91 show the first calculations of optical spectra of Li_2S , a compound that one expects to find in a discharged sulfur cathode complexed with diglyme solvent molecules using DFT. The team systematically increased the number of solvent molecules in the simulations. In Figure 91 it is seen that the spectra calculated with and without diglymes are qualitatively quite different because of interactions between the diglyme molecules and lithium ion, and the effect of these transitions on molecular orbitals. Since adding diglyme molecules increases the size of the system, as well as the computational cost by orders of magnitude, the team is attempting to find the minimum number of solvent molecules needed to achieve numerical convergence of spectra. The team evaluated systems with 2, 4, 6, and 8 diglymes for Li_2S complex, and convergence as seen with 8 diglymes included. The team's work shows the importance of including explicit solvent molecules in excited states spectra calculation. The team plans to continue exploring the steps necessary for reliably computing excitation spectra for lithium polysulfides systems. The team also completed building a cell to measure UV-Vis spectra from sulfur cathodes.

Patents/Publications/Presentations

Presentation

- 231st ECS meeting, New Orleans, Louisiana (May 2017): “Theoretical Uv-Vis Spectral Fingerprints for Li-S Reaction Intermediates in an Ether Based Electrolyte”; D. Wang, T. Pascal, N. Balsara, and D. Prendergast.

Task 8.3 – Novel Chemistry: Lithium Selenium and Selenium Sulfur Couple (Khalil Amine, Argonne National Laboratory)

Project Objective. The project objective is to develop a novel S_xSe_y cathode material for rechargeable lithium batteries with high energy density and long life, as well as low cost and high safety.

Project Impact. Development of a new battery chemistry is promising to support the goal of PHEV and EV applications.

Approach. The dissolution of lithium polysulfides in nonaqueous electrolytes has been the major contribution to the low energy efficiency and short life of Li/S batteries. In addition, the insulating characteristics of both end members during charge/discharge (S and Li_2S) limit their rate capacity. To overcome this problem, sulfur or Li_2S are generally impregnated in a carbon-conducting matrix for better electronic conductivity. However, this makes it difficult to increase the loading density of practical electrodes. It is proposed here to solve the above barriers using the following approaches: (1) partially replace S with Se, (2) nano-confine the S_xSe_y in a nanoporous conductive matrix and (3) explore advanced electrolytes with suppressed shuttle effect.

Out-Year Goals. This new cathode will be optimized with the following goals:

- A cell with nominal voltage of 2 V and energy density of 600 Wh/kg.
- A battery capable of operating for 500 cycles with low capacity fade.

Collaborations. This project engages in collaboration with the following: Professor Chunsheng Wang of University of Maryland, Dr. Yang Ren and Dr. Chengjun Sun of APS at ANL, and Dr. Luis Estevez at PNNL.

Milestones

1. Investigating the impact of fluorinated solvents for Se-S systems. (Q1 – Completed December 2016)
2. Investigating the effect of the pore volume of carbon matrix on high-loading Se-S systems. (Q1 – Complete)
3. Investigating the effect of the pore size and specific surface area of carbon matrix on high-loading Se-S systems. (Q2 – Complete)
4. Development of Se-S/carbon composites with high loading and high performance. (Q3 – Complete)
5. Exploration of novel electrolytes for high-loading Se-S systems. (Q4 – In progress)

Progress Report

In the last two quarters, the team has studied pore size and pore volume effects on the electrochemistry of high loading selenium-sulfur systems. It has found that high pore volume is essential for obtaining high specific capacity and stable cycle performance; however, it is not necessary for pore size to be small (2-10 nm) when using advanced electrolytes.

This quarter, given the high pore volume of HPC1 (6.053 cc/g), the team further prepared a S/HPC1-85% composite with an ultrahigh sulfur loading of 85 wt% through melt-diffusion strategy. Figure 92 shows its cycle performance in DOL/ANL-1 electrolytes at 840 mA/g within a voltage range of 1.0-3.0 V. The cell still maintains a reversible capacity of over 600 mAh/g after 100 cycles of charge/discharge, demonstrating good cycle performance even with such high sulfur loading. CE was measured to be 93% for the first cycle, and then was maintained at around 100% after subsequent cycling; this indicated a suppression of the shuttle effect.

The shuttle effect of Li-S and Li-Se batteries comes from parasitic reactions between polysulfides or polyselenides and lithium anode, and would thus lead to capacity degradation. To gain insight into parasitic reactions of S/HPC1-85%, the team further used a home-built, high-precision source meter system to measure the leakage current, which can be used as a quantitative indicator for the reaction rate of the side reactions (that is, shuttle effect in Li-S and Li-Se batteries). After formation for 2 cycles, the cells were charged to different potential (2.15-2.45 V) and held for 20 h to get the static leakage current. As clearly shown in Figure 93, compared to the case in DOL/DME, the S/HPC1-85% with DOL/ANL-1 shows much lower leakage current.

Although the host material has a pore size of 40 nm, it can still present stable cycle life, good CE, and suppressed shuttle effect, even with 85 wt% sulfur loading. This good performance is attributed to the stable electrode/electrolyte interface. From this understanding, the difference between DME and ANL-1 would be their solvation ability with polysulfides. Therefore, the team further performed DFT calculation on the solvation energies between soluble polysulfides and DME or ANL-1. As shown in Table 3, the solvation energies of Li_2S_4 , Li_2S_6 and Li_2S_8 with ANL-1 are all lower than that in DME. This indicates that polysulfides would have less interaction with ANL-1, leading to less solubility and further improved cycle performance.

Table 3. Density functional theory calculation for solvation energy of polysulfides in DME and ANL-1.

			
	-1607.97 a.u.	-2404.37 a.u.	-3200.74 a.u.
Solvent	ΔG_{solv} KJ mol ⁻¹	ΔG_{solv} KJ mol ⁻¹	ΔG_{solv} KJ mol ⁻¹
DME	-71.22	-73.14	-85.91
ANL-1	-68.32	-69.92	-81.89

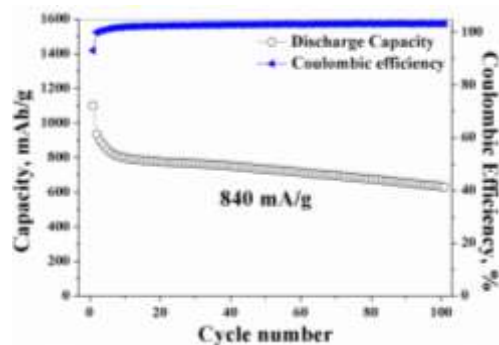


Figure 92. Cycle performance of S/HPC composite with 85 wt% sulfur loading.

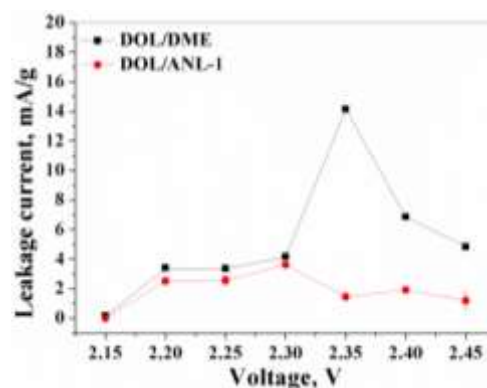


Figure 93. High-precision leakage current measurement on S/HPC cathode in DOL/DME and DOL/ANL-1 electrolytes.

In summary, by using advanced electrolytes, the team can stabilize the electrode/electrolyte interface by tuning the interactions between polysulfides/polyselenides and solvents. This finding provides new opportunities to develop high-performance Li-Se and Li-S batteries using host materials with large pore size but higher pore volume, which has been considered as less effective previously compared to meso-pore (2-10 nm) and micro-pore (< 2nm). Further exploration of novel electrolytes for Li-S and Li-Se batteries to achieve longer cycle life will continue.

Patents/Publications/Presentations

Publication

- Xu, Gui-Liang, and Hui Sun, Luis Estevez, Tianyuan Ma, Jianzhao Liu, Yang Ren, Cheng-Jun Sun, Xiaoyi Zhang, Yuzi Liu, Steve M. Heald, Zonghai Chen, and Khalil Amine. “Tuning the Electrode/Electrolyte Interface for High-Performance Space-Confined Selenium-Sulfur Cathodes of Lithium Batteries.” To be submitted in August 2017.

Task 8.4 – Multi-Functional Cathode Additives for Lithium–Sulfur Battery Technology (Hong Gan, Brookhaven National Laboratory; and Co-PI Esther Takeuchi, Brookhaven National Laboratory and Stony Brook University)

Project Objective. Develop a low-cost battery technology for PEV application utilizing Li-S electrochemical system by incorporating multi-functional cathode additives (MFCA), consistent with the long-term goals of the DOE EV Everywhere Grand Challenge.

Project Impact. The Li-S battery system has gained significant interest due to its low material cost potential (35% cathode cost reduction over Li-ion) and its attractive 2.8x (volumetric) to 6.4x (gravimetric) higher theoretical energy density compared to conventional Li-ion benchmark systems. Commercialization of this technology requires overcoming several technical challenges. This effort will focus on improving cathode energy density, power capability, and cycling stability by introducing MFCA. The primary deliverable is to identify and characterize the best MFCA for Li-S cell technology development.

Approach. TM sulfides are evaluated as cathode additives in sulfur cathode due to their high electronic conductivity. Electrochemically active additives are also selected for this investigation to further improve energy density of the sulfur cell system. In the first year, the project established individual baseline sulfur and TM sulfide coin cell performances and demonstrated strong interactions between sulfur and various MFCA within the hybrid electrode. During the second year, the project identified TiS_2 as the best MFCA candidate and demonstrated the particle size/BET surface area effect on Li-S cell electrochemical performance. In addition, sulfur electrode binder and carbon additives were optimized to achieve high sulfur loading up to 10 mg/cm^2 with good mechanical integrity. This year, the project targets to achieve optimized Li-S cell electrochemical performance by incorporating TiS_2 additive into the cathode formulation with new binder and new carbon additive. Electrode preparation process conditions and cell design factors will also be examined. The cell activation and cycling conditions will be defined, and 4 mAh sample cells will be built for DOE evaluation.

Out-Year Goals. This is a multi-year project comprised of two major phases to be completed in three years. Phase 1 was successfully completed during year 2, with selection of TiS_2 as the leading MFCA. Entering Phase 2, the project has completed binder and carbon selection. In the third year, tasks include cathode formulation optimization, process optimization, cell design optimization, cell activation, and testing optimization. At the end, the project will build 4 mAh sample cells for DOE testing. The mechanistic studies of MFCA and sulfur interaction will continue throughout the year to advance fundamental understanding of the system.

Collaborations. This project collaborates with Dong Su, Xiao Tong, and Yu-chen Karen Chen-Wiegart at BNL and with Amy Marschilok and Kenneth Takeuchi at SBU.

Milestones

1. Cathode formulation and process optimization with TiS_2 . (Q1 – Completed December 2017)
2. Cathode loading/density effect and power optimization. (Q2 – Completed March 2017)
3. Cell design and cell activation procedure development. (Q3 – Completed June 2017)
4. 4 mAh cell samples preparation and confirmation study. (Q4 – Initiated July 2017)

Progress Report

The team has completed the cathode optimization studies by defining the cathode chemical composition/formulation with TiS_2 additive, the cathode preparation process, and achievement of the high sulfur loading (up to 10 mg/cm^2 sulfur) with understanding of the cathode density-electrochemical performance correlation. This quarter, the focus was on the cell design optimization, including electrolyte-cathode interaction study and cell activation study, targeting to achieve $> 4 \text{ mAh}$ 2032 coin cells with good cycling.

Electrolyte-Cathode Interaction. The cathode density-performance relationship uncovered in the last quarter indicates the potential important role of electrolyte. Figure 94 shows the relationship between electrolyte to cathode weight ratio (E/C ratio) and the sulfur utilization under discharge current density ranging from 0.1 mA/cm^2 to 4.0 mA/cm^2 for cathodes with sulfur loading from 2.5 mg/cm^2 to 11.0 mg/cm^2 . With the team's 2032 coin cell design, the stable sulfur utilization can be achieved at all discharge rates when E/C ratio is ≥ 6.5 . Besides E/C ratio, electrolyte location also plays an important role. Although consistent with some literature report, the E/C ratio value is most likely cell-design dependent. The team also noticed that the cell cycle life and CE are strongly impacted by the sulfur loading and LiNO_3 concentration (Figure 95), suggesting the involvement of anode SEI. More detailed studies are in progress to understand the material interaction at the system level.

Cell Activation Study. Due to the non-conductive nature of sulfur active material, sulfur is not fully utilized during the cell cycling. The cell activation or “formation cycle” may pre-condition and redistribute the sulfur active material within the electrode conductive matrix that could improve the sulfur utilization in the subsequent cell cycles. Pre-cycling the Li-S coin cells at low discharge rate at RT and 50C was carried out, with and without initial discharge control. The influence of test temperature on cell initial sulfur utilization is shown in Figure 96 for cells with cathodes of $\sim 5.3 \text{ mg/cm}^2$ sulfur loading. Higher sulfur utilization is realized at 50C (80-85%) versus RT (62-64%). Interestingly, the cells activated at 50C with initial discharge-control resulted in higher sulfur utilization during the subsequent cycling at RT (Figure 97, +25% at cycle 40). These preliminary results indicate the possibility of achieving better sulfur utilization during cell cycling by simply modifying the cell activation conditions. More detailed material study is needed to understand the mechanism behind this observation.

This quarter, the team studied several critical cell design parameters. By incorporating the design controls, the viability of making 2032 coin cells that deliver $> 4 \text{ mAh}$ during cell cycling was demonstrated, meeting the Go/No-Go criteria.

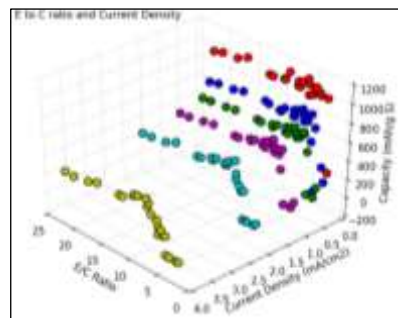


Figure 94. E/C ratio effect on Li-S cell power.

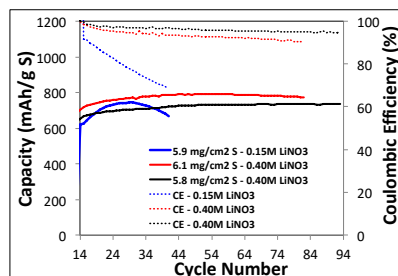


Figure 95. Effect of LiNO_3 concentration.

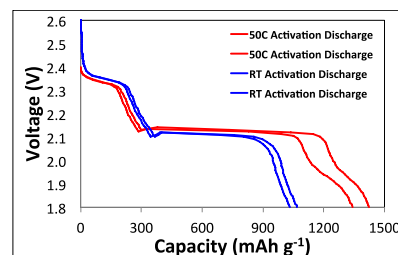


Figure 96. Temperature versus sulfur utilization.

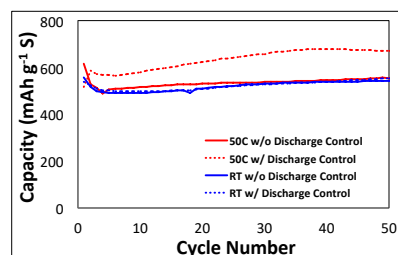


Figure 97. Li-S cell cycling after activation.

Patents/Publications/Presentations

Publication

- Sun, Ke, and Qing Zhang, David C. Bock, Xiao Tong, Dong Su, Amy C. Marschilok, Kenneth J. Takeuchi, Esther S. Takeuchi, and Hong Gan. “Interaction of TiS_2 and Sulfur in Li-S Battery System.” *J. Electrochem. Soc.* 164, no. 6 (2017): A1–A7.

Presentations

- MRS Spring Meeting, Phoenix, Arizona (April 17–21, 2017): “In Operando Synchrotron Multi-Modal Investigation for Structural and Chemical Evolution of Metal Sulfide Additives in Li-S Battery”; Ke Sun, Chonghang Zhao, Garth Williams, Jianming Bai, Eric Dooryhee, Juergen Thieme, Yu-chen Karen Chen-Wiegart, and Hong Gan.
- DOE Annual Merit Review, Washington D. C. (June 8, 2017): “Multifunctional Cathode Additives for Li-S Battery Technology”; Hong Gan, Ke Sun, Hellen Liu, Jian Huang, Avi Matarasso, Esther Takeuchi, Amy Marschilok, Kenneth Takeuchi, Christina A. Cama, Qing Zhang, David C. Bock, Rachel A. DeMayo, Dong Su, Sooyeon Hwang, Xiao Tong, Karen Chen-Wiegart, Chong Hang Zhao, Eric Dooryhee, Jianming Bai, Juergen Thieme, Simon Billinge, Maxwell Wesley Terban, and Xian Yang. Poster.

Task 8.5 – Development of High-Energy Lithium–Sulfur Batteries (Jun Liu and Dongping Lu, Pacific Northwest National Laboratory)

Project Objective. The project objective is to develop high-energy, low-cost Li-S batteries with long lifespan. All proposed work will employ thick sulfur cathode ($\geq 2 \text{ mAh/cm}^2$ of sulfur) at a relevant scale for practical applications. The diffusion process of soluble polysulfide out of thick cathode will be revisited to investigate cell failure mechanism at different cycling. Alternative anode will be explored to address the lithium anode issue. The fundamental reaction mechanism of polysulfide under the electrical field will be explored by applying advanced characterization techniques to accelerate development of Li-S battery technology.

Project Impact. The theoretical specific energy of Li-S batteries is $\sim 2300 \text{ Wh/kg}$, which is almost three times higher than that of state-of-the-art Li-ion batteries. The major challenge for Li-S batteries is polysulfide shuttle reactions, which initiate a series of chain reactions that significantly shorten battery life. The proposed work will design novel approaches to enable Li-S battery technology and accelerate market acceptance of long-range EVs required by the EV Everywhere Grand Challenge.

Out-Year Goals. This project has the following out-year goals:

- Fabricate Li-S pouch cells with thick electrodes to understand sulfur chemistry/electrochemistry in the environments similar to real application.
- Leverage the Li-metal protection project funded by the DOE and PNNL advanced characterization facilities to accelerate development of Li-S battery technology.
- Develop Li-S batteries with a specific energy of 400 Wh/kg at cell level, 1000 deep-discharge cycles, improved abuse tolerance, and less than 20% capacity fade over a 10-year period to accelerate commercialization of electrical vehicles.

Collaborations. This project engages in collaboration with the following:

- Dr. Xiao-Qing Yang (LBNL) – *In situ* characterization
- Dr. Deyang Qu (University of Wisconsin at Milwaukee) – Electrolyte analysis
- Dr. Xingcheng Xiao (GM) – Materials testing
- Dr. Jim De Yoreo (PNNL) – *In situ* characterization

Milestones

1. Study thick sulfur electrode ($\geq 4 \text{ mg/cm}^2$) with controlled porosity/thickness; demonstrate 80% capacity retention for 200 cycles. (Q1 – Completed December 31, 2016)
2. Investigate electrolyte and additive degradation mechanism with thick sulfur electrode. (Q2 – Completed March 31, 2017)
3. Identify approaches to minimize quick capacity drop and efficiency fluctuation occurring in thick sulfur electrode during initial cycles. (Q3 – Completed June 30, 2017)
4. Complete pouch cell assembly and testing by using optimized high energy cathode and electrolyte/additives. (Q4, September 30, 2017 – Initiated April 1, 2017)

Progress Report

Degradation mechanism of electrolyte additive LiNO_3 in sulfur cathode was studied in the last quarter by using *in situ* and *ex situ* techniques. It was found that chemical reactions between LiNO_3 and reductive lithium sulfide or polysulfide occur in sulfur cathodes and lead to accelerated LiNO_3 depletion. As a result, fast CE decay is usually observed in early cycling period (for example, first 5-10 cycles) of Li-S batteries, particularly when high mass loading sulfur cathodes are employed.

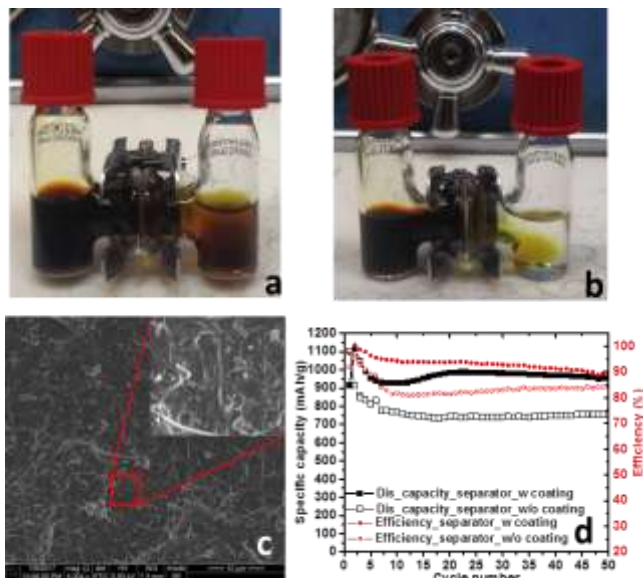


Figure 98. Visual comparison of polysulfide diffusion in H-cell using Celgard 2400 separator with (a) and without (b) cross-linked polyacrylic acid (C-PAA) coating for 1 h rest, (c) scanning electron microscopy image of C-PAA/carbon nanofiber (CNF)-coated separator, and (d) cycling capacity and Coulombic efficiency of Li-S cells using separator with and without C-PAA coating.

DME) and benchmark electrolyte (1M LiTFSI/DOL/DME) are separated by a Celgard 2400 separator with or without C-PAA coating. Polysulfide can easily cross pristine separator and migrate to the opposite chamber driven by concentration difference (Figure 98a), which, however, can be suppressed significantly when using a C-PAA coated separator (Figure 98b). In addition, CNF was introduced during the cross-linking of PAA, which provides reaction sites to reuse the blocked polysulfide on the separator. Figure 98c shows SEM image of the single-side coated separator, where cross-linked PAA and CNF form a relatively dense and electronic conductive coating layer. Effectiveness of the C-PAA coated separator on cell performance was verified in high loading sulfur cathodes (ca. 4 mg/cm^2). Using uncoated separator, the cell discharge capacity drops quickly from 1100 mAh/g to 810 mAh/g in first 5 cycles, accompanied by decreasing efficiency from 92% to 89% (Figure 98d). For the cell with C-PAA coated separator, the first cycle discharge capacity and efficiency are 915 mAh/g and 97%, respectively, which are maintained as high as 950 mAh/g and 96.4%, respectively, after 5 cycles, suggesting effectively suppressed polysulfide crossover. For long-term cycling stability of high-energy Li-S cells, multiple functional groups will be introduced onto each side of the separator to further inhibit polysulfide shuttle and stabilize lithium anode interface, respectively.

This quarter, the team investigated key factors causing early stage quick capacity decay in high loading sulfur cathodes by focusing on (1) polysulfide diffusion and methods to suppress it, (2) electrode structural stability upon repeated conversion of sulfur and lithium sulfide, and (3) electrolyte decomposition and passivation on conductive carbon components in cathodes. New understandings from this research provide a useful guideline for rational design of high-loading sulfur cathodes. Polysulfide dissolution and redistribution throughout Li-S cell is one of the main reasons for early stage capacity loss when excess electrolyte is used. To address this problem, the team designed a cross-linked polyacrylic acid (C-PAA) coated separator to inhibit free polysulfide diffusion. Blocking effect of C-PAA for polysulfide crossover was investigated with H-type cell (see Figure 98), where high concentration polysulfide contained solution ($0.15\text{M Li}_2\text{S}_6$ in 1M LiTFSI/DOL/

Patents/Publications/Presentations

Presentation

- BLI-X, IBM, Almaden, California (June 27 – 29, 2017): “Development of High Energy Sulfur Cathode for Lithium-Sulfur Batteries”; D. Lu, J. Xie, Q. Li, Y. Wang, S. Wilson, J.-G. Zhang, and J. Liu.

Task 8.6 – Nanostructured Design of Sulfur Cathodes for High-Energy Lithium-Sulfur Batteries (Yi Cui, Stanford University)

Project Objective. The charge capacity limitations of conventional TM oxide cathodes are overcome by designing optimized nano-architected sulfur cathodes. This study aims to enable sulfur cathodes with high capacity and long cycle life by developing sulfur cathodes from the perspective of nanostructured materials design, which will be used to combine with Li-metal anodes to generate high-energy Li-S batteries. Novel sulfur nanostructures as well as multi-functional coatings will be designed and fabricated to overcome issues related to volume expansion, polysulfide dissolution, and the insulating nature of sulfur.

Project Impact. The capacity and the cycling stability of sulfur cathode will be dramatically increased. This project's success will make Li-S batteries to power EVs and decrease the high cost of batteries.

Out-Year Goals. The cycle life, capacity retention, and capacity loading of sulfur cathodes will be greatly improved (200 cycles with 80% capacity retention, > 0.3 mAh/cm² capacity loading) by optimizing material design, synthesis, and electrode assembly.

Collaborations. This project engages in collaboration with the following:

- BMR PIs,
- SLAC: *In situ* X-ray, Dr. Michael Toney, and
- Stanford: Professor Nix, mechanics; and Professor Bao, materials.

Milestones

1. Investigate the Li-ion diffusion mechanism in different types of metal sulfides. (Q1 – Completed October 2016)
2. Identify the initial activation energy barrier of Li₂S on various metal sulfides. (Q1 – Completed December 2016)
3. Demonstrate the catalytic effect of Li₂S_x species on metal sulfides, enabling good performance of Li-S batteries. (Q3 – Completed April 2017)
4. Establish a standard procedure to quantitatively compare the polysulfide adsorption capability of candidate materials. (Q4 – Completed July 2017)

Progress Report

Last quarter, the team investigated the catalytic effect of Li_2S_x species on metal sulfides, and the results indicate that the addition of CoS_2 , VS_2 , and TiS_2 significantly improve the electrochemical performance of Li-S batteries. In this report, the team further establishes a standard procedure to quantitatively compare the polysulfide adsorption capability of various candidate materials.

Figure 99 presents data for the setup where 0.5 m^2 surface area of candidate materials is added to 3mM of Li_2S_6 in 4mL of 1,3-dioxolane/1,2-dimethoxyethane solution (DOL/DME, 1:1 by volume) for 3 hours. Li_2S_6 is a representative soluble long-chain polysulfide species and is prepared by chemically reacting sulfur with Li_2S in DOL/DME solution, which is a common electrolyte system for Li-S batteries. As Figure 99a illustrates, varying degrees of color change can be observed, which is attributed to interactions between candidate materials and polysulfide species. No observable color fading is associated with carbon black, suggesting weak physical adsorption. Other materials such as MoS_2 and TiO_2 demonstrate higher adsorption capability compared to carbon black, while CoS and TiN exhibit relatively low adsorption capability as indicated by the lack of significant color fading. In contrast, the polysulfide solutions become much lighter in color after the addition of V_2O_5 , MnO_2 , V_2O_3 , TiS_2 , and FeS , suggesting strong interactions between Li_2S_6 and these materials. However, the judgment of color shades is subjective to human eyes and is also hindered by the powder color of the candidate materials. Therefore, upon completion of the adsorption tests, 2 mL of the supernatant solutions are extracted from each sample to minimize the impact of powders, and UV-Vis is performed on these supernatant solutions for detailed examination.

Figure 99b illustrates the UV-Vis performance in the visible spectrum of varying concentrations of Li_2S_6 without addition of any candidate materials. There is strong absorbance toward the blue end of the visible spectrum, as blue is the complementary color of yellow. Unsurprisingly, higher concentrations of Li_2S_6 corresponds to darker shades of yellow and stronger absorbance around the blue spectrum. Figure 99c shows the performance of carbon black and the metal oxides adsorption test supernatant solutions. The results are in good agreement with previous visual inspections.

Carbon black demonstrates much higher blue spectrum absorbance corresponding to a higher concentration of Li_2S_6 remaining and thus weak polysulfide adsorption capability. In comparison to Figure 99b, it can be seen that very little Li_2S_6 is adsorbed by carbon black with 3 mM being the original concentration in each adsorption test sample. In contrast, V_2O_5 , MnO_2 , and V_2O_3 all illustrate much higher adsorption capability showing very low concentrations of Li_2S_6 remaining in the supernatant solutions. Ti_4O_7 , TiO_2 , SiO_2 , and Al_2O_3 exhibit moderate polysulfide adsorption capabilities. Similarly, Figure 99d

shows the performance of the metal nitride and metal sulfides. TiS_2 , FeS , and MoS_2 exhibit great polysulfide adsorption capabilities, CoS displays poor capability, and Cu_2S , CuS , TiN , and ZnS exhibit moderate capabilities. In Figure 99c-d, CoS and carbon black display background absorbance throughout the entire spectrum; this is likely due to the scattering effect of the sample powders, which do not settle well, as evident in Figure 99a, and are present in the supernatant solutions.

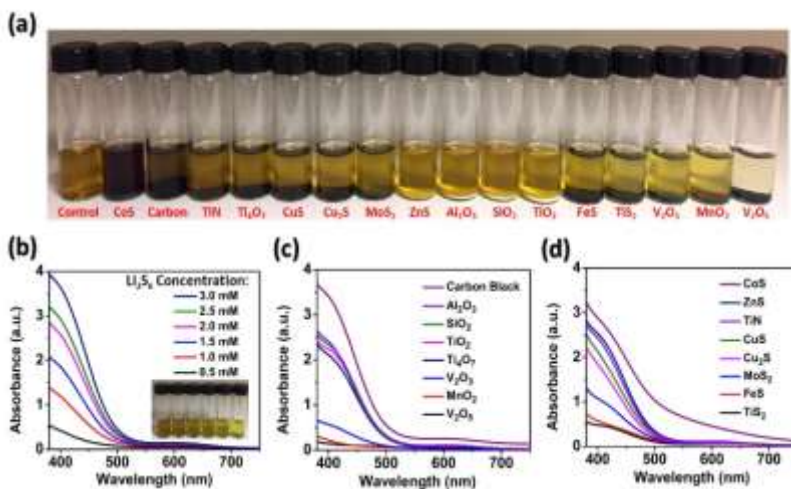


Figure 99. Li_2S_6 polysulfide adsorption test. (a) Photograph of setup. (b) UV-Vis data of varying concentrations of Li_2S_6 in DOL/DME solution without candidate materials. (c-d) With candidate materials added in 3 mM Li_2S_6 .

Task 8.7 – Addressing Internal “Shuttle” Effect: Electrolyte Design and Cathode Morphology Evolution in Lithium-Sulfur Batteries (Perla Balbuena, Texas A&M University)

Project Objective. The project objective is to overcome the Li-metal anode deterioration issues through advanced Li-anode protection/stabilization strategies including (1) *in situ* chemical formation of a protective passivation layer and (2) alleviation of the “aggressiveness” of the environment at the anode by minimizing the polysulfide shuttle with advanced cathode structure design.

Project Impact. Through formulation of alternative electrolyte chemistries as well as design, fabrication, and test of improved cathode architectures, it is expected that this project will deliver Li/S cells operating for 500 cycles at efficiency greater than 80%.

Approach. A mesoscale model including different realizations of electrode mesoporous structures generated based on a stochastic reconstruction method will allow virtual screening of the cathode microstructural features and the corresponding effects on electronic/ionic conductivity and morphological evolution. Interfacial reactions at the anode due to the presence of polysulfide species will be characterized with *ab initio* methods. For the cathode interfacial reactions, data and detailed structural and energetic information obtained from atomistic-level studies will be used in a mesoscopic-level analysis. A novel sonochemical fabrication method is expected to generate controlled cathode mesoporous structures that will be tested along with new electrolyte formulations based on the knowledge gained from the mesoscale and atomistic modeling efforts.

Out-Year Goals. By determining reasons for successes or failures of specific electrolyte chemistries, and assessing relative effects of composite cathode microstructure and internal shuttle chemistry versus that of electrolyte chemistry on cell performance, expected results are as follows: (1) develop an improved understanding of the Li/S chemistry and ways to control it, (2) develop electrolyte formulations able to stabilize the lithium anode, (3) develop new composite cathode microstructures with enhanced cathode performance, and (4) develop a Li/S cell operating for 500 cycles at an efficiency greater than 80%.

Collaborations. This is a collaborative work combining first-principles modeling (Perla Balbuena, TAMU), mesoscopic level modeling (Partha Mukherjee, TAMU), and synthesis, fabrication, and test of Li/S materials and cells (Vilas Pol, Purdue University). Balbuena also collaborates with M. Vijayakumar from PNNL.

Milestones

1. Complete electrochemical modeling of cell performance with electrolyte and cathode properties. (Completed December 2016)
2. Complete development of stable electrolytes. (Complete)
3. Produce 3-5 grams of C/S composite material. (Complete)
4. Complete scale-up of cathode composites, cell construction, and testing. (In progress)

Progress Report

New Cathode Synthesis. Pressurized “autogenic” synthesis routes, studied by Co-PI Vilas Pol at Purdue University, have produced homogeneous carbon-sulfur (C-S) composites with high sulfur content up to 74 wt%; the real sulfur content is controlled by optimization of the precursor ratio. Material characterization of these composites suggests pristine orthorhombic S_8 is transformed into amorphous sulfur species during the autogenic process. It is hypothesized that high sulfur content is enabled by homogeneous penetration of sulfur vapor into the porous carbon substrate, followed by homogeneous deposition as amorphous sulfur species. The synthesis scheme of the autogenically-derived carbon sulfur composite (with 40 wt% sulfur loading) and the electrochemical rate cycling results are shown in Figure 100. The performance of a conventional sample derived via ball milling is shown for comparison. When cycled at various cycling rates, the autogenically-derived C-S composite shows consistent capacity around 1100 Ah kg^{-1} between rates C/20 to 1C. After cycling at a slow rate of C/20, however, the capacity drops to ca. 700 Ah kg^{-1} . In comparison, the ball milled composite shows much lower capacity ca. 300 Ah kg^{-1} at 1C, higher capacity at C/20 rate, then a rapid drop in capacity to ca. 0 Ah kg^{-1} when returning to 1C rate. When analyzing the CE, the autogenic composite demonstrates better uniform efficiency across all rates near unity (ca. 100%) in comparison to the ball milled composite, which shows low efficiencies down ca. 20% at a fast 1 C rate.

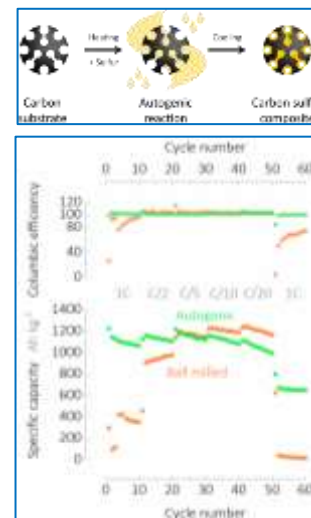


Figure 100. Synthesis scheme and electrochemical tests of C/S composite.

Analysis of Electrochemical Reduction of C/S Composites. The team developed a new model for studying the structure and electrochemical lithiation of the C/S composite. This model allows intimate mixing between sulfur and carbon by randomly dispersing graphene sheets up to 22 carbon atoms and 8-membered sulfur rings at 47 wt% sulfur and an approximate density of 1.67 g/cm^3 . Molecular dynamics simulations using a reactive force field carried out at 300 K and 1 atm revealed opening of most of the sulfur rings along with the formation of S-C bonds between sulfur chains of various lengths and the carbon atoms at the edges of the graphene sheets. Thus, the presence of discontinuous graphene sheets instead of continuous graphene layers allows a more realistic approach, as the low-coordinated carbon atoms at the edges of these graphene sheets favor C-S bond formation. Upon electrochemical lithiation, the team observed a quasi-linear volumetric expansion behavior upon lithium insertion, with an approximated total expansion of 65% at the end of lithiation. Experimental reports show a volumetric expansion up to 80% for lithiated sulfur structures, but the presence of carbon limits the expansion. The team also observed that graphene sheets tend to agglomerate into graphitic clusters due to van der Waals interactions between sheets, with most of the short-chain polysulfide species agglomerating around the edges. Thus, the team will obtain a detailed description of the Li_2S and Li_2S_2 precipitation, which is critical for the Li/S battery and is also discussed below based on mesoscopic simulations. In addition, the new model developed provides information on dissolution of the long-chain polysulfide species and is potentially useful to follow the shuttle effect at the molecular level.

Precipitation-Microstructure Interaction in Li/S Cathodes. Based on microstructure-scale simulations, effective property relations (for example, tortuosity) are developed and used to identify cathode resistances. If precipitation takes place in the form of film deposits, the electrode-electrolyte interface gets covered earlier and the cell shuts down due to predominant surface passivation. Alternatively, if precipitation occurs in a finger-like fashion, pore blockage is much more severe and causes cathode starvation. For intermediate morphologies, cathode resistance evolution has joint contributions from both. As cathode pristine porosity changes, it leads to different pore blockages. As precipitate morphology becomes more finger-like, cell performance improves in response to decreased surface passivation. On the other hand, at higher initial sulfur loading, increasing cathode porosity improves discharge capacity.

Patents/Publications/Presentations

Publications

- Nandasiri, M. J., and L. E. Camacho-Forero, A. M. Schwarz, V. Sutthanandan, S. Thevuthasan, P. B. Balbuena, K. T. Mueller, and M. Vijayakumar. “*In Situ* Chemical Imaging of SEI Layer Evolution in Li-S Batteries Using X-ray Photoelectron Spectroscopy.” *Chem. Mater.* 29, no. 11 (2017): 4728–4737.
- Liu, Z., and P. Balbuena, and P. P. Mukherjee. “Mesoscale Evaluation of Titanium Silicide Monolayer as a Cathode Host Material in Lithium-Sulfur Batteries.” *J. Minerals, Metals, and Materials Society*, in press. doi: 10.1007/s11837-017-2414-7.
- Chen, C.-F., and A. Mistry, and P. P. Mukherjee. “Correlating Impedance and Microstructure Evolution in Lithium-Sulfur Battery Cathodes.” Under review.
- Kamphaus, Ethan P., and Perla B. Balbuena. “First Principles Investigation of Lithium Polysulfide Structure and Behavior in Solution.” *J. Phys. Chem. C*. Under review.
- Liu, Zhixiao, and Perla B. Balbuena, and Partha P. Mukherjee. “Hole Polaron Diffusion in the Final Discharge Product of Lithium-Sulfur Batteries.” *J. Phys. Chem. C*. Submitted.
- Mistry, Aashutosh, and Partha P. Mukherjee. “Precipitation – Microstructure Interaction in Li-S Battery Cathode.” *J. Phys. Chem. Lett.* Under review.
- Liu, Zhixiao, and Aashutosh Mistry, and Partha P. Mukherjee. “Mesoscale Physicochemical Interactions in Lithium-Sulfur Batteries: Progress and Perspective.” *J. Electrochem. Energy Conv. Storage*. Under review.

Task 8.8 – Investigation of Sulfur Reaction Mechanisms (Deyang Qu, University of Wisconsin Milwaukee; Xiao-Qing Yang, Brookhaven National Laboratory)

Project Objective. With the advantages of the unique analytical assay developed in 2016, the primary objectives are to further conduct focused fundamental research on the mechanism for Li-S batteries, investigate the kinetics for the sulfur redox reaction, develop electrolytes and additives suitable for Li-S chemistry, and optimize the sulfur electrode and cell designs. In these objectives, special attention will be paid to investigation of the redox reaction of sulfur cathode, management for the solubility of polysulfide ions, formation of SEI layer and dead lithium on the surface of lithium anode, rechargeability of lithium anode in the solution containing polysulfide, and exploration of electrode and cell designs. Through such investigations, the Li-S chemistry will be studied systematically, and scientific understanding of the reaction mechanism can be well utilized to guide system engineering design.

Project Impact. The unique *in situ* electrochemical HPLC/MS technique will identify the soluble polysulfides real-time during the charge/discharge of a Li-S battery; thus, the mechanism can be revealed in detail. The project results will guide development of sulfur cathode and Li-S designs.

Approach. This project will use *in situ* electrochemical-MS, electrochemical-HPLC/MS, XPS, SEM, and XRD to study electrochemical reactions associated with sulfur electrodes. Electrochemical techniques such as AC impedance, rotation ring disk electrode, and galvanostat will be used to study the electrode process kinetics. The project is developing an *in situ* electrochemical optical method to investigate the surface of lithium anode during cycling of a Li-S cell.

Out-Year Goals. The out-year goal is to establish tools to investigate the interaction between dissolved sulfur and polysulfide ions with lithium anode, exploring the additives that can migrate such interaction. In addition, gain further understanding of the chemical behaviors of the polysulfide in the electrolyte and propose a valid mechanism for the Li-S reaction.

Collaborations. The PI, Deyang Qu, is the Johnson Control Endowed Chair Professor; thus, the University of Wisconsin at Milwaukee and BNL team have close collaboration with Johnson Controls' scientists and engineers. This collaboration enables the team to validate the outcomes of fundamental research in pilot-scale cells. This team has been closely working with top scientists on new material synthesis at ANL, LBNL, and PNNL, with U.S. industrial collaborators at GM, Duracell, and Johnson Control as well as international collaborators in Japan and South Korea. These collaborations will be strengthened and expanded to give this project a vision on both today's state-of-the-art technology and tomorrow's technology in development, with feedback from the material designer and synthesizers upstream, and from industrial end users downstream.

Milestones

1. Complete design and validation of the *in situ* electrochemical – microscopic cell for *in situ* investigation of lithium anode during cycling. (Q1 – Completed December 31, 2016)
2. Complete study of interaction between dissolved elemental sulfur and polysulfide ions with both the electrolytes and lithium anode. (Q2 – Completed March 31, 2017)
3. Complete investigation of chemical equilibriums among dissolved polysulfide ions during the course of discharge and recharge of Li-S batteries. (Q3 – Completed June 30, 2017)
4. Complete the preliminary engineering design and test for the rechargeable Li-S battery including electrode design and cell design. (Q4)

Progress Report

The team continued to utilize the unique HPLC-MS electrochemical technique to investigate the mechanism of sulfur redox reaction along with a traditional electrochemical method to investigate the electrochemical catalytic reaction of polysulfides on carbon electrodes.

To reduce the shuttle effect induced by the dissolved polysulfide ions, confining sulfur within various hosts, mostly conducting carbon-based materials, is regarded as one of the most efficient approaches to improve overall performance of Li-S batteries. Various carbon structures have been utilized as the cathodic matrix for sulfur. Generally, the nonpolar carbons are considered as incapable of immobilizing sulfur and its as-reduced products, owing to weak C-S interaction. Introducing defects or heteroatoms can effectively promote the chemical interaction with sulfur, suppress the shuttle effect, and synchronously accelerate the reaction kinetics.

The team adopted well-defined nanostructured substrate containing different planes (basal plane, step plane, and edge plane) on highly oriented pyrolytic graphite (HOPG) as model electrodes, and demonstrates the effect of defects on sulfur redox reactions. For the first time, the team's results directly indicate that electrochemical reduction and oxidation of sulfur are significantly affected by the carbon surface structure; namely, the electrochemical reversibility of sulfur redox reaction is much better on edge plane, compared with basal plane and step plane. This feature probably arises from higher affinities of sulfur and its as-reduced products to defect sites, which are abundant on the edge surface.

Two HOPG cylinders (separately denoted as HOPG-1 and HOPG-2) were adopted here, as shown in Figure 101a. Figure 101b schematically shows the corresponding structures, which were confirmed by XRD. Figure 102a shows the comparison of *iR*-free cyclic voltammetry (CV) curves for HOPG-1T, HOPG-1L, HOPG-2T and HOPG-2L. The CVs for the two edge planes (HOPG-1L and HOPG-2T) are similar, and both considerably differ from the basal plane (HOPG-1T) and step plane (HOPG-2L). Since the CVs of different surfaces (top surface and lateral surface) on the same electrode are quite different, it is obvious that this phenomenon should not result from the difference of the conductivity along and perpendicular to the graphite basal plane. The team adopted the reduction and oxidation peak potentials as an indicator of electrochemical reversibility. A clear correlation

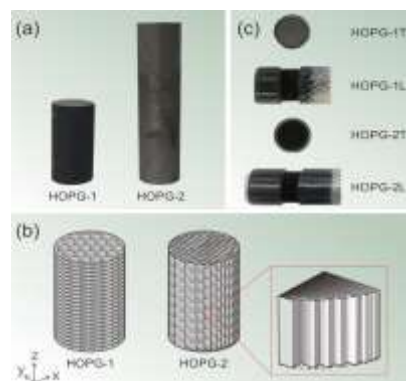


Figure 101. (a) Photograph of the two highly oriented pyrolytic graphite (HOPG) cylinders adopted in this paper. (b) Schematic illustration of the corresponding structures of HOPG-1 and HOPG-2. (c) Photographs of the geometrical configurations of the resulting working electrodes.

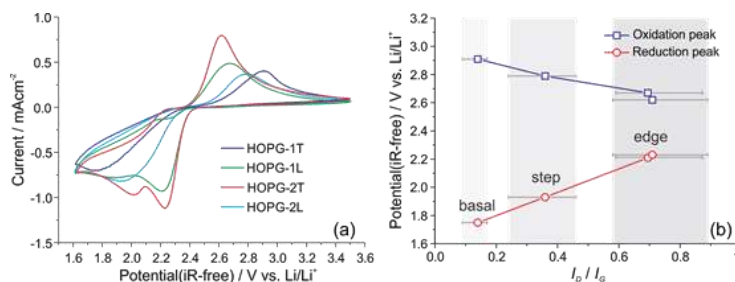


Figure 102. (a) *R*-free CVs of sulfur electrochemical reduction and oxidation on highly oriented pyrolytic graphite (HOPG)-1T (basal plane), HOPG-1L (edge plane), HOPG-2T (edge plane), and HOPG-2L (step plane) at a scan rate of 20 mV/s. (b) The relation between peak potential obtained from (a) and *I_D*/*I_O* obtained from Raman analysis.

between the reduction and oxidation peak potentials and *I_D*/*I_O* values extracted from Raman analysis was observed (Figure 102b). The reduction peak potential gradually increased and the oxidation potential simultaneously decreased with increasing the defect density. The sulfur redox reaction on the edge plane, which contains the highest defect density, exhibits a superior electrochemical reversibility compared to reactions on the step plane and the basal plane. Hence, the defect sites exhibit better electrocatalytic activity toward sulfur reduction and oxidation.

Patents/Publications/Presentations

Publication

- Wang, Gongwei, and Dong Zheng, Xiao-Qing Yang, and Deyang Qu. “Sulfur Redox Reactions on Highly Oriented Pyrolytic Graphite (HOPG) Electrodes: Direct Evidence for Superior Electrocatalytic Performance on Defect Sites.” *Carbon* 119 (2017): 460–463.

Task 8.9 – Statically and Dynamically Stable Lithium–Sulfur Batteries (Arumugam Manthiram, University of Texas – Austin)

Project Objective. The project objective is to develop statically and dynamically stable Li-S batteries by integrating polysulfide-filter-coated separators with a protected Li-metal anode through additives or a modified Li_2S cathode with little or no charge barrier during first charge. The project includes demonstration of electrochemically stable cells with sulfur capacities of $> 1,000 \text{ mA h g}^{-1}$ and cycle life in excess of 500 cycles (dynamic stability) along with positive storage properties (static stability) at $> 70 \text{ wt\%}$ sulfur content and $\sim 5 \text{ mg cm}^{-2}$ loading.

Project Impact. The combination of polysulfide-filter (PS-filter)-coated separator, Li-metal-protection additives, and Li_2S cathode modifications offers a viable approach to overcome the persistent problems of Li-S batteries. This project is systematically integrating the basic science understanding gained in its laboratory of these three aspects to develop the Li-S technology as the next-generation power source for EVs. The project targets demonstrating cells with sulfur capacities of over $1,000 \text{ mA h g}^{-1}$ and cycle life in excess of 500 cycles along with good storage properties at high sulfur content and loading that will make the Li-S technology superior to the present-day Li-ion technology in terms of cost and cell performance.

Approach. Electrochemical stability of the Li-S cells is improved by three complementary approaches. The first approach focuses on establishment of an electrochemically stable cathode environment by employing PS-filter-coated separators. The PS-filter coatings aim to suppress the severe polysulfide diffusion and improve the redox capability of Li-S cells with high-sulfur loadings. The study includes an understanding of materials characteristics, fabrication parameters, electrochemical properties, and battery performance of the PS-filter-coated separators. The second approach focuses on electrode engineering from two aspects. First, investigation of a Li-metal anode with coating- and additive-supporting approaches is aimed at improving the safety of Li-S cells. Second, research on activated- Li_2S cathode with little or no charge-barrier will promote performance and safety of the C- Li_2S cells. (3) Integration of the first two approaches would create statically and dynamically stable Li-S batteries for EVs.

Out-Year Goals. The overall goal is to develop statically and dynamically stable Li-S batteries with custom cathode and stabilized anode active materials. In addition to developing a high-performance battery system, a fundamental understanding of the structure-configuration-performance relationships will be established. Specifically, the optimization of the electrochemical and engineering parameters of PS-filter-coated separators aims at comprehensively investigating different coating materials and their corresponding coating techniques for realizing various high-performance custom separators. The developed PS-filter-coated separators can be coupled with pure sulfur cathodes with high-sulfur loading and content. Multi-functional PS-filter-coated separators, high-loading sulfur cathodes, stabilized-Li-metal anodes, activated- Li_2S cathodes, and novel cell design are anticipated to provide an in-depth understanding of the Li-S battery chemistry and to realize statically and dynamically stable Li-S batteries.

Collaborations. This project collaborates with ORNL.

Milestones

1. Analyze and improve dynamic electrochemical performances of Li-S cells. (Q1 – Completed December 2016)
2. Analyze and improve static electrochemical performances of Li-S cells. (Q2 – Completed March 2017)
3. Increase the sulfur loading of the cells. (Q3 – Completed June 2017)
4. Go/No-Go: Fabricate cells with high sulfur content/loading and good electrochemical stability. (Q4 – September 2017; In progress)

Progress Report

It is becoming increasingly clear that the Li-S battery chemistry and the electrochemical performances are distinctly different between low-loading sulfur cathodes ($< 4.0 \text{ mg cm}^{-2}$) and practically-relevant high-loading cathodes ($> 5.0 \text{ mg cm}^{-2}$). Accordingly, the team focused this quarter on improving electrochemical characteristics of high-loading sulfur cathodes by employing (i) PS-filter-coated separators and (ii) advanced cathode architectures. The team surpassed the target values of 5.0 mg cm^{-2} and 70 wt% sulfur that were set up to make the Li-S technology practically viable. The team has realized sulfur loading as high as 30 mg cm^{-2} and sulfur content up to 80 wt%.

Specifically, the team focused on PS-filter-coated separators fabricated with CNF using a layer-by-layer (LBL) coating method. The LBL CNF-coated separators enable the Li-S cells to achieve a high sulfur loading of 11.5 mg cm^{-2} and a high sulfur content of 72 wt%, including the mass of everything in the cathode region. The corresponding cells also realize a low electrolyte/sulfur (E/S) ratio of 7.5, compared to the E/S ratios of often > 20 or unknown in the literature, while still maintaining excellent cycle stability. Figure 103 shows that peak discharge capacities of the cells fabricated with the LBL CNF coatings #1 and #2 are 940 and $1,002 \text{ mA h g}^{-1}$. In consideration of their high sulfur loading and content, the areal capacities and energy densities attained are, respectively, $\sim 11 \text{ mA h cm}^{-2}$ and $\sim 23 \text{ mW h cm}^{-2}$. The cells exhibit high capacity-retention rates of 94% for 100 cycles. This high electrochemical utilization and stability imply that the LBL CNF coating enables the high-loading sulfur cathodes to have the energy densities higher than the commercial Li-ion batteries.

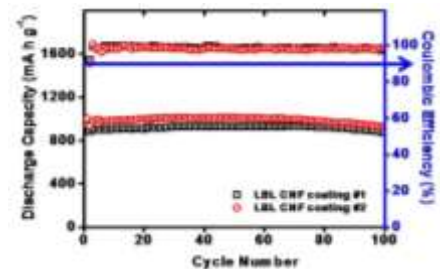


Figure 103. Cycling performance of the cells fabricated with LBL CNF-coated separators.

With the fulfillment of this quarter's milestones, the team is moving forward to design even better high-loading sulfur cathodes. Figure 104 shows high-loading cathodes (i) with pure sulfur powders in a shell-shaped carbon electrode as a core-shell (CS) cathode (Figure 104a) or (ii) with polysulfide catholytes in a cotton-carbon electrode as a cotton-carbon cathode (Figure 104b). Both cells exhibit good cyclability even with sulfur loadings reaching up to 30 mg cm^{-2} and sulfur contents up to 80 wt%, which are higher than the target values of 5 mg cm^{-2} and 70 wt%. The core-shell cathodes also exhibit good rate capability with high capacities from C/20 to C/2 rates (Figure 104a), and the cotton-carbon cathodes display high capacities of 900 and $1,172 \text{ mA h g}^{-1}$ at, respectively, C/5 and C/10 rates (Figure 104b). In addition, the E/S ratio is only 6.8 in the case of cotton-carbon cathode, which is much lower than the values generally used in the literature.

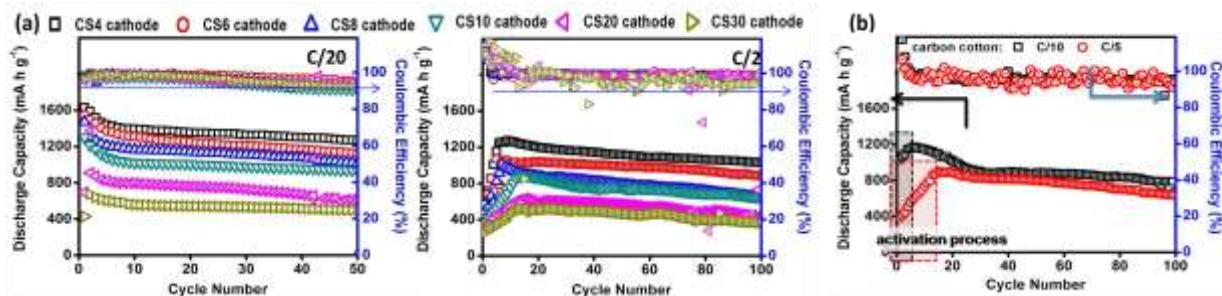


Figure 104. Cycling performance of the cells fabricated with (a) core-shell cathodes (sulfur loading of $4.0 - 30.0 \text{ mg cm}^{-2}$) and (b) cotton-carbon cathodes (sulfur loading of 30 mg cm^{-2}). The numbers in the legends CS4, CS6, ... CS30 in (a) refer to the sulfur loadings in mg cm^{-2} .

Patents/Publications/Presentations

Publications

- Chung, S.-H., and P. Han, C.-H. Chang, and A. Manthiram. “A Shell-Shaped Carbon Architecture with High-Loading Capability for Lithium Sulfide Cathodes.” *Advanced Energy Materials*. doi: 10.1002/aenm.201700537.
- Chung, S.-H. and A. Manthiram. “Lithium–Sulfur Batteries with the Lowest Self-Discharge and the Longest Shelf life.” *ACS Energy Letters* 2 (2017): 1056.
- Chung, S.-H., and P. Han, and A. Manthiram. “Quantitative Analysis of Electrochemical and Electrode Stability with Low Self-Discharge Lithium-Sulfur Batteries.” *ACS Applied Material & Interfaces* 9 (2017): 20318.

Presentations

- MRS Spring Meeting, Phoenix, Arizona (April 17 – 21, 2017): “Dynamically and Statically Stable Metal-sulfur Batteries with High Sulfur Loading”; A. Manthiram. Invited.
- 231st ECS Meeting, New Orleans, Louisiana (May 28 – June 1, 2017): “Lithium-Sulfur Batteries with an Ultrahigh-Sulfur-Loading Carbon-Cotton Cathode”; S.-H. Chung, C.-H. Chang, and A. Manthiram.
- DOE Annual Merit Review, Washington, D. C. (June 5 – 9, 2017): “Dynamically and Statically Stable Lithium-Sulfur Batteries”; A. Manthiram. Invited.
- International Conference on Materials for Advanced Technologies (ICMAT), Singapore, (June 18 – 23, 2017): “High Energy Density Lithium-Sulfur Batteries with High Sulfur Loading”; A. Manthiram. Invited keynote talk.

Task 8.10 – Electrochemically Responsive, Self-Formed, Lithium-Ion Conductors for High-Performance Lithium-Metal Anodes (Donghai Wang, Pennsylvania State University)

Project Objective. The project objective is to develop and deliver an electrochemically responsive self-formed hybrid Li-ion conductor as a protective layer for Li-metal anodes, enabling Li-metal anodes to cycle with a high efficiency of ~ 99.7% at high electrode capacity ($> 6 \text{ mAh/cm}^2$) and high current density ($> 2 \text{ mA/cm}^2$) for over 500 cycles. The project will also demonstrate prototype ~300 mAh Li-S battery cells with energy densities of ~200 Wh/kg and ~ 80% capacity retention for ~ 300 cycles at ~ 80% depth of discharge using Li-metal anodes with this protective layer.

Project Impact. This project aims to develop a new hybrid Li-ion conductor that enables safe and high-performance Li-metal anodes. The use of these high-performance Li-metal anodes in turn enables Li-S batteries with high energy density and long cycling life. Such anodes can also lead to a 50% increase in the energy density of conventional Li-ion batteries with Li-metal oxide cathodes. Meeting the technical targets will potentially develop a new high-energy-density lithium battery, promote increased adoption of EVs and PHEVs, and reduce petroleum consumption in the transportation sector by helping battery-powered vehicles become accepted by consumers as a reliable source of transportation.

Approach. The novel multiphase organo- Li_xS_y or organo- $\text{Li}_x\text{P}_y\text{S}_z$ hybrid ion conductors with tunable multi-functional organic components and controlled Li_xS_y and $\text{Li}_x\text{P}_y\text{S}_z$ inorganic components will be designed and prepared, and thus enable safe use of lithium metal with high CE. In the first year, the team will develop the organo- Li_xS_y lithium protection layers with tuned functionality: (1) finding appropriate composition and (2) developing appropriate synthesis and fabrication methods.

Out-Year Goals. Work will progress toward development of organo- Li_xS_y lithium protection layers with tuned functionality. Characterization, performance, and compatibility tests on materials and systems. Twelve baseline 300 mAh pouch cells using standard Li-metal anodes and high-performance carbon-sulfur cathodes will be delivered for independent verification.

Milestones

1. Development of the first-generation of organo- Li_xS_y lithium protection layers with tuned functionality. Conduct characterization and performance tests on the materials. (Q1 – Completed December 2016)
2. Deliver 12 baseline ~ 300 mAh Li-S cells for independent verification. (Q2 – Completed)
3. Optimize organo- Li_xS_y protective layer and demonstrate lithium anodes cycling with ~ 98.5% CE for ~ 200 cycles. (Q3)
4. Demonstrate lithium anodes with optimized organo- Li_xS_y protective layer and ~ 99% CE for ~ 200 cycles. (Q4)

Progress Report

Li-S baseline pouch cells were assembled and tested. The cathode with areal sulfur loading of around 4.2 mg cm^{-2} was made of sulfur, commercial carbon additives, and polyvinylpyrrolidone binder. The weight ratio of sulfur in the cathode is around 50%. 1 M LiTFSI and 0.4 M LiNO_3 in DOL/DME was used as electrolyte here. The electrolyte/sulfur (E/S) ratio is around 10 mL g^{-1} . Being cycled at C/30, the pouch cell shows an areal capacity of $\sim 5 \text{ mA h cm}^{-2}$, and the average CE is around 99% (Figure 105).

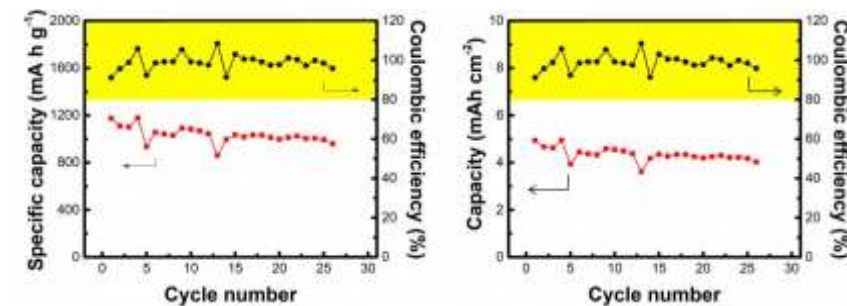


Figure 105. Cycling performance of Li-S pouch cell.

For Li-metal protection, SEI layers formed from electrolyte containing sulfur-containing polymer with 90 wt% sulfur (SCP-90) were characterized. The SEI layers formed from the control electrolyte, the S-Electrolyte and SCP-90-Electrolyte are named C-SEI, S-SEI, SCP-90-SEI, respectively. Morphologically, as shown in the SEM images (Figure 106), the C-SEI layer shows a porous and loose structure, indicating its continual break during the lithium plating/stripping process (Figure 106a). The S-SEI layer becomes smooth, but cracks are still observed (Figure 105b), which should be ascribed to non-continuous $\text{Li}_2\text{S}/\text{Li}_2\text{S}_2$ phase in the S-SEI layer. In contrast, the as-formed SCP-90-SEI layers show a mostly planar, smooth and uniform layer with no cracks (Figure 106c).

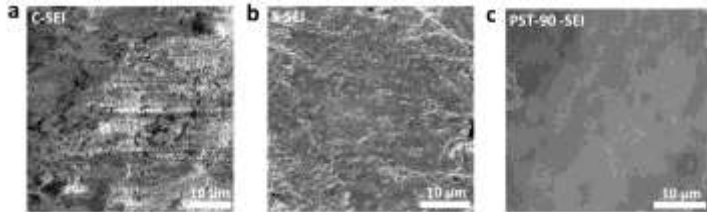


Figure 106. Scanning electron microscopy images of C-SEI layer (a), S-SEI layer (b), and SCP-90-SEI layer (c).

The morphology of SEI layers was further investigated using AFM. Figure 107 displays topographic images of different SEI layers. The C-SEI layer shows large granular features (Figure 107a), while small particulates are observed everywhere on the surface of S-SEI layer and cracks are also observed (Figure 107b). In contrast, the SCP-90-SEI layers are very smooth and uniform covering, as shown in Figure 107c. The 3D topographic features observed from AFM results are consistent with the SEM investigation (Figure 106). Such SEI layers can suppress the growth of lithium dendrites and thus prevent further contact of lithium with the electrolyte, which could lead to an enhanced CE, correspondingly.

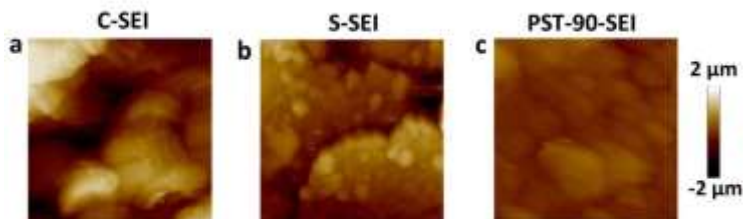


Figure 107. Atomic force microscopy images ($10 \times 10 \mu\text{m}^2$ scan size) of the C-SEI layer (a), S-SEI layer (b), and SCP-90-SEI layer (c).

TASK 9 – LITHIUM–AIR BATTERIES

Summary and Highlights

High-density energy storage systems are critical for EVs required by the EV Everywhere Grand Challenge. Conventional Li-ion batteries still cannot fully satisfy the ever-increasing needs because of their limited energy density, high cost, and safety concerns. As an alternative, the rechargeable lithium-oxygen (Li-O₂) battery has the potential to be used for long-range EVs. The practical energy density of a Li-O₂ battery is expected to be ~ 800 Wh kg⁻¹. The advantages of Li-O₂ batteries come from their open structure; that is, they can absorb the active cathode material (oxygen) from the surrounding environment instead of carrying it within the batteries. However, the open structure of Li-O₂ batteries also leads to several disadvantages. The energy density of Li-O₂ batteries will be much lower if oxygen has to be provided by an onboard container. Although significant progress has been made in recent years on fundamental properties of Li-O₂ batteries, research in this field is still in an early stage, with many barriers to be overcome before practical applications. These barriers include:

- Instability of electrolytes—The superoxide species generated during discharge or O₂ reduction process is highly reactive with electrolyte and other components in the battery. Electrolyte decomposition during charge or O₂ evolution process is also significant due to high over-potentials.
- Instability of air electrode (dominated by carbonaceous materials) and other battery components (such as separators and binders) during charge/discharge processes in an O-rich environment.
- Limited cyclability of the battery associated with instability of the electrolyte and other battery components.
- Low energy efficiency associated with large over-potential and poor cyclability of Li-O₂ batteries.
- Low power rate capability due to electrode blocking by the reaction products.
- Absence of a low-cost, high-efficiency oxygen supply system (such as oxygen selective membrane).

The main goal of this Task is to provide a better understanding on the fundamental reaction mechanisms of Li-O₂ batteries and identify the required components (especially electrolytes and electrodes) for stable operation of Li-O₂ batteries. PNNL researchers will investigate stable electrolytes and oxygen evolution reaction (OER) catalysts to reduce the charging overvoltage of Li-O₂ batteries and improve their cycling stability. New electrolytes will be combined with stable air electrodes to ensure their stability during Li-O₂ reaction. Considering the difficulties in maintaining the stability of conventional liquid electrolyte, the Liox team will explore use of a nonvolatile, inorganic molten salt comprising nitrate anions and operating Li-O₂ cells at elevated temperature (> 80°C). It is expected that these Li-O₂ cells will have a long cycle life, low over potential, and improved robustness under ambient air compared to current Li-air batteries. At ANL, new cathode materials and electrolytes for Li-air batteries will be developed for Li-O₂ batteries with long cycle life, high capacity, and high efficiency. The state-of-the-art characterization techniques and computational methodologies will be used to understand the charge and discharge chemistries. The University of Massachusetts/BNL team will investigate the root causes of the major obstacles of the air cathode in the Li-air batteries. Special attention will be paid to optimization of high-surface carbon material used in the gas diffusion electrode, catalysts, electrolyte, and additives stable in Li-air system and with capability to dissolve lithium oxide and peroxide. Success of this project will establish a solid foundation for further development of Li-O₂ batteries toward their practical applications for long-range EVs. The fundamental understanding and breakthrough in Li-O₂ batteries may also provide insight on improving performance of Li-S batteries and other energy storage systems based on chemical conversion processes.

Highlight. ANL discovered a new approach to determine the composition of the discharge product in Li-O₂ batteries, which is critical for further development of Li-O₂ batteries.

Task 9.1 – Rechargeable Lithium-Air Batteries (Ji-Guang Zhang and Wu Xu, Pacific Northwest National Laboratory)

Project Objective. The project objective is to develop rechargeable Li-O₂ batteries with long-term cycling stability. The FY 2017 objective is to stabilize Li-metal anode in Li-O₂ batteries and to investigate the temperature effect on oxygen reduction reaction (ORR) and OER processes of the Li-O₂ chemistry.

Project Impact. Li-air batteries have a theoretical specific energy that is more than five times that of state-of-the-art Li-ion batteries and are potential candidates for use in next-generation, long-range EVs. Unfortunately, the poor cycling stability and low CE of Li-air batteries have prevented their practical application. This work will explore a new electrolyte and electrode that could lead to long cyclability and high CEs in Li-air batteries that can be used in the next-generation EVs required by the EV Everywhere Grand Challenge.

Out-Year-Goals. The long-term goal of the proposed work is to enable rechargeable Li-air batteries with a specific energy of 800 Wh/kg at cell level, 1000 deep-discharge cycles, improved abuse tolerance, and less than 20% capacity fade over a 10-year period to accelerate commercialization of long-range EVs.

Collaborations. This project collaborates with Chongmin Wang of PNNL on characterization of cycled air electrodes by TEM/SEM and with Jinhui Tao of PNNL on characterization of Li-metal anodes by *in situ* AFM.

Milestones

1. Investigate temperature effect on ORR and OER of Li-O₂ batteries. (Q1 – Completed December 2016)
2. Identify factors that affect stability of Li-metal anode in Li-O₂ batteries. (Q2 – Completed March 2017)
3. Develop surface coating or electrolyte additive to stabilize Li-metal anode and improve cycle life of Li-O₂ battery. (Q4 – In progress; initiated March 2017)

Progress Report

This quarter, an electrolyte additive (lithium difluoro(oxalato)borate, LiDFOB) was investigated to further stabilize Li-metal anode in Li-O₂ batteries. The voltage profiles of Li||Li cells cycled at 0.2 mA cm⁻² based on the 1 M LiTf-Tetraglyme electrolyte with 2 wt% LiDFOB additive and the control electrolyte (1M LiTf-Tetraglyme) are compared in Figure 108a. Much more stable Li-metal plating/stripping is observed with the presence of LiDFOB additive under both areal capacities of 0.1 mAh cm⁻² and 1.0 mAh cm⁻², while a rapid increase in polarization of cells with control electrolyte is indicative of severe corrosion of lithium metal upon cycling. This phenomenon can be attributed to the formation of a robust protective SEI film induced by the LiDFOB additive, thus leading to stabilization of lithium metal and more stable lithium metal plating/stripping processes. To further study the effect of the additive on the cycling of Li-O₂ batteries, the project also tested Li-O₂ cells by using the regular CNTs air-electrodes with the two LiTf-TEGDME electrolytes with and without LiDFOB additive at a current density of 0.1 mA cm⁻². The cycling performance of Li-O₂ cells with (Figure 108b) or without LiDFOB additive (Figure 108c) clearly demonstrates that introduction of LiDFOB is beneficial for enhancement in cycling stability of Li-O₂ batteries.

In addition to the above work, the project also conducted *in situ* one-step optimization of RuO₂/CNTs catalysts for Li-O₂ batteries and achieved great improvement on the cycle life of Li-O₂ battery (Figure 109). The discharge capacity of Li-O₂ cells based on ultra-small RuO₂/CNTs catalysts can be maintained at 1000 mAh g⁻¹ for 190 cycles. Reassembled cell that consists of aforementioned air-electrode after 190 cycles and a new lithium metal is able to continue the stable cycling for an additional 120 cycles at the same capacity of 1000 mAh g⁻¹. However, pristine cells can survive for only 54 cycles. These interesting results reveal that the optimized RuO₂/CNTs nano-catalysts possess not only very efficient catalytic capability, but also extremely high stability; the Li-metal protection is critical for high-energy-density Li-O₂ batteries.

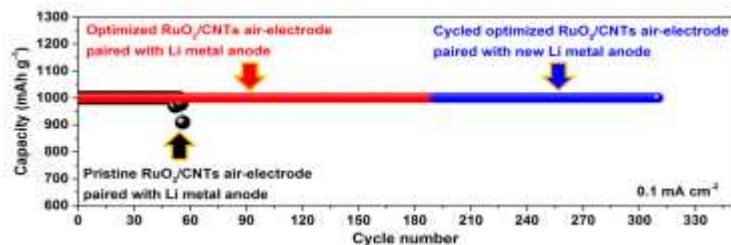


Figure 109. Li-O₂ cells with optimized RuO₂/carbon nanotubes (CNTs) air-electrode and Li-metal anode (after 190 cycles, cells based on above cycled air-electrode and new lithium metal), and pristine RuO₂/CNTs air-electrode and lithium metal, cycled at 0.1 mA cm⁻² in 1 M LiTf-Tetraglyme electrolyte.

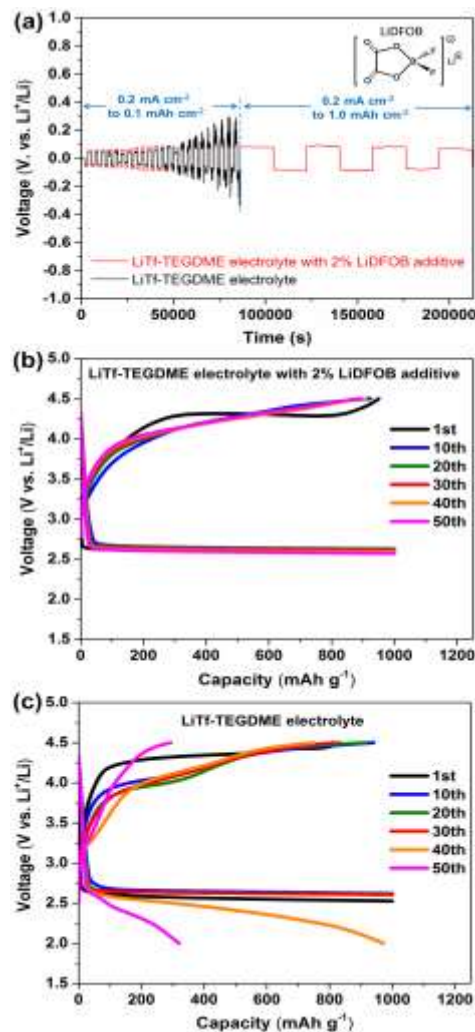


Figure 108. (a) Li-metal plating/stripping from Li||Li cells cycled at 0.2 mA cm⁻² in 1 M LiTf-Tetraglyme electrolytes with and without 2% LiDFOB additive. (b, c) Voltage profiles of Li-O₂ cells cycled at 0.1 mA cm⁻² in 1 M LiTf-TEGDME electrolytes with (b) and without 2% LiDFOB additive (c).

Patents/Publications/Presentations

Publication

- Liu, B., and W. Xu, J. Zheng, P. Yan, E. D. Walter, N. Isern, M. E. Bowden, M. H. Engelhard, S. T. Kim, J. Read, B. D. Adams, X. Li, J. Cho, C. Wang, and J.-G. Zhang. “Temperature Dependence of Oxygen Reduction Mechanism in Nonaqueous Li-O₂ Batteries.” Submitted.

Presentations

- 231st ECS meeting, New Orleans, Louisiana (May 30, 2017): “Stabilization of Lithium Metal in Optimized DMSO-Based Electrolytes for Li-O₂ Batteries”; B. Liu, W. Xu, P. Yan, S. Kim, M. H. Engelhard, X. Sun, D. Mei, J. Cho, C. Wang, and J.-G. Zhang.
- MRS Spring Meeting, Phoenix, Arizona (April 19, 2017): “Enhanced Cycling Stability of Li-O₂ Batteries through *In Situ* Formed Electrode Interface Layers”; B. Liu, W. Xu, P. Yan, J. Zheng, M. H. Engelhard, C. Wang, and J.-G. Zhang.

Task 9.2 – Efficient Rechargeable Li/O₂ Batteries Utilizing Stable Inorganic Molten Salt Electrolytes (Vincent Giordani, Liox)

Project Objective. The project objective is to develop high specific energy, rechargeable Li-air batteries having lower overpotential and improved robustness under ambient air compared to current Li-air batteries.

Project Impact. If successful, this project will solve particularly intractable problems relating to air electrode efficiency, stability, and tolerance to the ambient environment. Furthermore, these solutions may translate into reduced complexity in the design of a Li-air stack and system, which in turn may improve prospects for use of Li-air batteries in EVs. Additionally, the project will provide materials and technical concepts relevant for development of other medium temperature molten salt lithium battery systems of high specific energy, which may also have attractive features for EVs.

Approach. The technical approach involves replacing traditional organic and aqueous electrolytes with a non-volatile, inorganic molten salt comprising nitrate anions and operating the cell at elevated temperature (> 80°C). The research methodology includes powerful *in situ* spectroscopic techniques coupled to electrochemical measurements (for example, electrochemical MS) designed to provide quantitative information about the nature of chemical and electrochemical reactions occurring in the air electrode.

Out-Year-Goals. The long-term goal is to develop Li-air batteries comprising inorganic molten salt electrolytes and protected lithium anodes that demonstrate high (> 500 Wh/kg) specific energy and efficient cyclability in ambient air. By the end of the project, it is anticipated that problems hindering use of both the lithium anode and air electrode will be overcome due to materials advances and strategies enabled within the intermediate (> 80°C) operating temperature range of the system under development.

Collaborations. This project funds work at Liox Power, Inc.; LBNL (Prof. Bryan McCloskey: analysis of air electrode and electrolyte); and California Institute of Technology (Prof. Julia Greer: design of air electrode materials and structures).

Milestones

1. Demonstrate discharge specific energy and energy density ≥ 500 Wh/Kg and ≥ 800 Wh/L, respectively, based on air electrode mass and volume. (Q1 – Completed December 2016)
2. Scale-up downselected cell components for 4 mAh and 10 mAh cells. (Q2 – Completed March 2017)
3. Demonstrate ≥ 10 cycles at $\geq 90\%$ round-trip energy efficiency in laboratory-scale Li-air cells comprising a molten nitrate electrolyte and protected lithium electrode. (Q3 – Completed June 2017)
4. Fabricate and test 4- and 10-mAh cells. (Q4 – Initiated July 2017)

Progress Report

The third-quarter milestone was accomplished. A laboratory-scale Li-air cell comprising a molten nitrate electrolyte and protected lithium electrode has demonstrated ≥ 10 cycles at $\geq 90\%$ round-trip energy efficiency. The cycling performance of 2-electrode lithium cells comprising a solid electrolyte and a molten salt electrolyte contained within the cathode was investigated. The molten salt electrolyte consisted of binary alkali metal nitrate mixture and the solid electrolyte of a LLZO 1 cm² disc of about 400 microns. Cells were operated at 175°C to ensure good solid electrolyte performance and a molten state for nitrate salts. The cathode chemistry consisted of either the classical lithium-oxygen chemistry to form Li₂O₂ as the discharge product, or, the electrochemical reduction of nitrate anions to form Li₂O and nitrite species.

Figure 110 shows the third discharge/charge cycle of protected Li-anode cells using an alkali metal nitrate molten salt catholyte. On the left, the cell uses a porous carbon cathode and is cycled under O₂ gas. A typical discharge plateau (~2.7 V) is observed, consistent with ORR and the formation of solid lithium peroxide within the cathode porous structure (Super P carbon). Relatively high discharge capacity in Li/O₂ cell (1360 mAh/g of carbon, ~6.5 mAh/cm²) was achieved. However, the high temperature seemed to accelerate carbon decomposition in O₂ cell, leading to poor reversibility and cyclability. Post mortem analysis by XRD revealed large quantities of Li₂CO₃ deposited on the cathode surface. On the right plot, the cell uses a porous nickel cathode and is cycled under argon gas. The typical ~2.5 V discharge plateau corresponds to electrochemical reduction of nitrate anion based on the following cathode reaction: $2\text{Li}^+ + 2\text{e}^- + \text{NO}_3^- \rightarrow \text{Li}_2\text{O} + \text{NO}_2^-$. Lithium oxide fills up the cathode porous structure, while nitrite anion dissolves in the melt. The project observed a 45% active material utilization (nitrate anion reduction) with high reversibility; however, the high discharge capacity was maintained for only a few cycles.

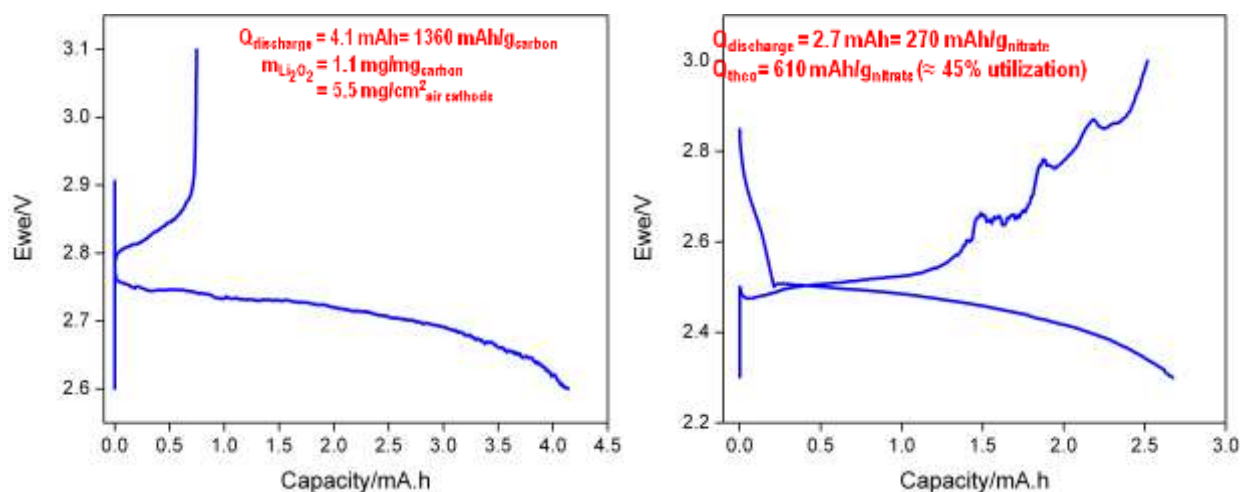


Figure 110. (left) Li/O₂ cell voltage profile at 175°C using Super P Carbon:PTFE (95:5 wt%) cathode at 0.05 mA/cm² current density (m_{carbon} = 3 mg, m_{nitrate} = 6.5 mg). (right) Molten nitrate lithium cell voltage profile at 175°C using nanoporous nickel cathode (Ni:LiNO₃-KNO₃ eutectic 50:50 wt%) at 0.05 mA/cm² current density (m_{Ni} = m_{nitrate} = 10 mg).

Ongoing work will use engineering cell fixtures to study solid electrolytes, as well as fabricate and test 4- and 10-mAh cells.

Task 9.3 – Lithium–Air Batteries (Khalil Amine and Larry A. Curtiss, Argonne National Laboratory)

Project Objective. This project will develop new cathode materials and electrolytes for Li-air batteries for long cycle life, high capacity, and high efficiency. The goal is to obtain critical insight that will provide information on the charge and discharge processes in Li-air batteries to enable new advances to be made in their performance. This will be done using state-of-the-art characterization techniques combined with state-of-the-art computational methodologies to understand and design new materials and electrolytes for Li-air batteries.

Project Impact. The instability of current nonaqueous electrolytes and degradation of cathode materials limits the performance of Li-air batteries. The project impact will be to develop new electrolytes and cathode materials that are stable and can increase cycle life and improve efficiency of Li-air batteries.

Approach. The project is using a joint theoretical/experimental approach for design and discovery of new cathode and electrolyte materials that act synergistically to reduce charge overpotentials and increase cycle life. Synthesis methods, in combination with design principles developed from computations, are used to make new cathode architectures. Computational studies are used to help understand decomposition mechanisms of electrolytes and how to design electrolytes with improved stability. The new cathodes and electrolytes are tested in Li-O₂ cells. Characterization along with theory is used to understand the performance of the materials used in the cell and make improved materials.

Out-Year Goals. The out-year goals are to find catalysts that promote discharge product morphologies that reduce charge potentials and find electrolytes for long cycle life through testing and design.

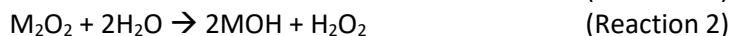
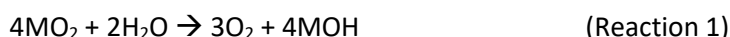
Collaborations. This project engages in collaboration with Professor Kah Chun Lau (University of California at Norridge), Professor Amin Salehi (University of Illinois at Chicago), Professor Yang-Kook Sun (Hanyang University), Professor Yiyang Wu (Ohio State University), and Dr. Dengyun Zhai (China).

Milestones

1. Investigation of new architectures for platinum catalysts using hollow nanocarbon cages. (Q1 – Complete)
2. Development of new characterization techniques for determination of the composition and conductivity of discharge products in Li-O₂ batteries. (Q2 – Complete)
3. Design and synthesis of new catalysts for cathode materials based on metal organic frameworks for low charge overpotentials. (Q3 – Complete)
4. Investigation of uniformly synthesized metal clusters as catalysts and nucleation sites for controlling efficiency of Li-O₂ cells. (Q4 – In progress)

Progress Report

Fundamental understanding of catalysts and electrolytes in Li-oxygen batteries is important for development of advanced energy storage systems with potential for long-range EVs. An important aspect of developing catalysts and electrolytes in this program is determining the composition of the discharge product (that is, whether it is lithium peroxide or a mixture of lithium peroxide and some other lithium oxides such as lithium superoxide). Previously, the project reported a titration technique that depends on the reaction of a Li-O₂ discharge product with a Ti(IV)OSO₄ solution as a diagnostic technique to distinguish between Li₂O₂ and LiO₂ in a discharge product. The method provides an accurate technique to detect the amount of Li₂O₂ present, but does not determine the amount of LiO₂ present. In the present work, the project has extended this method to assess the amount of LiO₂ present to make it a more powerful tool to provide quantitative information on the amounts of both LiO₂ and Li₂O₂ present in the discharge product. The two titration techniques are based on the hydrolysis reactions of LiO₂ and Li₂O₂ given by reactions 1 and 2, respectively.



The postulated mechanism for hydrolysis of LiO₂ derived was derived in this study and is shown in Figure 111. This concerted reaction explains the lack of H₂O₂ as a product that is detected for hydrolysis of Li₂O₂.

To develop a titration technique to determine the amount of the LiO₂ discharge product, the project tested for the expected LiOH product from Reaction 1, which is the reaction of water with LiO₂. This was done by pH measurement of a solution after addition of a known quantity of H₂O to a cathode after one discharge cycle in a Li-O₂ cell with an Ir-rGO cathode under the same conditions as described for the titration based on Ti(IV)OSO₄ solution described last quarter. The resulting solution was strongly basic with a pH of 11.84, consistent with the presence of OH⁻ anion from LiOH. In addition, by analysis of the current used and the discharge time, it is possible to determine quantitatively the amount of OH⁻ anion produced. In the case of the discharge product from the Ir-rGO electrode, this is 95% of that expected based on Reaction 1. Thus, this new titration method confirms that LiO₂ is present in the discharge product, consistent with other characterization techniques such as DEMS and Raman. It also provides a new technique for assessing Li-O₂ product composition.

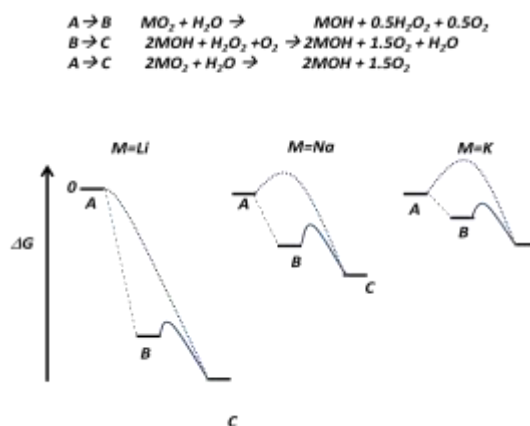


Figure 111. Reaction mechanisms for the hydrolysis of MO₂ (Reaction 1). For M=Li the reaction bypasses the formation of H₂O₂ and forms LiOH, the quantity of which is measured by pH titration.

Patents/Publications/Presentations

Patent

- Lu, Jun, and Khalil Amine, Larry A Curtiss, Kah Chun Lau, Yang-Kook Sun, Yun Jung Lee, and Xiangyi Luo. Lithium-Oxygen Batteries Incorporating Lithium Superoxide. 2017/1/24, US Patent Office, Patent number 9553316.

TASK 10 – SODIUM–ION BATTERIES

Summary and Highlights

To meet the challenges of powering the PHEV, the next generation of rechargeable battery systems with higher energy and power density, lower cost, better safety characteristics, and longer calendar and cycle life (beyond Li-ion batteries, which represent today's state-of-the-art technology) must be developed. Recently, Na-ion battery systems have attracted increasing attention due to the more abundant and less expensive nature of the sodium resource. The issue is not insufficient lithium on a global scale, but what fraction can be used in an economically effective manner. Most untapped lithium reserves occur in remote or politically sensitive areas. Scale-up will require a long lead time, involve heavy capital investment in mining, and may require the extraction and processing of lower quality resources, which could drive extraction costs higher. Currently, high costs remain a critical barrier to the widespread scale-up of battery energy storage. Recent computational studies on voltage, stability, and diffusion barriers of Na-ion and Li-ion materials indicate that Na-ion systems can be competitive with Li-ion systems.

The primary barriers and limitations of current state-of-the-art of Na-ion systems are as follows:

- Building a sodium battery requires redesigning battery technology to accommodate the chemical reactivity and larger size of sodium ions.
- Lithium batteries pack more energy than sodium batteries per unit mass. Therefore, for sodium batteries to reach energy densities similar to lithium batteries, the positive electrodes in the sodium battery need to hold more ions.
- Since Na-ion batteries are an emerging technology, new materials to enable sodium electrochemistry and the discovery of new redox couples, along with the diagnostic studies of these new materials and redox couples, are important.
- In sodium electrochemical systems, the greatest technical hurdles to overcome are lack of high-performance electrode and electrolyte materials that are easy to synthesize, safe, and non-toxic, with long calendar and cycling life and low cost.
- Furthermore, fundamental scientific questions need to be elucidated, including (1) the difference in transport and kinetic behaviors between sodium and lithium in analogous electrodes; (2) sodium insertion/extraction mechanism; (3) SEI layer on the electrodes from different electrolyte systems; and (4) charge transfer in the electrolyte–electrode interface and Na⁺ ion transport through the SEI layer.

This task will use synchrotron-based *in situ* X-ray techniques and other diagnostic tools to evaluate new materials and redox couples, to explore fundamental understanding of the mechanisms governing the performance of these materials, and provide guidance for new material developments. This task will also be focused on developing advanced diagnostic characterization techniques to investigate these issues, providing solutions and guidance for the problems. The synchrotron based *in situ* X-ray techniques (XRD and hard and soft XAS) will be combined with other imaging and spectroscopic tools such as HRTEM, MS, and TXM.

Task 10.1 – Exploratory Studies of Novel Sodium-Ion Battery Systems (Xiao-Qing Yang and Seongmin Bak, Brookhaven National Laboratory)

Project Objective. The primary objective is to develop new advanced *in situ* material characterization techniques and to apply these techniques to explore the potentials, challenges, and feasibility of new rechargeable battery systems beyond the Li-ion batteries, namely the Na-ion battery systems for PHEVs. To meet the challenges of powering the PHEV, new rechargeable battery systems with high energy and power density, low cost, good abuse tolerance, and long calendar and cycle life must be developed. This project will use synchrotron-based *in situ* X-ray diagnostic tools developed at BNL to evaluate the new materials and redox couples, exploring the fundamental understanding of the mechanisms governing the performance of these materials.

Project Impact. The VTO Multi-Year Program Plan describes the goals for battery: “Specifically, lower-cost, abuse-tolerant batteries with higher energy density, higher power, better low-temperature operation, and longer lifetimes are needed for development of the next-generation of HEVs, PHEVs, and EVs.” If this project succeeds, the knowledge gained from diagnostic studies and collaborations with U.S. industries and international research institutions will help U.S. industries develop new materials and processes for a new generation of rechargeable battery systems beyond Li-ion batteries, such as Na-ion battery systems, in their efforts to reach these VTO goals.

Approach. This project will use synchrotron-based *in situ* X-ray diagnostic tools developed at BNL to evaluate the new materials and redox couples to enable a fundamental understanding of the mechanisms governing the performance of these materials and to provide guidance for new material and new technology development regarding Na-ion battery systems.

Out-Year Goals. The out-year goals are as follows: (1) Complete the synchrotron based *in situ* XRD and absorption studies of MXene type material V_2C as new cathode material for Na-ion batteries during charge-discharge cycling, and (2) complete the preliminary synchrotron-based X-ray absorption studies of $NaCuMnO_2$ as new cathode material for Na-ion batteries.

Collaborations. The BNL team has been working closely with top scientists on new material synthesis at ANL, LBNL, and PNNL, with U.S. industrial collaborators at GM and Johnson Controls, and with international collaborators.

Milestones

1. Complete the *in situ* XRD studies of one type of MXene material V_2C as new anode material for Na-ion batteries during charge-discharge cycling. (Q1 – Completed December 2016)
2. Complete *in situ* hard X-ray absorption studies at vanadium K-edge of one type of MXene material V_2C as new anode material for Na-ion batteries during charge-discharge cycling. (Q2 – Completed March 2017)
3. Complete soft X-ray absorption studies at vanadium L-edge, carbon, and oxygen K-edge of one type of MXene material V_2C as new anode material for Na-ion batteries at different charge-discharge states. (Q3 – Completed June 2017)
4. Complete the synchrotron based X-ray absorption at copper and manganese K-edge for a new $NaCuMnO_2$ cathode material for Na-ion batteries during charge-discharge cycling. (September 2017 – In progress)

Progress Report

The third milestone was completed, and progress on the fourth-quarter milestone, scheduled for completion in September, was made.

BNL has been focused on studies of a new cathode material for Na-ion batteries. A V_2C material, as a new member of the 2D TM carbides, so-called MXenes, was synthesized and studied as anode materials for Na-ion batteries. The *ex situ* soft x-ray absorption studies (sXAS) at vanadium L-edges of MXene material V_2C during charge-discharge cycling was carried out. Figure 112 shows the V $L_{2,3}$ -edge sXAS spectra collected from five V_2CT_x electrodes cycled to different voltages using both (a) bulk sensitive total fluorescence yield (TFY) and (b) surface-sensitive total electron yield (TEY). The overall sXAS spectra can be divided into two regions, the L_3 -edge at the energy range of 510-520 eV and the L_2 -edge at 520-530 eV. It is apparent that L_3 -edge in TFY spectra display dramatic voltage-dependent changes, which are related to the vanadium redox reactions in the bulk V_2CT_x . The 516.7 eV peak intensity decreases from 1 V to 0.1 V and increases from 0.1 V to 3 V, while the lower energy peak at 513 eV shows just the opposite trend. The two sXAS features are related to the two different oxidation states of V (that is, the high energy peak at 516.7 eV represents a higher oxidation state, and its intensity increases when the average oxidation state of vanadium increases). Therefore, the changes in sXAS intensity and line shape changes clearly demonstrate the reduction of the V ions during the initial discharge from 1.0 V down to 0.1 V. Unlike in the V K-edge spectra, where the reduction of average oxidation of vanadium was indicated by the edge shift to lower energy, for the L_3 edge spectra, such reduction is indicated by the reduction of intensity ratio of 516.7 eV/513 eV peaks, which can be clearly observed by the significant enhancement of the 513 eV peak intensity at 0.1 V (sodiated). Due to the sensitivity of the TM L-edge sXAS to the valence 3d, the data in Figure 112 also show clearly that the V L-edge line shape does not fully recover when the V_2CT_x electrode is charged back to 3V from its discharged state (0.1 V). This indicates that the V redox is not fully reversible in the initial cycle, which is consistent with the low CE obtained by electrochemical test. Another observation is that the surface-sensitive TEY spectra (Figure 112b) show much weaker change, compared with that of the bulk probing TFY (Figure 112a), indicating less changes in vanadium oxidation states at the surface of V_2CT_x electrode during cycling. Combining these results with those of XRD and V K-edge XANES, it can be concluded that the redox reaction of vanadium mainly takes place in the bulk of V_2CT_x during Na^+ intercalation/deintercalation, rather than at the surface.

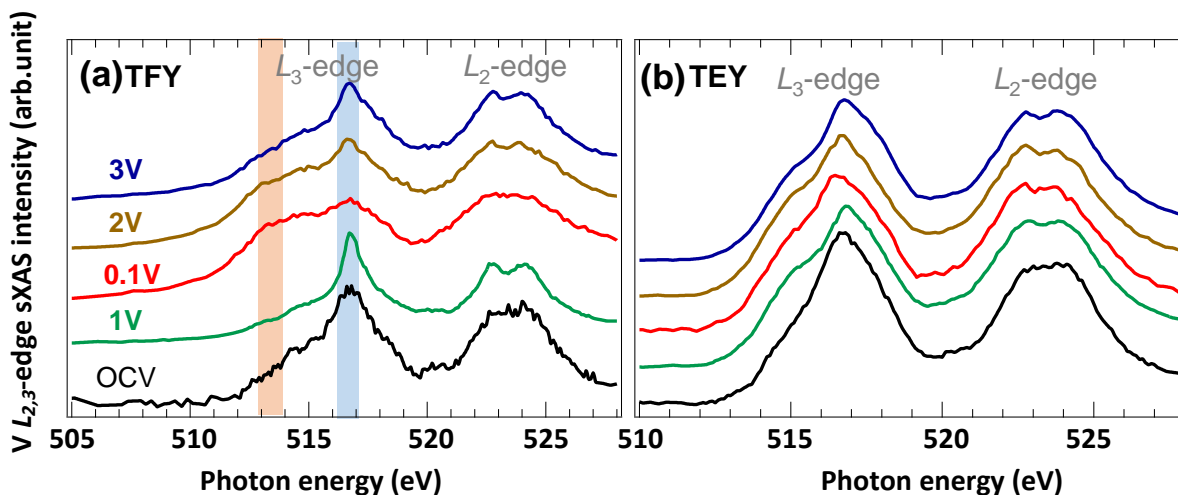


Figure 112. V $L_{2,3}$ -edge sXAS spectra collected on electrodes that are cycled to different voltages. (a) Bulk-sensitive total fluorescence yield (TFY), and (b) surface-sensitive total electron yield (TEY).

Patents/Publications/Presentations

Publication

- Yao, Hu-Rong, and Peng-Fei Wang, Yue Gong, Jienan Zhang, Xiqian Yu, Lin Gu, Chuying OuYang, Ya-Xia Yin, Enyuan Hu, Xiao-Qing Yang, Eli Stavitski, Yu-Guo Guo*, and Li-Jun Wan. “Designing Air-Stable O₃-Type Cathode Materials by Combined Structure Modulation for Na-Ion Batteries.” *J. Am. Chem. Soc.* 139, no. 25 (2017): 8440–8443. doi: 10.1021/jacs.7b05176, Publication Date (Web): June 9, 2017.

Presentation

- Third International Forum on Cathode & Anode Materials for Advanced Batteries, Ningbo, China (April 12 – 14, 2017): “Studies of New Electrode Materials for Next Generation of Batteries Using Synchrotron Based *In situ* X-ray Diffraction and Absorption as well as TXM Techniques”; Enyuan Hu, Xiqian Yu, Yongning Zhou, Yingchun Lyu, Yahong Xu, Xiao-Qing Yang*, Seong-Min Bak, Hung-Sui Lee, Xuelong Wang, Yijin Liu, Zhaoxiang Wang, Lin Gu, Hong Li, Xuejie Huang, and Liquan Chen. Invited.